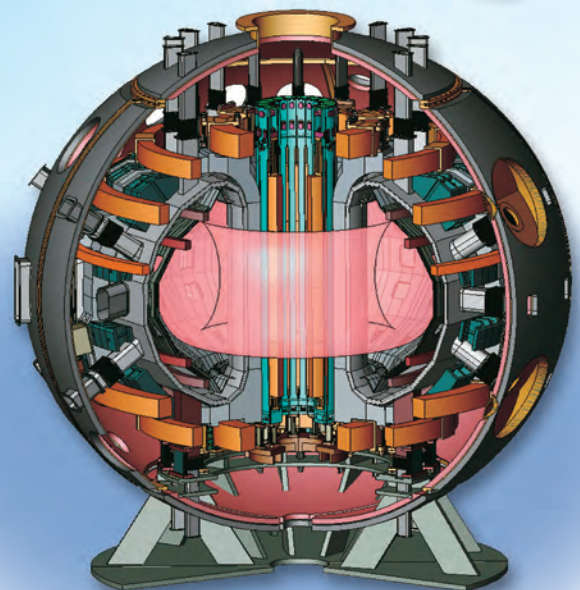


2007

# JAEA R&D Review



Underground Geological Inspection



JT-60SA

# *Message from the President*

岡崎俊雄

*President Toshio Okazaki*



Welcome to this second issue of “JAEA R&D Review”, informing you of the current R&D activities of the Japan Atomic Energy Agency (JAEA).

Two years have passed since the establishment of JAEA. We are now reaching the halfway point of the first mid-term plan, a very important period for the achievement of our goals in the R&D activities planned in this term. In addition, for the sake of stable supply of energy and resolution of global environmental problems, the importance of nuclear energy was recognized at the G8 Summit held in Heiligendamm, Germany in June, 2007. With regard to nuclear energy, JAEA is the sole comprehensive R&D institution aiming at facilitating both basic research and practical application programs in Japan. In other words, our research areas cover the whole range from science to technology for peaceful and safe uses of nuclear energy. Through our activities, JAEA has been contributing significantly to creating and improving various innovative technologies related to nuclear energy.

In the field of Fast Breeder Reactor (FBR) cycle technology designated as a “Key Technology of National Importance” by the government of Japan, JAEA has been making great efforts to restart “MONJU” (a prototype FBR) and also has been promoting R&D of the FBR cycle for commercialization. Furthermore, JAEA is constructing two underground research laboratories where R&D projects for disposal of high-level radioactive waste are being undertaken. In the field of fusion energy, JAEA strongly promotes the ITER Project and Broader Approach Project which are recognized as Strategically Prioritized Science and Technology, and is entering in the main activities of these projects with various kinds of tests. In the R&D for utilization of quantum beams, JAEA is concentrating efforts for the start-up of “J-PARC” in FY 2008.

The mission of JAEA is to improve the quality of life for all people by innovative advancements in nuclear energy. I strongly believe that JAEA will achieve this goal and become one of the world's most authoritative and comprehensive institutes, what we call a Center of Excellence (COE) for creative and reliable nuclear energy R&D.

This publication constitutes a review of our achievements in the year 2006. It not only provides you with a flavor of some of the work that has been carried out, but also invites you to check the references and contact with the researchers if there are any topics that you wish to learn about. I expect that you will take a few minutes to go to some of the following pages. I would be greatly pleased if I could hear from you with any comments on this publication.

I hope that you enjoy this publication. Thank you very much for your interest.



## 1 *Research and Development of Advanced Nuclear System*

**Toward Early Commercialization of the Fast Reactor Cycle, as One of the “Key Technologies of National Importance”** 8

—Launch of FaCT Project—

1. Handling Nuclear Data Accurately and Efficiently 9  
—Lattice Calculation Code Combining Ultra-Fine and Fine Group Calculations—
2. Ideal Fuel Cladding Materials for Fast Breeder Reactor Irradiated at Highest Temperature in the World 10  
—Microstructure Stability Evaluation of a Heavily Neutron-Irradiated Oxide Dispersion Strengthened Steel for Advanced Nuclear Reactors—
3. Toward Realization of Minor-Actinide Recycling in a Fast Reactor Cycle System 11  
—Development of Fabrication Technology of Advanced Oxide Fuel Containing Americium—
4. Accurate Temperature Analyses of FBRs in Low Flow Conditions 12  
—Heat Conduction and Heat Transfer between Subassemblies—
5. Experimental Study on Gas Entrainment Phenomena 13  
—Simultaneous Measurements of Flow Velocity Fields and Free Surface—
6. Achieving Efficient Fuel Handling 14  
—Study on the Fuel Handling System in a Commercial SFR—
7. Higher Accuracy in the Inspection of Heat Exchanger Steam Generator Tubes of Nuclear Fast Reactors 15  
—Suppression of Sodium Adhesion ECT Signal Achieved by Numerical Simulations—
8. Investigation of Strength of Structural Material Using Controlled Temperature Fluctuation Loading 16  
—High Cycle Thermal Fatigue Tests in Sodium for Fast Reactor Design—
9. Analysis Shows that Reactor Trip Failure Probability Is Extremely Small 17  
—Anticipated Transient without Scram (ATWS) Frequency Evaluation of FBR “MONJU”—
10. Analysis of “MONJU” Thermal Transient Margin 18  
—Analysis of “MONJU” Thermal Transient Margin Based on Measured Plant Performance—
11. The Challenge of Maintaining Safety in an Extreme Environment 19  
—Development of an ISI Device for the Reactor Vessel of “MONJU” Fast Breeder Reactor—

## 2 *Research and Development on Geological Disposal of High-Level Radioactive Waste*

**R&D Supporting the Technology and Reliability of Geological Disposal in Japan** 20

1. Development of a Novel Knowledge Management System for Geological Disposal 21  
—Preliminary Design of Management Functions and Knowledge Base—
2. Characterization of Potential Changes in Geological and Disposal Environment Caused by Natural Phenomena 22  
—Development of Evaluation Procedure for HLW Disposal System Perturbation Scenarios—
3. Possibility of Superlong-Lifetime Container for Geological Disposal 23  
—Corrosion Behavior of Copper Overpack in Low Oxygen Concentration Environment—
4. Integration and Management of Mass Transfer Coefficient in Geological Environment 24  
—Development and Operation of Web Site for Diffusion Database (DDB)—
5. Finding Ancient Temperatures 25  
—Reconstruction of Past Climate Using Pollen Records from the Small Basin Deposit—
6. Underground Survey Using the Blasting Vibration During Shaft Excavation in the MIU-Site 26  
—Underground Imaging Technique Using a Geophysical Method—
7. Estimation of a Groundwater Flow by Minute Tilt 27  
—Estimation of Hydrogeological Structures by an Inverse Analysis of Tilt Data—

- |  |    |
|--|----|
| 8. Estimation of Groundwater Quality from Specific Resistance Values<br>–Improvement of Geostatistically-Based Estimation of Groundwater Quality–              | 28 |
| 9. Estimation of the 3D Distribution of Groundwater Chemistries<br>–Hydrochemical Investigation in the Horonobe Underground Research Laboratory (URL) Project– | 29 |
| 10. Inference of Hydrogeological Structure from Geological Observations<br>–Development of Fracture Investigation Techniques for Sedimentary Rocks–            | 30 |

### 3 Nuclear Fusion Research and Development

#### For Practical Use of Fusion Energy 31

- |   |    |
|---|----|
| 1. Accomplishment of the Conceptual Design of JT-60SA through Collaboration of Japan and Europe<br>–JT-60SA Program for ITER-Supporting and ITER-Complementing Research–                              | 32 |
| 2. The Search for the Plasma Rotation Needed for High Pressure Plasma<br>–Finding the Minimum Plasma Rotation Suppressing Plasma Distortion–  | 33 |
| 3. Sharpening Plasma Shape Improves Pressure Limit<br>–Stabilization of the Edge Localized Mode by Sharpening the Plasma Shape–   | 34 |
| 4. Suppression Mechanism of Turbulent Electron Heat Transport<br>–Simulation Study of Microscopic Electron Turbulence in Tokamaks–  | 35 |
| 5. Development of Full Scale First Wall of Fusion Blanket<br>–R&D of Diffusion Bonding for Fusion Blanket Manufacturing–  | 36 |
| 6. Developing a Method for Suppressing Irradiation Hardening of F82H by Heat Treatment Utilizing the Difference in the Hardening of Weld Joints   | 37 |
| 7. Measurement of Tritium Production Rate in Blanket with High Accuracy<br>–Development of Measurement and Calculation Methods in Breeder Layer–  | 38 |
| 8. Material Allowing Stable Fuel Supply to Fusion Reactor<br>–Development of Advanced Tritium Breeder Materials for Fusion Reactor–   | 39 |
| 9. Research on Interaction between Tritium and Metal<br>–Pyramid-Like Blisters Formed by Hydrogen-Induced Local Superplasticity–  | 40 |
| 10. Neutron Shielding Resin Can Be Used in the High Temperature Environment of a Fusion Device<br>–Development of Neutron Shielding Resin that Has High Heat Resistance and High Mechanical Strength– | 41 |

### 4 Quantum Beam Science Research

#### Taking a Leading Role in Quantum Beam Technology 42

- |  |    |
|--|----|
| 1. Study Suggests the Existence of Ferroelectric Ice in Outer Space<br>–A Neutron Diffraction Study of Ice XI–   | 43 |
| 2. Elucidation of Plant Growth Regulation by Ion Beams<br>–The <i>SMAP1</i> Gene Regulates Sensitivity to Plant Hormone–   | 44 |
| 3. Discovery of Phonons Causing Superconductivity in Diamonds<br>–Looking for “Room Temperature-Superconductors” in Diamonds–  | 45 |
| 4. Discovery of Activation Enhancement Mechanism of DNA Repair Promoting Gene <i>pprA</i><br>–Role of Radiation Response Protein LexA2–                                  | 46 |
| 5. Anomalous Spin Structure in Frustrated Magnet<br>–Spin-Lattice Coupling Observed by a Neutron Scattering Technique–   | 47 |
| 6. Functional Diagnosis of Photosynthesis in a Leaf<br>–Quantitative Kinetic Analysis of Photosynthetic Functions Using Positron Emitting Tracer Imaging System (PETIS)– | 48 |

7. Photons Create New Heavy Elements in Supernovae	49
– Photodisintegration Reaction Nucleosynthesis in Supernova Explosions –	
8. Neutron Control by Magnetic Field	50
– Development of Magnetic Optics to Highly Polarize and Focus Neutrons –	
9. Promising Biodegradable Plastic for Industrial Applications	51
– OFF-ON Control of Biodegradability in Polymer with Radiation and Chemical Modifications –	
10. Direct Observation of Itinerant to Localized Transition of Heavy Electrons	52
– Toward the Understanding of Heavy Fermion Materials –	
11. Water Behavior in Concrete Observed Using Neutrons	53
– Application to Deterioration Diagnostics of Concrete Structures –	
12. Detection of Electric Circuit Malfunction Caused by Galactic Cosmic Rays	54
– Mechanism of Transient Current Induced by High Energy Heavy Ions in Semiconductor Devices –	
13. Clear Observation of Poorly Visible Objects Using High-Function X-rays	55
– Generation of High-Brightness, High-Contrast X-rays by Terawatt Laser –	

## 5 Nuclear Safety Research

<b>To Enforce Safety Regulations and to Ensure Nuclear Safety and Confidence</b>	56
1. For Risk-Informed Safety Management in Nuclear Power Plants	57
– Development of the Procedure for Uncertainty Analysis of Source Terms –	
2. Evaluating the Influence of Hydrogen Absorption in the Clad on Fuel Failure	58
– Failure of High Burnup Fuel in Reactivity Initiated Accident –	
3. Degradation of Cladding Ductility Affected by Cooling History	59
– Effect of Cooling History on Cladding Ductility under LOCA Conditions –	
4. Boiling Heat Transfer Enhancement by Irradiation	60
– Improvement of Critical Heat Flux by Radiation Induced Surface Activation –	
5. Evaluating the Fracture Resistance of a Reactor Pressure Vessel under Pressurized Thermal Shock	61
– Structural Reliability Evaluation of Aged Components in Nuclear Plants Based on Probabilistic Fracture Mechanics (PFM) –	
6. Preparation for Nuclear Criticality Safety Evaluation of High-Burnup Fuel Cycle in the Near Future	62
– Development of a High-Precision Evaluation Method for Nuclear Criticality Safety of a 5 to 10 % <sup>235</sup> U-Enriched Uranium Fuel System –	
7. Thermal Properties of Additional Material Used in MOX Fuel Fabrication Facility	63
– Investigation of Data and Evaluation Model of Pyrolysis Properties of Zinc Stearate –	
8. Mass Transport Retardation Studies under In Situ Conditions	64
– Radionuclide Migration Experiments in a Rock Fracture at a Depth of 240 m –	
9. Evaluating the Radionuclide Concentrations at which Radioactive Materials Can Be Released from Regulatory Control	65
– Clearance Level Calculation System Development –	

## 6 Advanced Science Research

<b>Advanced Basic Research to Create the Future</b>	66
1. Unusual Magnetic and Orbital Ordering in Np Compounds	67
– Neutron Scattering Study of Actinides in JRR-3 –	
2. Large Magnetoresistance Effect Found in Fullerene-Cobalt Thin Films	68
– Organic Molecule Mediates Electron Spin –	
3. A New Method for Material Synthesis under a Million G	69
– Research into New Materials Utilizing “Mega-Gravitoronics” –	

- |   |    |
|---|----|
| 4. Artificial Enzymatic Synthesis of Cellulose  | 70 |
| – Elucidation of Self-Organization Mechanism of Reaction Products by Using Small-Angle Neutron Scattering Method –  |    |
| 5. Dependence of Yield of DNA Damage Refractory to Enzymatic Repair on Ionization & Excitation Density of Radiation | 71 |
| – Exploring the Induction Mechanism of Clustered DNA Damage –   |    |

## 7 *Nuclear Science and Engineering Research*

### **Formation of Basis for R&D of Nuclear Energy, and Creation of Innovative Nuclear Energy Utilization Technology** 72

- |  |    |
|--|----|
| 1. Experimental Investigation of Thermal Margin in Tight-Lattice Rod Bundle  | 73 |
| – Large-Scale Experiments under High Pressure Conditions –   |    |
| 2. Proposal for Future Waste Management  | 74 |
| – Reduction of the Repository Size for the High Level Wastes (HLW) by Introducing Partitioning and Transmutation (PT) Technology – |    |
| 3. Attempts to Improve Radiolytic Stability of Amidic Extractants for the Separation of Actinides                                  | 75 |
| – Development of an Improved Extractant, Based on the Reaction Mechanism of Radiolysis –   |    |
| 4. Toward Clarification of Minor Actinides Behavior in Pyrochemical Processes  | 76 |
| – Preparation of Minor Actinide Chlorides without the Use of Corrosive Gases –   |    |
| 5. Radiation Dose Assessment for a Heavily Exposed Person without any Dosimeters   | 77 |
| – Dose Assessment by Measuring Activated Sodium in the Body –  |    |
| 6. Estimation of Quality and Quantity of DNA Damage Sites  | 78 |
| – New Method to Characterize DNA Damage Produced by Radiation –  |    |
| 7. Demonstration of Excellent Safety Characteristics of HTGR   | 79 |
| – Coolant Flow Reduction Test Using HTTR –   |    |
| 8. Outstanding Economic Efficiency of HTGR for Electricity Generation  | 80 |
| – Design Study on the HTGR with Gas Turbine –  |    |

## 8 *Nuclear Fuel Cycle Technological Development*

### **To Establish the Nuclear Fuel Cycle** 81

- |  |    |
|--|----|
| 1. Accurate Measurement of Plutonium Nitrate Solution  | 82 |
| – Accuracy & Reliability by Digital-Quartz Transducers Confirmed by Comparison of Two Densities and by Applying Them to Solution Mass Monitoring – |    |
| 2. Contributions to Safeguards and Further Efficiency  | 83 |
| – Safeguards Improvement for the Tokai Reprocessing Plant –  |    |

## 9 *Development of Technology on Nuclear Cycle Backend*

### **R & D for Decommissioning and Rad-Waste Management** 84

- |  |    |
|--|----|
| 1. Cutting Method for a Narrow Space with Little Heat Generation | 85 |
| – Dismantling of the Core by the Abrasive Water Jet Cutting –    |    |
| 2. Measurement of Low Concentrations of Tritium in Concrete      | 86 |
| – Confirmation of Tritium Contaminant Clearance –                |    |

## 10 *Computational Science and E-Systems Research*

### **Atomic Energy R&D by Computer Simulation** 87 —Toward Establishment of Advanced Technology for Atomic Energy R&D—

1. A Simulation Study of Intricate Crack Shapes 88  
—Large-Scale Simulation of Stress Corrosion Cracking Shape—
2. Detection of Nuclear Plant Structure Vibration 89  
—Vibration Analysis Technology for Simultaneous Evaluation of Different Wavelengths—
3. Measuring Twisting Modulus of DNA 90  
—Predicted Effects of Local Conformational Coupling and External Restraints on the Torsional Properties of Single DNA Molecules—
4. Nanosecond Neutron Detection with Superconductor MgB<sub>2</sub> 91  
—Ultra-Fast Response Revealed by Simulations and Experiments—

## 11 *Scientific & Technical Development for Nuclear Nonproliferation*

### **Scientific & Technical Development for Nuclear Nonproliferation Supporting Peaceful Use of Nuclear Energy** 92

1. Design of Safeguards System for an Advanced Nuclear Fuel-Cycle System 93  
—Development of Safeguards System Simulator—

## 12 *Development of Experimental Techniques / Facilities at JAEA R&D Centers* 94

1. Shortening the Modification Period in “MONJU” 98  
—Discussion of One-Loop Operation of Primary Heat Transport System in Fast Breeder Reactor “MONJU” and the Execution—
2. Heavy Ion Beams Lead the Way to Super Heavy Element Science 99  
—Development of Heavy Ion Injector in Terminal of Tandem Accelerator—
3. Toward a Better Understanding of High Burnup Fuel Behavior during Scenario Accidents in Nuclear Power Reactors 100  
—Design of Experimental Capsule for Irradiated Fuel Experiments—
4. Precise Estimation of the State of Oceans in the Past, Present and Future 101  
—Simulation of the Marine Diffusion of Radioactive Materials Using LAMER—
5. Study on Physical Properties of Fast Reactor Fuel for Future Commercialization 102  
—Study on Thermal Conductivities of Uranium-Plutonium Mixed Oxide Fuels—
6. Measurement and Analysis of Deflection of Fuel Pins Irradiated in a Fast Reactor 103  
—Evaluation of Irradiation Effects Using the X-ray CT Technique—
7. Measuring Irradiation Time until Metal Specimen Rupture in Sodium Cooled Reactor 104  
—In-Pile Creep Rupture Experiment of Cladding Materials for Fast Reactor—
8. Upgrading of HTTR Burnup Characteristics Evaluation Method 105  
—Improvement of BP Burnup Characteristics—
9. Fabrication of a Micro-Scale Arc de Triomphe by MeV Focused Proton Beams 106  
—Development of a 3-Ds’ Fine Fabrication Technique Using High Energy Submicron Ion Beams—
10. Battle Against Water Inflow: Five-year History of Mizunami Underground Research Laboratory 107  
—Development of Post-Grouting Technology for Deep Shaft—

## Toward Early Commercialization of the Fast Reactor Cycle, as One of the “Key Technologies of National Importance”

— Launch of FaCT Project —

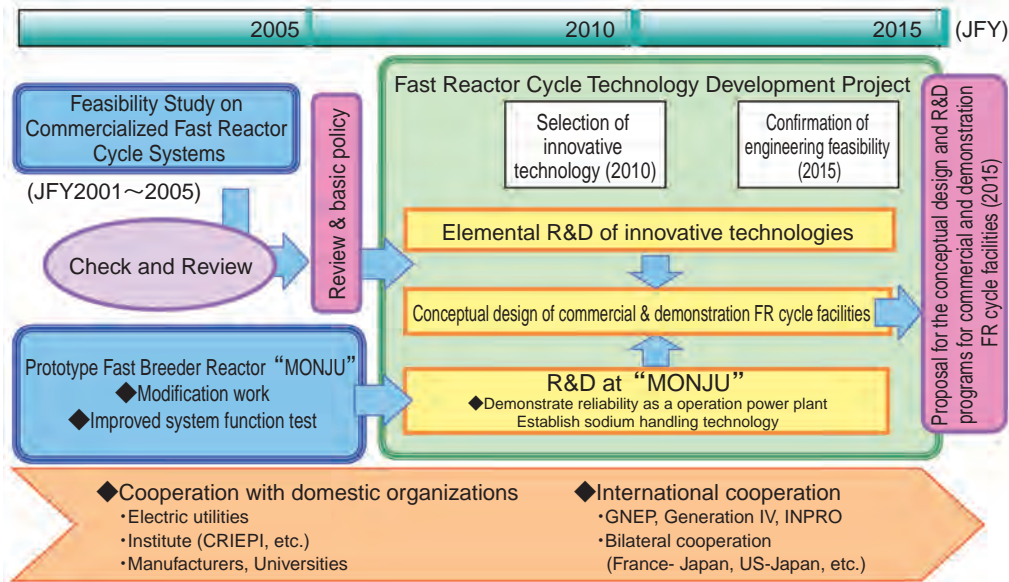


Fig.1-1 Fast Reactor Cycle Technology Development Project

The 2nd phase of the “Feasibility Study on Commercialized Fast Reactor (FR) Cycle Systems” (hereinafter referred to as “FS”) was completed by a Japanese joint project team comprising the Japan Atomic Energy Agency (hereinafter referred to as “JAEA”), electric utilities, and the Central Research Institute of Electric Power Industry at the end of March 2006. This was part of an R&D program aiming to present an appropriate conceptual design for a commercial FR cycle system by 2015. As a result of this FS, we found that the best concept is the combination of a sodium-cooled FR with oxide fuel, advanced aqueous reprocessing, and simplified pellet fuel fabrication, which meet requirements for economical competitiveness, safety, reduction of environmental burden, efficient utilization of nuclear fuel resources, proliferation resistance and technical feasibility.

The FR cycle technology was listed as a one of the “Key Technologies of National Importance” in the “Science & Technology Basic Plan” of Japan. In the previous fiscal year, the R&D program and commercialization of a FR cycle were discussed on a national level as part of a “Framework for Nuclear Energy Policy”. The Committee for Nuclear R&D (a subdivision of the Council for Science and Technology of MEXT) assessed the results of 2nd phase of FS, and discussed the path to an R&D program to commercialize the FR cycle. The committee selected the

above combination as a significant concept with high feasibility for commercialization, and suggested that JAEA should accelerate its development by focusing on the practical application of innovative technology.

We did strategic research in the FS to make our future goal clear, and then changed our R&D emphasis to “Technology Development concentrating on commercialization” by using “MONJU”, “JOYO” and our other recycling facilities, while aggressively pursuing international cooperation, based on the R&D policy of MEXT and the “Basic Policy on Research and Development of FR Cycle Technologies over the Next Decade” of the Japan Atomic Energy Commission. In addition, with the shift from the “concept” to the “actual system”, JAEA changed the project name from FS to “FaCT (Fast Reactor Cycle Technology Development)”. Further, we reviewed the existing organization in order to better promote the FaCT project, and established an executive organization headed by the JAEA president to coordinate between the R&D directorate and the facility site.

Using practical applications of innovative technology and the R&D results obtained at “MONJU”, we will conduct intensive R&D to present by 2015 an R&D program for conceptual design and realization of a commercial and demonstration FR cycle facility, as shown in Fig.1-1.

# 1-1 Handling Nuclear Data Accurately and Efficiently

## — Lattice Calculation Code Combining Ultra-Fine and Fine Group Calculations —

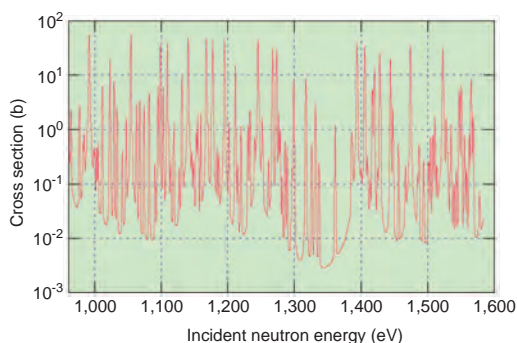


Fig.1-2 Energy dependence of  $^{238}\text{U}$  capture cross section

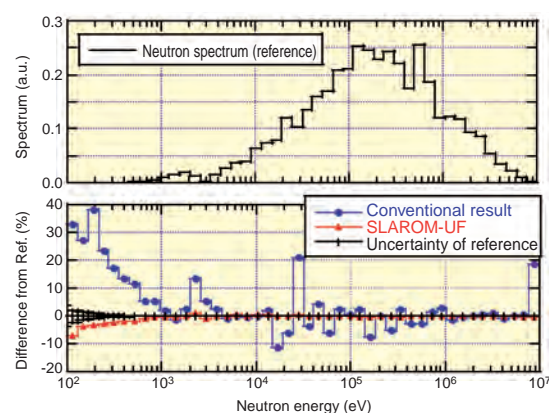


Fig.1-3 (upper) Analysis accuracy of neutron spectrum of “JOYO” MK-I core. Neutron spectra in an infinite lattice calculation using SLAROM-UF and using the conventional method are compared with regard to the difference from the reference (a continuous Monte Carlo calculation shown in the upper half). Use of SLAROM-UF almost eliminates the difference.

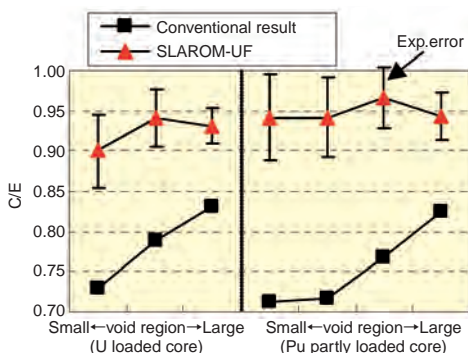


Fig.1-4 (left) Accuracy of sodium void reactivity analysis of criticality experimental data

The experimental data on BFS criticality experiment simulating Russian fast reactor BN-600 is analyzed. Use of SLAROM-UF improves the C/E ratio, thus reducing the regional dependence of the data.

In fast reactor analyses, it is important to evaluate neutron reactions accurately over the energy range from 100 eV to several MeV, where neutron cross sections have resonances at certain energies, where the probability of neutron reactions fluctuates rapidly (Fig.1-2).

In a conventional method, a discrete 70-group cross section set has been used, and effects of resonances are tabulated in advance. This method causes several dozen percent error in a sodium void reactivity analysis. Furthermore, the constants used were optimized to a specific reactor type of “MONJU”, so that errors occur depending on core sizes, etc.

There is a continuous energy Monte Carlo code free from error; however, it is not suitable either for calculations of very small values of the sodium void reactivity or for a detailed physical investigation.

Thus, we developed a code based on a deterministic method with accuracy comparable to the Monte Carlo code. The basic idea of the code is a combination of two kinds of calculations: an ultra-fine group (UF) calculation (approx.

100,000 groups) and a fine group calculation (max. 900 groups). The UF calculation covers the energy range below about 50keV where resonances are remarkable. Its group structure is so fine as to distinguish each resonance. Effective cross sections are efficiently created by solving a slowing down equation focusing only on elastic scattering and absorption. The fine group calculation follows the conventional method except for use of the effective cross section created in the UF calculation and use of a sufficiently fine energy structure above the 50keV that resonances of structural materials can be treated accurately.

Performances of the developed code “SLAROM-UF” are shown in Fig.1-3 and Fig.1-4. SLAROM-UF gives accuracy comparable to a continuous energy Monte Carlo code, and a drastic improvement is observed in its agreement with experimental values as well.

SLAROM-UF has the capability of the conventional calculation and can be used either for a rough or a very detailed calculation, depending on accuracy required. It has already been used in the analysis of “MONJU”.

### Reference

Hazama, T. et al., Development of a Fine and Ultra-Fine Group Cell Calculation Code SLAROM-UF for Fast Reactor Analyses, Journal of Nuclear Science and Technology, vol.43, no.8, 2006, p.908-918.

# 1-2 Ideal Fuel Cladding Materials for Fast Breeder Reactor Irradiated at Highest Temperature in the World

## — Microstructure Stability Evaluation of a Heavily Neutron-Irradiated Oxide Dispersion Strengthened Steel for Advanced Nuclear Reactors —

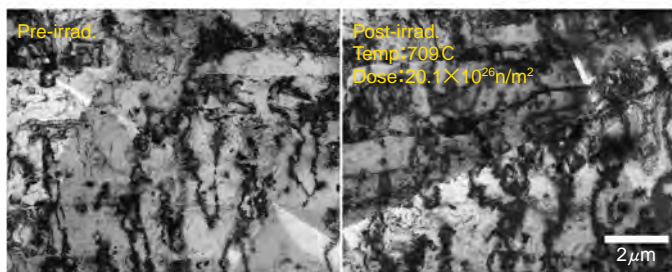


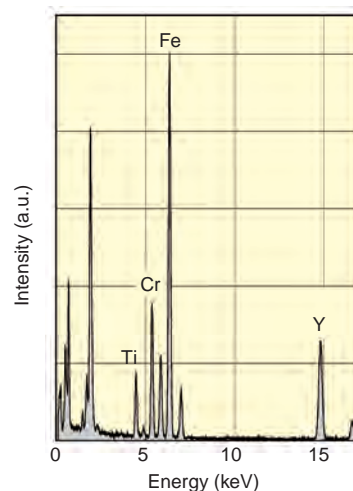
**Fig.1-5 A comparison of microstructure between pre- and post-irradiated ODS steels**

Irradiation effect on microstructures of ODS steel (MA957) was evaluated by comparing these before and after heavy neutron-irradiation at elevated temperature in the fast reactor “JOYO”. The microstructures of MA957 were little changed even after the irradiation, because dislocations with high density were stabilized by oxide particles.



**Fig.1-6 Bright and dark field images of oxide pinning dislocation and EDS from the oxide**

Transmission electron microscope observation and EDS analyses were conducted for understanding the effect of oxide particles on stability of mesoscopic scale structure under irradiation. We found that the oxide particle, which is composed of yttrium (Y) and titanium (Ti), effectively pinned dislocation under irradiation at elevated temperature.



Oxide Dispersion Strengthened (ODS) steel is one of most promising nuclear reactor materials because of its superior swelling resistance and excellent high temperature strength. We are developing a cladding tube of ODS steel for a Fast Breeder Reactor (FBR) to achieve higher thermal efficiency in the FBR system.

Important issues in the development of ODS steel are as the following; (1) To establish the cladding tube fabrication technology for ODS steel on a commercial scale, and (2) to inspect and demonstrate successive property changes of the irradiated ODS steel up to the target total dose in the FBR ( $5.0 \times 10^{27} \text{ n/m}^2; E > 0.1 \text{ MeV}$ ).

For solving the problems involved in irradiation testing and study, we are acquiring irradiation data by the following two steps. (i) The performance limit of this kind of alloy is being estimated prior actual testing of our originally-developed ODS steels by testing the commercially fabricated ODS steel MA957. Subsequently, (ii) we are planning to

demonstrate irradiation tolerance of our ODS steel as the cladding tubes by exposing it to the target doses.

Information on heavy neutron-irradiation of ODS steel at elevated temperatures has been obtained for the first time in the world. Fig.1-5 is a comparison of the microstructure before and after irradiation, indicating that the microstructural stability of MA957 is maintained even under this severe environment. On the other hand, Fig.1-6 is a bright and dark pair of images showing oxide pinning dislocation and Energy Dispersive Spectrum (EDS) from the oxide. We found that the oxide particle, which is composed of yttrium (Y) and titanium (Ti), effectively pinned dislocation under irradiation at elevated temperature.

In near-future plans, post irradiation tests of our originally-developed cladding tube made of ODS steels are scheduled, and we hope to confirm and demonstrate the irradiation tolerance of these materials.

### Reference

Yamashita, S. et al., Microstructural Development of a Heavily Neutron-Irradiated ODS Ferritic Steel (MA957) at Elevated Temperature, Journal of Nuclear Materials, vol.367-370, 2007, p.202-207.

# 1-3 Toward Realization of Minor-Actinide Recycling in a Fast Reactor Cycle System

## — Development of Fabrication Technology of Advanced Oxide Fuel Containing Americium —

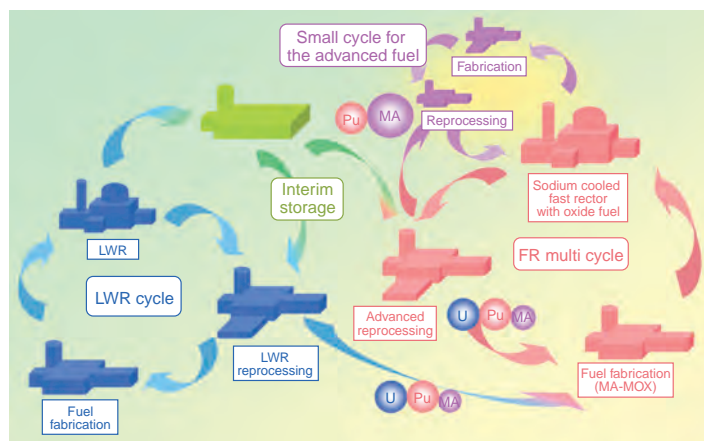


**Fig.1-7 FR cycle scheme that incorporates advanced oxide fuel**

The system is composed of three sub-cycles: an LWR cycle, main FR multi cycle and small cycle. This separation strategy of the advanced oxide fuel cycle can lead to load reduction of the main FR cycle.

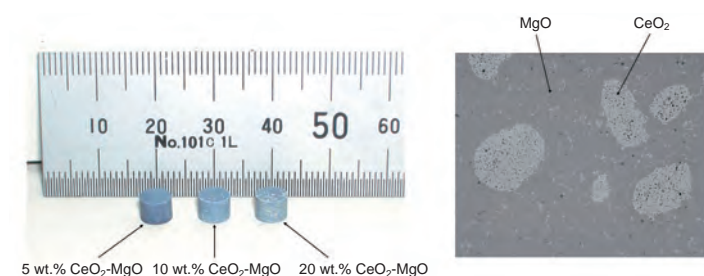


**Fig.1-9 Appearance and microstructure of the advanced oxide fuel**  
Advanced oxide fuel with MgO having good characteristics, i.e., no defects, high density, and homogeneous dispersion of a spherical host phase, was obtained.



**Fig.1-8 Fabrication process of macro-dispersed type fuel**

Fabrication tests of advanced oxide fuel were done by a powder metallurgy that could be adapted to present commercial manufacturing technology.

Minor actinides (MAs), which are recovered from spent nuclear fuel, are of special concern because of their lasting radiotoxicity and decay heat. Therefore, recovery and recycling of MAs in fast reactors (FRs) are key technologies for the successful realization of the FR cycle system, which can lead to a reduced environmental burden and a sustainable energy supply. The most promising candidate fuel for such FRs is considered to be a mixed oxide (MOX) fuel doped with 1~5wt.% of MAs. On the other hand, the MAs should be incinerated as soon as possible in the introductory phase of FRs since a large amount of MAs accumulate during extended operation of a light water reactor (LWR). Therefore, an advanced oxide fuel with a high content of MAs combined with inert matrix (IM), e.g. magnesium oxide (MgO) or Molybdenum (Mo), has been proposed for rapid incineration of MAs. These advanced oxide fuels have advantages in containing a large amount of MAs and enhancing thermal and physical properties better than the standard MOX fuel. Treatment of the advanced oxide fuel separate from the standard MOX fuels in the fabrication and reprocessing stages as in dedicated small-scale facilities was considered (Fig.1-7). This leads to concentration/ isolation of MAs by a small treatment cycle, for a small impact on the main FR cycle. The problem here is that the existing fabrication processes for such advanced oxide fuels are based on

advanced/complicated procedures which are not adaptable to the presently used commercial manufacturing technology, i.e. powder metallurgy. Therefore, novel technology has to be optimized and established.

In preparation for this introductory phase of FRs, the purpose of this study is to establish a simple fabrication technique for advanced oxide fuel that is adaptable to the standard one, for the rapid deployment of advanced oxide fuel production. A basic study for fabrication of an Am-containing advanced oxide fuel with MgO was carried out using a powder metallurgical technique. Macro-dispersed (particles with diameter of more than  $100\mu\text{m}$ ) fuels were fabricated in the present work. This type of fuel is designed for the suppression of irradiation damage of the matrix mainly by fission products, which lead to degradation of thermal properties. Fig.1-8 shows the fabrication process of macro-dispersed type fuel by powder metallurgy. Fig.1-9 shows the appearance and microstructure of the advanced oxide fuel, cerium dioxide ( $\text{CeO}_2$ )-MgO.  $\text{CeO}_2$  was used as a surrogate for Am-oxide. Advanced oxide fuel with MgO that had good characteristics was obtained.

In future work, the fabrication and evaluation of Am-containing advanced oxide fuel will be carried out. These results will be reflected in the further development of MA recycling in FR cycle systems.

### Reference

Osaka, M. et al., Research and Development of Minor Actinide-Containing Fuel and Target in a Future Integrated Closed Cycle System, Journal of Nuclear Science and Technology, vol.44, no.3, 2007, p.309-316.

# 1-4 Accurate Temperature Analyses of FBRs in Low Flow Conditions — Heat Conduction and Heat Transfer between Subassemblies —

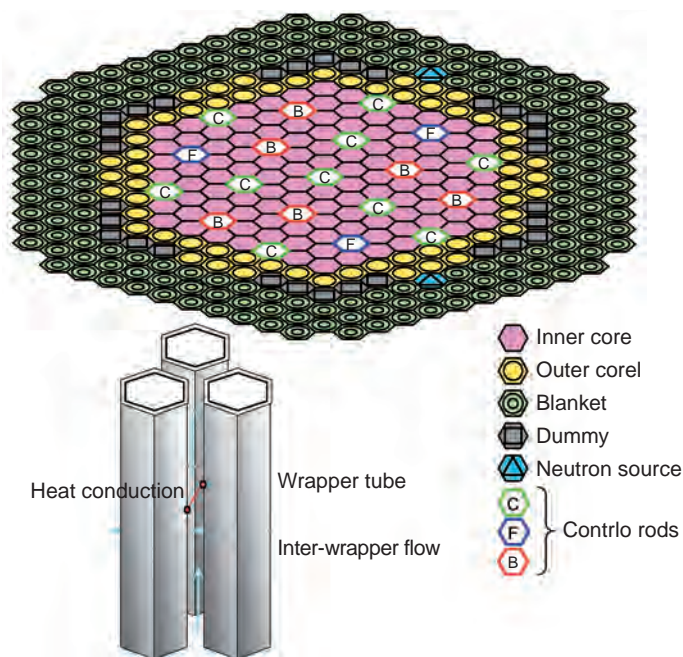


**Fig.1-10 (upper) Core of “MONJU” and inter-subassembly heat transfer (ISHT) model**

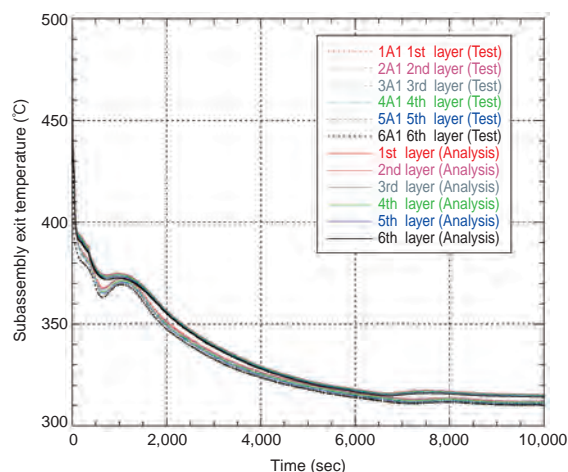
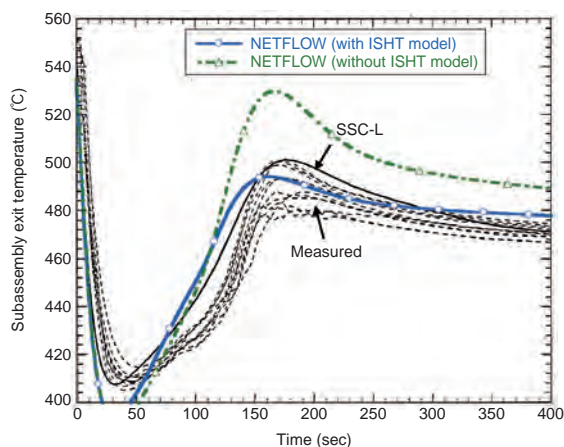
Heat transport from the center of the core to peripheral subassemblies is evaluated by heat conduction of sodium and heat transfer caused by inter-wrapper flow.

**Fig.1-11 (upper right) Comparison of “JOYO” assembly exit temperature (at 3rd layer)**

The ISHT model is validated through a calculation of the natural circulation test conducted at the “JOYO” reactor with 100 MW irradiation core. Exit temperatures are overestimated when the ISHT model is not used.

**Fig.1-12 (lower right) Comparison of “MONJU” subassembly exit temperature during reactor trip from 45% thermal power**

Subassembly exit temperatures during turbine trip test were calculated with a calculation model of the NETFLOW code from the primary heat transport (HT) system to the 3rd HT system. The Monju reactor was cooled by forced circulation at 1/10 of the rated flow rate by pony motors after the scram, and flow distribution was appropriate even at low flow rates. There was little temperature difference between subassemblies at the center and at the periphery. This situation was properly calculated by the code.



The NETFLOW code has been developed in order to simulate simply and accurately complex flow systems like heat transport systems (HTSs) and auxiliary cooling systems of a nuclear power plant. The calculation accuracy has been confirmed through analyses in light water reactor systems and test results of the forced circulation of the “MONJU” reactor. This code is already provided to graduate school students for their education.

In order to do accurate simulation under low flow rate conditions of the liquid metal cooled fast reactors, a model to calculate the heat transfer between subassemblies (SAs) was proposed and validated. In this model, six neighboring SAs' overall heat transfer coefficients for heat conduction by liquid metal and for low flow heat transfer around SAs, i.e. inter-

wrapper flow, were applied (Fig.1-10). Generally, temperature at the center SA is higher than the peripheral SAs. It is realistic that SAs should be analyzed by radial layers from the center outward rather than one by one. Therefore, the model calculated temperatures from data matrices consisting of kinds (fuels, blankets, control rods, and reflectors) and numbers of SAs neighboring the SA in question. The results are shown in Fig.1-11 and Fig.1-12; exit SA temperatures are simulated, like the SSC-L code developed in USA. Since exit temperatures were calculated appropriately, the temperature behavior can be understood before a calculation with a 3D model is done. The present ISHT model can be applied to other one-dimensional plant dynamics codes.

## Reference

Mochizuki, H., Inter-Subassembly Heat Transfer of Sodium Cooled Fast Reactors: Validation of the NETFLOW Code, Nuclear Engineering and Design, vol.237, issue 19, 2007, p.2040-2053.

# 1-5 Experimental Study on Gas Entrainment Phenomena

## — Simultaneous Measurements of Flow Velocity Fields and Free Surface —

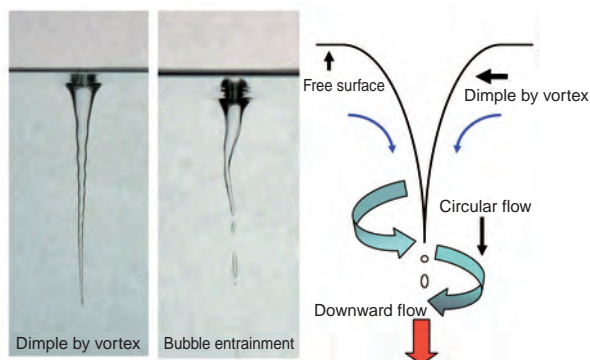


**Fig.1-13 Overview of gas entrainment due to surface vortices**

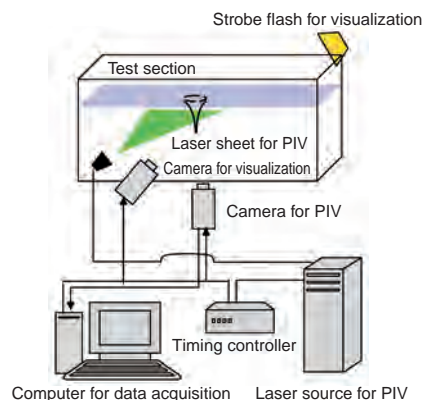


**Fig.1-14 Measurement system of the velocity field and the shape of free surface**

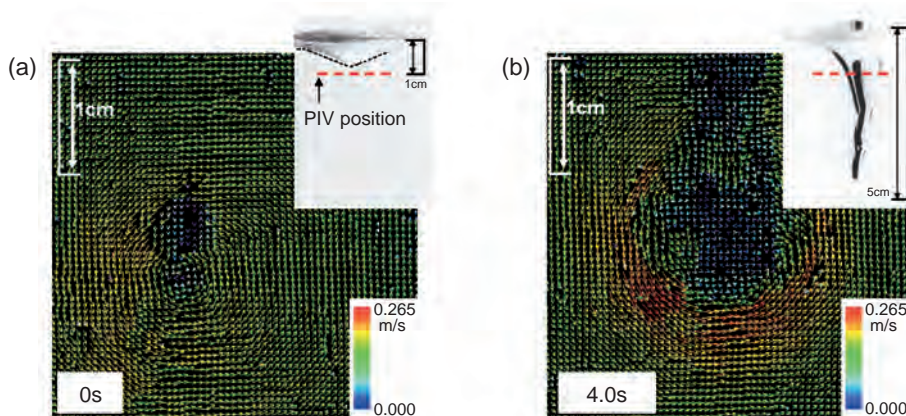


**Fig.1-15 Velocity field and shape of free surface obtained by the laser measurements**

The upper right picture shows the surface shape of the vortex and the measurement position of PIV (1mm below the bulk free surface). The left side figure shows the velocity profiles on the horizontal plane at  $t = 0s$ , and  $t = 4s$  in the right side figure.

JAEA has proposed and investigated an innovative design for a Sodium-cooled Fast Reactor in the FaCT project of FBR cycle system. One of the key concepts of the reactor is a reactor vessel more compact than previous designs for high cost performance, i.e., reduction of construction cost. However, this design causes higher flow velocity in the reactor vessel, and this causes cover gas entrainments at the free surface in the reactor vessel. In order to realize this compact design, we have to prevent the gas entrainments, and it is now one of the significant thermal hydraulic issues. The most significant type of gas entrainment is caused by surface vortices as shown in Fig.1-13. The surface vortices may result in the gas entrainment even if velocity near the free surface is relatively low. It is necessary to clarify the onset condition and development process to establish the criterion to prevent this type of gas entrainment. Thus, a basic water experiment was carried out to grasp the mechanism of the phenomena by measuring the velocity fields inside of the

vortices.

According to a mock up experiment, vortices that appear in the actual reactor would develop and decline intermittently. To clarify such transient behaviors, the velocity field and the surface shape were measured simultaneously by using a measurement system combining Particle Image Velocimetry (PIV) and surface visualization as shown in Fig.1-14.

As a result, we could make instantaneous measurements of the surface shape and the velocity field inside of the vortex at the same time as shown in Fig.1-15. Then, it was shown that there was a strong correlation between the circular flow around the vortex and the gas core length which developed. From the comparison between the result of  $0s$  (a) and  $4.0s$  (b), the gas core development was delayed after the velocity increase. These results will be used for the verification of a numerical analysis, and also to improve the guidelines for prevention of gas entrainments.

### Reference

Ezure, T. et al., Transient Behavior of Gas Entrainment Caused by Surface Vortex, Proceedings of 5th Korea-Japan Symposium on Nuclear Thermal Hydraulics and Safety (NTHAS-5), Jeju, Korea, 2006, p.94-99.

# 1-6 Achieving Efficient Fuel Handling

## — Study on the Fuel Handling System in a Commercial SFR —

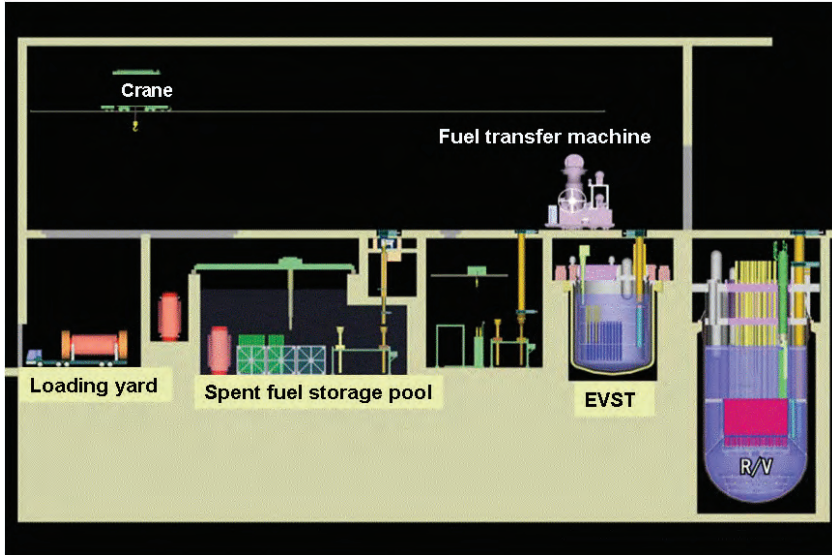


**Fig.1-16 Fuel handling system of JSFR**

Spent fuel discharged from the reactor vessel (RV) is stored in a spent fuel storage pool after decreasing its decay heat in an external vessel storage tank (EVST). New fuel is received into the EVST and transferred to the RV through the reverse route of the spent fuel.

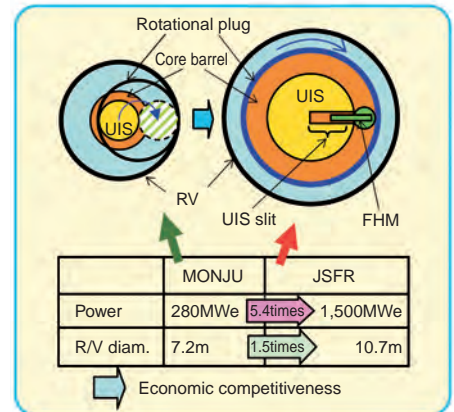


**Fig.1-17 Type of FHM and diameter of RV**

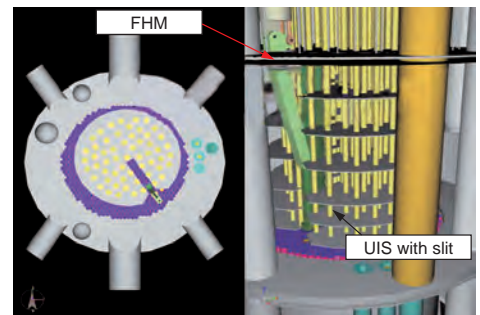


**Fig.1-18 UIS with slit and FHM**

The fuel handling system for a sodium-cooled fast reactor (SFR) is required to allow remote handling, isolating the sodium from the air because the chemically active sodium surrounds the fuel. Reliable and safe fuel handling systems have been developed for “JOYO” and “MONJU”.

The fuel handling system of the future commercial SFR (JAEA SFR; JSFR) studied in the FaCT project is composed of an in-vessel fuel handling machine, an outside-the-vessel fuel handling machine and, an outside-the-vessel fuel storage tank (EVST), etc. as in “MONJU” (Fig.1-16). However, in order to increase economic competitiveness further, we are now attempting simplification and size reduction of the fuel handling system through innovative technologies.

For the in-vessel fuel handling machine, we have been developing a new fuel handling machine (FHM) that is different from the ones in “JOYO” and “MONJU” and suitable for a compact reactor vessel (RV). In case of “MONJU” (280 MWe), its RV diameter is three times larger than that of the reactor core barrel, because the core upper internal structure (UIS) has to be displaced from its normal position right above the reactor core to the periphery when refueling. JSFR (1,500 MWe) has an FHM and UIS, and both of them are attached under the rotational plug the same as in

“MONJU”, but its UIS has a narrow slit space in which the fuel gripper unit of the FHM is able to move horizontally and approach any fuel assembly under the UIS by rotational movement, enabling refueling. In this design, the UIS need not be displaced widely when refueling. Therefore, a much larger RV diameter can be avoided in the design of JSFR, even with increase in the reactor output power up to 1,500 MWe (Fig.1-17).

However, as the size of the UIS’s slit space is limited (width: 0.41m, height: 5.9m and depth: 2.6m), it is necessary to develop the FHM that can smoothly discharge and charge the fuel assembly at the specified position in this narrow space, meeting design requirements such as compactness, stiffness, and precise positioning (Fig.1-18). Based on the results of our design study, we are now planning to fabricate an FHM and perform a test to confirm its function.

In the R&D program for the fuel handling system, in addition to using R&D experience gained with “JOYO” and “MONJU”, we will acquire design data and confirm intended functions through mock-up tests and so on, especially for innovative designs and concepts. The results of these tests will be adequately reflected in the design study of the JSFR fuel handling system.

**Reference**

Japan Atomic Energy Agency, Feasibility Study on Commercialized Fast Reactor Cycle Systems Technical Study Report of Phase II- (1) Fast Reactor Plant Systems 2006, JAEA-Research 2006-042, 2006, 1807p. in CD-ROM attached (in Japanese).

# 1-7 Higher Accuracy in the Inspection of Heat Exchanger Steam Generator Tubes of Nuclear Fast Reactors

— Suppression of Sodium Adhesion ECT Signal Achieved by Numerical Simulations —

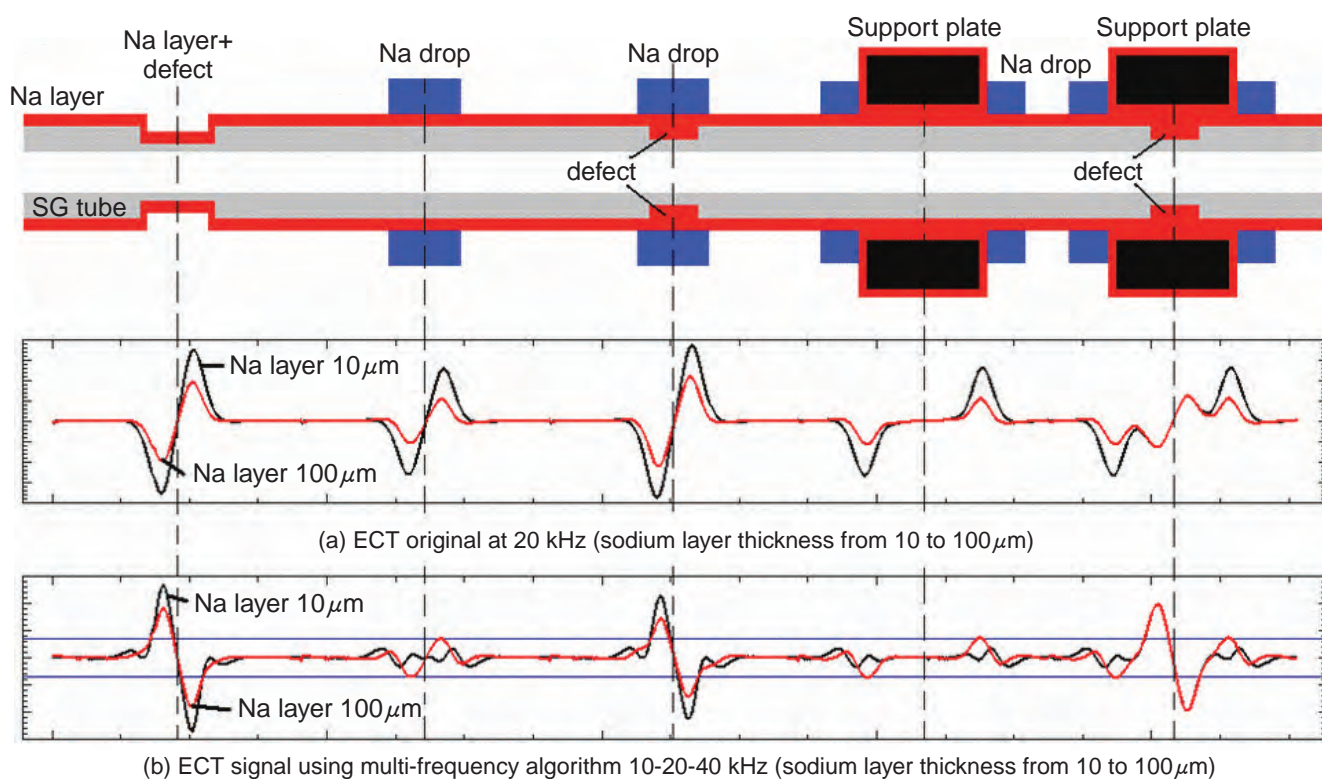


**Fig.1-19 Comparison between the original ECT signal and multi-frequency ECT algorithm signal**

In nuclear fast breeder reactors (FBR), liquid sodium is used as an intermediate heat-transfer fluid, and only the steam generator (SG) tube wall separates the steam-water inside of its pipe and the liquid sodium flowing outside it. Earlier defect detection, before wall penetration occurs, during the in-service inspection (ISI) is required to increase the safety of SG tube component in order to avoid the powerful chemical reaction between water and sodium. The SG tubes integrity are checked on a regular basis using either ultrasound or eddy current testing (ECT).

In the ECT, the ECT coils are inserted inside of the SG tubes and by monitoring the changes in their impedance variations in SG tube thickness can be detected. However, sodium is highly electrically conductive, and its presence on the outer tube surface can interfere with the electromagnetic disturbance signal from existing defects. The unknown sodium signal is accurately modeled, using numerical

simulations to estimate the range of the signal when sodium layer adhesion thickness varies between 10 and 100  $\mu\text{m}$ . A tuned multi-frequency ECT algorithm was constructed, using numerical simulations, for the specific ECT inspection probe which is able to suppress the signal from sodium structures such as: layers of unknown thickness or drops.

This algorithm acts as a filter, being able to delete also the support plate (SP) signal and possible sodium drops located nearby and extract and enhance only the defect signal. The result of the developed multi-frequency ECT algorithm is shown in Fig.1-19 where signals from sodium structures and SP signals are reduced, independently of sodium layer thickness.

Accurate numerical ECT simulations are an effective tool to indicate and develop ways to enhance ECT inspection, even when dealing with unknown sodium structures, increasing therefore the safety of SG tubes.

## Reference

Mihalache, O. et al., Analysis of Defect Detection in Steam Generator Tubes of FBR, Under Support Plates and in the Presence of Sodium, Using Multi-Frequency Eddy Currents Algorithm, Proceedings of 15th International Conference on Nuclear Engineering (ICONE15), Nagoya, Japan, 2007, ICONE15-10211, in CD-ROM.

# 1-8 Investigation of Strength of Structural Material Using Controlled Temperature Fluctuation Loading

## — High Cycle Thermal Fatigue Tests in Sodium for Fast Reactor Design —

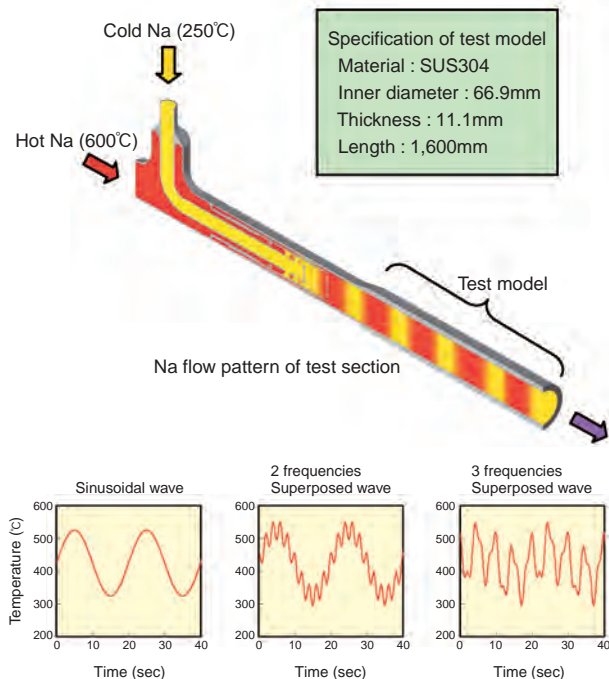


Fig.1-20 Test section structure and Na temperature histories

In nuclear power plants, it is necessary to assess possibilities of material failure by high cycle thermal fatigue due to the mixing of different temperature fluids, because thermal stress could occur in structural material by the cyclic temperature fluctuations of the fluids. It has been established that thermal stress depends on the frequency of temperature fluctuations. Therefore, we propose a high cycle thermal fatigue assessment method that includes the frequency effect in the thermal stress assessment, in the development of high temperature structural material assessment technology. In order to confirm the validity of this assessment method, we developed sodium (Na) temperature controlled thermal fatigue test equipment (SPECTRA). SPECTRA can accurately control the frequency of temperature fluctuation using Na, which is a coolant for a fast reactor. The thermal fatigue tests were then carried out for SUS304 steel, which is one of the main structural materials of fast reactors.

SPECTRA use electromagnetic pumps to control continually the ratio of high (600°C) and low (250°C) temperature Na fluids to produce temperature variations with various waveforms and frequencies. The temperature variations then initiate and propagate fatigue cracks in the test model of structural material (Fig.1-20). Major features of this equipment are (1) it can control temperature variation with sine wave frequency parameters while there is constant flow, (2) it can provide axially symmetric temperature variation in the test model to avoid complex thermal stress distribution, (3) it can efficiently obtain the data on the crack initiation as well as the crack propagation with one test model, giving the axial distribution of large and small thermal stresses, (4) it can generate temperature variations

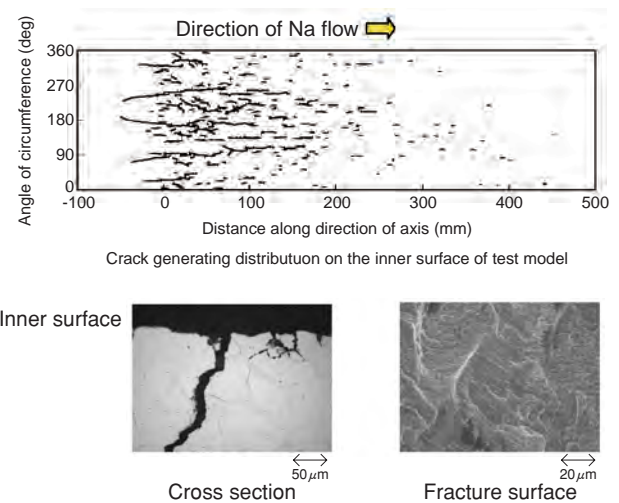


Fig.1-21 Fatigue damage observation after 160,000cycles at frequency 0.05Hz

Metallurgical observation of the damaged test model clarifies crack initiation, propagation, and mechanism, and gives verification data for an assessment method.

with superposed wave forms by combining different frequency waves, and so on.

The thermal fatigue tests were carried out under sine wave temperature variations with frequencies between 0.05-0.5Hz, which were generated by SPECTRA. In these tests, Na temperature was controlled at an average of 425°C and with a fluctuation of 200°C. The total flow rate was kept at 300 l/min by mixing high/low temperature Na fluids each flowing at 150 l/min in an antiphase manner into the test model.

From the test results, it was proved that there was a difference in the initiation and propagation of cracking, depending on the frequency. For example, at frequency 0.05 Hz, after 160,000 cycles of temperature variation, a crack occurred at the inner surface of the test model and penetrated to the outer surface (Fig.1-21). However at frequency 0.2Hz, even after 260,000 cycles, the inner surface crack did not reach the outer surface. There is a significant difference in fatigue life with these two frequencies. Therefore, it has been confirmed that even under the same amplitude of temperature fluctuation, depending on the difference of frequency, the thermal stress on the structural material will change, impacting on its fatigue life, the test proving the phenomenon that was previously known through theoretical modeling. These results will be used as verification data of the high cycle thermal fatigue assessment method.

In the future, we are planning to perform a test of superposed short period and long period waves. This test will be to assess the specific qualities of structural materials under random variations caused by actual irregular temperature fluctuations. In this way, the effects of complex temperature variations on structural materials will be studied.

### Reference

Kawasaki, N., Kobayashi, S., Hasebe, S. et al., SPECTRA Thermal Fatigue Tests under Frequency Controlled Fluid Temperature Variation-Transient Temperature Measurement Tests-, Proceedings of 2006 ASME Pressure Vessels and Piping Division Conference (PVP2006) /International Council on Pressure Vessel Technology (ICPV11), Vancouver, Canada, 2006, ICPV11-93548, 8p., in CD-ROM.

# 1-9 Analysis Shows that Reactor Trip Failure Probability Is Extremely Small — Anticipated Transient without Scram (ATWS) Frequency Evaluation of FBR “MONJU” —

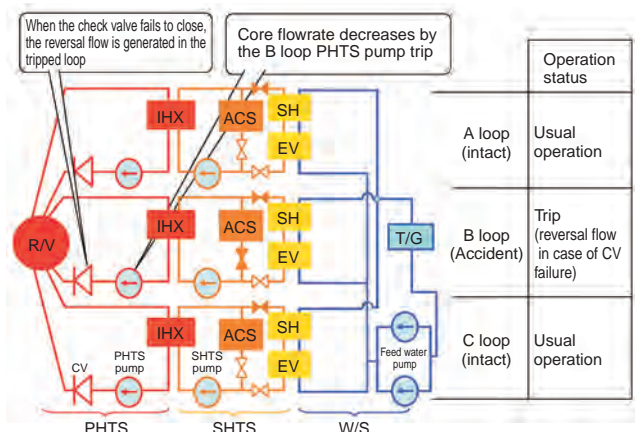


Fig.1-22 1loop PHTS pump trip event

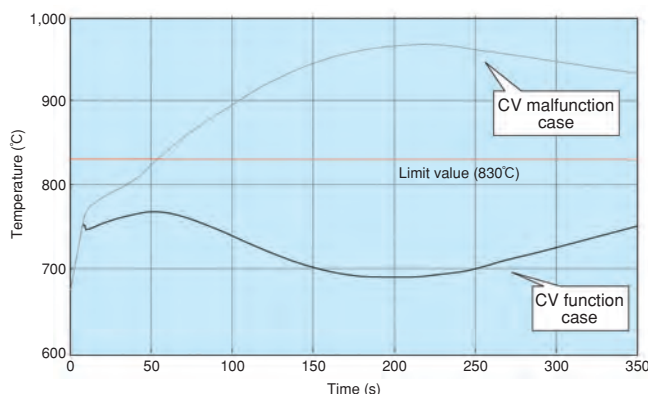


Fig.1-23 Fuel cladding temperature in 1loop PHTS pump trip without scram

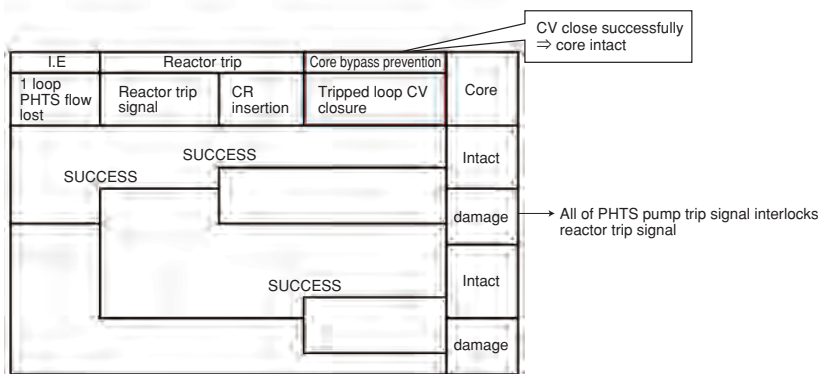


Fig.1-24 1loop PHTS pump trip sequence event tree

Safety of a nuclear power plant has been improved with reliable measures for the following three stages: prevention of abnormal event occurrence, the suppression of abnormal event expansion, and the reduction of radioactive material release.

The probabilistic analysis approach is effective to evaluate these improved reliability of safety measures whose failure probabilities are very small.

As one specific probabilistic safety assessment of “MONJU”, the frequency of Anticipated Transient without Scram (ATWS) was evaluated.

Fig.1-22 shows one ATWS event where a pump trip event in one loop of the primary heat transport system (PHTS) is explained. The B loop PHTS of three cooling loops in “MONJU” has its pump tripped. It is shown that the core coolant flow is secured if the check valve of the tripped loop closes, by hydraulic effect from the intact loops. The PHTS pump trip in this loop generates a reactor trip signal; however, reactor trip failure is supposed in this case. We also suppose the failure of the check valve closure in this evaluation.

As shown in Fig.1-23, fuel cladding temperature behaviors were analyzed in the PHTS pump trip of one loop without scram. As analytical result, in the case with the check valve functioning, the maximum cladding temperature was below the temperature limit for reactor core intactness.

All of event sequences in the sequence event tree analysis shown in Fig.1-24 were evaluated. The first branch divides according to whether the reactor trip signal is generated by the one loop PHTS pump trip successfully or not. If the reactor trip signal was generated, the next branching in this sequence centers on control rod insertion failure. If the reactor trip signal generation failed, the next branching in this sequence centers on check valve closure. The failure probabilities of these safety features are analyzed by the system fault tree. These probabilities are estimated as  $10^{-10}$  -  $10^{-5}$  per demand, and thus these safety features function reliably.

The total ATWS frequency of “MONJU” is estimated as  $10^{-8}$  per reactor year. These studies indicate that the ATWS frequency of “MONJU” is sufficiently small and thus that the safety functions have high reliability.

**Reference**

Sotsu, M. et al., ATWS Frequency Evaluation of FBR MONJU, Proceedings of 14th International Conference on Nuclear Engineering (ICONE 14), Miami, USA, 2006, ICONE14-89377, in CD-ROM.

# 1-10 Analysis of “MONJU” Thermal Transient Margin

— Analysis of “MONJU” Thermal Transient Margin Based on Measured Plant Performance —

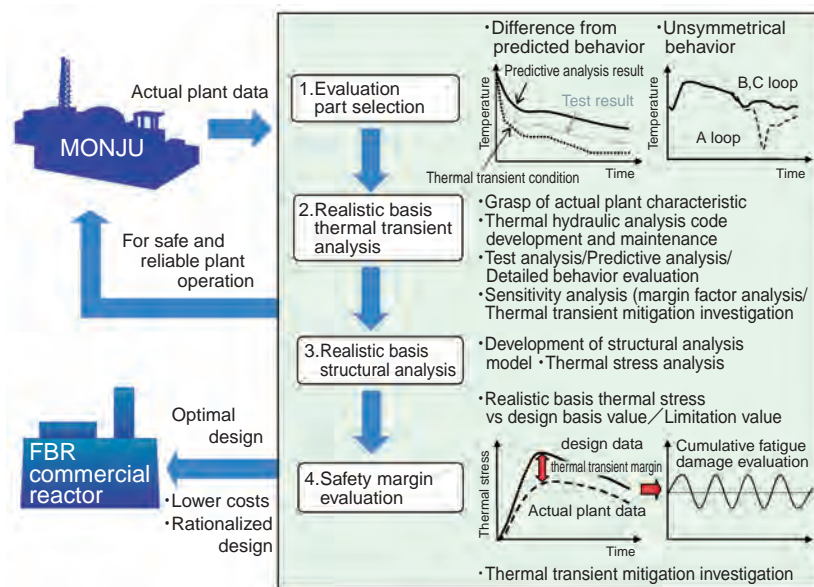


Fig.1-25 Thermal transient margin evaluation technique

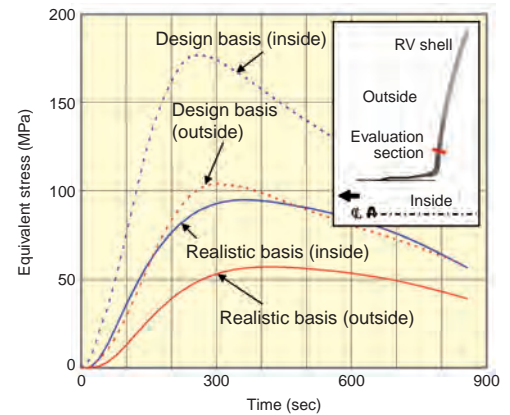


Fig.1-26 RV outlet nozzle thermal stress analysis result

To develop plant technologies for safe and reliable operation of “MONJU” and to further expand the technologies for design optimization of future FBR plants, we have evaluated the design technique applied to “MONJU” by using the measurement data obtained through actual operation.

In “MONJU”, the coolant sodium temperature heated by the reactor core increases up to 500°C or more. The difference in temperature of coolant sodium between reactor inlet and outlet exceeds 100°C in “MONJU”. Therefore, the integrity of the equipment against reactor trips is verified by examining the influence of severe thermal transients. This paper clarifies the realistic thermal transient of the reactor trip of the actual plant, and evaluates the design margin. Fig.1-25 is an outline of the thermal transient margin evaluation technique.

In a reactor trip test at 40% power capacity, coolant temperature change at the reactor vessel (RV) outlet was faster than the pre-test forecast. And, the feed water temperature change at the evaporator (EV) was higher than the pre-test forecast.

Analysis of the coolant temperature behavior at the RV outlet confirmed the influence of the flow conditions of the low-temperature and the high-temperature sodium that passes through the RV outlet from the upper reactor core. Then, a model of the thermal-hydraulic analysis code was developed with finer partitioning of the area etc. By these

improvements, coolant temperature change at the RV outlet was more accurately simulated. In addition, coolant temperature change at RV outlet due to a reactor trip at rated power was simulated by the same code. Fig.1-26 shows thermal stress analysis of RV outlet nozzle based on the simulated temperature and flow rate changes and the design analysis. The actual thermal stress was less than the design analysis result, by a margin of about 50%.

Moreover, to reproduce better the phenomenon of the high temperature steam flowing into EV feed water inlet, we added a backflow analysis function to this code. By these improvements, EV feed water inlet temperature behavior was simulated more accurately than before. In addition, EV feed water inlet temperature change due to a reactor trip at rated power was simulated by the same code. By thermal stress analysis of the EV feed water tube sheet based on simulated temperature and flow rate changes, we confirmed that the EV feed water tube sheet had enough margin in its fatigue accumulation coefficient, well below its limit value of 1.0.

We will use the improved thermal-hydraulic analysis code and the thermal transient margin evaluation results in the operating plan and the forecast analysis for our next test. Moreover, we plan to advance the design technology steadily, based on the real data obtained from the trial operation, for safe and steady plant operation and development of an FBR commercial reactor.

## Reference

Mori, T. et al., Margin Analysis of MONJU Thermal Transient Based on Measured Plant Performance, Proceedings of 14th International Conference on Nuclear Engineering (ICONE14), Miami, USA, 2006, ICONE14-89379, in CD-ROM.

# 1-11 The Challenge of Maintaining Safety in an Extreme Environment

## — Development of an ISI Device for the Reactor Vessel of “MONJU” Fast Breeder Reactor —

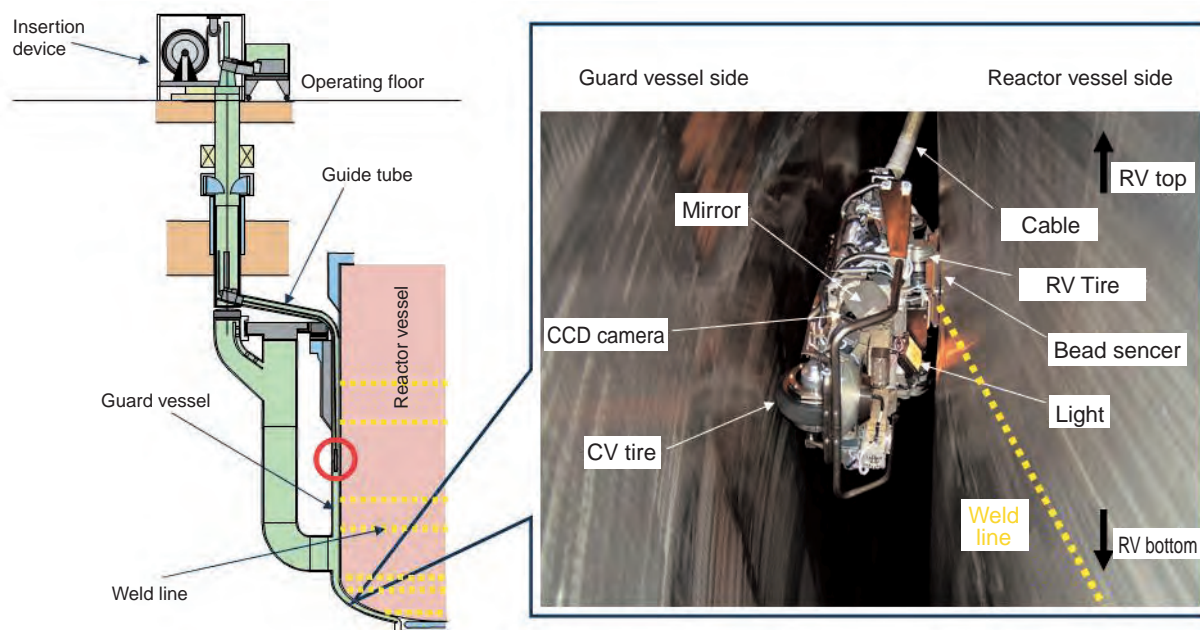


Fig.1-27 The operational environment of the inspection machine (Photo of operation in the mock-up facility)

Table 1-1 Chief inspection conditions

Temperature	Max 200°C
Dose rate	Max 10Gy/hr
Atmosphere	N <sub>2</sub> , Inhibition water
Remote control	About 50m
Narrow space	About 300mm

In-service inspection (ISI) by visual inspection is carried out to confirm the integrity of the main components of “MONJU” Fast Breeder Reactor (FBR). The reactor vessel (RV) contains both nuclear fuel and coolant sodium. Unlike a light water reactor, the examination area in FBR is an extreme environment where human access is not possible (Table 1-1). In order to inspect this extreme environment, a remote controlled inspection device (ID) was developed. The inspection-machine insertion device is installed on the operating floor where it is accessible to humans. The ID is taken down to the RV through a guide tube using a car gondola and it is inserted in the 300 mm clearance between the RV and guard vessel. After coming out of the gondola, the ID can run by itself, moving and inspecting the test area. The ID supports its own weight using the force of a spring. The remote control of the ID running between the trackless

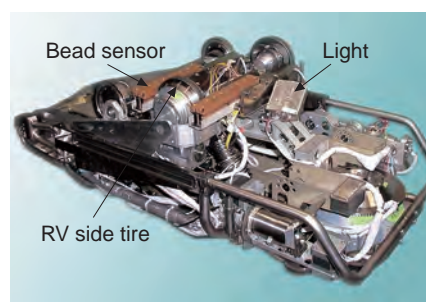


Fig.1-28 External view of the inspection device

vertical wall surfaces is carried out using a 50m long cable. A bead sensor is used in this case to detect and follow the weld line that is to be visually inspected and inspected by a CCD camera (Fig.1-27). Until now, due to limited heat resistance and radiation durability it could employ only a 30,000 pixels fiberscope. However, the newly developed inspection device (Fig.1-28) uses a cooling system for a 410,000 pixels CCD camera, attaining a very accurate inspection.

The presence of sodium leakage marks is determined during the visual inspection. An attached electromagnetic acoustic transducer (EMAT) ultrasonic probe, which is now under development, checks and detects flaws before actual leakage occurs. Research and development are still continuing to improve the inspection device for use in extreme environments, for a better inspection and higher safety of the reactor components.

### Reference

Tagawa, A. et al, Development of the ISI Device for Fast Breeder Reactor MONJU Reactor Vessel, Journal of Power and Energy Systems, vol.1, no.1, 2007, p. 3-12.

## R&D Supporting the Technology and Reliability of Geological Disposal in Japan

High-level radioactive waste (hereafter, HLW) is generated when we utilize nuclear power. In Japan, reprocessing is done to recover uranium and plutonium remaining in spent fuel from power generating reactors, for recycling into useful fuel. The liquid remaining after such retrieval is finished is vitrified to produce a chemically and physically stable glass, which is HLW. International consensus has been reached that HLW can be disposed of in stable deep geological strata (geological disposal) so as to be isolated from human environments for a long term. Waste glass inserted in an over pack (e.g. carbon steel) with a bentonite buffer around that will be placed at a depth below 300m in the Japanese proposal (Fig.2-1).

For initiating repository operation in the late 2030s, the Nuclear Waste Management Organization of Japan (NUMO), with responsibility for implementing geological disposal of HLW, is now calling for municipalities to volunteer as candidate siting areas and be surveyed, which is the first stage in the final disposal project. The first application came this January from Toyo town, Kochi prefecture, but it was withdrawn after the subsequent mayoral election in April.

To ensure safe implementation of geological disposal, we have conducted R&D in various fields, e.g. geoscientific research, engineering development, and performance assessment (PA) of the geological disposal system.

A particular JAEA R&D activity is to promote the projects of two Underground Research Laboratories (URLs): one at Mizunami city situated in crystalline rock and the other at Horonobe town situated in sedimentary rock (Fig.2-2). The results of the 1st R&D Phase (investigations from the surface) were entered in the 2006 report. Phase 2, excavation of shafts and drifts, is underway. Research on geological phenomena such as fault and volcanic activities also has progressed.

At the same time, we are conducting laboratory experimental studies at the Tokai research center. The relatively large-scale and non-radioactive experiments, performance assessment of the multibarrier system supported by extensive computer analysis, and research to obtain basic data concerning the chemical properties and migration behavior of radionuclides under geological disposal

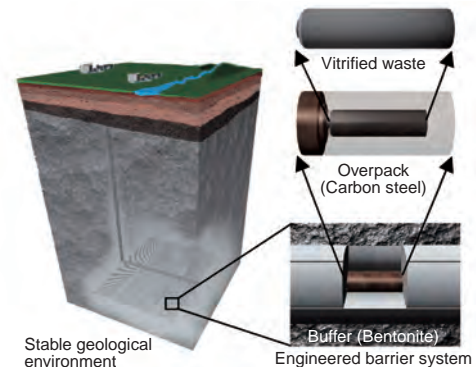


Fig.2-1 Concept of geological disposal

conditions have been carried out. These studies are linked with the geological environment data obtained from the URLs. In 2006, JAEA's diffusion database of radionuclides was released on the Web to serve as an important tool for safety assessment.

Geological disposal of HLW will be a long term project of more than one hundred years. It is supported by huge amounts of extremely diverse information which must be organized to reveal multiple lines of evidence relevant to safety. Management of knowledge is a very important issue for this long-term disposal program. JAEA has conducted a project to develop the next generation novel knowledge management system (KMS). Various evidence and information derived from a wide range of R&D activities will be managed systematically and made transmittable in a knowledge base in the KMS. In March 2007, the base-line design of KMS was completed.

In July 2005, a "Geological Disposal R&D Coordination Council" was established to coordinate wide ranging R&D which is being carried out by JAEA and ANRE (Agency for Natural Resources and Energy). In this council, JAEA and related R&D organizations have discussed their respective roles, created a co-operation framework to integrate R&D results into a database, and prepared a roadmap for the implementation of geological disposal. The roadmap was reported at an open council symposium in March 2007.

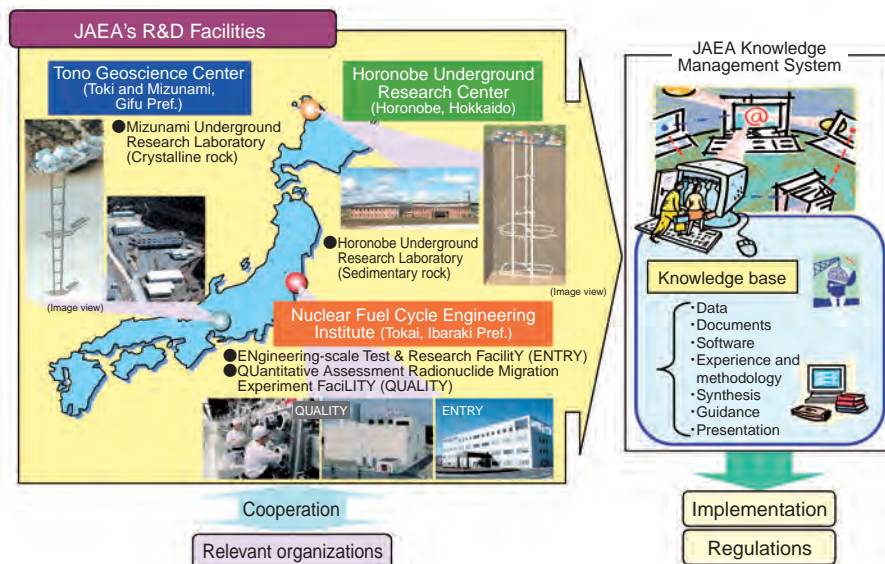


Fig.2-2 JAEA's R&D activities on geological disposal technology

## 2-1 Development of a Novel Knowledge Management System for Geological Disposal – Preliminary Design of Management Functions and Knowledge Base –

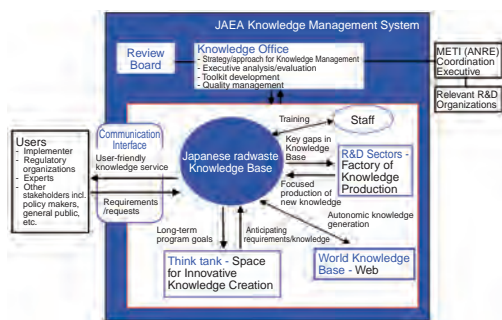


Fig.2-3 Fundamental concept of JAEA KMS

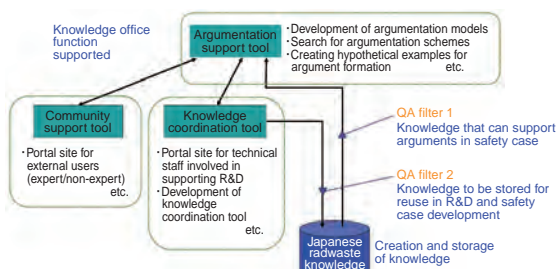


Fig.2-5 An illustration of the present concept for linkage of toolkits to provide an “intelligent assistant”

The implementation process for the geological disposal of high-level waste (HLW) utilizes vast quantities of information, data, experience, understanding, etc. – which can be defined broadly as “knowledge”. In order to improve confidence in the safety of geological disposal, it is necessary to collate, integrate and quality assure appropriate knowledge, extending it where needed with focused studies and taking particular account of advances in diverse areas of science and technology that are of relevance here. We, therefore, have initiated a project to develop a “next generation” knowledge management system (KMS), which will incorporate an “intelligent assistant”, utilizing advanced electronic information management technology.

Based on the fundamental KMS concept (Fig.2-3), preliminary design of the required management functions and Knowledge Base (KB) has been carried out. In this design, a framework of knowledge management that optimizes production, dissemination, and use of the relevant knowledge is proposed, based on a concept that regards construction of the safety case as chains of arguments and counter-arguments (argumentation model, Fig.2-4).

In addition to this argumentation support tool, a knowledge coordination tool for experts and community-ware for interested non-experts have been specified as required system components. Fig.2-5 illustrates the present concept of subcomponent toolkits, which are combined to function as

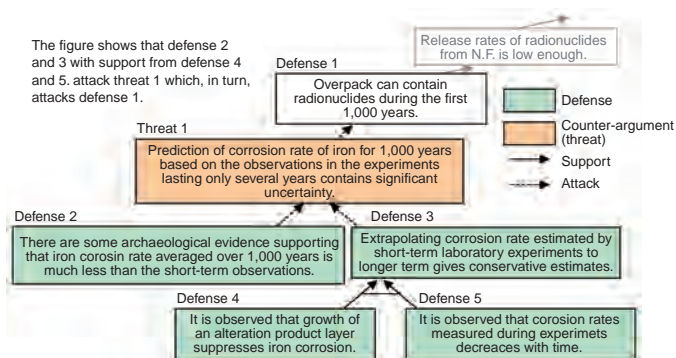


Fig.2-4 An example of argumentation model

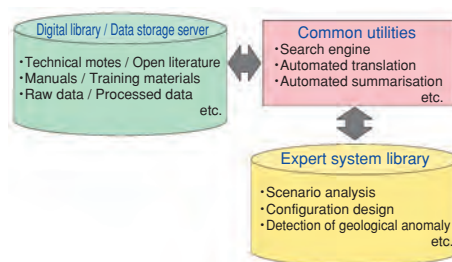


Fig.2-6 Outline of the present conception of the KB in the JAEA KMS

the “intelligent assistant”. In this concept, an “argumentation support tool” aids development of argumentation models, searching for alternative argumentation schemes, and creating hypothetical examples for argumentation. This tool mainly supports the knowledge office. The “knowledge coordination tool”, on the other hand, provides a portal site for technical staff involved in supporting R&D, providing access to the KB and tools that help them put their work in the context of appropriate safety case components and argumentation schemes. The “community support tool” provides a portal site specifically for external users, tailored to facilitate use by both expert and non-expert stakeholders.

The present concept for the KB is illustrated in Fig.2-6, although again this is currently under development and hence should be regarded as a provisional conceptual outline only. The present concept envisages a “digital library/data storage server”, an “expert system library” and an additional group of “common utilities”. In any case, as emphasized above, the key aspect of the KB is its flexibility to provide output structured to any desired application. A priority, therefore, is the implementation of user-friendly search engines, which allow such tailoring of output.

Taking account of both present requirements and possible future needs of users, we will develop a prototype of a novel KMS within the current 5-year R&D program (up to fiscal year 2010).

### Reference

Umeki, H., Osawa, H. et al., Fundamental Concept of Knowledge Management System for Geological Disposal Technology, JAEA-Research 2006-078, 2006, 45p. (in Japanese).

## 2-2 Characterization of Potential Changes in Geological and Disposal Environment Caused by Natural Phenomena

— Development of Evaluation Procedure for HLW Disposal System Perturbation Scenarios —

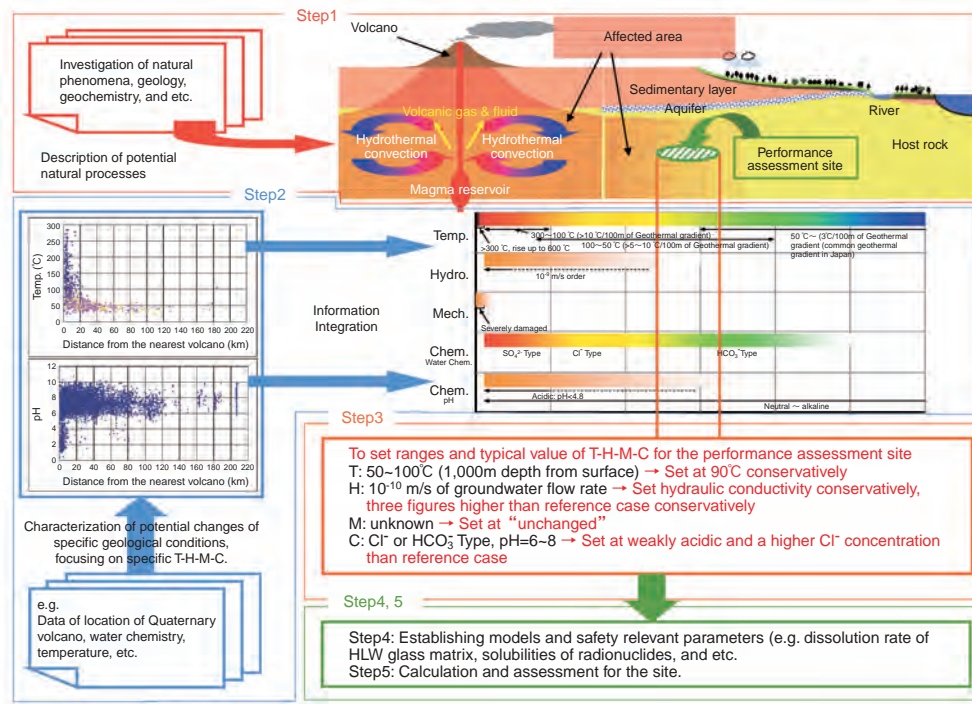


Fig.2-7 Illustration of evaluation procedure of the potential impact of natural phenomena (e.g. Volcanism)

We have developed a formal evaluation method to assess the potential impact of natural phenomena (earthquakes and fault movement, volcanism, uplift, subsidence and erosion, and climatic and sea-level changes) on a HLW Disposal System.

In the "H12" project, JNC developed generic and conservative initial perturbation scenarios, by which to examine other perturbation scenarios. As results of the development of the H12 perturbation scenarios, two points were highlighted for consideration in subsequent work: for improvement of the scenarios, from the viewpoints of reality, transparency, traceability, consistency, and avoiding extreme overconservatism.

Building on this initial work, we have developed a new procedure for creating such perturbation scenarios based on further studies of the characteristics of these natural perturbation phenomena in Japan. The approach to effectively creating the perturbation is divided into five steps (Fig.2-7):

Step 1: Description of potential natural processes and their impacts on the geological environment.

Step 2: Characterization of potential changes of geological environment in terms of T-H-M-C (Thermal – Hydrological –

Mechanical – Chemical) processes. The focus is on determining specific T-H-M-C parameters that influence geological barrier performance, utilizing the input from Step 1.

Step 3: Classification of potential influences, based on similarity of T-H-M-C perturbations. This leads to development of perturbation scenarios to serve as a basis for consequence analysis.

Step 4: Establishing models and parameters for performance assessment.

Step 5: Calculation and assessment.

This study focuses on identifying key T-H-M-C processes associated with perturbations in Step 2. This framework has the advantage that it reliably maintains traceability during the scenario construction processes, facilitating the production and structuring of suitable records. In this framework, scenario development work proceeds in a stepwise manner, to ensure clear identification of the impact of processes associated with these phenomena on a HLW disposal system. Output is organized to create credible scenarios with required transparency, consistency, traceability and adequate conservatism.

### Reference

Kawamura, M. et al., Study on Evaluation Method for Potential Impacts of "Natural Phenomena" on a HLW Disposal System, Proceedings of East Asia Forum on Radioactive Waste Management Conference, Taiwan, 2006, p.350-367.

## 2-3 Possibility of Superlong-Lifetime Container for Geological Disposal — Corrosion Behavior of Copper Overpack in Low Oxygen Concentration Environment —

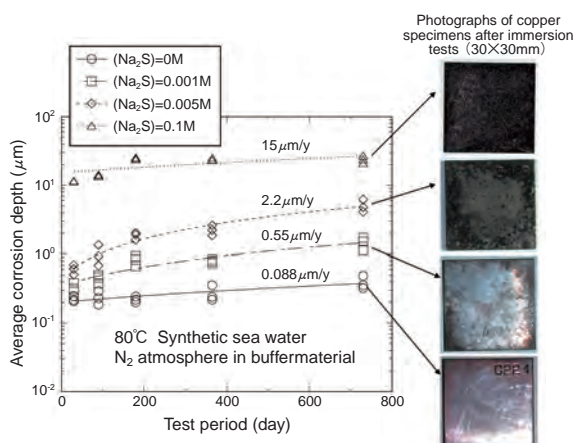


**Fig.2-8 Influence of sulfide concentration on the corrosion of pure copper**

As the sulfide concentration was increased, the corrosion rate became larger with a thicker growth of black corrosion product. The corrosion product was identified as  $\text{Cu}_2\text{S}$  by X-ray diffraction analysis.

Overpack is a container for high-level radioactive waste disposal which is expected to prevent the contact of groundwater with vitrified waste at least for 1000 years. We have studied possible overpack materials, carbon steel in particular, and basic knowledge for designing the overpack including corrosion behavior has been obtained. However, the reliability of the repository system will be improved if a lifetime of overpack far beyond 1000 years could be achieved. Carbon steel is sufficiently strong to ensure a lifetime of 1000 years, since the corrosion rate in deep underground environment has been estimated to less than several  $\mu\text{m}/\text{y}$ . However, it is difficult to achieve a much longer lifetime, over tens of thousands of years, with carbon steel. Therefore, we have investigated alternative metals such as titanium and copper as candidate materials for the longer lifetime overpack.

Among the candidate overpack materials, copper is an only metal that is immune to corrosion under anaerobic conditions. The deep underground environment has inherently low oxygen concentration so that copper have a potential to achieve semi-permanent non-corrosion subject to change in the environmental conditions. However, such chemical stability of copper is known to be lost in the presence of sulfide ( $\text{H}_2\text{S}$ ,  $\text{HS}^-$  and  $\text{S}^{2-}$ ). Therefore, we have been studying the effect of sulfide concentration on the corrosion behavior of copper under anaerobic conditions. As an example of our experimental results, the relationship between the sulfide concentration and the corrosion rate is shown in Fig.2-8. It was confirmed that the corrosion rate of copper increased with sulfide concentration. In case of 0.001M sulfide, the corrosion rate was less than  $1 \mu\text{m}/\text{y}$ , and

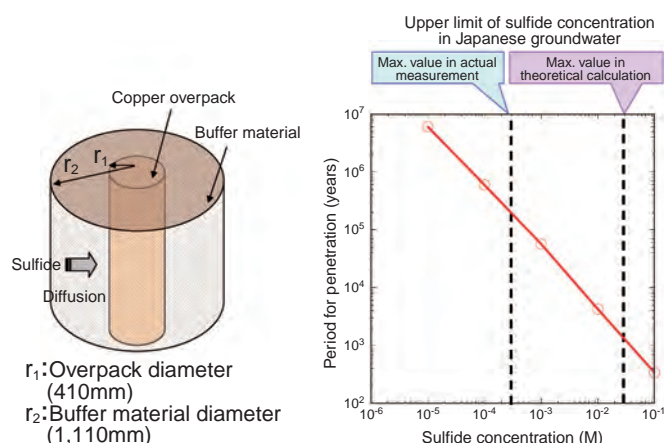


**Fig.2-9 Schematic of the model for the evaluation of corrosion depth and the corrosion lifetime estimated by the model as a function of sulfide concentration**

The lifetime was assumed to be the period for 10 mm penetration. Copper overpack can have a long lifetime of over a hundred thousand years if the sulfide concentration is less than 0.0006M.

linear extrapolating the experimental data yields and estimate of less than 1 mm corrosion in 1000 years. Since the copper overpack will be designed to have corrosion allowance of several centimeters, longer lifetime far beyond 1000 years could be achieved. In order to make the long term evaluation for an actual repository system, we performed a model calculation of long term corrosion depth assuming the present repository design. The buffer material which consists primarily of bentonite was installed around the overpack, so that the sulfide would contact the overpack surface only by diffusion through the buffer material. Consequently, the corrosion rate will be controlled by diffusion rate of sulfide in buffer material. The sulfide flux to the overpack surface was converted into the corrosion rate and the overpack lifetime was estimated as a function of sulfide concentration. As shown in Fig.2-9, if sulfide concentration is not over 0.0003M, the upper limit of actual measured data for general groundwater in Japan, a lifetime of several hundred thousand years is possible. However, if some kind of peculiar effect such as microbial action is assumed, the sulfide concentration can theoretically rise to 100 times higher. In such case, a very long lifetime cannot be expected.

Although copper have a potential of achieving an extremely long lifetime depending on the environmental conditions as above, it is necessary to clarify observe the environmental conditions and its long-term evolution if copper is selected as an overpack material. We are planning to extend our knowledge of the corrosion of copper in order to contribute to material selection, overpack designing and assessment of its long term integrity.

### Reference

Taniguchi, N. et al., Effect of Sulfide on the Corrosion Behavior of Pure Copper under Anaerobic Condition and Possibility of Super Long Lifetime for Copper Overpacks, JAEA-Research 2007-022, 2007, 64p. (in Japanese).

## 2-4 Integration and Management of Mass Transfer Coefficient in Geological Environment — Development and Operation of Web Site for Diffusion Database (DDB) —

**Table 2-1 Main data fields in DDB system**

name of field	detail
De	effective diffusion coefficient
De information	boundary condition, condition of solution agitation, etc.
Type	acidic crystalline rock, Basic crystalline rock, Sedimentary rock (sandstone, mudstone, tuff, etc.)
Element	element name
Species	chemical species
Solid information	place of sample production, type, size of sample disk, shape, pretreatment, mixtures, mineral composition, grain size, isoelectric point, etc.
Dry Density	value of dry density
Porosity	value of porosity
Experimental method	In-diffusion, through diffusion, back to back, etc.
Solution Index	kind of sample solution
Tracer	kind and concentration of tracer
Contact time	sample immersion time for nuclide diffusion in sample
Temperature (C)	temperature of experimental system
Redox condition	Eh (vs SHE), atmosphere condition (anoxic or oxid),
Author	author of source literature
Title, Vol., Num. etc.	title, vol., num., etc. of source literature
publication year	publication year of source literature
Others	other additional information
Quality information	Information concerning quality of data

**Fig.2-10 Main interface form of data search**

We have developed a diffusion database (DDB) to manage and utilize diffusion coefficients and related data. The diffusion coefficient is one of the most important values in investigating the migration behavior of various radionuclides in solid substances. Diffusion data have been collected for their contribution to the safety assessment of geological disposal of radioactive waste. The web site of the DDB has been opened to researchers in similar fields where it has been of valuable use.

The DDB has comprehensive data related to a wide range of diffusion coefficients, e.g. porosity, experimental method, and composition of solution of the sample (refer to Table 2-1), which have been collected by literature survey. The DDB is able to manage and extract the data that a user needs, by setting search conditions. The diffusion database contains information of original literature, so that the user can access detailed information of original sources. The diffusion data

managed in DDB are diffusion coefficients of radionuclides in rocks in Japan and related data (about 300) taken from a survey of literature published from 1980 to 1998 to apply for “H12: Project to Establish the Scientific and Technical Basis for HLW Disposal in Japan” (published in 1999).

In order to make the DDB more accessible, the form of the window of data search and display was modified. Through this improvement, search conditions are selected and displayed simultaneously as shown in Fig.2-10.

The DDB is operated by Microsoft-Access, and is accessed through a Web site (URL: <http://migrationdb.jaea.go.jp>). In order to expand the scope of the DDB, diffusion coefficients of elements in buffer materials and related data for performance assessment of geological disposal have been investigated and compiled. These data will be added to the DDB in the near future.

### Reference

Tochigi, Y. et al., Diffusivity Database (DDB) System for Major Rocks and Buffer Materials (Released on 2007/Specification), JAEA-Data/Code 2007-010, 2007, 14p. (in Japanese).

## 2-5 Finding Ancient Temperatures

### — Reconstruction of Past Climate Using Pollen Records from the Small Basin Deposit —

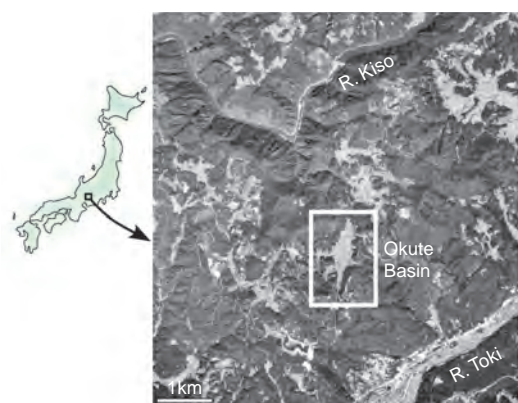


**Fig.2-11 Location of the study area (Okute Basin, Mizunami City, Gifu Prefecture)**

The Okute Basin is located near the summit of a hilly area.



**Fig.2-12 Pollen fossil of *Pinus parviflora***

Picture by Professor Yoshimune Morita, Okayama University of Science.

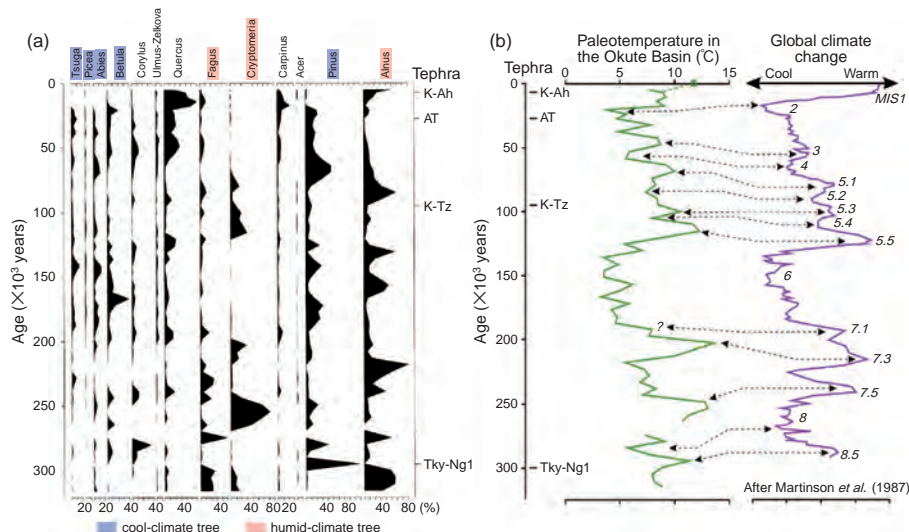


**Fig.2-13 Pollen composition in the Okute Basin core boring and the past temperature reconstructed by pollen analysis**

(a) Pollen percentage distribution of the Okute core boring  
(b) The past temperature reconstructed by modern analogue technique (green) and global climate change (purple).

We have conducted research to develop methods for precise reconstruction of the past climate in an inland area of Japan, as a part of our research into geological disposal of high-level radioactive waste (HLW). As a case study, we investigated the pollen species and their compositional ratios in the stratigraphy of the Okute Basin (Mizunami City, Gifu Prefecture) (Fig.2-11). The pollen (Fig.2-12) preserved in the sediments of the Okute Basin provide an almost continuous record for the past 300,000 years, because the basin is located near the summit of a hilly area and has not been subjected to erosion by large rivers.

Based on the pollen records, the past climate of the Okute Basin has been reconstructed as follows: 300,000 years ago the Okute Basin had a warm climate, with Beech (*Fagus*) and Alder (*Alnus*) forests dominant at that time. Subsequently, rapid cooling occurred and mean annual temperature decreased 5 degrees Celsius. Afterwards, repetitive warm and cool periods occurred every few tens of thousands of years.

In the cold period, a boreal landscape prevailed in the Tono area, with *Tsuga* (*Tsuga*), Firs (*Abies*), Spruce (*Picea*) and Pine (*Pinus*) forests being dominant.

Reconstructed temperatures during the past 300,000 years in the Okute Basin are consistent with global temperature changes reconstructed from analysis of deep-sea sediments. Consequently, climate change in the Okute Basin (Central Japan) is consistent with and therefore linked to global temperature changes (Fig.2-13).

Although paleoclimate changes that occurred during the last several tens of thousands of years were reconstructed in many inland areas in Japan, long-term (>300,000 years), continuous reconstructions have had limited success until now. This research will have a marked impact on paleoclimatology studies and understanding.

As a future research, reconstruction of the past landforms and the geomorphic development is planned to evaluate the effect of climatic changes on landscape morphology.

#### Reference

Sasaki, T., Moriya, T. et al., Reconstruction of Depositional Environment and Paleoclimate Changes from a Small Basin Deposit during the Past 300,000 Years, Central Japan, *Daiyonki-Kenkyu*, vol.45, no.4, 2006, p.275-286 (in Japanese).

## 2-6 Underground Survey Using the Blasting Vibration During Shaft Excavation in the MIU-Site

### — Underground Imaging Technique Using a Geophysical Method —

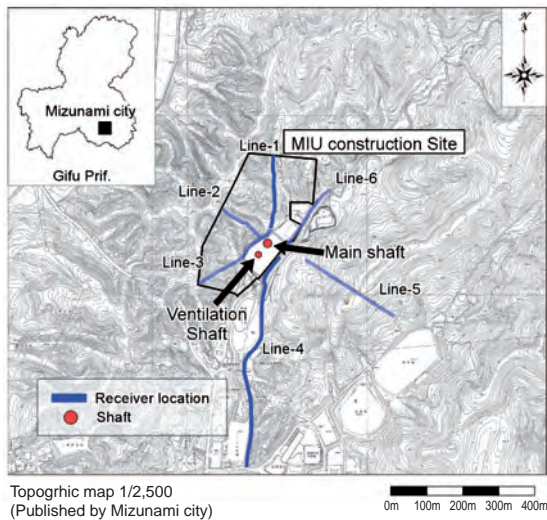


**Fig.2-14 Survey location**

This figure shows the location of receivers to observe the blasting vibration. The interval between receivers is 10 m.

It's very important for the geological modeling of the disposal sites of HLW to understand the three-dimensional structure of geological elements (e.g. geological boundary and fault) that influence the groundwater flow. Generally, remote sensing, airborne geophysical surveys, surface geophysical surveys, geological mapping, borehole investigation etc. are applied to obtain the geological information from the surface. In this paper, the underground imaging technique using the blasting vibration during shaft excavation is introduced, as one more surface geophysical method.

We are constructing the Mizunami Underground Research Laboratory (MIU) in Mizunami city, Japan. The MIU is composed of two shafts to depth of 1,000 m (Main shaft:  $\phi$  6.5 m, Ventilation shaft:  $\phi$  4.5 m) and drifts every 100 m. In this study, the blasting vibration, which is generated by the shaft excavations, was used as a seismic source, and the imaging of subsurface structure was attempted. This method is similar to a conventional reflection seismic survey. Geophones were arranged in regular array on the surface as

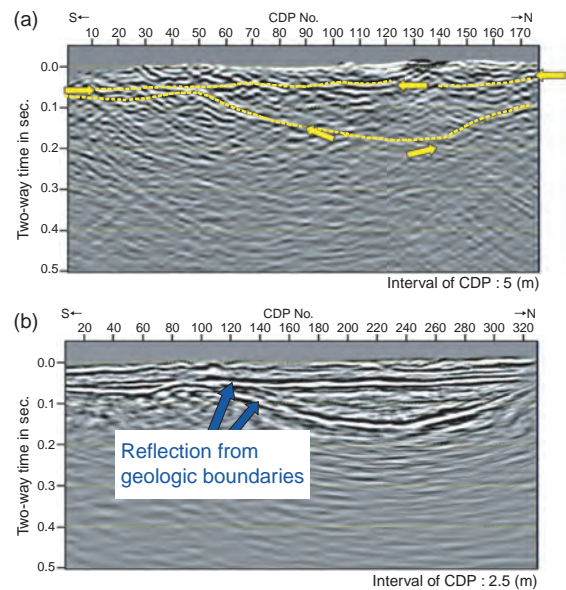


**Fig.2-15 Comparison of the reflection seismic profile made from excavation vibration records (a) and conventional shot reflection seismic profile (b)**

Yellow block arrows and dashed lines of (a) indicate main reflectors.

shown in Fig.2-14. However, this method doesn't need seismic source shots at regular intervals like a conventional reflection seismic survey. This method can synthesize the same number of shot records as the receivers, with only one seismic source event. The reflection response can be obtained by the cross-correlation of the transmission responses on the surface.

Fig.2-15 shows a reflection seismic profile made from synthesized shot records taken in Line-1 and Line-4 (a) and a conventional reflection seismic profile (b). The reflectors in the reflection seismic profile made from synthesized shot records are confirmed.

A clearer subsurface structure image can be obtained by adding more vibrations produced during the MIU construction.

An advantage of this method is that one can simulate a number of extra shot records proportional to the number of receivers. Therefore, it can be easy to investigate in three-dimensions from the surface.

#### Reference

Shiraishi, K., Matsuoka, T. et al., Seismic Interferometric Imaging from a Point Source in the Ground, Journal of Seismic Exploration, vol.15, 2006-2007, p.323-332.

## 2-7 Estimation of a Groundwater Flow by Minute Tilt

### — Estimation of Hydrogeological Structures by an Inverse Analysis of Tilt Data —

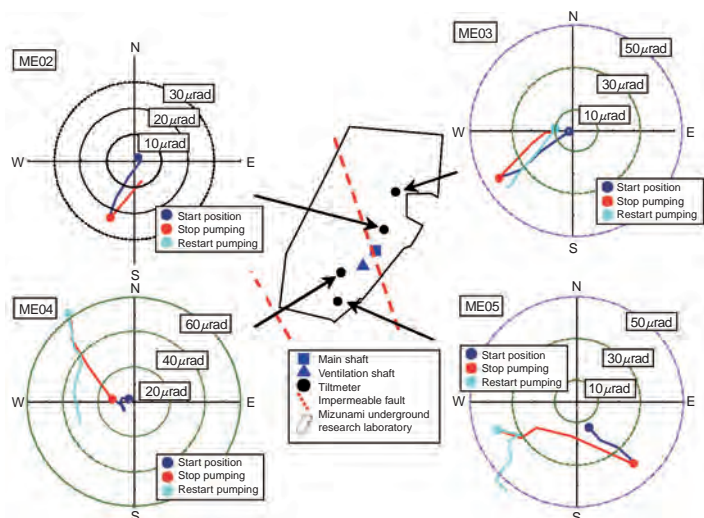


**Fig.2-16 Measurement result of tiltmeter**

The tilt direction and tilt angle change in response to change of groundwater flow during shaft excavation, excavation and pumping stop, and excavation and pumping restart.

In R&D on geological disposal technology of high-level radioactive waste (HLW) and construction of large-scale structures underground which protects the environment, it is important to evaluate groundwater flow deep underground.

To evaluate the groundwater flow, it is necessary to study the distribution of hydraulic conductivity, pore pressure and hydrogeological structures which control the groundwater flow. Generally, these data can be obtained by borehole investigation. However, investigations and observations using many boreholes require too much cost and time, and it is important to develop a simple method to complement the borehole investigation data.

We developed a simple method to characterize the hydrogeological structures by measuring the minute tilt movement of the ground surface in collaborative research with Tohoku University.

In this research, we developed and modified the method for estimating a deep groundwater volume change by an inverse analysis of tilt change caused by the groundwater flow measured by borehole testing and inflow to a large-scale structure. To test the applicability of this method, we performed an inverse analysis using a tilt data obtained from in situ measurement to estimate the hydrogeological

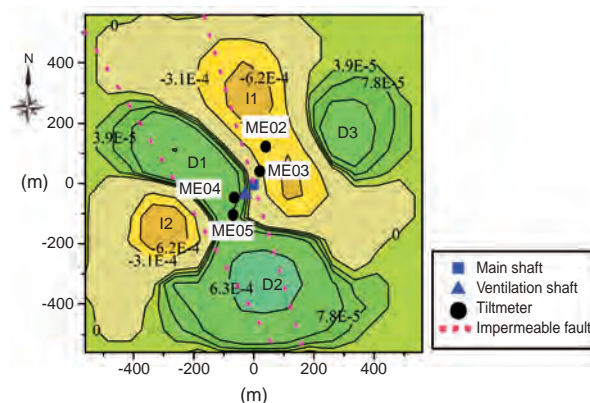


**Fig.2-17 Result of inverse analysis**

The value shows change of groundwater volume per unit volume of rock. D1, D2 and D3 show a center of a groundwater decreasing area (cold color). I1 and I2 show a center of a groundwater increasing area (warm color).

structures.

In the Mizunami Underground Research Laboratory, tilt data measured by four tiltmeters with a resolution of  $10^{-9}$  radians was used. This measurement data shows that the tilt change is caused by the groundwater flow change accompanying shaft excavation (Fig.2-16).

From the result of estimation of a groundwater volume change at the depth of ground level -160m by an inverse analysis using the tilt data during shaft excavation, it was estimated that the groundwater volume decreasing area extended to the north-northwest and to the south-southeast of the shafts (Fig.2-17).

The result indicates that the decrease in groundwater volume occurred mainly in the area surrounded by two impermeable (low permeability in the normal direction to the fault plane) faults which were already characterized and studied in previous research work. Therefore this decrease of groundwater volume is caused by inflow to the shafts supplied by the groundwater from this restricted area. This result is consistent with previous research, and thus the method we developed is a one effective way to estimate the hydrogeological structures.

#### References

- Nakatani, K., Takeuchi, S. et al., Development of a Method for Estimating Underground Water Flow by Tiltmeters and Model Analysis, Journal of MMIJ, vol.123, no.1, 2007, p.17-25 (in Japanese).  
 Nakatani, K., Takeuchi, S. et al., Evaluation of Underground Water Flow during Excavation of Shafts by Inversion of Tilt Data, Journal of MMIJ, vol.123, no.1, 2007, p.26-32 (in Japanese).

## 2-8 Estimation of Groundwater Quality from Specific Resistance Values — Improvement of Geostatistically-Based Estimation of Groundwater Quality —

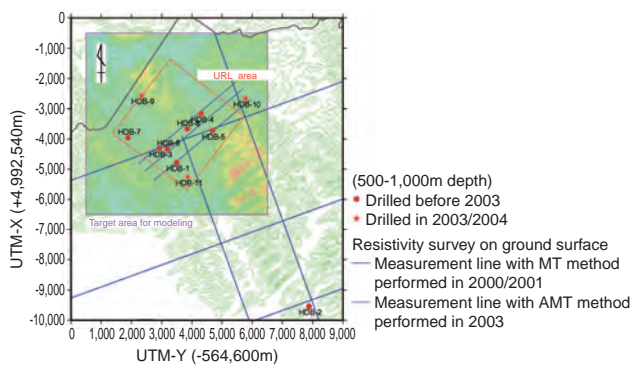


Fig.2-18 Location and time of resistivity surveys

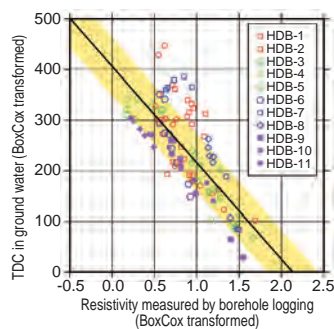


Fig.2-19 Relationship between measured resistivity and TDC in ground water

As a part of the Horonobe Underground Research Laboratory (URL) project, JAEA carried out surface-based investigations of soft sedimentary formations in a 3km × 3km area (the URL location) in Japan. The R&D work for URL construction is going on. This report gives an outline for a study aimed at understanding the geological environment and its change due to URL construction from ground surface measurements.

Different kinds of geological surveys: helicopter, seismic reflection, and resistivity of the ground surface, were carried out in the surface - based investigation phase. Especially, the resistivity surveys with different scales and resolutions were carried out step by step, such as from a helicopter with very large scale and low resolution, the survey on ground surface with medium scale and medium resolution and borehole loggings in deep boreholes with small scale and high resolution (Fig.2-18). In URL area, there was good correlation between resistivity and total dissolved composition (TDC) in groundwater as seen in Fig.2-19.

In this study, we constructed a 3-D resistivity model in URL area by integration of the results of the different kinds of resistivity surveys based on a geostatistical method (Step wise kriging). Moreover, the different data sets made as the project progressed and the 3-D model developed from each data set were qualitatively evaluated for confidence and uncertainty by referring to the latest borehole investigation etc. The advantage of this methodology is that the confidence

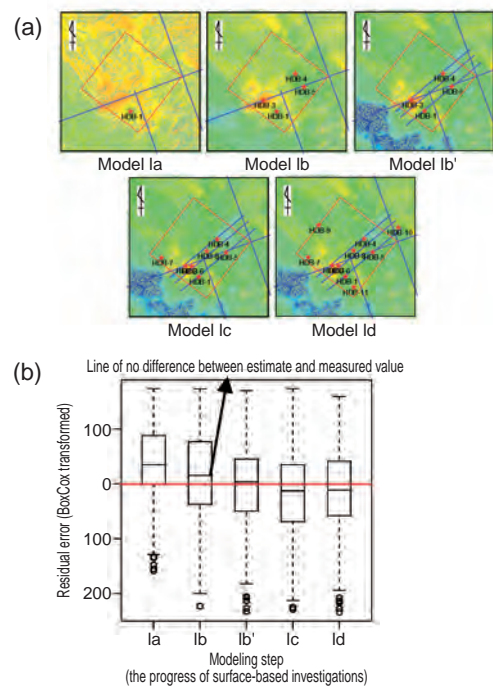


Fig.2-20 Change of the confidence level on 3-D model for TDC in ground water in each investigation steps

(a) Change of distribution by data addition (b) Change of the residual error and its deviation ( $1\sigma$ )

and uncertainty of a model can be evaluated in statistical sense.

Fig.2-20 shows the distribution of TDC in ground water calculated from the 3-D resistivity models (Fig.2-20 (a)) and the residual error of the predicted values and their deviation range with regard to the measured values in each progressive step (Fig.2-20 (b)) in the surface-based investigation. The confidence and uncertainty of the 3-D distribution of TDC in groundwater is effectively improved close to the area where a resistivity survey was done (Fig.2-20 (a)). The residual error approached zero with the data addition, but its deviation range did not improve. The result suggests that the uncertainty of a geological environment is difficult to eliminate by simple data addition and it is necessary to plan investigations considering other characteristics of the environment.

In future work, the resistivity survey in URL area will be repeated every year, and the constructed 3-D models of resistivity, TDC in groundwater and hydraulic conductivity will be verified and improved based on the results. Moreover, the extent of effects of the URL excavation will be estimated as well. This methodology is expected to be a useful tool to understand geological environments and their changes from the ground surface observations made in a pre-investigation state, during construction, and after closure of a real repository.

### Reference

Honda, M., Matsui, H. et al., Study on Geological Environment Model Using Geostatistics Method (Joint Research), JAEA-Research 2007-028, 2007, 91p. (in Japanese).

## 2-9 Estimation of the 3D Distribution of Groundwater Chemistries

### — Hydrochemical Investigation in the Horonobe Underground Research Laboratory (URL) Project —

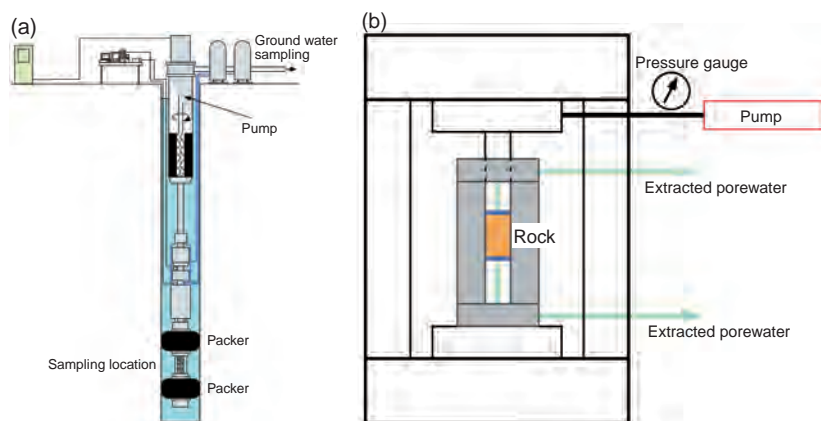


**Fig.2-21 (a) Groundwater pumping system**

After the packers were inflated, the drilling fluid was removed from the packed-off interval with a pump. During the pumping, the tracer concentration was measured at the site to estimate the contamination of the groundwater by the drilling bentonite fluid.

**(b) Equipment of extracting porewater**

The core is subjected to high pressure (ca. 70~100 MPa). 10~30 cc of porewater was extracted from the 200 cc core in two weeks.

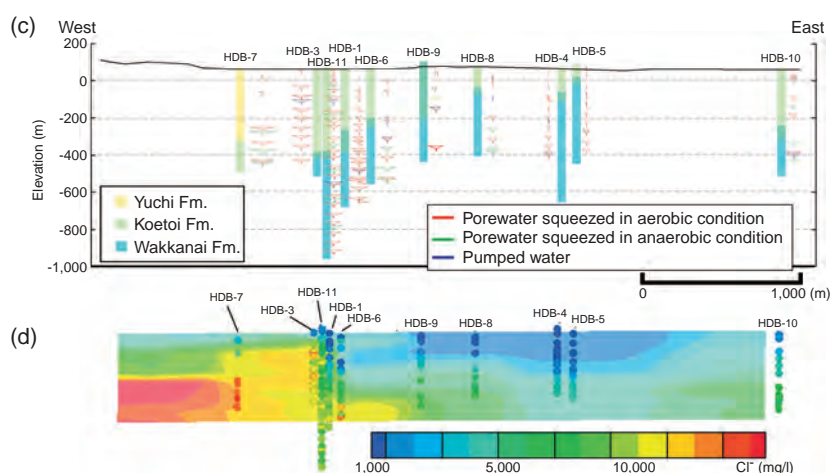


**Fig.2-22 (c) Geological columns and Hexadiagram**

This figure shows hexadiagrams of groundwater chemistries. The distribution of groundwater chemistries changes from the fresh water system (Na-HCO<sub>3</sub> type) to saline water system (Na-Cl type) with the depth.

**(d) Estimated pattern by inverse - distance interpolation of water samples**

3-D distributions of groundwater chemistries were estimated by using a geostatistical method (inverse-distance interpolation method) based on the borehole location and sampling depth. As a result, the zone at the east side of Omagari fault has a low concentration of chloride ion (Cl<sup>-</sup>), down to deep levels.

In Japan, the high-level radioactive wastes (HLW) generated with the reprocessing of used fuels are planned to be disposed in the ground deeper than 300 meters. The groundwater will be pumped up during the construction and operation phase of the disposal facility. It is suggested that the geological environments around the facility will be changed. In this research, the techniques to estimate the distributions of groundwater chemistries from the ground level (GL) to about GL -500m before constructing the facility were developed.

The chemical data of meteoric water, river water, groundwater and porewater were used for the estimation. The chemical data of 18 groundwater and 170 porewater samples were analyzed (Fig.2-22(c)) during 11 borehole investigations (HDB-1 to HDB-11). The boreholes were Our research results show clearly that the bentonite fluid influences the groundwater chemistry. The groundwater was sampled in the hydraulic packer test (Fig.2-21(a)).

The porewater was extracted by squeezing in a suitably-designed high pressure cell. This technique has been successfully utilized by the British Geological Survey (BGS) in the Nirex site investigations (Fig.2-21(b)).

The inverse - distance interpolation method was applied to these data, and three dimensional distributions of groundwater chemistries have been estimated (Fig.2-22(d)). As the result, the distribution revealed a change in groundwater chemistry from the fresh water system (Na-HCO<sub>3</sub> type) to saline water system (Na-Cl type) with increasing depth. It is understood that the boundary depth of the fresh water and saline water is different in the east and west portions of the area.

We will simulate and discuss the evolution process of these groundwater chemistries in the future. Also, the validity of this geochemical model will be confirmed by comparison with the groundwater chemistry changes during the construction and operation of the underground facility.

#### Reference

Hama, K., Kunimaru, T. et al., The Hydrogeochemistry of Argillaceous Rock Formations at Horonobe URL Site, Japan, Physics and Chemistry of the Earth, Parts A/B/C, vol.32, issues 1-7, 2007, p.170-180.

## 2-10 Inference of Hydrogeological Structure from Geological Observations — Development of Fracture Investigation Techniques for Sedimentary Rocks —

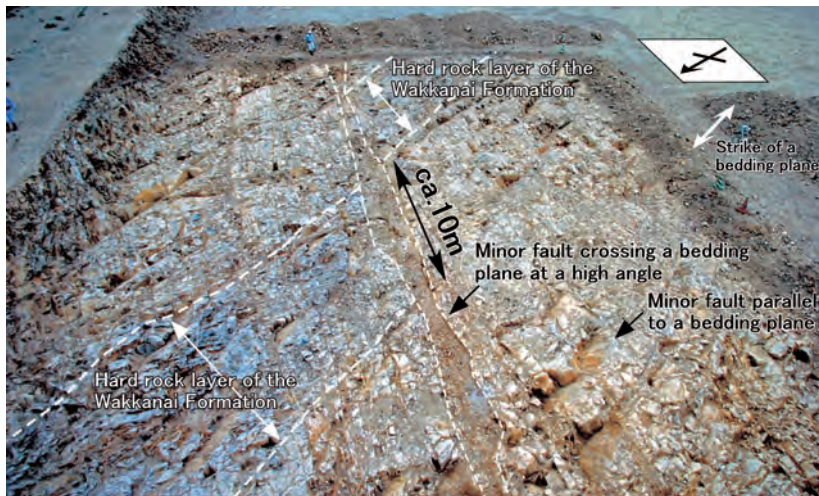


**Fig.2-23 The observed outcrop**

An outcrop exposed by heavy equipment. MFCs and MFPs can be observed within sedimentary rocks (the Wakkanai Formation). The hard rock layer of the formation has a sinistral strike-slip with about 10 m displacement along the MFC at the outcrop's center. We recorded the geological characteristics of MFCs and MFPs in detail.

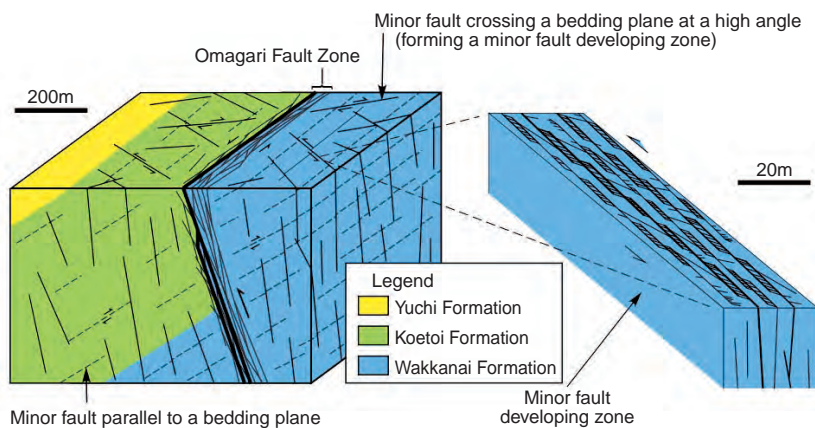


**Fig.2-24 A conceptual model for WCFs**

MFCs (particularly MFDs) are considered to be high potential WCFs, but the potential of MFPs is low. The Omagari Fault shown in this figure, not mentioned in the text, is inferred to be a high potential WCF from other investigations. Solid lines: high potential WCF; broken lines: low potential WCF

In order to evaluate migrations of radionuclides in rock masses around a geological repository for high-level radioactive wastes, ground water flow must be analyzed. For the ground water flow's analysis, the hydrogeological structure, i.e. distributions of hydraulic conductivities in rock mass, must be understood, in particular the water-conducting features (WCFs) which have high hydraulic conductivities.

The hydrogeological structure is inferred by an analysis integrating geological observations and in-situ permeability test data. If water-conducting features can be characterized to some degree only from geological observations, we can perform in-situ permeability tests selectively and infer the hydrogeological structure efficiently.

In this study, we performed geological observations for fractured sedimentary rocks in the Horonobe area, northern Hokkaido, Japan, and researched characteristics and distributions of WCFs in the rock mass (Fig.2-23).

Most of fractures in the rock mass were divided by their orientations and surface's occurrence into two types of faults;

a minor fault crossing a bedding plane at a high angle (MFC) and a minor fault parallel to a bedding plane (MFP). In addition, MFCs, particularly collected in a high density zone called a minor fault developing zone (MFD), were inferred to be high potential WCFs, based on the nature of their alterations, orientations, densities and crosscutting relations. This inference agrees with the results of in-situ permeability tests and the spots where there is water loss during drilling.

Based on the orientations, direction of displacements, and crosscutting relations of MFCs, it is inferred that they were formed after uplifting, by residual stress which accumulated during folding. Based on this origin, it is inferred that MFCs are to be found in and around folds, which is actually confirmed at outcrops and boreholes.

In this way, hydrogeological structure was feasibly inferred to some degree from geological observations (Fig.2-24). We will be studying the relationships between the uncertainty of inferred results and a quantity/quality of investigations.

### Reference

Ishii, E. et al, A Case Study of Analysis of Faults in Neogene Siliceous Rocks, Oyo Chishitsu, vol.47, no.5, 2006, p.280-291 (in Japanese).

## For Practical Use of Fusion Energy

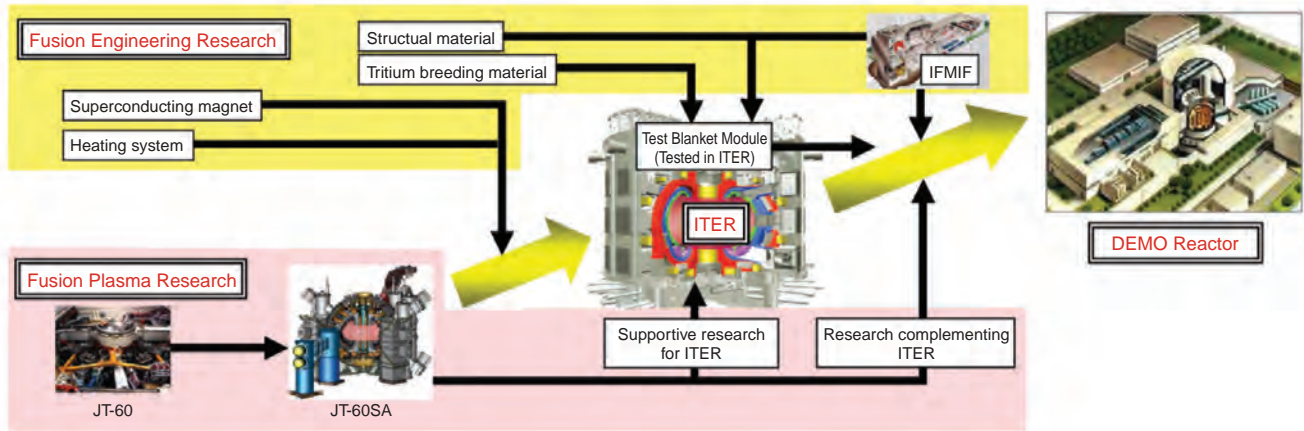


Fig.3-1 Development of the Fusion DEMO Reactor

In the fusion research and development field, R&D into three fields that are keys to the fusion development needed for the practical use of fusion energy are being pursued: the ITER project, the fusion plasma research, and the fusion engineering research. We are intensively engaged in international cooperation not only in the ITER project, but also in R&D over a broader area pursued by Japan and EU (Broader Approach Activity) etc (Fig.3-1).

### ITER (International Thermonuclear Experimental Reactor) Project

The ITER project is an international cooperative project to demonstrate the scientific and technical feasibility of fusion energy through construction and operation of an experimental reactor. The participants are Japan, EU, US, Russia, China, Korea, and India, more than half of the world population. The experimental reactor, “ITER”, is scheduled to be constructed in Cadarache in France. The international agreement on the construction and operation of “ITER” was signed by seven participating parties in Paris in November 2006. We are to become the domestic agency of the ITER project in Japan and will play an important role in the project.

### Fusion Plasma Research

Studies for the JT-60SA plan (upgrade of JT-60 to a superconducting machine) to support the ITER project and to seek the advanced performance of a core plasma for the DEMO reactor were begun as one of the broader approach activities through the cooperation of Japan and EU. Topic 3-1, “Accomplishment of the Conceptual Design of JT-60SA Through Collaboration of Japan and Europe” concerns this upgrade, making a wide range of experiments possible by using existing equipment of JT-60 to the maximum, and adopting advanced technologies.

The critical requirement for the DEMO reactor is to attain a high level of economical efficiency, namely, to sustain a high fusion power in a reactor core of compact size. It is necessary to improve the plasma pressure (temperature  $\times$  density) for that. Topic 3-2, “The Search for the Plasma Rotation Needed for High Pressure Plasma”, is the first research in the world that experimentally showed that a high plasma pressure can be maintained stably using JT-60. Moreover, major progress was achieved in theoretical research in parallel with the experiment. Topic 3-3,

“Sharpening Plasma Shape Improves Pressure Limit”, clarified theoretical guidelines to achieve high plasma pressure, and Topic 3-4, “Suppression Mechanism of Turbulent Electron Heat Transport”, verified that the heat insulating layer discovered by experiment is a self-organization phenomenon, the same as the formation of a jet in a planet atmosphere, by first-principle simulation of electron turbulent flow. In the future, great progress in fusion plasma research through the combination of experiment and theory is expected.

### Fusion Engineering Research

The fuel of fusion energy is deuterium and tritium. A large quantity of deuterium exists in seawater. The tritium hardly exists naturally at all, but it can be produced from lithium, which is also contained plentifully in seawater. In the fusion reactor, the energy of the neutrons resulting from fusion reactions is extracted with the device “Blanket”, and here tritium is also produced. Topic 3-5 and Topic 3-6, “Development of Full Scale First Wall of Fusion Blanket” and “Developing a Method for Suppressing Irradiation Hardening of F82H by Heat Treatment Utilizing the Difference in the Hardening of Weld Joints” are research results needed for the development of a manufacturing method of Blanket and a method of controlling the stiffening caused by neutron irradiation, using ferritic steel (F82H) which is a low activation material developed by us. On the other hand, the development of a breeding material and the accurate evaluation of the tritium production rate are necessary for the development of Blanket so that it can efficiently produce tritium. The research into tritium breeding by Blanket has progressed steadily due to the results of Topic 3-7 and Topic 3-8, “Measurement of Tritium Production Rate in Blanket with High Accuracy” and “Material Allowing Stable Fuel Supply to Fusion Reactor”. Moreover, the development of materials other than those for Blanket were also advanced as shown in Topic 3-9 and Topic 3-10, “Research on Interaction between Tritium and Metal” and “Neutron Shielding Resin can be used in the High Temperature Environment of a Fusion Device”.

Thus, we aim at the utilization of fusion energy in the middle of the 21st century, through a comprehensive approach to the necessary research, including fusion plasma and fusion engineering technologies centering on the ITER project.

# 3-1 Accomplishment of the Conceptual Design of JT-60SA through Collaboration of Japan and Europe

— JT-60SA Program for ITER-Supporting and ITER-Complementing Research —

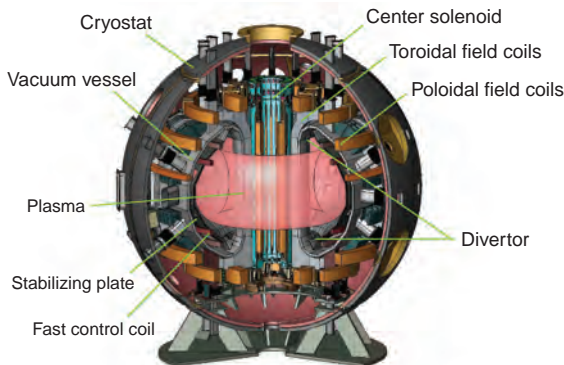


**Fig.3-2 Structure of the JT-60SA device**

The tokamak device is contained in a cryostat (insulated container) to keep superconducting coils at ultra low temperature. In the vacuum vessel, high heat-resistant divertors, stabilizing plates, and high speed control coils are installed to keep a plasma stable.

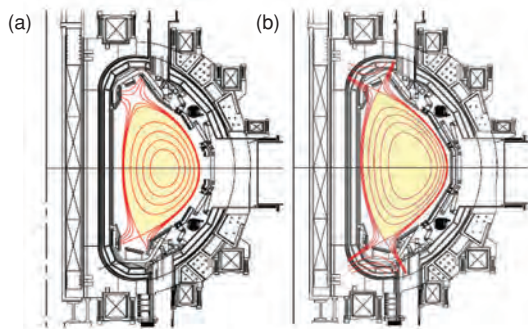


**Fig.3-4 Plasma configurations suitable for ITER-supporting and ITER-complementing research**

Since the ITER-like configuration (a) has the same magnetic structure as ITER, experimental results obtained can be directly used to optimize ITER operations. The high  $\beta$  oriented configuration (b) has a magnetic configuration favorable to sustain high pressure plasmas, and is used for research for DEMO.

“JT-60SA” is a tokamak-type fusion experimental device with superconducting coils (hereafter SC) (Fig.3-2). This device will be constructed as an updated version of the present “JT-60U” as a joint project of the ITER Satellite Tokamak Program of Japan and Europe and the Japanese National Centralized Tokamak Program (JT-60SA program). The main objectives consist of ITER-supporting research directly contributing to “ITER” and ITER-complementing research for DEMO reactors, executed in parallel with ITER. The latter aims at studying high  $\beta$  (high pressure) plasmas necessary for economically feasible DEMO reactors with high power density, and establishing a method for its steady operation (Fig.3-3).

The conceptual design of JT-60SA has been completed recently after four years of design activities. JT-60SA is capable of sustaining a plasma current of 5.5 MA for 100 s by electromagnetic induction. The SC system consists of the center solenoid with  $\text{Nb}_3\text{Sn}$  as in ITER and the toroidal coil and poloidal coils with  $\text{NbTi}$ , which were determined through optimization for the 5.5 MA operation. Two typical plasma configurations with different cross-sectional shapes are established in one device; an ITER-like configuration with almost the same aspect ratio  $A$  (a ratio of major radius to minor radius of a plasma), elongation factor  $\delta$  and triangularity  $k$  as ITER, and a high  $\beta$  oriented configuration with low  $A$ , high  $\delta$  and high  $\kappa$  suitable for studying high

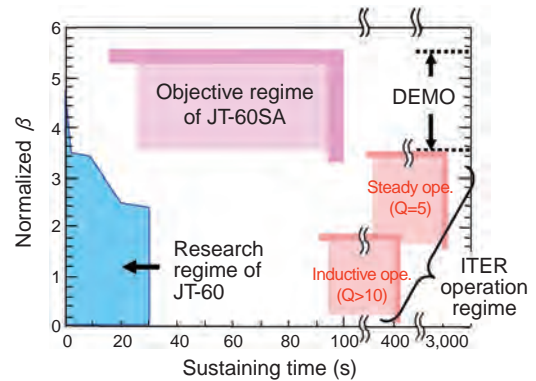


**Fig.3-3 Objective regime of the JT-60SA program**

The power density of a fusion reactor is roughly proportional to the square of normalized  $\beta$  ( $\beta_N$ ; index of plasma pressure). High power density operation expected in the DEMO reactor requires stable operation of plasma with normalized  $\beta_N$  of 3.5-5.5.

pressure plasmas. Upper and lower divertor shapes and the arrangement of poloidal coils were optimized for these configurations (Fig.3-4). Stabilizing plates and fast control coils are installed in the vacuum vessel, to improve the stability of the plasma. The heating power necessary for achieving high temperature and high density break-even class plasmas and steady state high  $\beta$  plasmas has been assessed from simulation results, and the neutral beam injection of 34 MW and the electron cyclotron heating of 7 MW are provided. Since the heat flux to the divertor is estimated to reach  $15 \text{ MW/m}^2$  with such high power injection, a mono-block-type carbon-fiber-composite divertor with high cooling efficiency has been designed. On the other hand, nuclear heating of the SCs by secondary  $\gamma$ -rays and activation of the device and air (argon) by thermal neutrons must be reduced because these phenomena hinder the operation and maintenance. This is resolved by circulating borated water in the double wall of the vacuum vessel and filling boron-doped concrete in the wall of the cryostat.

The conceptual design was made mainly by JAEA, incorporating requirements of Satellite Tokamak Program to the JT-60SA program, and has been reviewed by Japanese and European experts. The JT-60SA program officially started in June, 2007 as a 10 year program with 7-year construction and 3-year experimental periods.

## Reference

M. Kikuchi et al., JT-60SA Project for JA-EU Broader Approach Satellite Tokamak and National Centralized Tokamak, Puruzuma, Kaku Yugo Gakkai-shi, vol.82, no.8, 2006, p.455-469 (in Japanese).

## 3-2 The Search for the Plasma Rotation Needed for High Pressure Plasma — Finding the Minimum Plasma Rotation Suppressing Plasma Distortion —

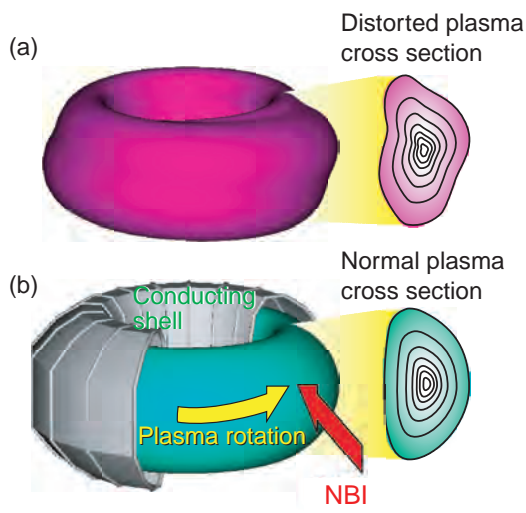


**Fig.3-5 Schematic drawing of suppressing plasma distortion**

- (a) Plasma distorts with increase in plasma pressure.  
 (b) Plasma distortion suppressed by plasma rotation in the conducting shell, because the eddy current flows so as to suppress the plasma distortion.

To realize a fusion reactor with high fusion output power density (small size and high power output means an economical attractiveness), high pressure plasma (= plasma temperature  $\times$  density) is required. However, the high pressure makes it hard to sustain the plasma confinement due to plasma distortion (Fig.3-5 (a)), and therefore, how the plasma distortion can be stabilized is a key issue in increasing the pressure limit. For this problem, a theoretical prediction was made that the plasma distortion can be suppressed by plasma rotation, which can be driven by neutron beam injections (NBIs), in a conducting shell. However, it should be pointed out that extra NBI could be required to gain enough rotation, because in “ITER” and future reactors it will be more difficult to drive the plasma rotation than in present tokamaks. For this reason, it is important to clarify the threshold of the plasma rotation which can suppress plasma distortion as well as making experimental verification of this theoretical prediction.

In almost all tokamaks, since the direction of NBI is only one direction, the power applied for high pressure plasma also causes large plasma rotation. Thus, a low plasma

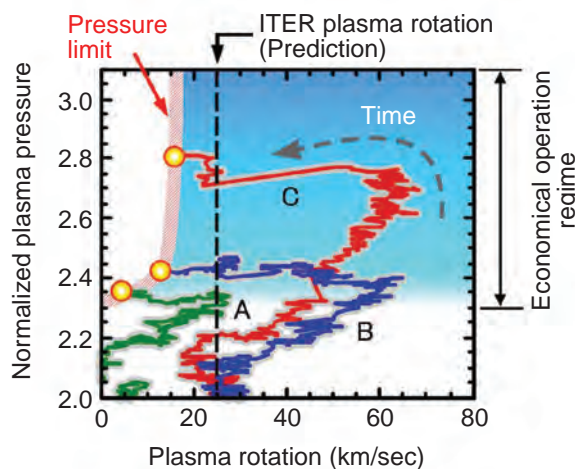


**Fig.3-6 Experimental results showing the required plasma rotation for suppressing the plasma distortion**

Plasma pressure and rotation was changed over time by adding NBI. It is found that the plasma distortion can be suppressed by a plasma rotation lower than that predicted for “ITER” and future reactors. A, B and C stand for the changes over time of three cases where the combination with NBI was different. Plasma distortion occurred at the yellow circles.

rotation in a simulation of a future reactor is difficult to realize in experiment. In contrast, since the JT-60U makes NBI in different directions, we can try to control the plasma rotation using a combination of NBIs while keeping the high plasma pressure. In consequence, we can realize similar plasmas with a low rotation in “ITER” and future reactors, and thus we can find the plasma rotation required to suppress the plasma distortion for the first time. The results are shown in Fig.3-6. In the three cases, A, B and C, the combination of NBI direction and power are different, and in each case power is adjusted over time. In this way, the plasma rotation at which the plasma distortion appears was successfully obtained. It was found that when the plasma rotation becomes less than 20 km/sec, the plasma began to distort and the confinement is degraded at the same time. This threshold of plasma rotation is only about 15% of the theoretical prediction. These results indicate that we can operate in an economical regime where the plasma rotation is quite sufficient to suppress the plasma distortion even if the plasma rotation is low as predicted in “ITER” and future reactors.

### Reference

Takechi, M., Matsunaga, G. et al., Identification of a Low Plasma-Rotation Threshold for Stabilization of the Resistive-Wall Mode, Physical Review Letters, vol.98, 2007, p.055002-1-055002-4.

### 3-3 Sharpening Plasma Shape Improves Pressure Limit — Stabilization of the Edge Localized Mode by Sharpening the Plasma Shape —

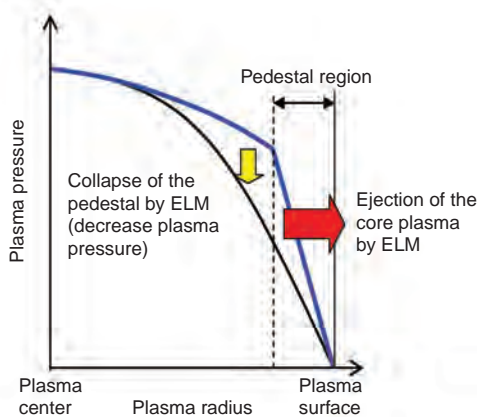


**Fig.3-7 Pattern diagram of the collapse of the edge pedestal structure in the edge localized mode (ELM)**

The pedestal structure of the plasma pressure (blue line) will collapse when the pressure becomes too high and the edge localized mode (ELM) is generated. After such a collapse, the pressure profile becomes smooth.

From the economical point of view, a fusion reactor needs to confine high pressure plasma stably. The so-called “H-mode plasma” whose plasma pressure exhibits a pedestal structure near the plasma surface (Fig.3-7) is desirable to increase the total plasma pressure. However, when the pressure of this pedestal region becomes too high, an instability called the edge localized mode (ELM) sometimes induces the collapse of the pedestal structure. This collapse ejects the high temperature plasma to the outside of the confined region, and it decreases the total pressure of the confined plasma. Therefore, understanding the conditions which stabilize ELM is an important issue for high pressure plasma.

Previous studies revealed experimentally and theoretically that a large collapse near the plasma edge is induced by the Type-I ELM, which is one of the ideal magnetohydrodynamic (MHD) instabilities called peeling-ballooning mode, and this MHD mode can be stabilized by changing the plasma cross-section from circular to “D-shape”. However, the impact of the “D-shaping” on the ELM stability changes in different experimental devices. This result implies that the stability of this MHD mode will depend on not only the “D-shaping” but

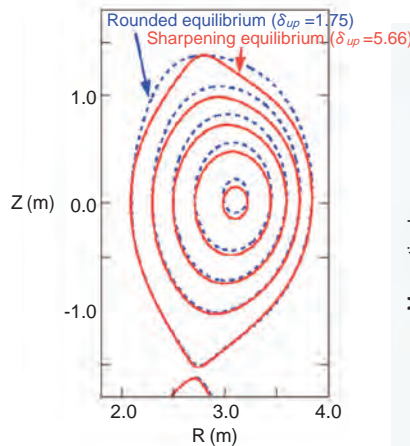


**Fig.3-8 Plasma cross-sections of the equilibria whose sharpness are different**

We investigated numerically the ability of equilibria whose sharpness at the top of the cross-section are different to prevent the unstable peeling-ballooning mode. (The parameter  $\delta_{up}$  expresses the sharpness. This parameter increases as the cross-section becomes sharper.)

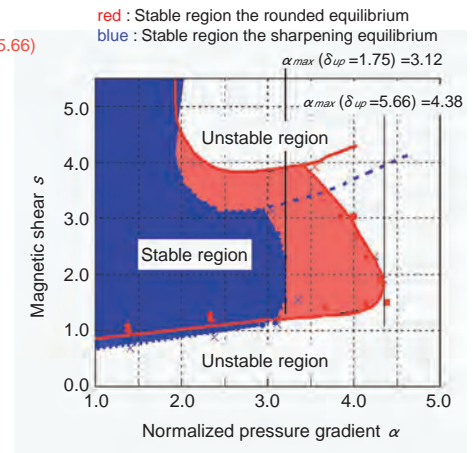


**Fig.3-9 Expansion of the MHD stable region by increasing the sharpness**

MHD stability diagram on the plasma pressure gradient and the magnetic shear plane. The stable region expands as the sharpness increases from  $\delta_{up}=1.75$  (blue region) to 5.66 (red region). This expansion improves the maximum pressure gradient at which stability can be maintained by over 30%.

also other shaping effects.

To investigate these shaping effects, we developed the linear ideal MHD stability code MARG2D, and analyzed the effect of the sharpness near the top of the plasma surface (Fig.3-8) on the stability of the peeling-ballooning mode. As a result, we reveal that the peeling-ballooning mode can be stabilized by sharpening the plasma top shape, even when the ellipticity and the triangularity, which are the shaping parameters to express the “D-shape” of the cross-section are almost unchanged. This stabilization increases the maximum pressure gradient at which stability can be maintained. For example, by changing the plasma top shape as shown in Fig.3-8, the maximum pressure gradient increases over 30% as shown in Fig.3-9. Moreover, we found this stabilization is caused by increasing near the top of the plasma the magnetic shear - the change of the direction of the magnetic field line from the center to the surface of plasma.

This experimentally verified stabilizing effect of the sharpness in JT-60U is theoretically explained in this study. Based on this result, greater plasma performance can be realized in ITER and JT-60SA.

#### Reference

Aiba, N. et al., Effects of ‘Sharpness’ of the Plasma Cross-Section on the MHD Stability of Tokamak Edge Plasmas, Nuclear Fusion, vol.47, no.4, 2007, p.297-304.

### 3-4 Suppression Mechanism of Turbulent Electron Heat Transport – Simulation Study of Microscopic Electron Turbulence in Tokamaks –

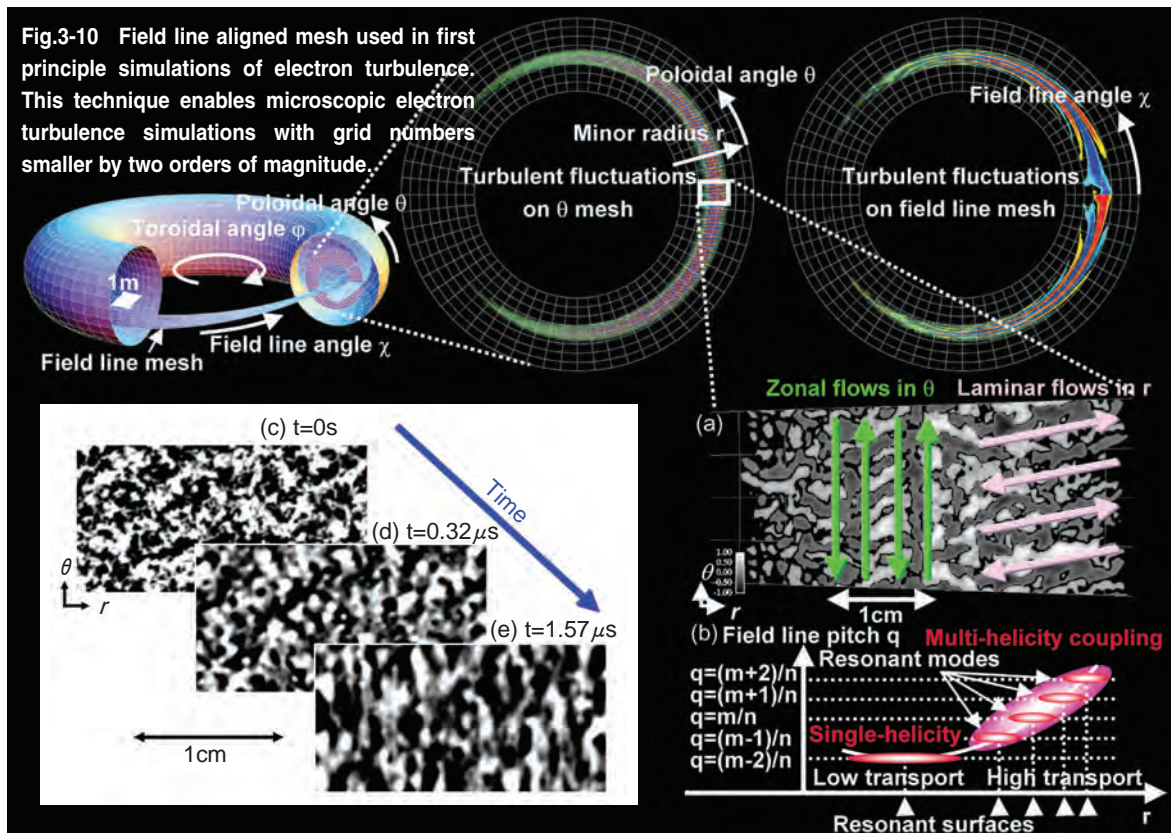


**Fig.3-12 Contour plots of electric potential observed in electron turbulence simulations of self-organization processes**

Single-helicity electron turbulence, which is a model for a barrier region in Fig.3-11 (a), is evolved from random turbulent fields (c). These pass through a transient state (d), and then the system is relaxed to form turbulent structures with zonal flows (e).

**Fig.3-11 First principle simulations of electron transport barriers**

(a) is a contour plot of the electric potential and (b) shows coupling structures of resonant modes characterized by mode numbers (m,n) in (θ, φ) directions. In a barrier region, zonal flows are produced by self-organization processes of single-helicity (2D-like) turbulence.

In tokamak research, it is one of critical issues to sustain high temperature plasmas efficiently by suppressing turbulent transport, which dissipates the heat from the reactor core. Up to now, ion turbulence (characteristic wave length  $\lambda \sim 5\text{mm}$ ) has been studied based on first principle simulations. However, calculation of the microscopic electron turbulence ( $\lambda \sim 0.1\text{mm}$ ) which is important especially in burning plasmas in “ITER”, where the electron heating by  $\alpha$ -particles becomes dominant, in experimentally relevant parameters is prohibitively costly. To overcome this difficulty, we developed a new simulation technique using field line aligned mesh (Fig.3-10), and succeeded in simulating the

electron turbulence. By using this simulation, we studied the electron turbulence in a transport barrier region, which is often observed in recent experiments. The results show that in a barrier region, zonal flows are produced which suppress heat flux from a core (Fig.3-11 (a)), and that this effect can be expected to occur also in future large devices. Further analyses on turbulent structures clarified that they have two dimensional (2D) like character, which is similar to that found in atmospheres of planets, and that zonal flows are generated from self-organization processes similar to those of East-West zonal jets on planets (Fig.3-12).

**References**

Idomura, Y. et al., Global Profile Effects and Structure Formations in Toroidal Electron Temperature Gradient Driven Turbulence, Nuclear Fusion, vol.45, no.12, 2005, p.1571-1581.  
 Idomura, Y., Self-Organization in Electron Temperature Gradient Driven Turbulence, Physics Plasmas, vol.13, no.8, 2006, p.080701.1-080701.4.

## 3-5 Development of Full Scale First Wall of Fusion Blanket — R&D of Diffusion Bonding for Fusion Blanket Manufacturing —

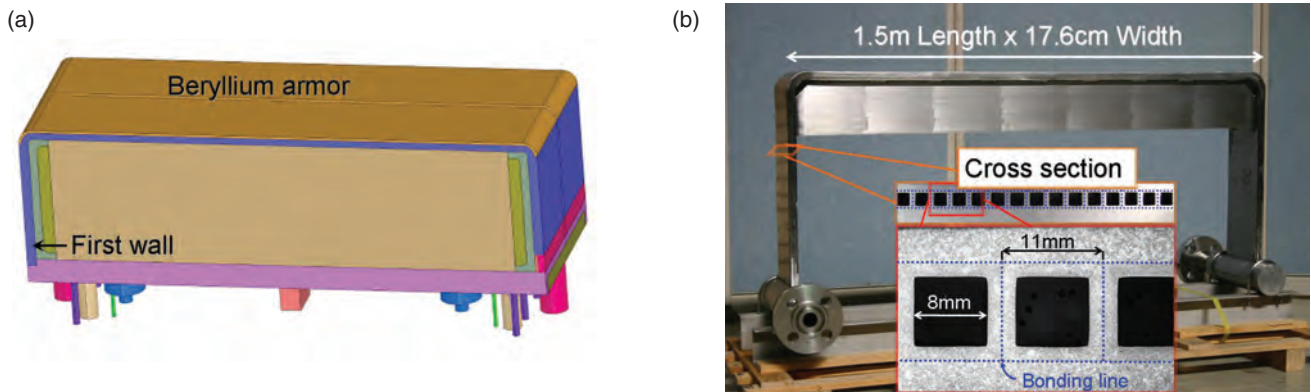


**Fig.3-13 Fusion blanket and newly developed first wall components**

(a) The light brown region is armor material, and the blue region is the first wall.

(b) The first wall includes fifteen square cooling channels. Ultra sonic tests did not find any defects in the wall.

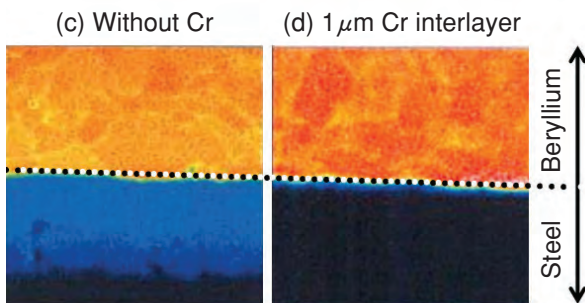


**Fig.3-14 Elemental analysis of the interface of Be/RAF, after (c) HIP at 1,233 K without chromium foil, and (d) HIP at 1,023 K with 1  $\mu$ m chromium interlayer. The blue region in (c) shows brittle inter metallic compound.**

We have developed two key technologies for fusion blanket components. The first one is a fabrication process of a first wall structure of the fusion blanket. The second one is a joint between the dissimilar metals beryllium (Be) and steel. These were developed from the Hot Isostatic Pressing (HIP) method. HIP is a kind of diffusion bonding method. The work-pieces are pressurized under high temperature argon atmosphere.

Fusion blanket is an important in-vessel component, which works as an energy converter, and it also produces tritium as a fusion fuel. It is to be loaded in ITER for demonstration of power production. The First Wall (FW) is the wall facing fusion plasma. The wall is exposed to high heat load and high flux neutron radiation. Therefore the FW has built-in cooling channel and its structural material is a reduced activation ferritic steel (RAF), which demonstrates superior resistance to radiation damage. However, the surface of the FW component must be covered with a low atomic number element, such as Be, for stable plasma operation (Fig.3-13). We applied the HIP method to fabrication of the built-in cooling channel of the FW component and the joint between

Be and RAF.

For the FW fabrication, we developed precision RAF square tubes to minimize assembly gaps which cause excess deformation around joint interfaces. And we also optimized HIP and post HIP heat treatment conditions to avoid microstructural change which causes degradation in material properties such as ductility and toughness. The FW fabricated with these techniques demonstrated good dimension stability without degradation in mechanical properties. As for the Be/RAF dissimilar joint, it is well known that Be forms brittle intermetallic compounds with iron. Therefore we used chromium foil as a diffusion barrier and carefully set the HIP temperature to control diffusion of Be. We found that 1  $\mu$ m chromium foil effectively worked as a diffusion barrier at 1,023 K. The chromium foil suppressed Be diffusion and it made a strong dissimilar joint (Fig.3-14).

We are intensively competing with the other “ITER” participating countries in the R&D of blanket manufacturing. We have developed these technologies prior to the others, and we have made a great advance towards the fusion power production.

### Reference

Hirose, T. et al., Joining Technologies of Reduced Activation Ferritic/Martensitic Steel for Blanket Fabrication, Fusion Engineering and Design, vol.81, issues 1-7, 2006, p.645-651.

### 3-6 Developing a Method for Suppressing Irradiation Hardening of F82H by Heat Treatment Utilizing the Difference in the Hardening of Weld Joints

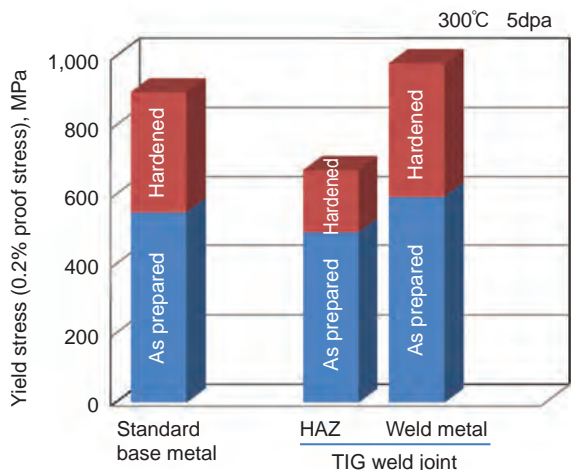


**Fig.3-15** Yield stress of the base metal and TIG weld joints of F82H, i.e. heat affected zone (HAZ) and weld metal, before and after irradiation. Irradiation hardening of HAZ is smaller than that of base metal and weld metal.

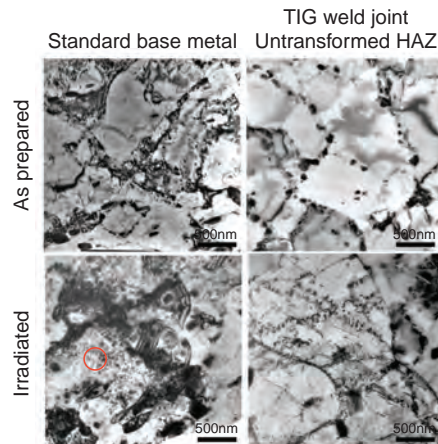
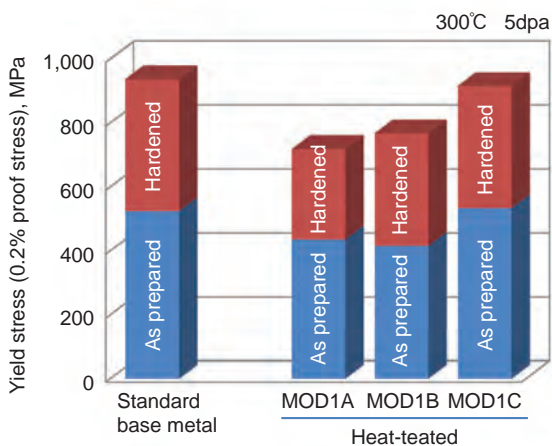


**Fig.3-16 TEM microstructure of base metal and untransformed TIG-HAZ region before and after irradiation.** Dislocation loops dominate in irradiated base metals (indicated by ○) is not observed in untransformed TIG-HAZ region.



Heat treatment conditions

F82H standard base metal  
1,040°C×30min, 750°C×1hour

F82H MOD1A  
(Untransformed HAZ region equivalent)  
800°C×30min, 700°C×10hours

F82H MOD1B  
(Transformed HAZ region equivalent ver.1)  
860°C×30min, 700°C×10hours

F82H MOD1C  
(Transformed HAZ region equivalent ver.2)  
920°C×30min, 700°C×10hours

**Fig.3-17 Yield stress of standard and heat-treated F82H, simulating the thermal history of TIG-HAZ region**

The F82H heat treated under conditions simulating the thermal history of untransformed HAZ region (Mod-1 A) exhibits less hardening upon irradiation than the others.

Reduced activation ferritic/martensitic steels (RAFMs) are the leading candidates for the fusion blanket structural material. F82H (Fe-8Cr-2W- V,Ta) is the one of the RAFMs which has been developed by JAEA. The key issue now is how to suppress the irradiation hardening and embrittlement induced by neutron irradiation at temperature below 350°C.

In the course of research into irradiation hardening, it was found that the irradiation hardening at the heat affected zone (HAZ) of a TIG weld joint is much smaller than that of the standard base metal and the TIG weld metal (Fig.3-15). TEM observation of these regions revealed that dislocation loops, which are recognized as the key feature causing irradiation

hardening, are not observed in the untransformed HAZ region (Fig.3-16). Based on these results, F82H was heat treated in a manner simulating the thermal history of HAZ region, and then neutron irradiated. A tensile test revealed that the heat treating which simulates the thermal history of untransformed HAZ region yielded the smallest hardening (Fig.3-17).

This research was conducted as the part of the collaborative program for testing structural materials in mixed-spectrum reactors of JAEA and US Department of Energy.

**Reference**

Wakai, E. et al., Effect of Initial Heat Treatment on DBTT of F82H Steel Irradiated by Neutrons, Fusion Science & Technology, vol.47, no.4, 2005, p.856-860.

### 3-7 Measurement of Tritium Production Rate in Blanket with High Accuracy — Development of Measurement and Calculation Methods in Breeder Layer —

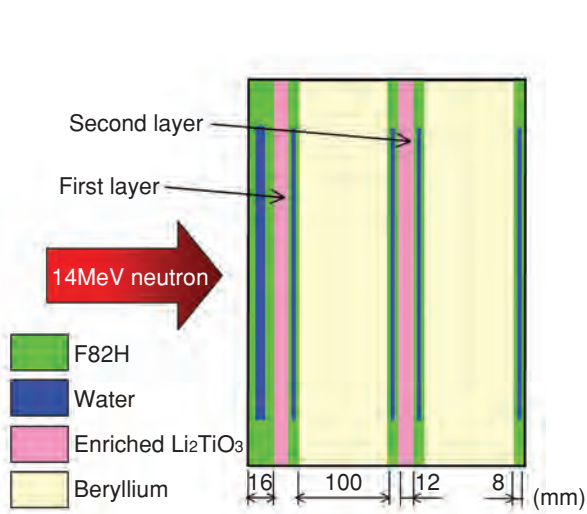


**Fig.3-18 Neutronics experiment with multi-layered blanket mockup**

We constructed a multi-layered blanket mockup composed of a First Wall panel (F82H and water), enriched  $\text{Li}_2\text{TiO}_3$  breeding layer (40% enrichment), beryllium layer, and partition panel (F82H and water). We irradiated it with 14 MeV neutrons, and measured tritium production rates in the  $\text{Li}_2\text{TiO}_3$  layer.

Tritium Breeding Ratio (TBR) is defined as a ratio of the tritium produced by nuclear reaction between neutron and lithium in a blanket to that consumed by the DT reaction in a fusion reactor. Future fusion blankets are required to supply tritium as a fuel by themselves. Therefore we pursued development of a blanket with TBR of more than unity.

The TBR has been estimated by numerical calculations such as a Monte Carlo method for the blanket design, but the accuracy of these calculations has not been fully investigated for complicated blanket configurations so far. In order to solve this issue, 14 MeV neutron irradiation experiments have been conducted with partial mockups of the fusion blanket using the Fusion Neutronic Source (FNS) facility at JAEA, and we have performed neutronics studies to validate the calculation accuracy of TBR.

In the blanket, small enriched tritium breeder ( $\text{Li}_2\text{TiO}_3$ ) pebbles 1 mm in diameter were packed in a breeder layer 12-15 mm in thickness. It is expected that tritium production rates (TPRs) change by more than one order of magnitude in the breeder layer. The TPR refers to tritium production from one lithium nucleus and one source neutron generated by the DT reaction. In order to measure this sharp change of the TPR, we developed two kinds of TPR detectors in this study. One is an enriched breeder pellet detector, and different thick pellets are applied corresponding to the change of the TPR.

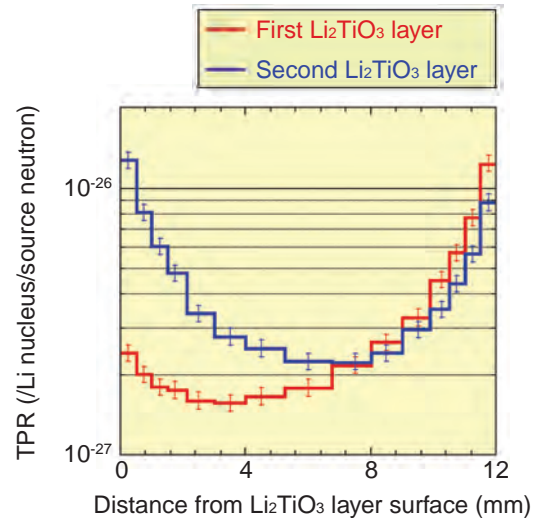


**Fig.3-19 Measured TPR distributions**

By installing the fabricated 40% enriched  $\text{Li}_2\text{CO}_3$  pellets 13 mm in diameter and 0.5-2 mm in thickness in the  $\text{Li}_2\text{TiO}_3$  layer of the multi-layered blanket mockup, and using them as the TPR detector, we could successfully measure the detailed distribution of the TPR for the first time.

The other is a very thin bed of small breeder pebbles serving as detectors. In order to model the blanket, we constructed a multi-layered slab configuration mockup composed of heat-resistant structure (F82H), coolant (water), breeder (enriched  $\text{Li}_2\text{TiO}_3$ ), neutron multiplier (beryllium), and a pebble bed mockup composed of F82H, beryllium and small breeder pebbles. Fig.3-18 shows the multi-layered mockup. We put the enriched pellet detectors and the pebble bed detectors in these mockups, and irradiated the mockups with 14 MeV neutrons. For the first time, we successfully measured a detailed distribution of the TPR in a blanket mockup (Fig.3-19). We have established a data base for the accurate prediction of the TPR distribution.

In addition, we studied design calculation uncertainty of the TBR based on these experimental results. We proposed new calculation method for the pebble bed layer. In the previous blanket design for the pebble bed layer, we mixed pebbles and voids homogeneously, and performed calculations using this geometry. In this study, we modeled each pebble and void accurately with a hexagonal close-packed heterogeneous geometry for the pebble bed layer used in our experimental analysis. As a result, we got indications that calculations with our TBR design have uncertainty of less than 10%, and so made great progress in the development of the fusion reactor blanket.

#### Reference

Sato, S. et al., Measurement of Tritium Production Rate in Water Cooled Pebble Bed Multi-Layered Blanket Mockup by DT Neutron Irradiation Experiment, Nuclear Fusion, vol.47, no.7, 2007, p.517-521.

## 3-8 Material Allowing Stable Fuel Supply to Fusion Reactor — Development of Advanced Tritium Breeder Materials for Fusion Reactor —

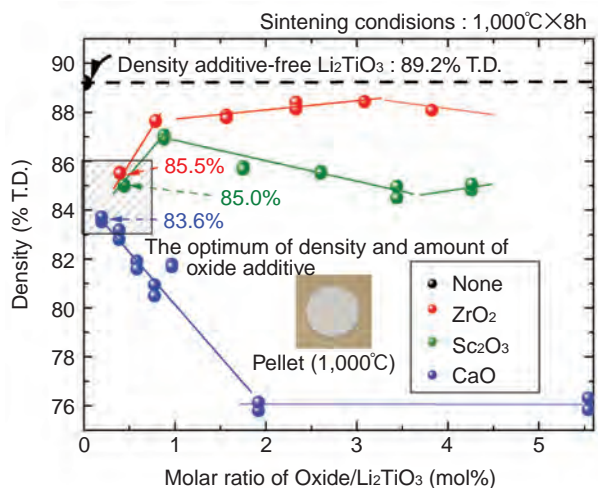


**Fig.3-20 Density of Sintered  $\text{Li}_2\text{TiO}_3$  with different amounts of oxide additives**

The density of the sintered pellet was restrained by adding an oxide ( $\text{ZrO}_2$ ,  $\text{Sc}_2\text{O}_3$ , and  $\text{CaO}$ ) to  $\text{Li}_2\text{TiO}_3$ . The reduction of tritium release due to grain growth when  $\text{Li}_2\text{TiO}_3$  is used for a long time at high temperatures could be prevented by adding the oxide as a grain growth control material.

Tritium (T) doesn't exist in the natural world, but a fusion reactor uses deuterium (D) and T as fuel in the DT nuclear fusion reaction. Therefore, it is necessary to irradiate lithium (Li) filled to the fusion reactor blanket with neutrons, thus producing T artificially. Among materials including Li, Lithium titanate ( $\text{Li}_2\text{TiO}_3$ ) has a good T release properties and so is attracting attention. On the other hand, when  $\text{Li}_2\text{TiO}_3$  is used in an  $\text{H}_2$  atmosphere for a long time at high temperature, crystal grains grow, and the Ti in  $\text{Li}_2\text{TiO}_3$  is reduced. Thus, there is a problem that the amount of the T release decreases. It is necessary to develop a method of controlling  $\text{Li}_2\text{TiO}_3$  crystal grain growth so that it is not reduced easily with the  $\text{H}_2$  gas. This research dealt with improvement of  $\text{Li}_2\text{TiO}_3$  by the addition of oxides.

$\text{CaO}$ ,  $\text{ZrO}_2$ , and  $\text{Sc}_2\text{O}_3$  were investigated as the added oxide. The sample was sintered at  $1,000^\circ\text{C}$ , and made into pellets (Fig.3-20). The dependence of decrease in density after sintering upon addition of small amounts of oxide was

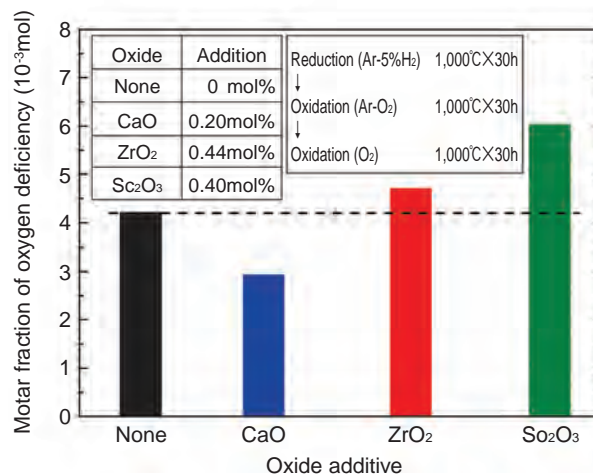


**Fig.3-21 Molar fraction of oxygen deficiency of  $\text{Li}_2\text{TiO}_3$  with oxide additives**

Because tritium, the fuel of the fusion reactor, is collected by hydrogen ( $\text{H}_2$ ) gas,  $\text{Li}_2\text{TiO}_3$  is used in an  $\text{H}_2$  atmosphere. Ti in  $\text{Li}_2\text{TiO}_3$  was reduced in the hydrogen atmosphere, causing oxygen loss, but the oxygen loss could be lowered by adding  $\text{CaO}$ .

obtained from the density of the sintered pellets and the amount of the oxide addition (Fig.3-20).

Next, the reduction of  $\text{Li}_2\text{TiO}_3$  with added oxide in the  $\text{H}_2$  atmosphere was examined by means of thermogravimetry. If  $\text{Li}_2\text{TiO}_3$  is reduced with  $\text{H}_2$ , O loss is caused. The amount of the oxide addition was adjusted to achieve the optimum density as shown in Fig.3-20. The color of the sample changed from white into thin blue if the sample was reduced, and a weight decrease due to O loss was observed. Fig.3-21 shows the calculated O deficiency in the samples.  $\text{Li}_2\text{TiO}_3$  with  $\text{CaO}$  added had less oxygen deficiency than the other kinds of  $\text{Li}_2\text{TiO}_3$ .

The overall results suggest that the oxide additives are able to control not only the growth of the grain size but also the amount of oxygen deficiency. Thus, the present study confirmed the efficacy of oxide addition to  $\text{Li}_2\text{TiO}_3$  in developing high-temperature resistant breeding materials.

### Reference

Hoshino, T. et al., Non-Stoichiometry of  $\text{Li}_2\text{TiO}_3$  under Hydrogen Atmosphere Condition, Fusion Engineering and Design, vol.75-79, 2005, p.939-943.

### 3-9 Research on Interaction between Tritium and Metal — Pyramid-Like Blisters Formed by Hydrogen-Induced Local Superplasticity —

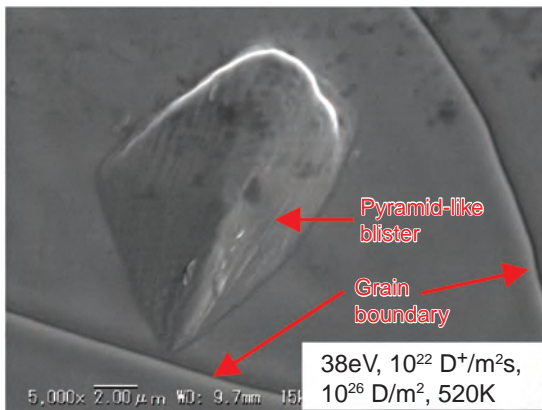


Fig.3-22 Pyramid-like blister on tungsten

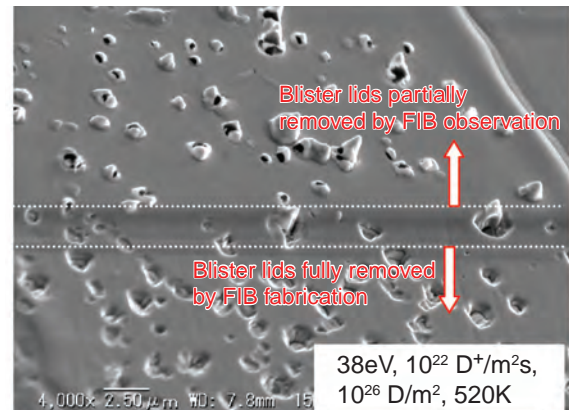


Fig.3-23 Internal features of small blisters

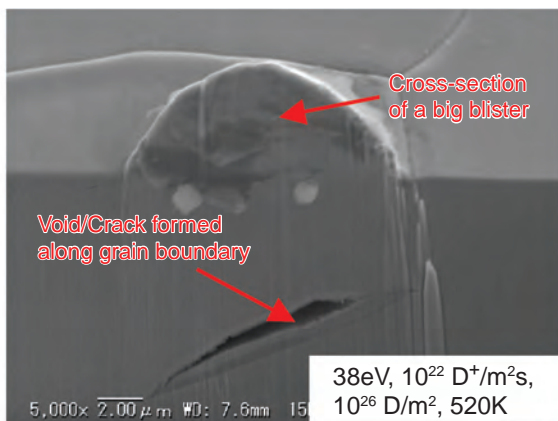


Fig.3-24 Cross-section of a big blister

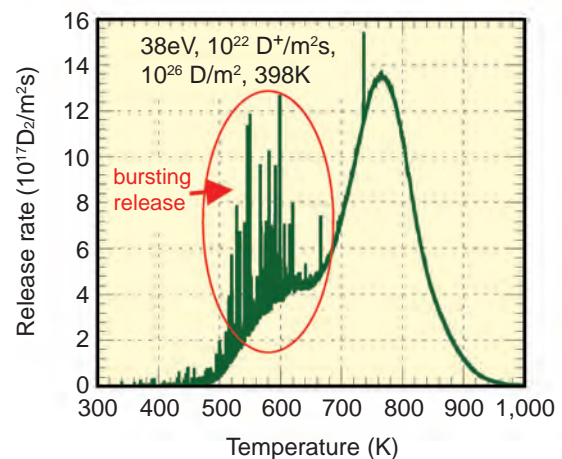


Fig.3-25 Deuterium release rate (0.5 K/s)

Gas (hydrogen, helium, etc.) ion implantation into solids will cause surface structures like blisters. For blisters formed by ions with energy higher than 1 keV, the cavity filled with gases between the surfaced layer and the bulk is generally assumed to be of a lenticular shape with a typical ratio of height against inner diameter of base of about 0.05.

Tungsten is a most promising plasma facing material because of its high melting point. Thus, we investigated its blistering and deuterium retention by exposing recrystallized tungsten samples to simulating edge plasma at fusion reactors (energy: a few tens of eV; flux:  $10^{22}$  D<sup>+</sup>/m<sup>2</sup>s; fluence: up to  $10^{27}$  D/m<sup>2</sup>). As shown in Fig.3-22 and Fig.3-23, two kinds of high-dome blisters appeared at the tungsten surface after deuterium plasma exposure. One is a big blister with magnitude of greater than a few microns and various shapes, even pyramids (Fig.3-22), and the other is a small blister with

size of less than a few microns (Fig.3-23). The ratio of height against inner diameter for both blisters is one-order greater than that reported before, indicating local superplasticity. In addition, there were cavities inside small blisters (Fig.3-23), whereas there were voids/cracks along the grain boundary beneath the big blisters but no hollow lid formed (Fig.3-24). Furthermore, bursting release of deuterium with sudden peaks was observed during heating (Fig.3-25).

These high-dome blisters were considered to be formed by hydrogen-induced local superplasticity due to the generation of atom vacancies and subsequent formation and clustering of hydrogen and vacancies which diffuse deeply into the bulk (i.e. diffusion of tungsten atoms to the surface). Blister formation is a drawback to tungsten as plasma facing material. Since the mechanism has been revealed, efforts will be made to develop techniques for alleviating blistering.

#### Reference

Shu, W.M. et al., Blister Bursting and Deuterium Bursting Release from Tungsten Exposed to High Fluences of High Flux and Low Energy Deuterium Plasma, Nuclear Fusion, vol.47, no.3, 2007, p.201-209.

## 3-10 Neutron Shielding Resin Can Be Used in the High Temperature Environment of a Fusion Device

— Development of Neutron Shielding Resin that Has High Heat Resistance and High Mechanical Strength —

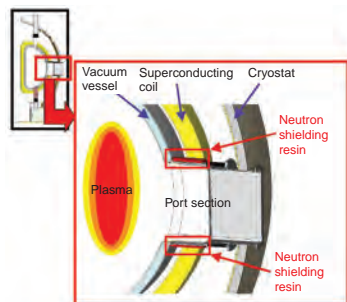


**Fig.3-26 Cross Section of JT-60 Superconducting Modification with Enlarged View of the Port Section**

It is necessary to decrease the heat given to the restricted space around the port section of the superconducting coil by the radiation. (The vacuum vessel is a container where the high temperature plasma is confined. The cryostat is a container to insulate the superconducting coil at an extremely low temperature.)



**Fig.3-27 Test piece of the developed resin**

Used for the neutron shielding characteristics experiment. The size is  $40 \times 40 \times 5 \text{ cm}^3$ .

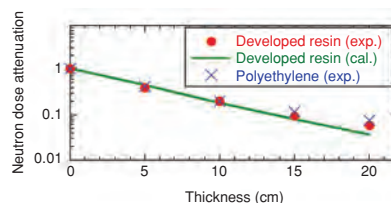


**Fig.3-28 Neutron dose attenuation in the new resin and polyethylene using  $^{252}\text{Cf}$  source**

The neutron shielding performance of the resin was almost the same as the polyethylene.

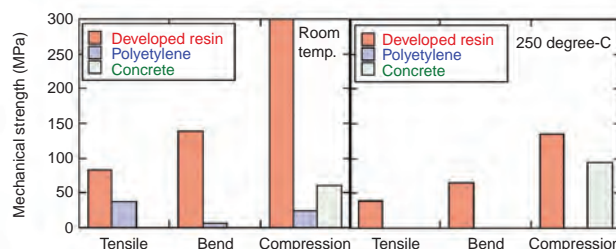


**Fig.3-29 Mechanical strength of the new resin and existing neutron shielding materials**

The new resin has higher mechanical strength than polyethylene and concrete both at room temperature and  $250^\circ\text{C}$ .

In the JT-60 modification there is a device with a new addition of a superconducting coil. The device will be operated with deuterium plasma and a deuterium beam, but no blanket is planned. Therefore, some shielding structure is required for the DD neutrons ( $E_n=2.45 \text{ MeV}$ ) in order to suppress nuclear heating at the superconducting coil. The DD neutrons will be shielded mainly by the water in the double walled vacuum vessel. However at the port duct where the double wall structure is not available, another neutron shield material will be required. Such a neutron shielding material is required to be resistant to the baking temperature of the vacuum vessel,  $150\sim 300^\circ\text{C}$ . The neutron shielding material, such as resin, will be installed outside the vacuum vessel of the device, between the port wall and the superconducting coils (Fig.3-26).

When the plasma quenches, a big electromagnetic force is generated in the vacuum vessel and the structure materials. Therefore, it is necessary to have mechanical strength in the neutron shielding material. In addition, lightness of the materials in the narrow part around the port section is indispensable. Neither heat resistance nor strength is found in borated polyethylene. We evaluated resins as the raw material. Ten kinds of test materials were produced. Six consisted of epoxy-based resin, two consisted of the glass fiber, one consisted of polyurethane and the last one consisted of phenol-based resin. Only the phenol-based resin and the glass fiber were useful above  $250^\circ\text{C}$ . Further

improvement of the phenol-based resin to reduce production cost was carried out.

In the next step, modification of the resin so that it will capture the thermal neutrons was investigated. At first, we tried to mix boric acid into the resin. However, it was difficult to produce neutron shielding material having more than 5cm thickness. We tried developing a neutron shielding resin by mixing boron carbide ( $\text{B}_4\text{C}$ ) with phenol-based resin that had improved heat-resistance (Fig.3-27). The density of the resin was  $1.8\text{g}/\text{cm}^3$ . The heat-proof temperature was more than  $300^\circ\text{C}$  by the determination of the temperature of deflection under load in a test according to the Japanese Industrial Standard (JIS).

Mechanical strength characteristic of the developed resin and existing neutron shielding materials are shown in Fig.3-29. The developed resin has enough mechanical strength at both room temperature and  $250^\circ\text{C}$ . The resin was compared with concrete. The volume of the resin was 1/2 that of concrete. The weight of the resin was 1/2~1/3 that of concrete. Thus, the resin used is expected to be much lighter than the concrete.

Finally, the neutron shielding performance of the developed resin using  $^{252}\text{Cf}$  neutron source was almost the same as that the polyethylene (Fig.3-28). Thus, a neutron shielding resin that could be used in a high temperature environment was developed. This resin is suitable for application to the port section of the vacuum vessel.

### Reference

Morioka, A. et al., Development of a Heat-Resistant Neutron Shielding Resin for the National Centralized Tokamak, Purazuma, Kaku Yugo Gakkai-shi, vol.81, no.9, 2005, p.645-646.

## Taking a Leading Role in Quantum Beam Technology

Quantum beams include electromagnetic waves (laser, X-ray,  $\gamma$ -ray, etc.), leptons (electron, positron, etc.) and hadrons (proton, neutron, ion, etc.), which possess the characteristics of both wave and particle. We are utilizing neutrons from research reactors, ions and electrons from accelerators,  $\gamma$ -rays, intense ultra-short pulsed lasers and synchrotron radiation, the sources of which are operated in the Kansai district, Tokai village and Takasaki city (Fig.4-1). We are promoting R&D activities as described below, making advances in science and technology and promoting industry through establishment and popularization of “quantum beam technology” as a core technology for innovation in science and technology.

### What capabilities of quantum beams should we focus upon?

The fact that each quantum interacts with an atom or molecule enables fabrication with a precision of nm (the capability to “create”). The quantum beams can also observe atomic arrangement and electronic states, and identify elements in matter, through which material properties can be explored (the capability to “observe”). Moreover, as quantum beams can locally deposit huge amount of energy, they can attack cancer cells, causing little damage to other tissues (the capability to “cure”).

### In which science and technology areas are we involved?

We promote R&D activities, mainly in the “Four Priority Fields to be Promoted” in the “Science and Technology Basic Plan”: development of a highly durable fuel cell membrane in the nanotechnology and materials area, structural analysis of proteins for drug discovery in the life sciences and biotechnology area, development of materials and technologies for environmental protection in environmental

sciences and energy area, and development of radiation-resistant semiconductors in the information and communication technology area. In addition, in the advanced medical treatment area, technique for miniaturization of particle beam radiotherapy equipment by generating proton beams with high intensity lasers is envisioned.

### What steps are we taking to promote R&D?

First, we are developing techniques to generate high quality quantum beams. We succeeded in developing the world’s highest performance supermirror for highly efficient transport and focusing of neutrons, and in generating protons up to 2.2 MeV through laser-driven acceleration.

Second, we seek to advance techniques of quantum beam application, to provide R&D results where they will lead to technological innovation and open up new possibilities. We succeeded in developing polarized neutron analysis and high magnetic field X-ray diffractometry, and applying them to determine the fine magnetic structure of magnetically frustrated compounds, and also discover a protein with new DNA repair mechanism. Moreover, as introduced in Topic 4-1, we demonstrated a new application of quantum beams to basic sciences, by proposing the existence of ferroelectric ice in the universe.

Third, for those techniques near the stage of practical use, we promote industrial application through technology transfer. For instance, we applied radiation-induced cross-linking and graft techniques utilizing electron beams and  $\gamma$ -rays to develop a mm-wave antenna substrate with low loss of electrical power, and to create a new flower variety by ion beam breeding. Moreover, we promote internal collaborations; for instance, applying neutrons and synchrotron radiation to residual stress measurement to solve issues in the Fast Breeder Reactor project.

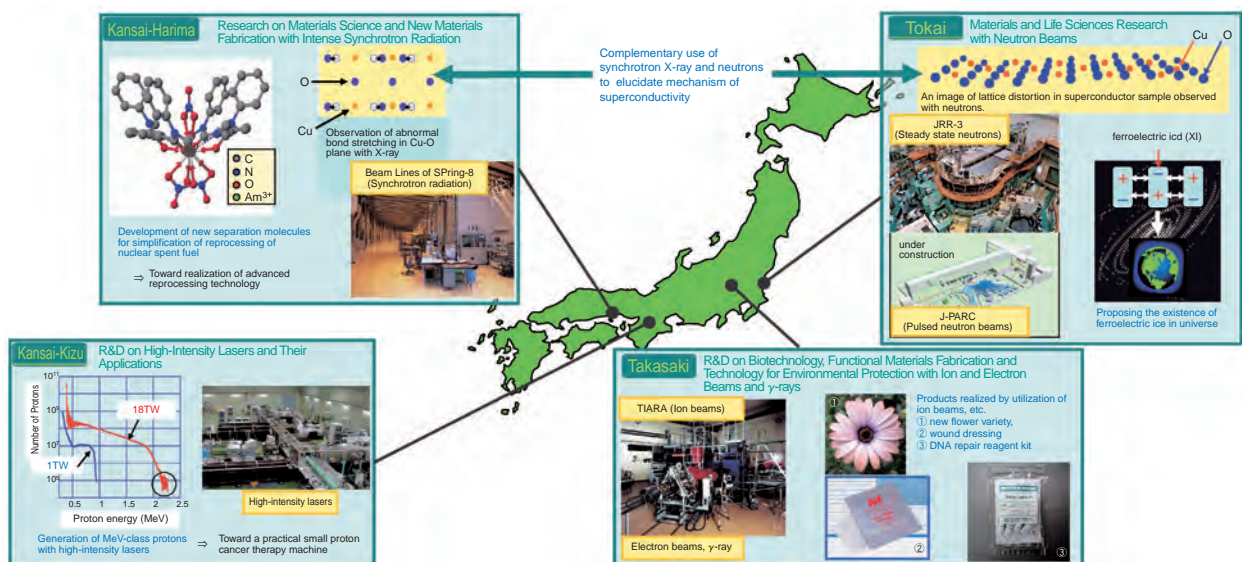
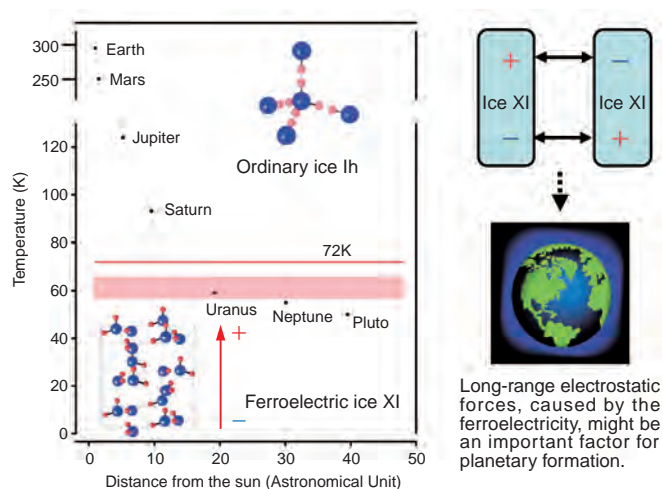


Fig.4-1 Quantum beam facilities in JAEA, with respective R&D topics

## 4-1 Study Suggests the Existence of Ferroelectric Ice in Outer Space — A Neutron Diffraction Study of Ice XI —



**Fig.4-2** The area (below the red line of 72 K) where ice XI exists as a stable form in the solar system. The red area represents temperatures (57 - 66 K) at which ice Ih is able to transform to ice XI. Uranus and its satellites are in the red area. The surface temperature of Neptune, Pluto and their satellites is cooler, but just below the surface of these objects the temperature is in the red area. Blue and red circles are oxygen and hydrogen. Since water molecules are aligned along the c-axis (vertical direction), ice XI has ferroelectricity.

Neutrons are sensitive to hydrogen (H), and a neutron diffraction study gives us accurate information about H atoms. Recently, we made an imitation of the ice of cold space and measured neutron diffraction of the ice. We found that the position of hydrogen became ordered at the temperatures (below  $-200^{\circ}\text{C}$ ) of Uranus, Neptune and Pluto. H of the water molecule ( $\text{H}_2\text{O}$ ) has a positive charge. When H is ordered, ice polarizes to have a positive and negative end and becomes ferroelectric. Based on the neutron measurements, we propose that ferroelectric ice, named ice XI, exists in the universe (Fig.4-2).

In ordinary ice, named ice Ih, H is equally distributed around adjacent oxygen atoms. Ice Ih has no polarization. On the other hand, ice XI polarizes as indicated by the red arrow in Fig.4-2. Thus, the particles of ice XI have long-range electric attraction to each other. The small ice XI of several micrometers in solar nebula may grow quickly and attract electrons and ions. This special character of ice XI becomes a key that solves the mystery of planet formation and material evolution.

The structure of ice was examined in detail by our neutron

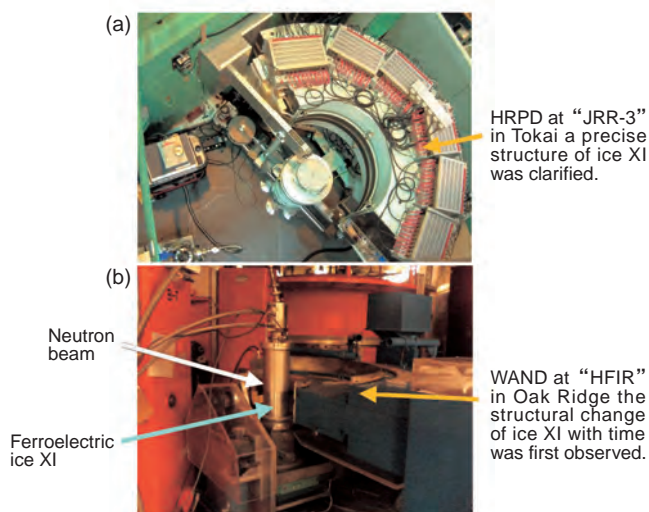


**Fig.4-3** (a) High Resolution Powder Diffractometer (HRPD) located at our research reactor (JRR-3) in Tokai. We revealed the structure of ferroelectric ice in detail using HRPD. The formation processes of ferroelectric ice were investigated by the Wide-Angle Neutron Diffractometer (WAND, (b)). WAND at the High Flux Isotope Reactor (HFIR) of the Oak Ridge National Laboratory is operated under the "US-Japan Cooperative Program on Neutron Scattering".

diffractometer (Fig.4-3(a)) in Tokai. The structural changes with time were investigated by a high intensity diffractometer (Fig.4-3(b)) at a high flux reactor of the Oak Ridge National Laboratory. From the time-resolved measurements, we found the temperature conditions for the transformation of the largest fraction of ice into ice XI using the lowest level of impurity dopant. The red area in Fig.4-2 represents temperatures (57-66 K) at which ice Ih is able to transform to ice XI. Once ice XI is formed at this temperature condition, it remains in this form at any temperature below 72 K. The ice Ih with dopant transforms to ice XI in one week. The movement phenomenon observed in this hydrogen over the course of one week is estimated to take about 10,000 years in ice without the catalyst. Therefore, ice in outer space which anneals at temperatures of 57-66 K and is kept below 72 K for 10,000 years becomes ferroelectric ice XI.

This research suggests that future telescopes will find huge ferroelectric ice in space. We expect that there is ferroelectric ice XI on Uranus, Neptune, and Pluto, their satellites, and icy objects in the outer solar system. A neutron study concerning ice forms inside these objects is underway.

### Reference

Fukazawa, H. et al., Existence of Ferroelectric Ice in the Universe, *Astrophysical Journal Letters*, vol.652, no.1, 2006, p.L57-L60.

## 4-2 Elucidation of Plant Growth Regulation by Ion Beams — The *SMAP1* Gene Regulates Sensitivity to Plant Hormone —

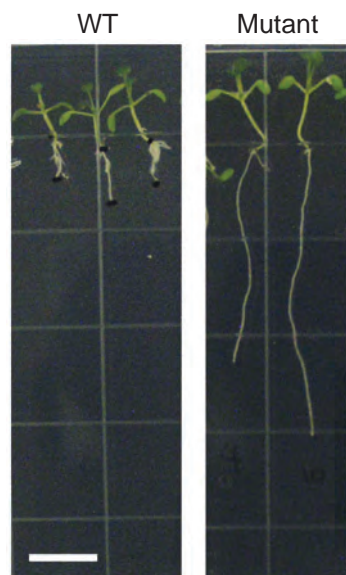


**Fig.4-4 Phenotype of the mutant**  
On a medium with 2,4 - dichlorophenoxyacetic acid (2,4-D), wild type (WT) plant exhibits short root with large number of lateral roots, whereas the ion beam-induced mutant has a long root with no visible lateral roots.

When living organisms are exposed to ionizing radiation, mutants are generated as a consequence of change in DNA sequence. Because ion beams give higher energy to a more localized area than  $\gamma$ -rays, it can delete and translocate larger DNA fragments. The characteristic effects of ion beams enable them to facilitate generation of novel mutants and greatly contribute to the research field of plant breeding.

Inducing mutants is also helpful for basic science. Numerous mutants are used for elucidating a mechanism of plant growth regulation. The number of required mutants has increased as research in this field has progressed, and the capacity of traditional mutagens such as chemical reagents to produce mutants has reached the saturation point. This fact prompted us to isolate novel mutants that are helpful in elucidating plant growth regulation by taking advantage of the characteristic effects of ion-beams.

We screened mutants exhibiting altered response to plant hormone auxin, which controls plant growth and differentiation, from approximate 30,000 Arabidopsis seedlings propagated from ion beam-irradiated seeds. We successfully obtained a mutant with novel characteristics: normal response to natural auxin indoleacetic acid (IAA) but

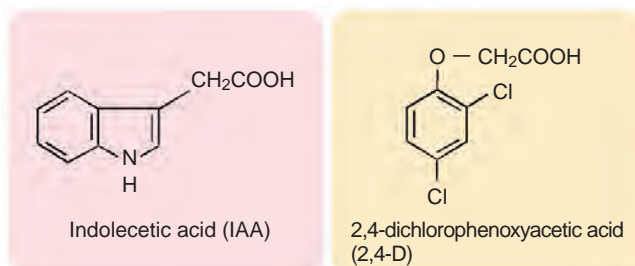


**Fig.4-5 Structure of Auxin**  
Indole-3-acetic acid (IAA) and 2,4-D are types of auxin, the most frequently used plant hormone in biotechnology and agriculture.

SMAP1	----	SMAMDVDDLEAMEILNEGGLVS	----	DNKLA	-----	DADFFNKFDDDFDDTDIN	-----
TETRAODON	GPYVDL	DEVQLCVFLWQAGGSTGLLMD-LAANEKAV	-----	HSDFFNDFEDLFDDDDI	-----		
HUMAN	GPYVDL	DEAG-----GSTGLLMD-LAANEKAV	-----	HADFFNDFEDLFDDDDIQ	-----		
XENOPUS	GPYVDL	DEAG-----GSTGLLMD-LAANEKAV	-----	HADFFNDFEDLFDDDDIQ	-----		
DANIO	GPYVDL	DEAG-----GSSGLLMD-LAANEKAV	-----	HSDFFNDFEDLFDDDDIQ	-----		
MOUSE	AQEGGGSQL	YCETHPQAGGSTGLLMD-LAANEKAV	-----	HADFFNDFEDLFDDDDVQ	-----		
DROSOPHILA	G-YMEMDESG	-----GATGMMMDHLPSNDKHV	-----	HADFFYNDFFDLFEDENWAKMKTDGKQ	-----		
RICE	PGGVNEWEDSPGEMESEAAASAVGMGMMEVDADDRHPPSSSLPIDADFFNFSFPDDFDDQDLA	-----			-----		

**Fig.4-6 Amino acid sequences of SMAPs from various organisms**

A part of the amino acid sequence of Arabidopsis SMAP1 was aligned with that of SMAPs from other organisms. Amino acids identical and similar to those of SMAP1 are marked in red and orange, respectively.

less sensitivity to synthetic auxin 2,4-dichlorophenoxyacetic acid (2,4-D) (Fig.4-4, Fig.4-5). DNA analysis revealed a 44,000 base pair deletion, which was probably caused by the ion-beam, in mutant DNA. There were ten putative genes in this deleted region. We introduced small DNA fragments derived from this deleted region one at a time to the mutants. We found a fragment that recovers the wild type phenotype and so identified the gene that is responsible for the unique auxin response of the mutant. Because the gene encodes very small and acidic protein, we named it as SMAP1 gene (Fig.4-6). Interestingly, database search revealed that the *SMAP1*-like genes are present not only in plant but also in animal genomes, implying that the *SMAP* genes might be involved in a still unknown regulatory mechanism which plays a pivotal role and has been evolutionally conserved. To date, there have been no reports about the function of *SMAP* genes. Our finding by using ion beams showed the importance of the gene in plant growth regulation. Elucidation of the molecular mechanism by which *SMAP1*-encoded protein regulates auxin-directed growth and of the roles of *SMAP* genes in other organisms are future challenges.

### Reference

Rahman, A., Oono, Y. et al., A Small Acidic Protein 1 (SMAP1) Mediates Responses of the Arabidopsis Root to the Synthetic Auxin 2,4-Dichlorophenoxyacetic Acid, *The Plant Journal*, vol.47, no.5, 2006, p.788-801.

## 4-3 Discovery of Phonons Causing Superconductivity in Diamonds — Looking for “Room Temperature-Superconductors” in Diamonds —

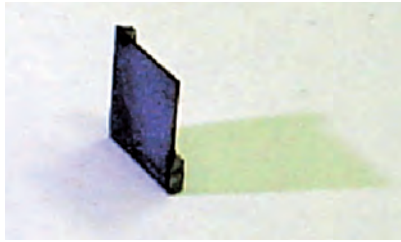


**Fig.4-7** Boron doped Diamond manufactured by a CVD method. The thickness of the sample is about 100  $\mu\text{m}$ .

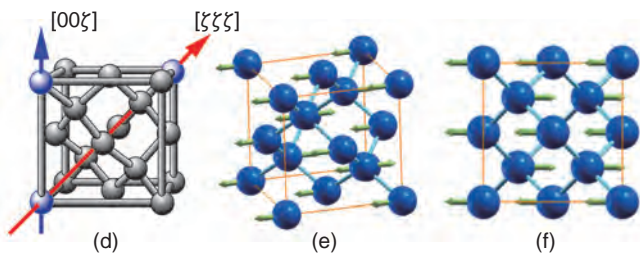


**Fig.4-9** (d):Crystal structure of diamond (e):LO-mode at  $\Gamma$ -point(shown in 3D) (f): LO-mode(top view)

It is well-known that the metal becomes a superconductor with zero resistivity at low temperatures. The mechanism of this superconductivity is believed that phonons mediate the coupling of two electrons at very low temperature, although they have minus charge repelling each other. This pair is called a Cooper-pair. Pure diamond is a wide band-gap insulator. When it is boron doped at a high concentration beyond the metal-to-insulator transition, more than  $3 \times 10^{20} \text{ cm}^{-3}$ , it shows superconductivity remarkably high temperature  $T_c$  for an impurity doped material with low carrier density. It is expected that if the mechanism of this superconductivity is made clear, the way to manufacture room-temperature superconductors will be guided. Therefore, we studied the phonon of boron-doped diamond superconductors in detail. The phonon is characterized by its (1) traveling direction, (2) magnitude, and (3) energy. The relation among them is called phonon dispersion relation. We have studied the lattice dynamics in a highly boron-doped single crystal diamond whose  $T_c$  is about 4.2 K, comparing it to that of pure diamond (Fig.4-7). We focused on the Longitudinal Optical phonon mode (LO-mode), which is the highest energy

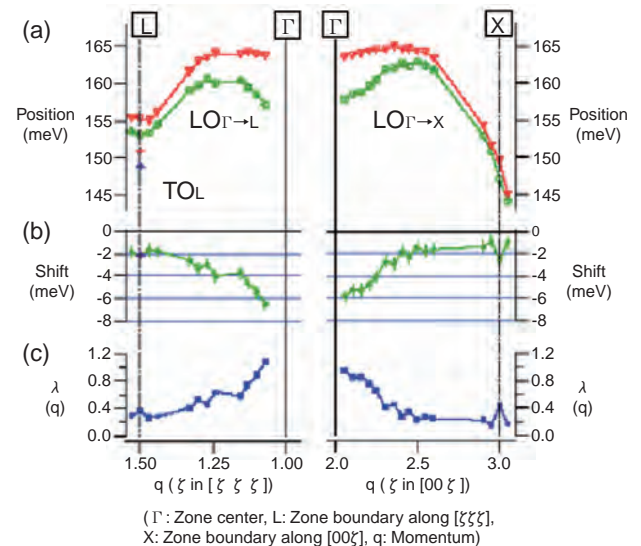


**Fig.4-8** (a): Observed LO-mode of non-superconducting diamond, N, (red), superconducting diamond, S, (green) (b): Softening curve: peak shift for sample S with respect to sample N as a function of momentum (c): Momentum dependent electron-phonon coupling parameter  $\lambda(q)$

phonon. Fig.4-8 shows the observed phonon dispersion relation of the LO-mode. Fig.4-9 (d) shows the observed phonon direction in real space relative to the cubic symmetry. As it can be seen in Fig.4-8, a difference in the phonon dispersion in non-superconducting and superconducting diamonds was observed; that is, the LO-mode is softened in a superconducting diamond. This phonon softening is purely dependent on the absolute value of the momentum  $q$  in the two high-symmetry directions. The softening is the biggest at the  $\Gamma$  point, and becomes small towards the zone boundary in both  $[\zeta \zeta \zeta]$  and  $[00\zeta]$  directions. The atomic movement at  $\Gamma$  is shown in Fig.4-9 (e) and (f) in a real space. On the other hand, no softening was observed in the acoustic phonon mode. These observations indicate that electrons are coupled to the highest energy LO-phonon mode, and this interaction could play a key role in the superconductivity of boron doped-diamonds. This observation has stimulated theoretical works to design new superconductors having higher  $T_c$ . The present work was made possible by the success in growing good single crystals and by the third generation synchrotron radiation (SR) source.

### Reference

Hoesch, M., Fukuda, T., Mizuki, J. et al., Phonon Softening in Superconducting Diamond, Physical Review B, vol.75, no.14, 2007, p.140508-1-140508-4.

## 4-4 Discovery of Activation Enhancement Mechanism of DNA Repair Promoting Gene *pprA*

### — Role of Radiation Response Protein LexA2 —

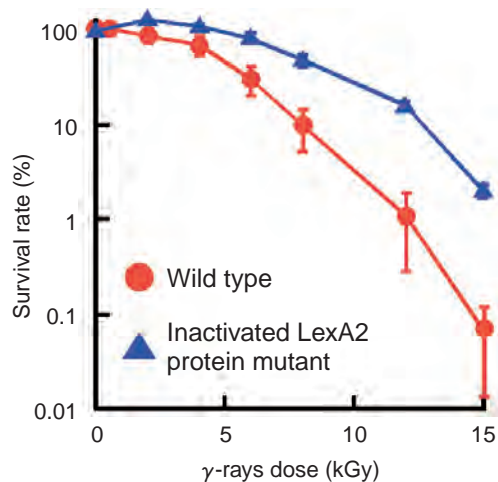


**Fig.4-10 Survival curves for  $\gamma$ -rays**

The inactivated LexA2 protein mutant strain was generated, and the  $\gamma$ -ray survival rate was investigated. The radioresistance in the inactivated LexA2 protein mutant strain was much higher than that of wild type, indicating that the DNA damage is promptly repaired in the inactivated LexA2 protein mutant strain.

The radiation response of microorganisms including their DNA repair mechanisms have actively been studied using *Escherichia coli* from 1970's. It is well known that *E. coli* possesses a mechanism of increasing the intracellular level of DNA repair proteins following radiation-induced DNA damage. RecA (Recombinase) and LexA (Locus for X-ray sensitivity) proteins play important roles in the DNA damage response and repair mechanisms in *E. coli*. On the other hand, we made clear that RecA protein contributes to the radiation response mechanism of the radioresistant bacterium *Deinococcus radiodurans*, but LexA protein is not involved. Furthermore, we identified a novel DNA repair-promoting protein PprA (Pleiotropic protein promoting DNA repair), which plays a critical role in the radioresistance. However, the relationship between RecA and PprA proteins in the radiation response mechanism remained to be elucidated.

*D. radiodurans* possesses LexA2 protein which has amino acid sequence similar to LexA. Integrating bioinformatics and molecular biology, we generated an inactivated LexA2 protein mutant strain and confirmed that the radioresistance of *D. radiodurans* was increased by the inactivation of LexA2 protein (Fig.4-10). In 1999, the whole genomic DNA sequence of *D. radiodurans* was published by The Institute for Genome Research, USA. We found that there was an

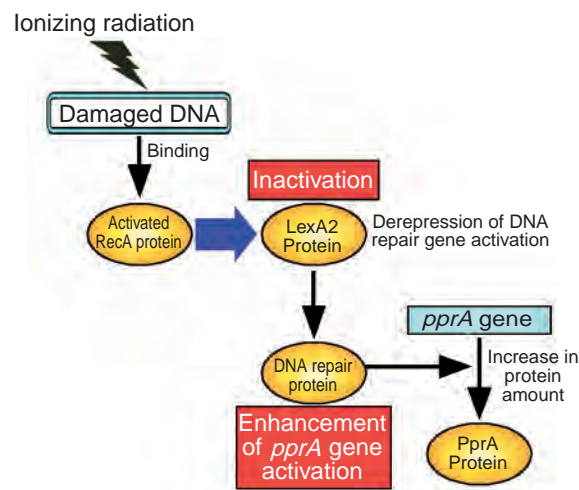


**Fig.4-11 The radiation response mechanism of *Deinococcus radiodurans***

Ionizing radiation induces DNA damage. RecA protein is activated by binding to the damaged DNA, and inactivates LexA2 protein as a repressor. Consequently, activation of DNA repair genes regulated by LexA2 protein is derepressed. Since the constitutive activation of *pprA* gene is disadvantageous for cell growth, it is usually repressed. By this derepression, *pprA* gene is activated, and damaged DNA is repaired.

error in the published sequence of *lexA2* gene region. There have been several studies performed based on the wrong sequence. After determining the correct *lexA2* DNA sequence, we investigated the characteristics of LexA2 protein that has the correct amino acid sequence in detail. As a result, we found that RecA protein is activated by its binding to damaged DNA. The interaction of activated RecA and LexA2 proteins resulted in inactivation of LexA2 protein as a repressor. Activation of DNA repair genes regulated by LexA2 protein was then derepressed. Consequently, activation of *pprA* gene was enhanced by this derepression, and thereby the intracellular level of PprA protein was increased (Fig.4-11). Thus, the increase in radioresistance of the inactivated LexA2 protein mutant strain is explained in part by this series of events.

Currently, PprA protein is being commercialized as a highly efficient DNA repair reagent. The results of this research should be applicable to improve the production efficiency of PprA protein in a manufacturing process. In future, by analyzing the crystal structure of a DNA repair protein complex, molecular mechanism of protein-protein interaction will be made clear in detail. This will lead to the development of drug discovery science using novel DNA repair protein complexes of great use for advanced medicine.

#### Reference

Satoh, K. et al., Down-Regulation of Radioresistance by LexA2 in *Deinococcus radiodurans*, Microbiology, vol.152, no.11, 2006, p.3217-3226.

## 4-5 Anomalous Spin Structure in Frustrated Magnet — Spin-Lattice Coupling Observed by a Neutron Scattering Technique —

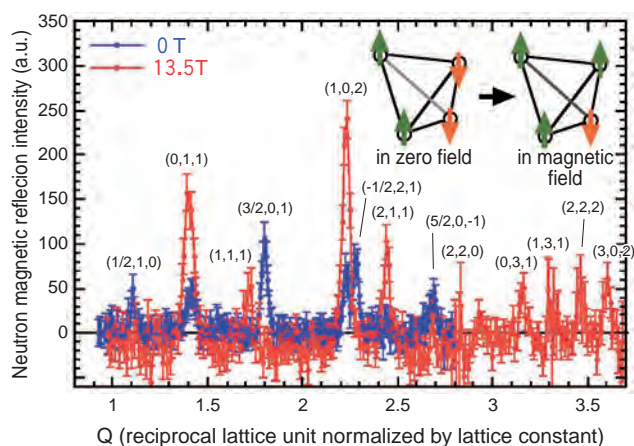


**Fig.4-12** Neutron powder diffraction patterns at 0 T (blue symbols) and 13.5 T (red symbols). Only magnetic reflections are shown. The magnetic structures were determined using magnetic structural analysis. In zero field, the spin arrangement is two-spin-up and two-spin-down in one tetrahedron. On the other hand, in the magnetization plateau phase, the spin arrangement is three-spin-up and one-spin-down.

In the spinel antiferromagnet  $\text{ACr}_2\text{O}_4$  (A: non-magnetic elements), the magnetic  $\text{Cr}^{3+}$  ions form the most frustrated lattice, a three-dimensional network of corner-sharing tetrahedra, a so-called “pyroclore lattice”. Furthermore, since  $\text{Cr}^{3+}$  has no orbital degree of freedom, the Jahn-Teller distortion is not expected and a highly symmetric cubic structure is maintained. As a result, it is predicted that magnetic ordering is suppressed down to very low temperatures due to the strong magnetic frustration. However, in real materials, a long-range magnetic ordering appears at a very low temperature, accompanying a structural distortion. This is an interesting phenomenon called “spin Jahn-Teller effect”, originating from strong spin-lattice coupling. This phenomenon is related to the spin-Peierls transition in the quantum spin system, at which spin dimers are induced by a structural distortion, and is also related to functional multiferroics, in which (anti)ferromagnetism and (anti)ferroelectricity coexist.

Another interesting phenomenon in  $\text{ACr}_2\text{O}_4$  is that a magnetization plateau is observed in a wide range of magnetic field. Theoretical studies predicted that the magnetization plateau is stabilized with strong spin-lattice coupling. However, experimental studies to determine the crystal and magnetic structures in the plateau phase have not been performed yet. We performed neutron and X-ray

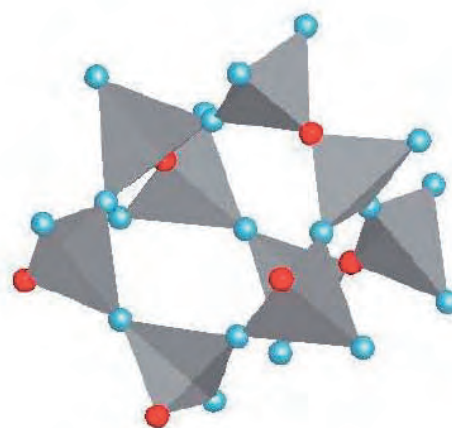


**Fig.4-13** Crystal and magnetic structures of the  $\text{Cr}^{3+}$  ions in the magnetization plateau phase in  $\text{HgCr}_2\text{O}_4$  determined by neutron and X-ray diffraction techniques. Blue and red circles represent up and down spins, respectively. The distance between the blue circles is elongated and the distance between blue and red circles is contracted. This structural distortion stabilizes the magnetic structure, indicating a strong spin-lattice coupling.

diffraction measurements in  $\text{HgCr}_2\text{O}_4$ , which has a magnetization plateau phase above  $\sim 10$  T, to elucidate the spin-lattice coupling in this interesting system.

We first performed neutron diffraction experiments in zero magnetic field at the JRR-3 facility and determined the magnetic structure. Fig.4-12 shows the typical neutron magnetic diffraction patterns at 0 and 13.5 T. With increase in the magnetic field, the neutron magnetic diffraction pattern changes at around 10 T, indicating that the magnetic structure changes dramatically. Although there were several possible magnetic structures in the plateau phase, we determined the magnetic structure uniquely, as shown in Fig.4-13, from magnetic structural analysis. Three spins out of four in one tetrahedron point in the direction of the magnetic field and one spin points opposite to the magnetic field. We also performed X-ray diffraction experiments under magnetic field at the SPring-8 facility and found that the crystal structure also changes in the plateau phase. Most importantly, the symmetry of the crystal structure is exactly the same as that of the magnetic structure, indicating that the structural distortion stabilizes the magnetic structure. Therefore, the spin-lattice coupling influences greatly not only the transition at zero field but also the field-induced transition. We clarified this important mechanism experimentally for the first time.

### Reference

Matsuda, M. et al., Spin-Lattice Instability to a Fractional Magnetization State in the Spinel  $\text{HgCr}_2\text{O}_4$ , *Nature Physics*, vol.3, no.6, 2007, p.397-400.

# 4-6 Functional Diagnosis of Photosynthesis in a Leaf

— Quantitative Kinetic Analysis of Photosynthetic Functions Using Positron Emitting Tracer Imaging System (PETIS) —

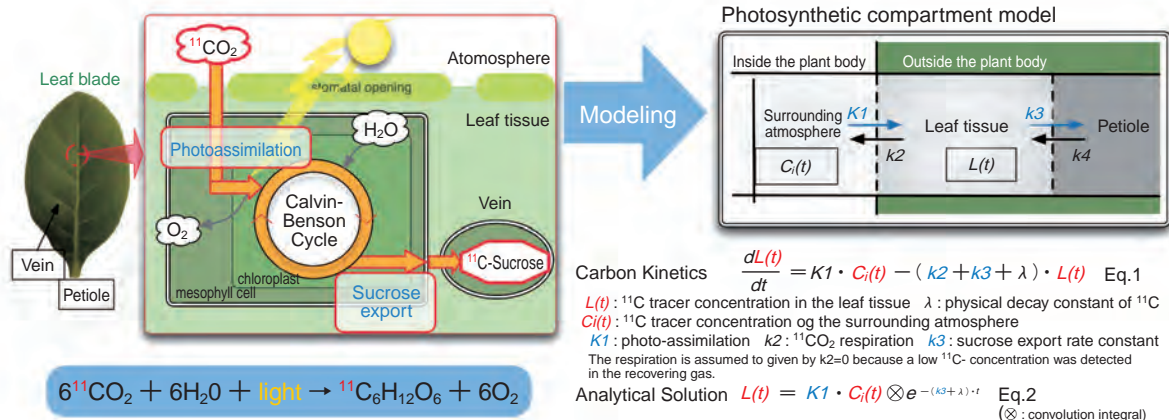


**Fig.4-14 Compartment model of photosynthesis and formulations of carbon transfer**

Carbon kinetics in a photosynthetic system (left) is simplified into three compartments, and the arrows indicate the carbon flows (right). By assuming equilibrium, the tracer balance can be expressed as Eq.1, and <sup>11</sup>C concentration in a leaf as Eq.2.

Carbon Kinetics  $\frac{dL(t)}{dt} = K1 \cdot C_i(t) - (k2 + k3 + \lambda) \cdot L(t)$  Eq.1

$L(t)$ : <sup>11</sup>C tracer concentration in the leaf tissue  $\lambda$ : physical decay constant of <sup>11</sup>C  
 $C_i(t)$ : <sup>11</sup>C tracer concentration of the surrounding atmosphere  
 $K1$ : photo-assimilation  $k2$ : <sup>11</sup>CO<sub>2</sub> respiration  $k3$ : sucrose export rate constant  
 The respiration is assumed to given by  $k2=0$  because a low <sup>11</sup>C- concentration was detected in the recovering gas.

Analytical Solution  $L(t) = K1 \cdot C_i(t) \otimes e^{-(k3+\lambda) \cdot t}$  Eq.2  
 (⊗: convolution integral)

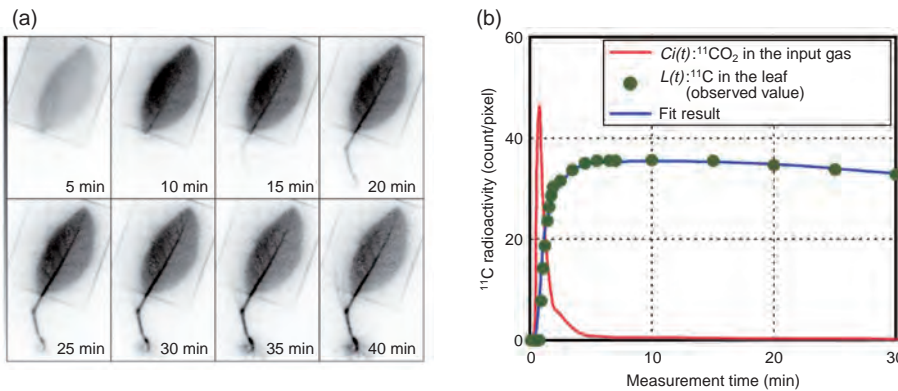


**Fig.4-15 Serial PETIS images and a graph of the time-activity**

(a) Serial images of carbon dynamics were acquired after <sup>11</sup>CO<sub>2</sub> exposure by PETIS. (b) Activity values of PETIS data over time (●) and the curve predicted by the model (—) are in good agreement.

Positron emission tomography (PET), which can image tracer dynamics, is used not only in clinical and animal studies but also in clinical practices, e.g. cancer diagnosis. In the field of plant physiology, various techniques have been developed for measuring the kinetics of the uptake of water, nutrients and environmental pollutants. However, most of the methods need invasive procedures. Hence, in order to fulfill the requirements for plant studies, the positron emitting tracer imaging system (PETIS) has been developed as a real-time monitoring scanner. To evaluate plant function quantitatively, we are studying the plant translocation systems of water and nutrients and the plant responses to environmental pollutants by observing isotope-labeled tracers with PETIS.

We have successfully imaged the carbon kinetics of photosynthesis and the export of the synthesized sucrose by using the PETIS and carbon-11-labeled carbon dioxide (<sup>11</sup>CO<sub>2</sub>). The acquired images of macro kinetics of carbon transport obtained by this measurement show a combination

of two kinds of physiological processes, i.e. photoassimilation and sucrose exporting. We devised a mathematical model based on the compartment model to analyze physiological processes that involve the exchange of the carbon compounds inside and outside a test leaf (Fig.4-14). Consequently, the observed data and the estimated curve are in good agreement, so that the present model appropriately expresses the carbon kinetics of photosynthesis, despite the use of a relatively simple model (Fig.4-15).

The newly-developed analytical method presented here is based on the compartment model of photosynthesis. Since it depicts the translocation systems of sugar and CO<sub>2</sub>, it can be applied to agricultural studies into increasing the efficiency of food production and to environmental studies into reducing the atmospheric level of CO<sub>2</sub> to solve the problem of global warming. Our imaging technique will facilitate not only basic research on plant physiology but also application of this research to resolve agricultural and environmental problems.

**Reference**

Kawachi, N. et al., Kinetic Analysis of Carbon-11-Labeled Carbon Dioxide for Studying Photosynthesis in a Leaf Using Positron Emitting Tracer Imaging System, IEEE Transactions on Nuclear Science, vol.53, issue 5, 2006, p.2991-2997.

## 4-7 Photons Create New Heavy Elements in Supernovae — Photodisintegration Reaction Nucleosynthesis in Supernova Explosions —

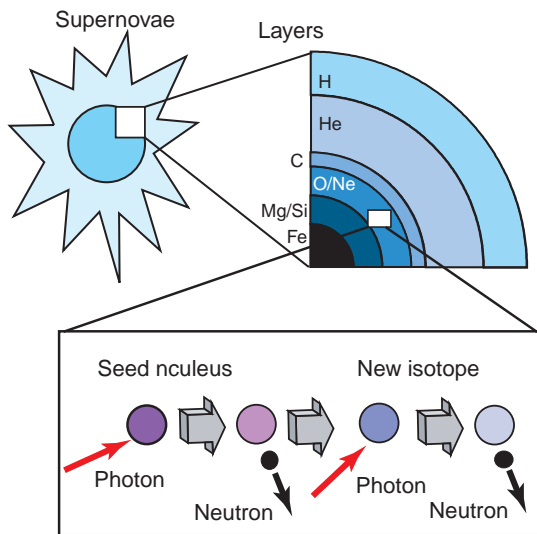


**Fig.4-16** Nucleosynthesis by photo-induced reactions in supernova explosions. New light isotopes in O/Ne layers are synthesized by photodisintegration reactions in the supernova explosions.

It has been well known that about 99% of elements heavier than the iron group were synthesized by neutron-induced reaction processes before the formation of the solar system. However, twenty-seven isotopes, so-called “p-nuclei”, can not be synthesized by the neutron-induced reaction processes. To account for the astrophysical origin of the p-nuclei, a photodisintegration reaction process in supernova explosions ( $\gamma$  process) has been proposed (Fig.4-16). Massive stars that are at least eight times heavier than our sun may have supernova explosions in the last evolutionary stage. In such explosions, new isotopes are produced by the photodisintegration reactions with high energy. We discovered an empirical law in the solar system, isotope ratios of a p-nucleus and a seed nucleus thereof that is heavier than the p-nucleus by two neutrons are almost constant. This law is the evidence that the most probable origin of the p-nuclei is the  $\gamma$  process.

There have been many stars born with various astrophysical conditions such as mass and metallicity. Our solar system was born from an interstellar medium, whose compositions originated from many stellar nucleosynthesis episodes under various astrophysical conditions. The

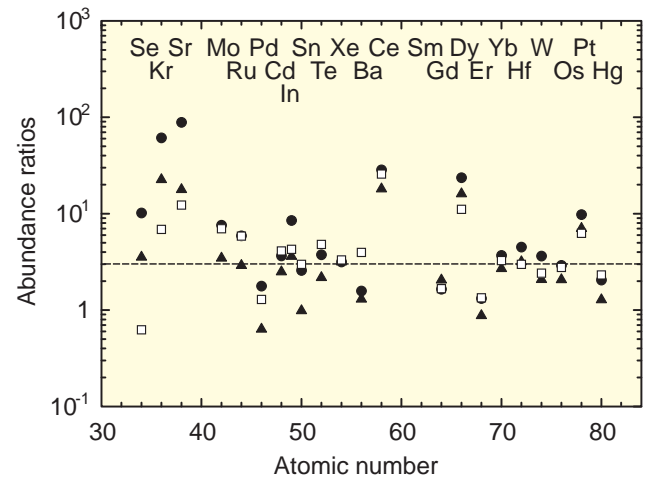


**Fig.4-17** Calculated ratios of isotopes created in supernova explosions under various astrophysical conditions. The filled circles, open squares, and triangles denote cases of a massive star, low-metallicity, and high explosion energy, respectively.

question what type of stellar nucleosynthesis dominantly affected individual isotopes of the solar system materials has remained.

To understand the mechanism of the  $\gamma$  process, we calculated nucleosynthesis models of supernovae under various astrophysical conditions such as mass, metallicity, and explosion energy (Fig.4-17). The calculated results showed that the abundance ratios of a p-nucleus to its seed nucleus are almost constant over a wide region of atomic number, even under different astrophysical conditions. Why is there such a universality which is independent of the astrophysical conditions ?

The mass of the  $\gamma$  process layer in a progenitor depends on the explosion energy and mass. Because peak temperature of the layer is, however, almost constant and independent of the explosions energy and mass, the photodisintegration reaction rates are almost constant. Therefore, the empirical law that the abundance ratios of nuclides are almost constant over the wide region holds for materials produced by individual nucleosynthesis processes. The composition of the solar system is the average of many different stellar products and hence this empirical law applies.

### Reference

Hayakawa, T. et al., Principle of Universality of  $\gamma$ -Process Nucleosynthesis in Core-Collapse Supernova Explosions, *Astrophysical Journal Letters*, vol.648, 2006, p.L47-L50.

## 4-8 Neutron Control by Magnetic Field

### — Development of Magnetic Optics to Highly Polarize and Focus Neutrons —

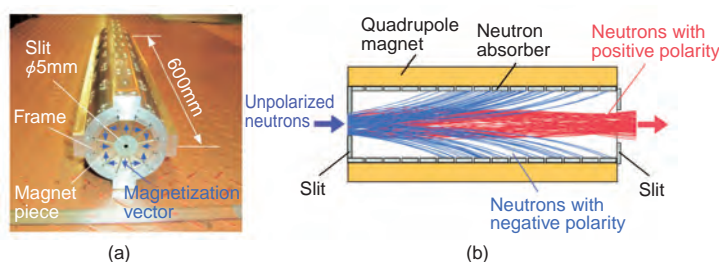


**Fig.4-18 (a) Neutron polarizer with permanent quadrupole magnet, (b) Neutron trajectory in the quadrupole magnet**

A quadrupole magnet separates unpolarized neutrons spatially into two polarized components with positive and negative spin. Highly polarized neutrons are obtained by passing one of these components through a slit.

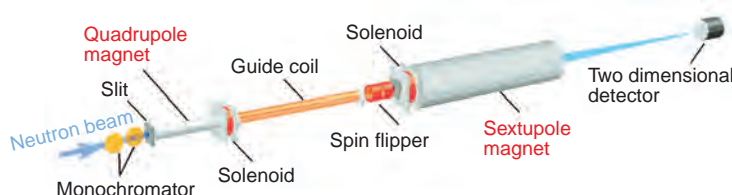


**Fig.4-19 Experimental apparatus to focus and highly polarize neutrons**

Monoenergetic neutrons are delivered to the permanent quadrupole magnet through a slit. Highly polarized neutrons selected by the quadrupole magnet are delivered to the permanent sextupole magnet through solenoids, a guide coil, and a spin flipper. The image of neutrons focused by the permanent sextupole magnet is observed with a two-dimensional detector placed in the focal plane.

A neutron is a valuable probe for the structural study of materials, which include light elements such as hydrogen atoms, or of magnetic materials, since it is scattered by nuclei and atomic magnetic moments. In order to increase the polarization of the neutron beam from about 96%, which can be obtained by a polarizer using magnetic supermirrors, to 99.9% and then apply the highly polarized neutrons to effective and precise analysis of the magnetic structure of magnetic materials, we have taken the lead in developing a neutron optical system to highly polarize and focus neutrons by using their property of being accelerated by a magnetic field gradient through the interaction between the magnetic field and the magnetic moment of neutron, and have evaluated the performance of this neutron optical system.

In the present neutron optical system we have used permanent quadrupole and sextupole magnets which produce quadrupole and sextupole magnetic fields in the beam path, to control the motion of neutron. A quadrupole magnet is superior for producing highly polarized neutrons by separating unpolarized neutrons spatially into two polarized components with positive and negative spin and so that one

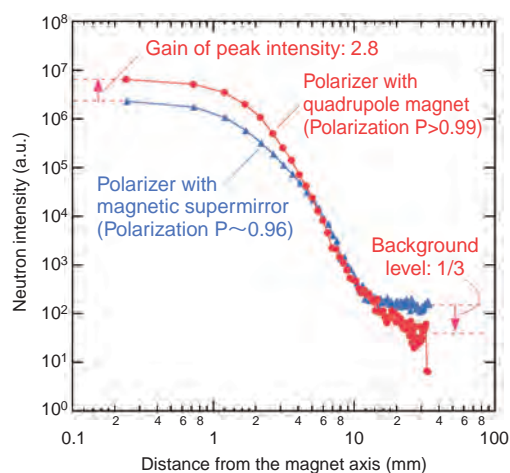


**Fig.4-20 Neutron beam profile observed with a two-dimensional detector**

The density of the polarized neutrons selected by the quadrupole magnet relative to the background level is about 10 times higher than that by magnetic supermirrors.

of these components can be selected (Fig.4-18). On the other hand, the sextupole magnet is suit to focus polarized neutrons finely at a focal point. Such fine polarization and focusing of neutrons is based on the structure of the multipole magnets, in which no materials scatters or absorbs neutrons in the beam path. We have evaluated the focusing performance of the polarized neutrons by the developed system at “JRR-3” as shown in Fig.4-19. The density of the neutrons polarized by the quadrupole magnet relative to the background level is about 10 times higher than that obtained by magnetic supermirrors as shown in Fig.4-20. We will make this developed system practical for the structural analysis of magnetic materials at JRR-3 and also improve it so that it is applicable to structural analysis using pulsed polychromatic neutrons at “J-PARC”.

This basic study on the neutron control with the multipole magnet has been performed in collaboration with RIKEN and KEK. The present study was financially supported in part by the Special Coordination Fund for Promoting Science and Technology of MEXT.

#### Reference

Oku, T., Suzuki, J. et al., Highly Polarized Cold Neutron Beam Obtained by Using a Quadrupole Magnet, *Physica B*, vol.397, 2007, p.188-191.

## 4-9 Promising Biodegradable Plastic for Industrial Applications

— OFF-ON Control of Biodegradability in Polymer with Radiation and Chemical Modifications —

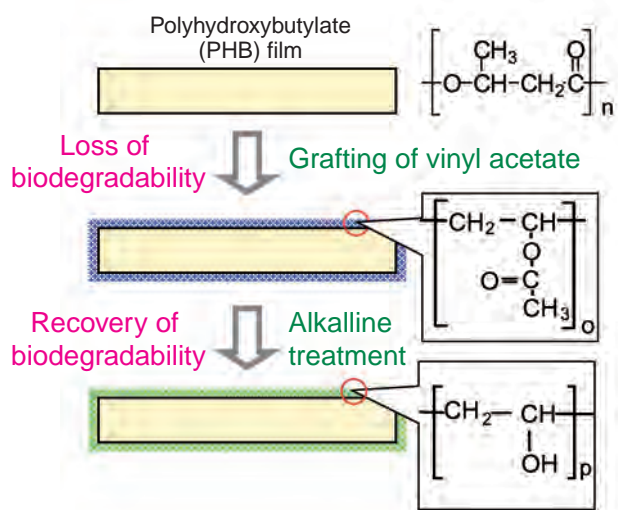


**Fig.4-21 OFF-ON control of biodegradability in PHB by graft polymerization**

Biodegradability of PHB film was suppressed by surface grafting of vinyl acetate (VAc). Alkaline hydrolysis converts grafted VAc to biodegradable polyvinyl alcohol. As a result, VAc-grafted PHB recovers its intrinsic biodegradability. This technique can provide a polymer, which is not degraded during use but which when discarded becomes degradable after alkaline treatment.

Biodegradable plastic is attractive as an environment-friendly polymer, which is finally decomposed, to water and carbon dioxide in the ground. In Japan, 6,000 tons of biodegradable plastic, 10% of world consumption, is used annually. Polyhydroxybutyrate (PHB) is biodegradable polyester, which is accumulated in the bodies of microorganisms. Though its mechanical strength is the same as that of polypropylene, PHB was rapidly degraded by native microorganisms even in anaerobic conditions. Thus, it has the ideal features of a biodegradable polymer, maintaining its mechanical strength like non-biodegradable plastic during use and having its biodegradability induced after disposal by chemical treatment.

Graft polymerization can introduce a polymer chain onto a trunk polymer, as in grafting for trees. In radiation-induced grafting, the active sites in the trunk polymer are produced with electron beams (EB) and  $\gamma$ -rays and reacted with a polymerizable reagent, so that the graft chain propagates. When vinyl acetate (VAc) was grafted on EB-irradiated PHB

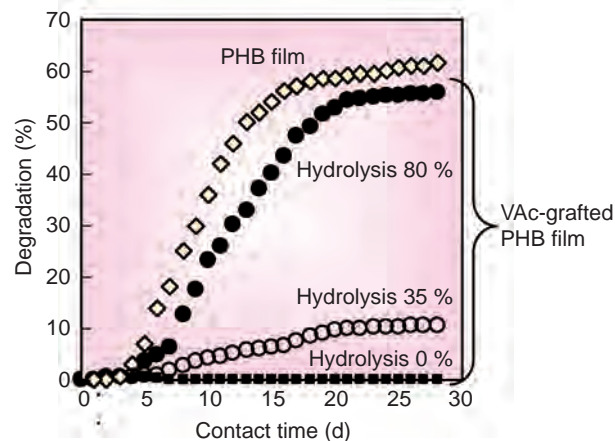


**Fig.4-22 Effect of hydrolysis on biodegradation of PHB film grafted by VAc**

VAc-grafted PHB did not show any biodegradation. Hydrolysis of VAc-grafted PHB with alkaline treatment induced biodegradation. The increment of hydrolysis increased the biodegradation of VAc-grafted PHB. Biodegradability of VAc-grafted PHB after 80% hydrolysis was equivalent to that of PHB alone.

film, a layer composed of polymeric VAc chains covered the PHB film as shown in Fig.4-21. Although PHB is biodegradable polymer, its biodegradability was lost by the overlay of non-biodegradable poly-VAc, which became 15% of PHB weight. Fig.4-22 shows the biochemical oxygen demand (BOD) of PHB film and VAc-grafted PHB films after various degrees of hydrolysis by alkaline treatment. The VAc-grafted PHB film did not exhibit any biodegradation at all. However, alkaline treatment hydrolyzes the grafted poly-VAc on the surface layer of PHB, changing the poly-VAc to biodegradable polyvinyl alcohol. As a result, VAc-grafted PHB recovered its biodegradability after alkaline hydrolysis. Hydrolysis of 80% of the poly-VAc resulted in the same level of biodegradability as that of the original PHB. Hence, the combination of graft polymerization and alkaline hydrolysis could realize the OFF-ON control of biodegradability. This technique will be applicable to a variety of biodegradable polymers in the future.

### Reference

Wada, Y., Tamada, M. et al., Biodegradability of Poly(3-hydroxybutyrate) Film Grafted with Vinyl Acetate: Effect of Grafting and Saponification, Radiation Physics and Chemistry, vol.76, 2007, p.1075-1083.

## 4-10 Direct Observation of Itinerant to Localized Transition of Heavy Electrons — Toward the Understanding of Heavy Fermion Materials —

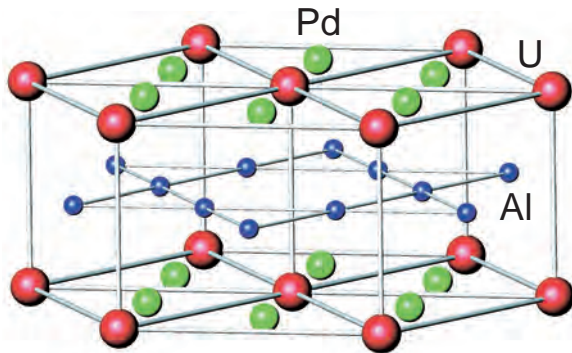


Fig.4-23 Crystal structure of UPd<sub>2</sub>Al<sub>3</sub>

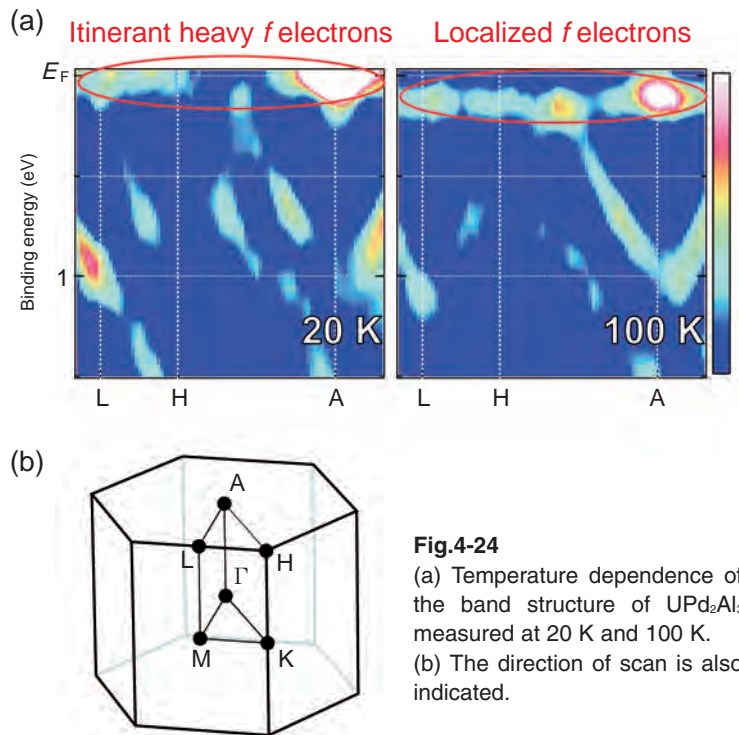


Fig.4-24

(a) Temperature dependence of the band structure of UPd<sub>2</sub>Al<sub>3</sub> measured at 20 K and 100 K.  
(b) The direction of scan is also indicated.

Electrons in solids have been conventionally classified as being either freely moving, “itinerant”, or bound to atom lattices, “localized”, depending on their properties. These opposing properties of electrons are both well understood. For heavy Fermion (HF) compounds, however, the *f* electrons display both itinerant and localized behavior depending on temperature. At high temperatures, their magnetic properties are well described by the ionic *f*-electron models, suggesting that the *f*-electrons behave as localized electrons. On the other hand, at low temperatures, their behaviors can be explained well by the “itinerant” *f*-electron model with heavy electron mass. These two models ascribe totally different natures to *f*-electrons, and how they transform between the localized and itinerant state as a function of temperature has never been understood on the level of their electronic structures. Furthermore, some HF compounds show unconventional superconductivity at very low temperatures, and have attracted much attention in recent years. Here we

studied the band structure of the HF antiferromagnetic superconductor UPd<sub>2</sub>Al<sub>3</sub> at low temperatures and high temperatures by angle-resolved photoelectron spectroscopy (ARPES), and discovered the temperature dependence of the electronic structure. Fig.4-23 shows the crystal structure of UPd<sub>2</sub>Al<sub>3</sub>. Fig.4-24 shows the band structure of UPd<sub>2</sub>Al<sub>3</sub> measured at 20 K and 100 K. At low temperature, 5*f* bands form a Fermi surface, suggesting that they have itinerant properties. On the other hand, at high temperature, the *f*-bands move toward higher binding energies, and are excluded from the Fermi surface. The present results demonstrate at the level of electronic structure how the same *f*-electrons can show both itinerant and localized behavior, and provide important information for a consistent description of the localized and itinerant nature of HF compounds. Moreover, we could clarify the band structure of HF superconductor for the first time. This is key information for the understanding of the unconventional superconductivity of HF compounds.

### Reference

Fujimori, S. et al., Itinerant to Localized Transition of *f* Electrons in the Antiferromagnetic Superconductor UPd<sub>2</sub>Al<sub>3</sub>, Nature Physics, vol.3, no.9, 2007, p.618-622.

## 4-11 Water Behavior in Concrete Observed Using Neutrons — Application to Deterioration Diagnostics of Concrete Structures —

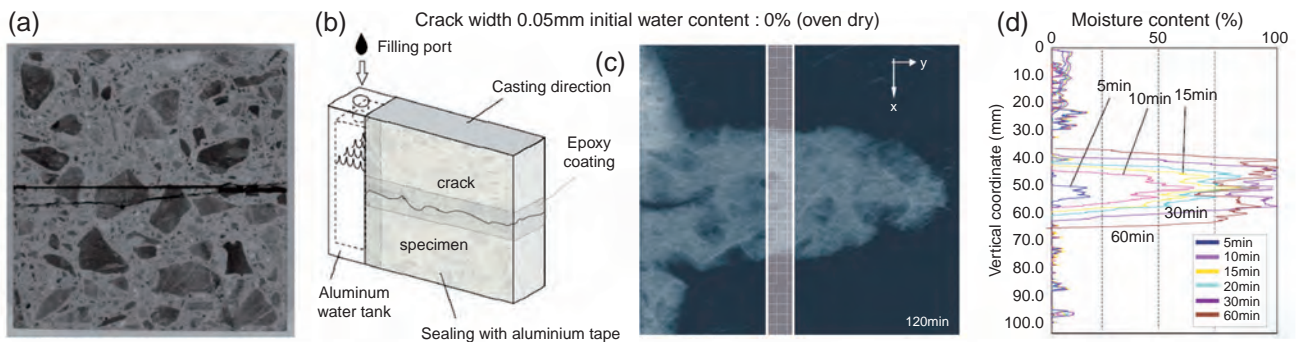


**Fig.4-25 Quantification of moisture content of concrete**

(a) Cutting plane of concrete specimen. (b) Specimen specifications. (c) Extracted image of moisture content only. (d) Change of the moisture concentration of the area sandwiched by the white lines along the vertical direction.

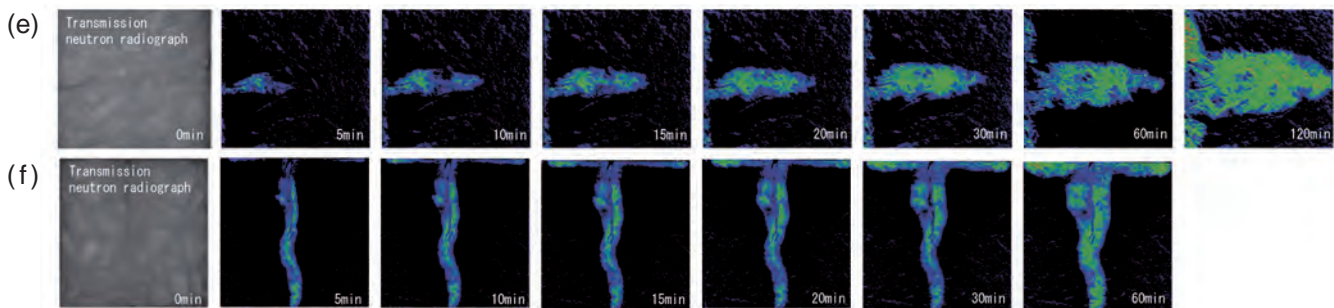


**Fig.4-26 Visualization of water behavior in a crack (e) horizontal crack (f) vertical crack**

With these images, moisture behavior in concrete can be obtained dynamically that was difficult to detect by existing method.

In Japan, improving the durability of concrete structures is one way to contribute to sustainable development of society, and it has also become a crucial issue from an environmental viewpoint. It is well known that moisture behavior in reinforced concrete is linked to phenomena such as cement hydration, volume change and cracking caused by drying shrinkage, reinforcing bar corrosion, and water leakage that affect the durability of concrete. Moisture content is commonly detected by using a humidity sensor of such material as ceramic or polymer. However, these techniques make measurements at discrete intervals with low resolution capability, and the devices are difficult to install without influencing the concrete or cement matrix system.

Fig.4-25 and Fig.4-26 show a typical image of water penetration behavior through the crack into a cementitious matrix that is successfully obtained by using the thermal neutron radiography facility (TNRF) of “JRR-3”. From these images, it is clearly confirmed that TNR can make visible the water behavior in/near the horizontal crack and can quantify the rate of diffusion and concentration distribution of moisture with high spatial and time resolution. And, by

making a detailed analysis it is observed that water penetrates through the crack immediately after pouring and its migration speed and distribution depends on the moisture condition in the concrete.

Furthermore, a lot of specialized information was obtained by using TNRF, such as moisture behavior during the cement hydration, water penetration into other building materials, and water retainment of recycled aggregate.

Thermal neutron radiography is expected to be useful as a method to detect phenomena related to building materials that cannot be grasped by the existing techniques. Also, it will contribute to more reliable design methods of newly constructed buildings and improved deterioration diagnosis techniques of existing buildings which were built during the high economic growth period.

Research into this theme has been started as one of the promotion programs of the Ministry of Education, Culture, Sports, Science and Technology in 2006, and this research was continued under the general facility research program of JAEA in 2007.

### Reference

Kanematsu, M., Iikura, H. et al., Visualization and Quantification of Water Behavior around Cracks by Neutron Radiography, Proceedings of the Japan Concrete Institute, vol.29, no.1, 2007, p.981-986 (in Japanese).

## 4-12 Detection of Electric Circuit Malfunction Caused by Galactic Cosmic Rays — Mechanism of Transient Current Induced by High Energy Heavy Ions in Semiconductor Devices —

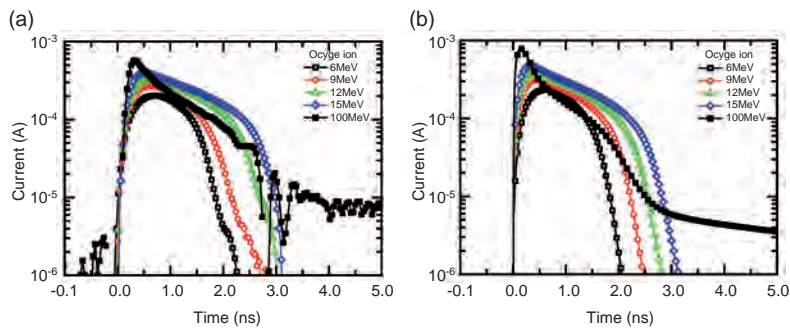


**Fig.4-27 Measured (a) and calculated (b) SET currents**

Peak values of SET current increase with increase in the energy of O ion. Simulating the carrier dynamics with a Drift-Diffusion model, reasonable agreement between measured and calculated values is obtained.

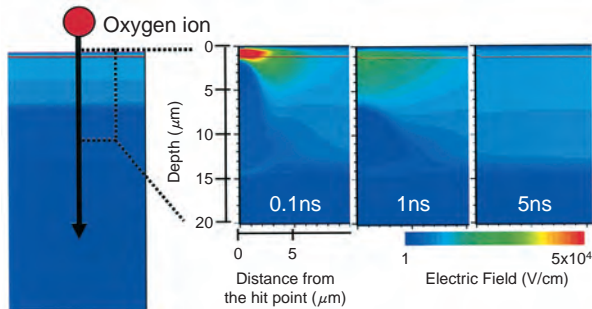


**Fig.4-28 Cross sectional images indicating the transient electric field after a 100 MeV O ion hits**

Electric field is instantaneously perturbed when the ion hits. The electric field returns to equilibrium at 5ns.

Electronic devices in space suffer from several long-term and short-term problems due to the high radiation levels. One such problem occurs when high energy heavy ions in Galactic Cosmic Rays (GCR) pass through sensitive portions of devices, where the electron-hole (e-h) pairs generated by the ion's energy loss can result in Single Event Transients (SET) that generate device damage or erroneous operation. In this study, to clarify the mechanism of GCR effect on carrier transport in junction diodes, the SET current induced by an ion was evaluated using a high bandwidth measurement system called Transient Ion Beam Induced Current (TIBIC) in conjunction with a 3 MV tandem and an AVF cyclotron accelerators. Fig.4-27 shows the measured SET currents resulting from Oxygen (O) ion with energies ranging from 6 to 100 MeV. In order to fully understand the carrier dynamics, we simulated the SET currents using the Synopsis TCAD. Since the ion initial track structure strongly affects SET current, the distributions of e-h pairs are calculated by considering the  $\delta$ -electron production with MeV ion penetration and keV  $\delta$ -electron transmission theory, instead of the cylindrical track structure generally accepted. As a result, the total collected charge obtained by time integration of SET current agrees well with the measured charge, errors being less than 10%.

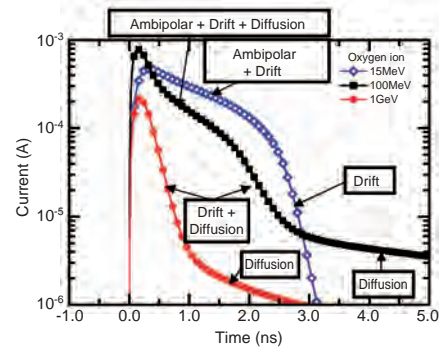


**Fig.4-29 Simulated transient current caused by O ions with energies of 15 MeV, 100 MeV, and 1 GeV**

Transient current is composed of ambipolar diffusion, drift, and diffusion currents.

Fig.4-28 shows two dimensional maps of the electric field after an O ion hits. We find that the electric field is instantaneously perturbed and the transient current is composed of ambipolar diffusion, drift, and diffusion currents. As shown in Fig.4-29 the contribution of these components to SET current waveform depends on the ion energy; that is, in the case of 15MeV O ions (1) the sum of ambipolar diffusion and drift currents and (2) only drift current, in the case of 100MeV (1) the sum of ambipolar diffusion, drift, and diffusion currents, (2) sum of drift and diffusion currents, and (3) only diffusion current. While energies used here are not high enough to simulate the energy spectrum of GCR, we predict the SET current due to GeV ions with the assistance of TCAD simulation. In contrast with 15 and 100MeV, in case of 1GeV, the ambipolar diffusion current does not flow any more, and the sum of drift and diffusion currents comprises the SET current waveform as shown in Fig.4-29.

By using TCAD simulations with carefully optimized models and parameters, the carrier dynamics and the energy dependence of SET current have been revealed. These results, together with further investigation, will aid future design of electronic devices intended for space applications.

### Reference

Onoda, S. et al., Transient Currents Generated by Heavy Ions with Hundreds of MeV, IEEE Transactions on Nuclear Science, vol.53, issue 6, 2006, p.3731-3737.

## 4-13 Clear Observation of Poorly Visible Objects Using High-Function X-rays — Generation of High-Brightness, High-Contrast X-rays by Terawatt Laser —

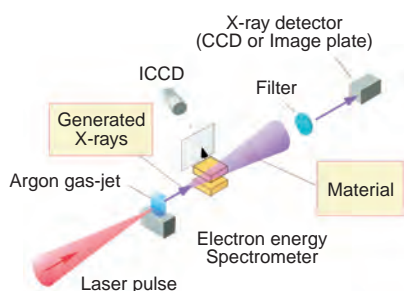


**Fig.4-30 A schematic of laser-plasma X-ray generation device**

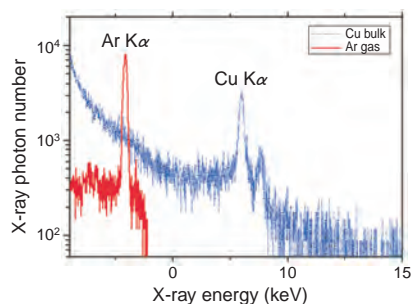


**Fig.4-31 Obtained X-ray spectrum (red)**

For comparison, an X-ray spectrum obtained with a previous laser-plasma X-ray device is also shown (blue).

In X-ray imaging, the absorption contrast method is usually used, in which an image is formed by intensity variations due to absorption of X-rays in a material. However, it is difficult to observe soft tissue or small animals clearly and in detail because of their low absorption efficiency. Therefore, the phase contrast method, in which the change of refraction of X-rays in the material instead of absorption is detected, becomes an alternative. It requires X-rays having good spatial coherence. Thus, a specially designed X-ray tube, a synchrotron light source from a large-size accelerator, or laser-plasma X-ray source are used for the purpose.

However, the X-ray tube and laser-plasma X-ray source are small but less bright, while the synchrotron radiation source is bright but huge, therefore a new X-ray device which is bright and compact is demanded.

In this study, we have developed such a new device by optimizing the conditions of laser irradiation. In a laser-plasma X-ray source, a laser irradiated on materials produces plasma, and then the accelerated electrons excite ions, which radiate X-rays through atomic transitions. The previous X-ray source produced some undesirable Bremsstrahlung, and thus the desired X-ray had low brightness. We succeeded in maximizing the X-ray photon numbers in the required spectral region by reducing the prepulse which is large in high intensity lasers and by controlling the focus position.

(a) Absorption contrast



(b) Phase contrast



**Fig.4-32 Absorption contrast (a) and phase contrast (b) imaging using the X-ray device**

These measures are effective in reducing undesired Bremsstrahlung X-rays, because the appropriate energy is thereby transferred to electrons. As shown in Fig.4-30 and Fig.4-31 Terawatt, 70 fs pulse width Ti: sapphire laser pulses were focused onto an Ar gas jet. We obtained high-contrast X-rays; that is, undesirable X-rays were suppressed and the desired X-rays had a higher intensity, as seen in Fig.4-31. This new X-ray source enables us to reduce the total X-ray dose on a material or living body and obtain sharp images. In addition, the peak brightness is  $10^{20}$  photons/s/mm<sup>2</sup>/mrad<sup>2</sup>, which is comparable to that of the synchrotron radiation. Because the pulse duration of this source is estimated to be on the order of 100 fs, it can be utilized to measure ultrafast phenomena.

We attempted absorption and phase contrast imaging of spiders with this source (Fig.4-32). Fine structure that cannot be seen in the absorption contrast image can be seen in the phase contrast image. Thus, we have demonstrated that this new X-ray source is suitable for phase contrast imaging.

This X-ray source produces spatially coherent, high brightness, high contrast X-rays. When this device is used in phase contrast computed tomography, it allows us to observe fine structure and reduces undesirable background X-ray dose to patients, and so this device is expected to be a useful new medical tool.

### Reference

Chen, L. M., Kando, M. et al., Phase-Contrast X-ray Imaging with Intense Ar  $K\alpha$  Radiation from Femtosecond-Laser-Driven Gas Target, Applied Physics Letters, vol.90, 2007, p.211501-1-211501-3.

## To Enforce Safety Regulations and to Ensure Nuclear Safety and Confidence

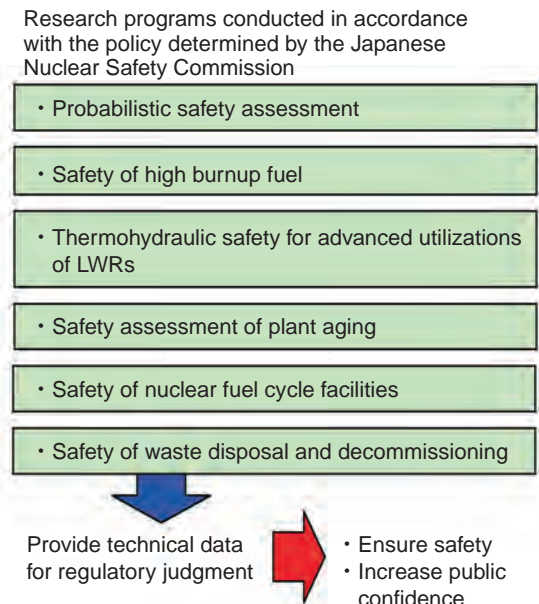


**Fig.5-1 Major tasks and roles of Safety Research**

To ensure the safety of nuclear installations, the regulatory authorities conduct strict investigations and inspections. Nuclear safety research is necessary to improve the safety regulations. The latest scientific and technical knowledge is essential for the development and improvement of the safety guidelines and regulatory criteria.

The Nuclear Safety Commission (NSC) proposed a “Prioritized Plan for Nuclear Safety Research” in July 2004, to be carried out in order to meet the future regulatory needs. The main tasks expected for us to accomplish are shown in Fig.5-1.

The results of nuclear safety research contribute to the maintenance and improvement of safety of the nuclear facilities and also to fostering public confidence in nuclear safety.

We have conducted various safety studies based on the Prioritized Plan for Nuclear Safety Research and have obtained many results in each field. In our research on risk-informed safety management in nuclear power plants, we developed a procedure for uncertainty analysis of source terms that is important for applications of PSA results such as the comparison of risk with safety goals (Topic 5-1). In the study on high burnup fuel safety, it was clarified that hydrogen absorption by the clad makes fuel failure possible under accident conditions (Topic 5-2). In addition, regarding fuel failure during reflooding by Emergency Core Cooling System, we have revealed that cladding gets brittle when it is slowly cooled to relatively low temperature before quench (Topic 5-3). In the safety assessment of advanced uses of a light water reactor, the possible enhancement of the boiling heat transfer by the wettability enhancement on the fuel clad surface due to the irradiation has been proved experimentally using the Japan Material Testing Reactor (Topic 5-4). We received awards from the Atomic Energy Society of Japan in

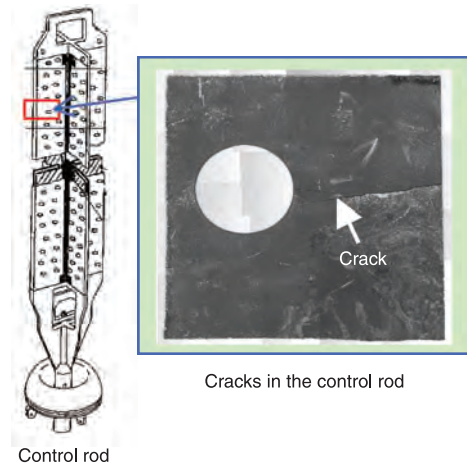


**Fig.5-2 Contribution to the investigation of cracks in the control rods with hafnium plates**

We carried out the investigations of cracks and damages in the control rod with hafnium plates at Unit 6 of Fukushima Daiichi Power Station, Tokyo Electric Power Company. The results were referred to in the investigation report (published on May 2006) by the Nuclear and Industrial Safety Agency (NISA).

2006 for these results. For research on the structural integrity assessment of reactor components, we have developed a probabilistic fracture mechanics analysis program, PASCAL ver.2, which considers the scattering and uncertainties of loads applied to the vessel, fracture toughness, and frequency of cracks with non-destructive examination and evaluates the conditional fracture probability of reactor pressure vessel (Topic 5-5). For research on safety evaluation of nuclear fuel cycle facilities, we have developed a high-precision criticality safety evaluation method that is applicable to 5% to 10%  $^{235}\text{U}$ -enriched uranium fuel cycle facilities expected in the future (Topic 5-6). Moreover, data of the thermal properties of additional material required for prediction of a criticality accident in the powder preparation process of a fuel fabrication plant was acquired (Topic 5-7). In the field of radioactive waste disposal and decommissioning safety research, radionuclide migration experiments were performed at a depth of 240 m under international collaboration with AECL to demonstrate retardation of radionuclide migration deep underground (Topic 5-8). We developed the probabilistic assessment code system (PASCLR ver.2) for evaluating the radionuclide concentrations (clearance levels) at which radioactive materials do not need regulatory control. The results calculated by this code will contribute to the future establishment of clearance levels for the uranium and TRU wastes by the regulatory body (Topic 5-9).

Moreover, we carried out the investigations of cracks and damages in the control rod with hafnium plates at Unit 6, Fukushima Daiichi Power Station, Tokyo Electric Power Company (TEPCO) in cooperation with the Japan Nuclear Energy Safety Organization (JNES), based on a request from the Nuclear and Industrial Safety Agency (NISA). The causes of crack generation and mechanisms of its growth were clarified by analysis (Fig.5-2).

## 5-1 For Risk-Informed Safety Management in Nuclear Power Plants — Development of the Procedure for Uncertainty Analysis of Source Terms —

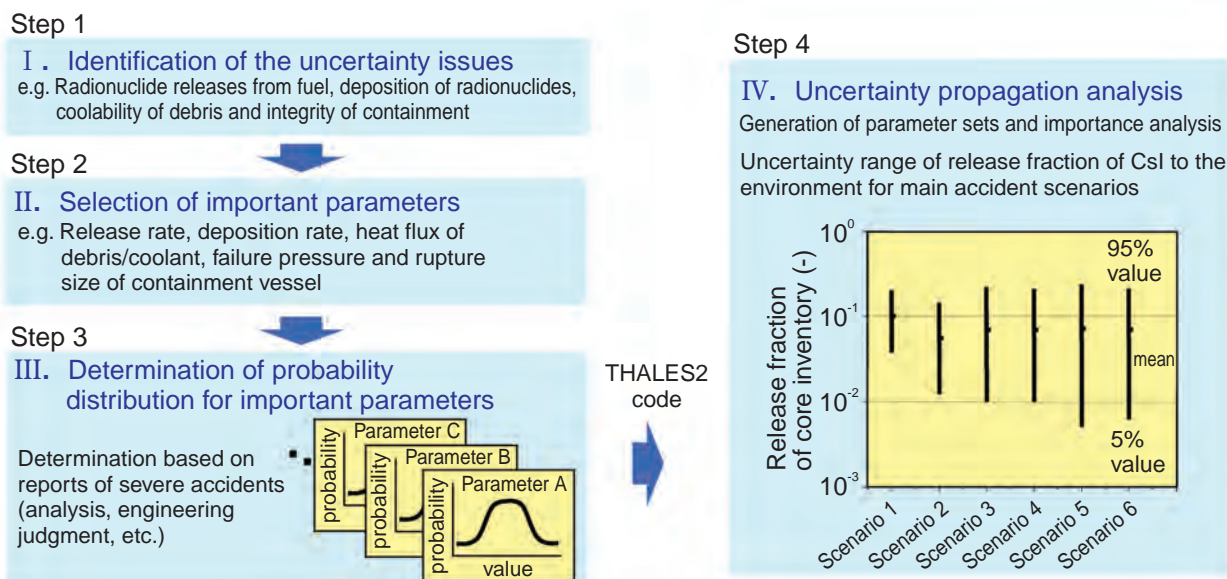


**Fig.5-3 Procedure of the uncertainty analysis of source terms and an example of results**

This procedure consists of four steps: "Identification of the uncertainty issues", "Selection of important parameters", "Determination of probability distribution for important parameters" and "Uncertainty propagation analysis". The result is obtained in the form of the cumulative probability distribution. The final result is represented by 5% , 95% and mean values.

Recently, the use of probabilistic safety assessment (PSA) methods is making rapid progress in the safety regulation and risk management of nuclear power plants in Japan. For the sake of maintaining the quality of PSA results, the Standards Committee of the Atomic Energy Societies of Japan (AESJ) is developing the standards for PSA procedures. Uncertainties should be considered in applications of PSA results such as the comparison of risk with safety goals.

In a PSA, source terms, defined as the timing and the characteristics of radionuclide release into the environment, are evaluated by using severe accident analysis codes which simulate thermal hydraulic and radionuclide behavior in the plant. Because of the complexity of severe accident phenomena and the computer resources thus needed, development of an efficient procedure of uncertainty analysis was needed. Therefore, we proposed a procedure for uncertainty analysis of source terms using the severe accident analysis code THALES2, and applied this procedure to the source term analysis of a BWR-5/Mark-II plant. This procedure consists of four steps. First, we identified

uncertainty issues that might have strong influence on source terms. We divided the progress of a severe accident into four stages, and selected important factors in each stage systematically. Next, we selected important parameters that can contribute to the uncertainty of each uncertainty issue. Then, the probability distributions of these important parameters were determined by surveying existing experimental and analytical studies. Finally, the uncertainties of these parameters were used to make estimates by the Monte Carlo method.

The uncertainty analysis was performed for six containment vessel overpressure-caused failure scenarios. Fig.5-3 shows the calculated release fractions of Cesium Iodide (CsI) to the environment. From these analyses, it was found that the release fractions of CsI to the environment (mean value) for all six scenarios are about 10% of the initial core inventory and the uncertainty ranges from one to two orders of magnitudes. This application confirmed the usefulness of this procedure. This procedure was reflected in the above-mentioned AESJ operations standards for level 2 PSA.

### Reference

Ishikawa, J. et. al., Uncertainty Evaluation of Source Terms under Severe Accident Conditions at LWRs, Nippon Genshiryoku Gakkai Wabun Ronbunshi, vol.5, no.4, 2006, p.305-315 (in Japanese).

## 5-2 Evaluating the Influence of Hydrogen Absorption in the Clad on Fuel Failure — Failure of High Burnup Fuel in Reactivity Initiated Accident —

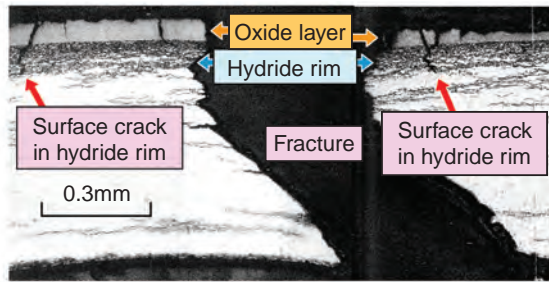


**Fig.5-4 Cross-section of high burnup PWR fuel clad which failed in the NSRR test**

The NSRR can simulate a Reactivity Initiated Accident (RIA). Embrittled clad of the high burnup PWR fuel failed in the test.

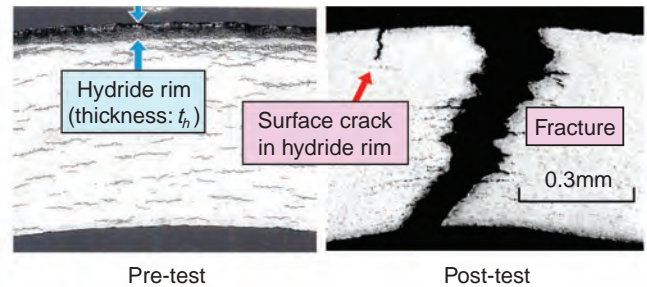


**Fig.5-5 Failure of fresh fuel with artificial hydride rim**

The influence of hydride rim on fuel failure was evaluated with fresh fuels with artificially produced hydride rim. The tests reproduced fracture features observed in the high burnup fuels, indicating that the hydride rim plays a key role in the high burnup fuel failure.

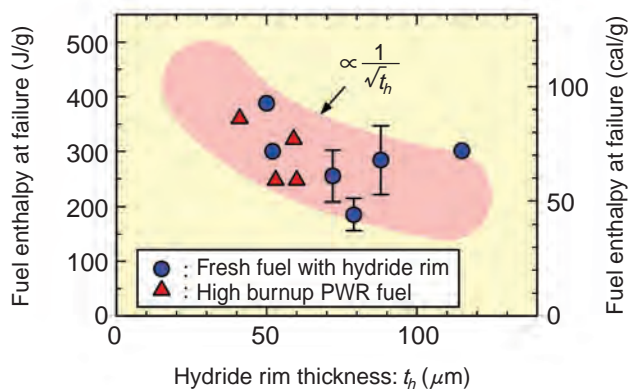


**Fig.5-6 Relation between hydride rim thickness and fuel enthalpy at failure**

The vertical axis denotes the fuel enthalpy at which fuel failed, an index for the fuel performance in RIA. Two test series show a consistent tendency, i.e., inverse proportion of fuel enthalpy to the square root of the hydride rim thickness ( $t_h$ ), which indicates the linkage with the stress intensity factor at the tip of a surface crack with a depth equal to  $t_h$ .

Extending the fuel utilization period in light water reactors, i.e. fuel burnup extension, is being promoted for more efficient use of the uranium resource and so on. The long-term use, however, increases the fuel clad corrosion and fission product accumulation in the fuels. Hence, the safety of burnup extension should be confirmed under accident conditions as well as under normal operation conditions. To determine high burnup fuel behavior and failure conditions in a Reactivity Initiated Accident (RIA), we have performed RIA-simulating power burst tests at the Nuclear Safety Research Reactor (NSRR).

Fig.5-4 shows a cross-section of the PWR fuel clad, which failed due to pellet thermal expansion at a power burst in the NSRR test. High burnup fuels typically have an oxide layer at the clad outer surface due to long-term contact with coolant water. As the hydrogen generated in the surface oxidation process was absorbed into the clad, the excess hydrogen precipitated mainly under the oxide layer and formed a “hydride rim” which is not as fragile as the oxide, but has higher brittleness than the normal regions.

Previous studies showed that the fuel can fail at lower fuel enthalpy, i.e. with smaller pellet expansion, when the clad oxide is thicker. The present study, however, focused on the influence of the hydride rim rather than the oxide layer, and performed RIA tests using a fresh fuel rod with an artificially produced hydride rim only. Fig.5-5 shows examples of the pre- and post-test clad cross-sections. The fracture shape and surface cracks observed in the case of the high burnup fuels were reproduced, indicating that the hydride rim plays a key role. In the relation between the hydride rim thickness ( $t_h$ ) and the fuel enthalpy at failure in Fig.5-6, results from the two test series show a consistent tendency of fuel enthalpy at failure being in inverse proportion to the square root of  $t_h$ . This curve can be explained as being due to the stress intensity factor at the surface crack tip, if the crack depth is regarded as  $t_h$ . Thus, it is suggested that the surface cracks in clad hydride rim are generated in the early stage of RIA, and one of them grows due to the stress concentration and results in a fracture. The knowledge obtained from this study will be reflected in advanced safety evaluation methods for RIA.

### Reference

Tomiyasu, K., Sugiyama, T. et al., Influence of Cladding-Peripheral Hydride on Mechanical Fuel Failure under Reactivity-Initiated Accident Conditions, Journal of Nuclear Science and Technology, vol.44, no.5, 2007, p.733-742.

## 5-3 Degradation of Cladding Ductility Affected by Cooling History

### — Effect of Cooling History on Cladding Ductility under LOCA Conditions —

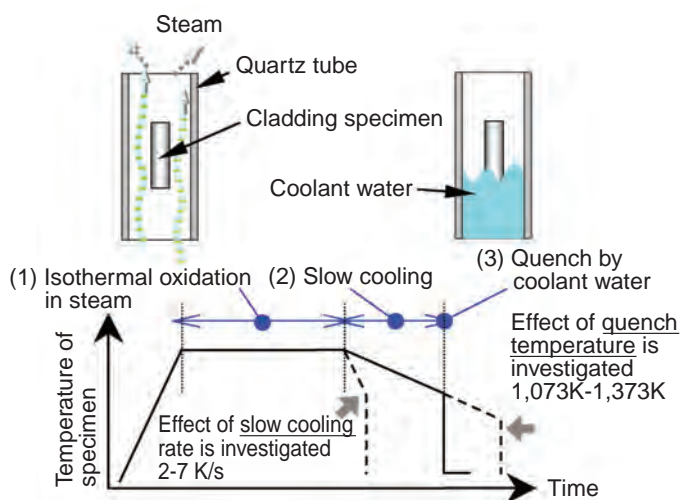


**Fig.5-7 Oxidation and quench test to simulate LOCA conditions**

Steam is supplied into the quartz tube and the cladding specimen is heated to 1,373K. After isothermal oxidation, steam supply is stopped and the specimen temperature is slowly lowered (slow cooling). Finally, coolant water is supplied to quench the specimen. These tests were conducted with different rates of slow cooling and quench temperatures. The oxidized specimens were subjected to the ring-compression test, in which a specimen was compressed in its radial direction, to investigate their ductility.

Loss-of-coolant accident (LOCA) is one of the postulated accidents in the safety design of a nuclear power plant. In a LOCA condition, the fuel temperature increases until the Emergency Core Cooling System (ECCS) starts to quench the fuel bundle in a few minutes. The water level in the reactor vessel is recovered by ECCS and the overheated fuel is cooled. A fuel rod consists of Uranium dioxide pellets and Zircaloy tube (cladding). When the cladding is severely oxidized and embrittled due to long time exposure to steam at high temperatures, fuel fracture might occur by thermal shock during the quench. Fuel fragments can block coolant channels and reduce coolability of the reactor core.

To avoid embrittlement of the fuel cladding, which would be dangerous in a LOCA, the safety criteria limits of the peak cladding temperature and of the ratio of the thickness of oxidized cladding were determined. These safety criteria were determined based on tests simulating the steps of a LOCA to clarify the conditions in which fracture occurs. In these tests, heated and oxidized cladding is slowly cooled and then quenched by re-flooding water. Simulation of the slow cooling process before the quench was considered necessary because the post quench ductility of the cladding might be affected by the change of cladding microstructure which is caused by the diffusion of oxygen atoms during slow cooling process. Data, which showed the effect of slow cooling on cladding ductility after quench were limited, and the

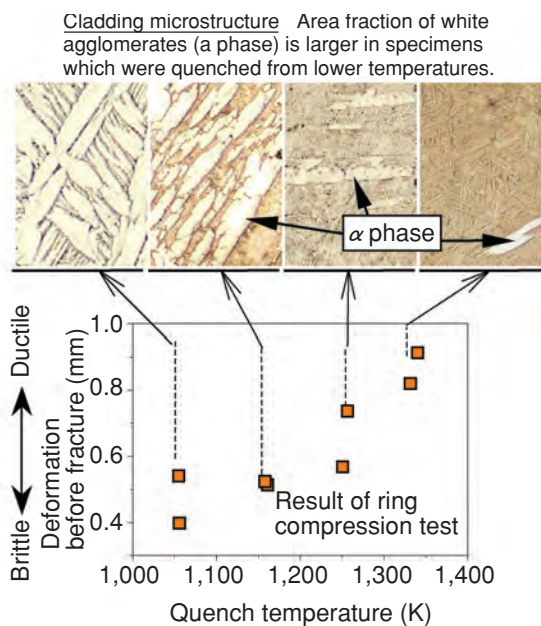


**Fig.5-8 Correlation between quench temperature and cladding ductility**

Ductility change of cladding specimens with different quench temperature was investigated. The ductility decreases with decrease in the quench temperature.

conditions under which the cladding ductility changes were not clear.

In the present study, cladding specimens were oxidized in steam at high temperatures, cooled slowly, and quenched by water flooding (Fig.5-7). These tests were conducted with different rates of slow cooling and quench temperatures in order to investigate their effects on the post quench ductility of the cladding. As a result, it was found that the post-quench ductility decreased with decrease in the quench temperature as shown in Fig.5-8. On the other hand, the effect of the slow cooling rate was negligible. In the metallurgical examination after oxidation (Fig.5-8), the area of the  $\alpha$  phase region, which appeared to be a white agglomerate, was large in the embrittled cladding specimens. The  $\alpha$  phase region is oxygen-rich, hard, and brittle compared to the matrix region around the agglomerates. The ductility reduction with the quench temperature decrease can be attributed to the relative increase in the area of  $\alpha$ -phase regions, which can be a preferential path for crack propagation.

LOCA-simulated experiments regarding fuel safety have been conducted with slow cooling processes. The present results indicate that the slow cooling processes give conservative conditions regarding cladding ductility. The present study provided useful information to establish an experimental method appropriate for the safety evaluation.

#### Reference

Udagawa, Y. et al., Effect of Cooling History on Cladding Ductility under LOCA Conditions, Journal of Nuclear Science and Technology, vol.43, no.8, 2006, p.844-850.

## 5-4 Boiling Heat Transfer Enhancement by Irradiation

### — Improvement of Critical Heat Flux by Radiation Induced Surface Activation —

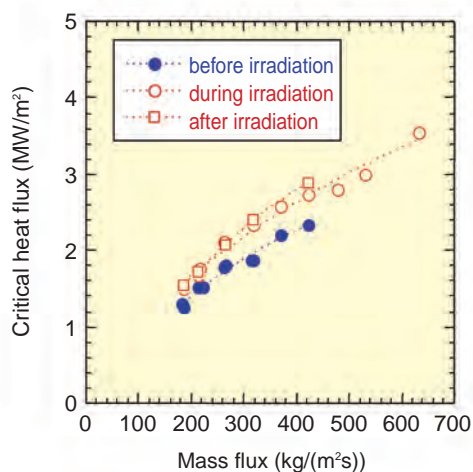


**Fig.5-9 Comparison of critical heat flux**

The critical heat flux increased during and after irradiation in JMTR core under forced convection boiling conditions.

The Radiation Induced Surface Activation (RISA) effect is now drawing significant research interest because it may enhance the wettability and coolability of an irradiated surface. The RISA effect, caused by the photochemical activation of an oxidized metal surface by heavy irradiation, was discovered recently. A large amount of a cumulative irradiation dose is required for the effect to appear. The heavy irradiation environment in a nuclear reactor should effectively improve the wettability and coolability, especially on the fuel rod surface. We have conducted an experimental study using the Japan Materials Testing Reactor “JMTR” in JAEA to investigate the applicability of the RISA effect to enhance heat removal under critical cooling conditions.

Boiling Water Reactor (BWR) is designed so that the fuel rod surface is always covered with continuous liquid film to prevent the excessive increase of surface temperature that occurs when there is depletion of liquid film, so-called dryout, which may pose a threat to fuel integrity. The maximum thermal power, at which a thin liquid film can exist on the fuel rod surface, is defined as the critical power in the thermal hydraulic design, which determines the operational power range of BWR.

The critical heat flux (CHF), defined as the critical power for a unit area of fuel rod surface, is usually evaluated by empirical correlations based on the extensive experimental data. In a recent experiment, it was learned that the CHF is dependent on the surface properties including the wettability. If the critical power is increased by the wettability enhancement due to the RISA effect, it may provide an additional margin to the nuclear fuel design and should be favorable for operational power uprate. The previous research

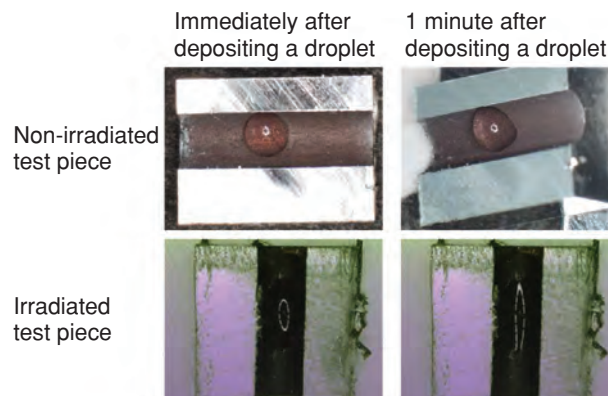


**Fig.5-10 Water droplet contact condition on test piece**  
Surface wettability of a flow channel of a water droplet changes to super-hydrophilic after a large cumulative irradiation in JMTR.

on the RISA effect using small irradiation facilities did not provide experimental evidence for increasing the CHF in the forced flow boiling condition.

Our experiments tested a water up-flow through a small diameter channel concurrent with gamma and neutron irradiation in the JMTR. These experiments were unique in that they dealt with forced flow boiling, rather than pool boiling, and were conducted under radiation dose rate and spectrum similar to those in the core of commercial BWRs. The test section had a 2-mm diameter flow channel and was heated electrically. Quasi-steady state experiments were conducted before irradiation (out-of-pile and in-pile before reactor operation), during irradiation and after irradiation (in-pile), under the same thermal hydraulic conditions using the same test section. This approach allowed direct evaluation of the RISA effect through comparison of experimental data.

The results are plotted against the mass flux in Fig.5-9. The CHF obtained during and after irradiation was larger by about 17%, on average, than that before irradiation. Fig.5-10 shows the observation of static spread of a liquid droplet put on the surface of the test piece, which was a part of the flow channel, before and after the irradiation. A super-hydrophilic state was achieved after the irradiation in JMTR, while a droplet remains in the original form for non-irradiated test piece.

In this way the RISA effect was confirmed for the first time in the case of forced convection boiling heat transfer on a metal oxide surface. The next stage experiment, under nearly real plant conditions, high pressure, high mass flux, and high heat flux, is being planned.

#### Reference

Sibamoto, Y. et al., In-Pile Experiment in JMTR on the Radiation Induced Surface Activation (RISA) Effect on Flow-Boiling Heat Transfer, Journal of Nuclear Science and Technology, vol.44, no.2, 2007, p.183-193.

## 5-5 Evaluating the Fracture Resistance of a Reactor Pressure Vessel under Pressurized Thermal Shock

— Structural Reliability Evaluation of Aged Components in Nuclear Plants Based on Probabilistic Fracture Mechanics (PFM) —

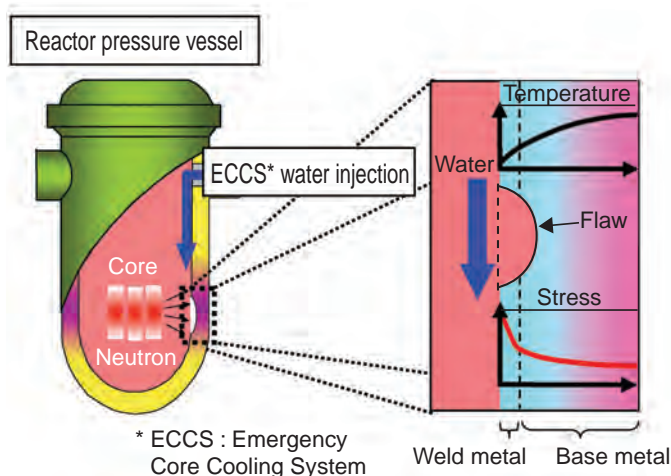


**Fig.5-11 The concept of PTS**

When a loss-of-coolant accident occurs in a reactor, the emergency core cooling system injects water in the RPV, resulting in cooling of the inside of the vessel with high pressure maintained. This induces a high tensile stress at the inner surface of the RPV, so called PTS. The structural integrity of the RPV during PTS should be evaluated assuming the existence of a flaw at the inner surface.

Some of the light water reactors (LWRs) in Japan have been operated for over 30 years. To assure the structural integrity of components is an important issue for the safe operation of these aged LWRs. Probabilistic Fracture Mechanics (PFM) has attracted a great deal of interest as a useful tool for evaluating the failure probability of aged components appropriately. In the PFM approach, the uncertainties of loads applied to structural components, the distributions of flaw size, and the probability of occurrence of flaws are considered.

We have developed a PFM analysis code PASCAL. This code evaluates the conditional probabilities of failure of a reactor pressure vessel (RPV) under transient loading conditions such as pressurized thermal shock (PTS), the concept of which is shown in Fig.5-11. The following is a brief description of the analysis function of PASCAL.

RPV steel is subjected to neutron irradiation from the reactor core, so that it tends to embrittle as operation continues. This phenomenon is evaluated using the embrittlement prediction equation formulated in Japan. For the assessment of structural integrity of the RPV, a flaw in the RPV wall is assumed to exist. The flaw size is chosen from among a distribution of flaw sizes using a random number

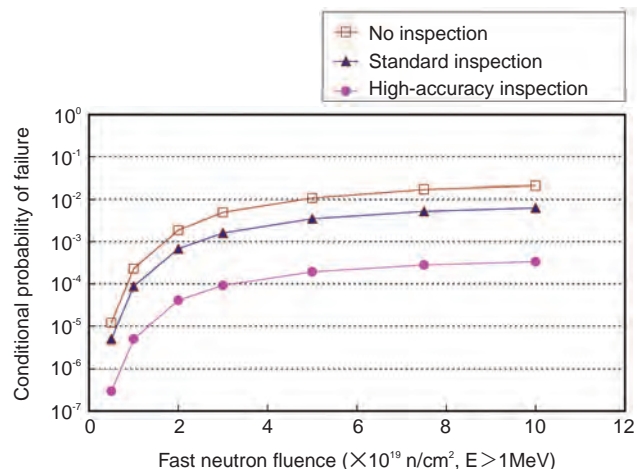


**Fig.5-12 The conditional probability of failure of an RPV as a function of fast neutron fluence computed with PASCAL**

The fast neutron fluence is the number of neutrons accumulated during an operation period per unit area at the vessel wall in an LWR. It increases as the operation time of the LWR increases. The conditional probability of failure increases with increase in the fast neutron fluence, as shown in the figure. It is clear that nondestructive inspection significantly reduces the probability of failure due to the occurrence of PTS.

(i.e. flaw sampling). The flaw is evaluated as to its growth and whether it penetrates the RPV wall during a PTS. The sampling is repeated, and the conditional probability of failure is calculated as the ratio of the number of failed flaws to the number of samples. In PASCAL, one can analyze easily by setting various parameters on graphical user interface (GUI) including the type of a transient, the chemical compositions in steel, and the accuracy of nondestructive inspection.

The effect of nondestructive inspection on the conditional probability of failure is shown in Fig.5-12. Any nondestructive inspection reduces the failure probability. Especially, the failure probability after an inspection with high accuracy was reduced to approximately 1/100 that where there was no inspection.

We are continuing research to incorporate the latest knowledge about evaluation items such as residual stress distributions in PASCAL, focusing on making a contribution to possible revisions of codes and standards.

This work was performed by JAEA under the contract research entrusted from the Ministry of Economy, Trading and Industry of Japan.

### Reference

Osakabe, K., Onizawa, K. et al., Development of Probabilistic Fracture Mechanics Analysis Code PASCAL ver.2 for Reactor Pressure Vessel, Nippon Genshiryoku Gakkai Wabun Ronbunshi, vol.6, no.2, 2007, p.161-171 (in Japanese).

## 5-6 Preparation for Nuclear Criticality Safety Evaluation of High-Burnup Fuel Cycle in the Near Future

### — Development of a High-Precision Evaluation Method for Nuclear Criticality Safety of a 5 to 10% <sup>235</sup>U-Enriched Uranium Fuel System —

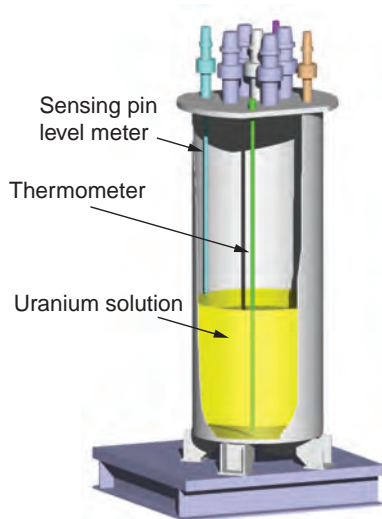


**Fig.5-13 Schematic diagram of the tank of the Static Criticality Experiment Facility STACY**

The critical height of 10% <sup>235</sup>U-enriched uranium solution was measured with precision of 0.2 mm with a sensing pin level meter (indicated in aqua blue). Besides the measurement error, errors in composition and temperature of the container and solution were considered, and these were limited so that their effect on the neutron multiplication factor was 0.001 or less.

From nuclear fuel cycle facilities including power reactors, various wastes are discharged. The amount of wastes can be reduced if fuels are burned for a longer duration. In order to introduce higher burnup uranium fuels, both the integrity and increased initial enrichment of fuels become important.

The former topic was discussed in Topic 5-3 of this review series in 2006. Research efforts related to the latter topic will be explained below.

The traditional nuclear fuel cycle restricts the upper limit of uranium enrichment to 5%. The use of uranium fuels in <sup>235</sup>U enrichment higher than 5% would reduce the critical mass. For example, when the means of criticality safety control is adjustment of the diameter of the cylindrical container for uranium solution, the diameter of the container should be reduced. A simple reduction of the container diameter would reduce the throughput, which should be avoided as much as possible. This minimum reduction can be realized by estimating precisely the required neutron multiplication factor (NMF); this is crucial for determining the cylinder diameter.

We have performed criticality experiments to confirm errors in the calculated NMF. The critical heights of 10% <sup>235</sup>U-enriched uranium solutions were measured to a high degree

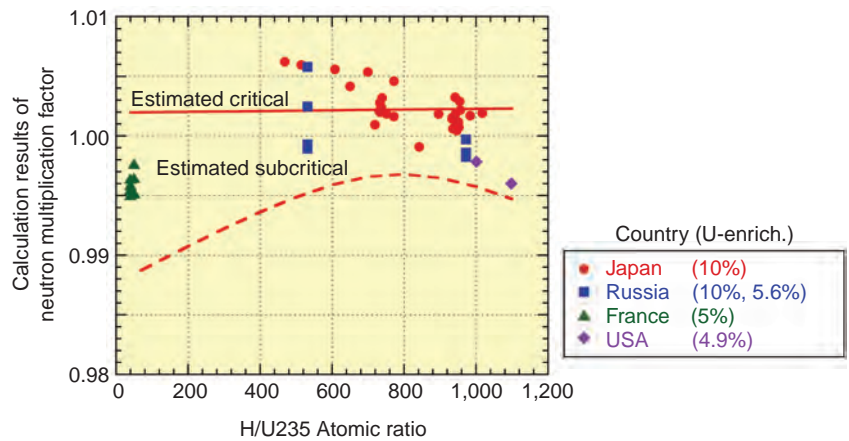


**Fig.5-14 Accuracy evaluation results of the current criticality calculation method**

The criticality calculation program MVP II and nuclear data library JENDL 3.3 were applied to analyze criticality experiments using 5% to 10% <sup>235</sup>U-enriched uranium solutions and powders, whose results are shown by the symbols. “Japan” indicates the results from STACY experiments. The solid line is the level at which criticality is most likely and the broken line is the level at which criticality is negligibly small, as calculated by the latest method applied to 10% <sup>235</sup>U-enriched uranium solution and powder systems.

of precision at the STACY facility (Fig.5-13).

By analyzing the data of criticality experiments, performed at STACY and at facilities in foreign countries and whose high precision was guaranteed through international cooperation, we evaluated the errors of calculations made with a combination of the computer program MVP II and the nuclear data library JENDL 3.3. The results of this analysis are shown as symbols in Fig.5-14. The NMF for critical conditions should be unity. However, the calculation results deviate and scatter from 1.0 because of errors in the computer code and nuclear data library. The estimated critical value of the NMF, at which systems are likely to become critical, and the estimated lower-limit value, below which systems are unlikely to be critical, were obtained by a statistical analysis and plotted as solid and broken lines, respectively in Fig.5-14. The dependences on uranium enrichment and on H/<sup>235</sup>U atomic ratio, which greatly affect neutron moderation, were considered. These considerations are expected to lead to a higher precision in criticality safety evaluation.

We are performing criticality experiments and analytical research as described above for preparing methods and data for nuclear criticality safety evaluation of high-burnup fuel cycles; these will be carried out in the near future.

#### Reference

Okuno, H., Development of a Statistical Method for Evaluation of Estimated Criticality Lower-Limit Multiplication Factor Depending on Uranium Enrichment and H/Uranium-235 Atomic Ratio, Journal of Nuclear Science and Technology, vol.44, no.2, 2007, p.137-146.

## 5-7 Thermal Properties of Additional Material Used in MOX Fuel Fabrication Facility — Investigation of Data and Evaluation Model of Pyrolysis Properties of Zinc Stearate —

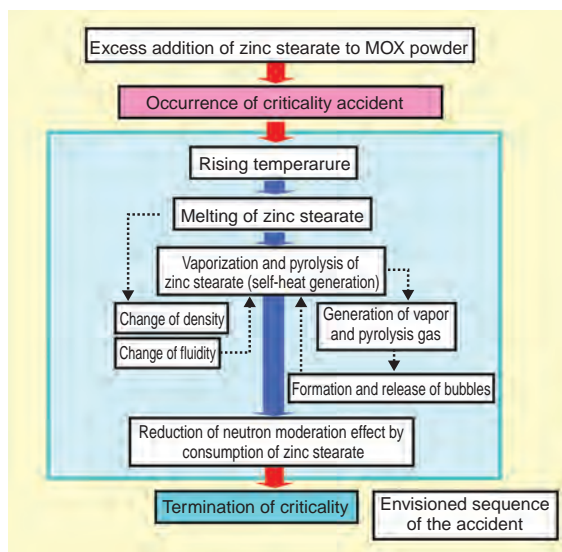


**Fig.5-15 Progress of criticality accident assumed in this study**

If a criticality accident is induced by excess addition of zinc stearate, the fluidity and density of the materials in the system would be changed by the melting and pyrolysis of the zinc stearate, which would occur because of the fission energy, and pyrolysis gas would be released. These would affect the kinetic characteristics of the MOX fuel and act as a negative feedback mechanism. Further, consumption of the zinc stearate by the pyrolysis should serve as a mechanism for termination of the criticality.

To confirm safety of a nuclear fuel facility, evaluation of the influence to the environment after a hypothetical criticality accident is important. Data and a method for estimating total fission number and time history of power are necessary for this evaluation. In the MOX fuel fabrication facility being planned, a dry process will be adopted as main process, but zinc stearate ( $((\text{CH}_3(\text{CH}_2)_{16}\text{COO})_2\text{Zn})$ ) will be added to the MOX powder as an additional material to adjust the density. If too much of the zinc stearate is added by mistake, the criticality characteristics of the MOX powder will be influenced because of its neutron moderation effect. If a criticality condition should be induced by the excess addition, melting and pyrolysis of the zinc stearate could be caused by the fission energy, and therefore, the kinetic characteristics of the MOX fuel would be affected in a feedback mechanism. Consumption of the zinc stearate by pyrolysis should be a criticality terminating mechanism (Fig.5-15). In this study, exothermic and endothermic properties and gas release behavior due to pyrolysis of zinc stearate were examined by differential scanning calorimeter (DSC) and pressure vessel tests, respectively, and an

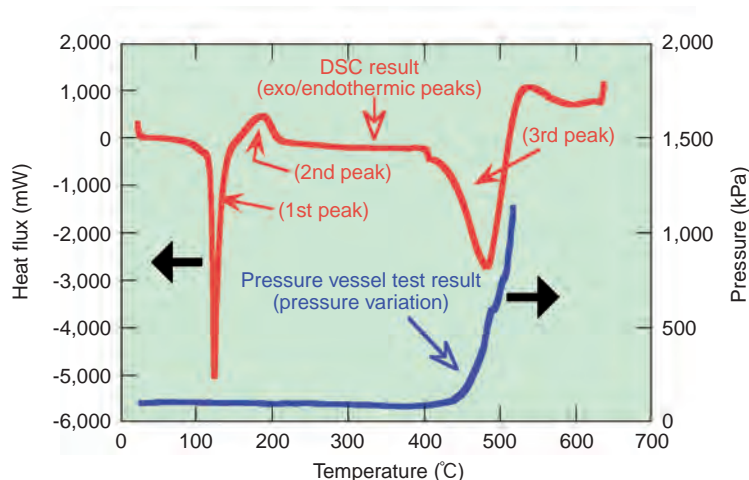


**Fig.5-16 Experiment results regarding pyrolysis properties of zinc stearate**

The results using a DSC showed that zinc stearate has a sharp endothermic peak at about 80°C (1st peak), a weak exothermic peak over about 150°C (2nd peak) and a large endothermic peak over about 400°C (3rd peak) with rising temperature. Since the rise in pressure with rise of temperature over 400°C was also observed in the pressure vessel test, in which pressure variation with rising temperature in a vessel containing the zinc stearate was measured, it is likely that pyrolysis of the material progresses rapidly when the temperature rises above 400°C.

evaluation model for pyrolysis properties of the zinc stearate during this accident was developed.

Fig.5-16 shows examples of the experiment results. From the DSC results, the zinc stearate was recognized as a stable material without radical exothermic reaction. It indicated some endo/endermic peaks with rising temperature and a large endothermic peak over about 400°C (3rd peak). Since the rapid rise in pressure over about 400°C was also observed in the pressure vessel test, the 3rd peak can be attributed to the progress of pyrolysis. The calorific values and reaction rates of the respective peaks were estimated from the DSC result and average molecular weight of the pyrolysis gas was estimated by the pressure vessel test result. Moreover, variation of the physical and chemical conditions of the zinc stearate during the accident could be simulated well using our calculation model based on the data. In the future, by establishing a link between this model and a detailed kinetic characteristic analysis code, a method for evaluating kinetic characteristics of the MOX fuel which takes fluidity and density variation with melting of the material into consideration will be investigated.

### Reference

Abe, H. et al., Investigation of a Model to Evaluate the Pyrolysis Properties of Zinc Stearate, Nippon Genshiryoku Gakkai Wabun Ronbunshi, vol.6, no.1, 2007, p.10-21 (in Japanese).

## 5-8 Mass Transport Retardation Studies under In Situ Conditions — Radionuclide Migration Experiments in a Rock Fracture at a Depth of 240m —



**Fig.5-17 Forklift transporting granite block containing natural fracture, quarried at a depth of 240 m**

The blocks were excavated from the natural fracture zone using a diamond wire saw. Care was taken to prevent ingress of cutting debris into the fracture during the excavation and to preserve the in situ geochemical conditions by making sure that there was a positive flow of water out of the formation. Injection and withdrawal ports were installed around the perimeter of the block.

In the Japanese program, high-level radioactive waste (HLW) is vitrified, encapsulated in a metal container called overpack, surrounded by engineered buffer material, and emplaced in a repository constructed in stable rocks at a depth of 300m or greater. In safety assessments of this disposal method, the possibility that long-lived radionuclides may be leached from the wastes and may subsequently be transported through surrounding rock masses must be considered. It is therefore necessary to understand the transport of radionuclides through water-bearing fractures in rocks surrounding the repository. For this purpose, in situ radionuclide migration experiments were performed at the 240-m level in Atomic Energy of Canada Ltd.'s (AECL) Underground Research Laboratory under a five-year cooperative research program with AECL.

Two granite blocks, each with a volume of  $\sim 1\text{m}^3$  and containing a single fracture were excavated from a water-bearing fracture zone with special care to minimize changes in the geochemical conditions (Fig.5-17). Migration experiments were performed by injecting  $^3\text{H}$ ,  $^{85}\text{Sr}$ ,  $^{95\text{m}}\text{Tc}$ ,  $^{237}\text{Np}$ ,  $^{238}\text{Pu}$ , and synthetic colloids, followed by groundwater injection.

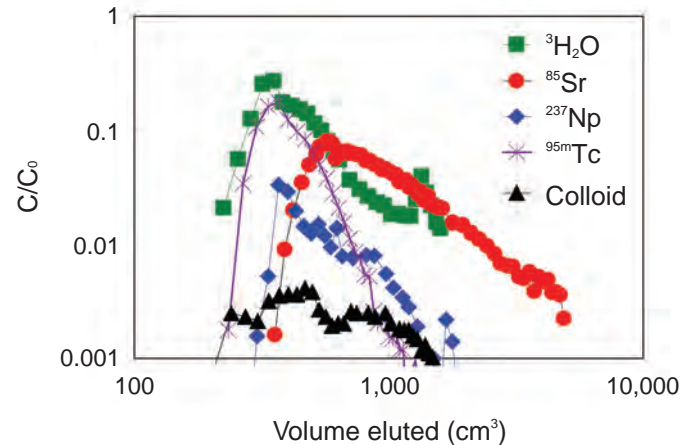


**Fig.5-18 Radionuclide and colloid elution profiles, normalized to the injection concentrations**

Transport of  $^{85}\text{Sr}$  in the fracture was retarded relative to the  $^3\text{H}_2\text{O}$  by diffusion into granite matrix and adsorption onto mineral surfaces. Plutonium was sorbed near the inlet to the fractures and was not detected in any of the eluted groundwater. The colloid elution exhibited a broad and low peak.

As predicted from earlier sorption studies, radionuclide transport by groundwater through the fractures was retarded by sorption on rock-forming minerals and was element-specific (Fig.5-18). Strontium exhibited weak reversible sorption. Plutonium was strongly sorbed near the inlet of the fractures, as shown by post-experiment radiometric analysis of the fracture surfaces. The elution peaks for  $^{95\text{m}}\text{Tc}$  and  $^{237}\text{Np}$  suggested that fractions of these radionuclides were transported without retardation and that the remainder was retained within the fractures. Transport of  $^{95\text{m}}\text{Tc}$  and  $^{237}\text{Np}$  can be explained by a kinetically slow redox reaction. The redox kinetics is often affected by microbial activities.

Colloid concentrations in the eluted groundwater were low, again as expected, and may have been controlled by sedimentation and diffusion into stagnant zones.

We demonstrated the retardation of radionuclide migration deep underground and gave possible mechanisms. Further investigations are needed to determine if the postulated mechanisms are valid over long periods of time, to be confident of the safety of the disposal. Of particular interest is whether colloids enhance or limit radionuclide migration in fractures.

### Reference

Yamaguchi, T. et al., Radionuclide and Colloid Migration Experiments in Quarried Block of Granite under In-Situ Conditions at a Depth of 240m, Proceedings of 15th International Conference Nuclear Engineering (ICONE15), Nagoya, Japan, 2007, ICONE15-10374, in CD-ROM.

## 5-9 Evaluating the Radionuclide Concentrations at which Radioactive Materials Can Be Released from Regulatory Control — Clearance Level Calculation System Development —

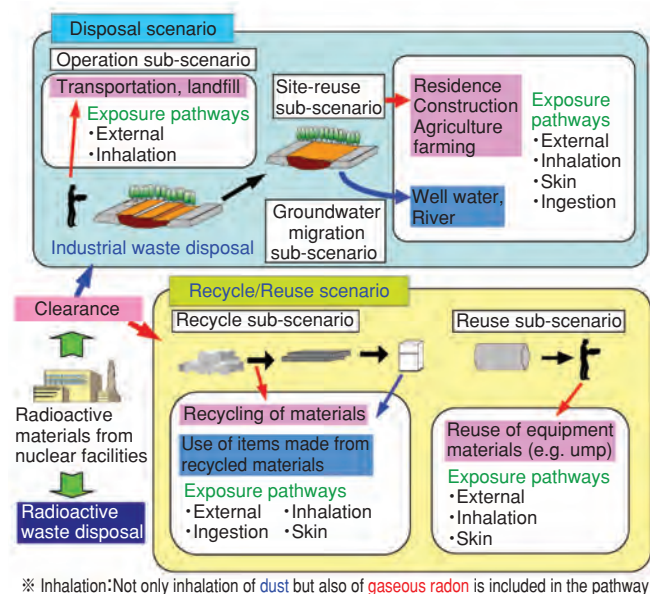


**Fig.5-19 Scenarios and exposure pathways used to derive the clearance levels for uranium waste and TRU waste**

The PASCLR ver. 2 computer code calculates the unconditional clearance levels for uranium waste and TRU waste. The clearance levels were obtained considering the set of scenarios and pathways shown in this figure. The two typical scenarios are landfill disposal of industrial waste and recycling or reuse of released materials.

Radioactive materials generated from operation and dismantling of nuclear facilities include those with extremely low levels of radioactivity. The clearance level concept is used to categorize such materials as not requiring treatment as radioactive wastes. The radionuclide concentration below which such treatment is not required is called the clearance level. The “cleared” material is either reused/recycled or disposed of as industrial waste. The Nuclear Reactor Regulation Law was amended to set the clearance levels for short-lived radionuclides contained in the waste from major nuclear facilities. It is also necessary to set the method for deriving the clearance levels of uranium and transuranium (TRU) wastes. These wastes contain long-lived radionuclides in decay chains.

We developed a probabilistic assessment code system (PASCLR ver.2) to derive the clearance levels of radionuclides contained in the uranium and TRU wastes. This code supports the dose estimation for the exposure pathways in two typical scenarios; landfill disposal of industrial waste

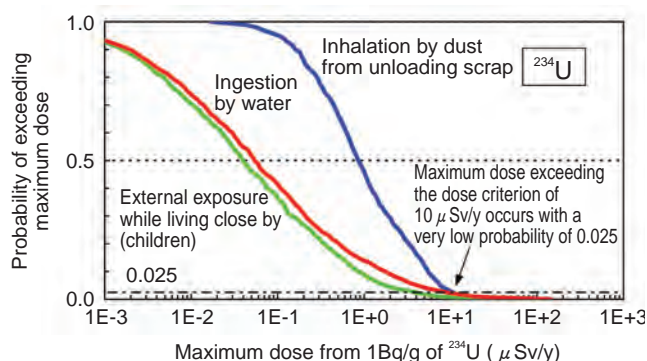


**Fig.5-20 The uncertainty analysis of a possible exposure dose from  $^{234}\text{U}$  contained in disposed waste**

The uncertainties accompanying calculated exposure doses based on deterministic analysis with typical parameter sets can be estimated by PASCLR ver. 2 computer code system using the Monte Carlo technique. This figure indicates that if the  $^{234}\text{U}$  concentration in the disposed waste is limited to 1 Bq/g, the maximum exposure dose (occurring due to the inhalation of dust during scrap unloading) is unlikely to exceed the dose criterion of  $10 \mu\text{Sv/y}$ ; the probability of receiving  $10 \mu\text{Sv/y}$  exposure is as low as 0.025.

and recycling or reuse of the released materials (Fig.5-19). The growth of daughter radionuclides in decay chains can lead to a high dose contribution over a long time periods. This code can estimate such long time effects for all exposure pathways considered. The contribution from gaseous radon ( $^{222}\text{Rn}$ ) is included in the calculations.

Uncertainties in the parameters used in the clearance level calculations include observational error and variations in the environmental conditions at the disposal site. The effect of these uncertainties on the clearance levels obtained from the deterministic analysis can be accounted for in a probabilistic calculation using the Monte Carlo technique (Fig.5-20).

These results, as well as consideration of the consistency of international clearance levels reported by the IAEA, will contribute to the future establishment of the clearance levels for uranium and TRU wastes by this regulatory body.

This work was performed by JAEA under contract with Nuclear and Industrial Safety Agency in Ministry of Economy, Trade and Industry.

### Reference

Takeda, S. et al., Development of PASCLR Code System Version 2 to Derive Clearance Levels of Uranium and Trans Uranium Wastes, JAEA-Data/Code 2006-003, 2006, 137p. (in Japanese).

## Advanced Basic Research to Create the Future

In the Advanced Science Research Center, new frontier research of nuclear energy and ionizing radiation expected to bear fruit in the future is conducted to discover new principles and phenomena, and furthermore to create new materials and technologies. In order to achieve these aims, we have four basic policies; (1) to pursue research for which the high level research capability (researchers and facilities) in JAEA is effectively used and which is difficult to do in other research organizations, (2) to achieve results before the rest of the world does, (3) to nurture a new basic research area until it becomes fruitful, (4) to explain and apply the research, thus fulfilling our responsibility to society, in conformity with the Third Science and Technology Basic Plan.

The following research is going on: nuclear physics and nuclear chemistry of superheavy elements, the nuclear shell structure, reaction dynamics and electrochemistry using heavy - ion beams of accelerators, synthesis of uranium

and transuranium compounds and measurement of their macroscopic quantities and electronic structure, clarification of magnetic structure, magnetic excitation, and the mechanism of superconductivity by using NMR,  $\mu$ SR, neutron scattering, and theoretical methods, design of novel materials using mega - gravitation and nano - particle deposition, topmost surface studies using bright and coherent positron beams, elucidation of interaction mechanism of heavy elements and studying the primary and fundamental processes in the interactions of ionizing radiation with matter (Fig.6-1).

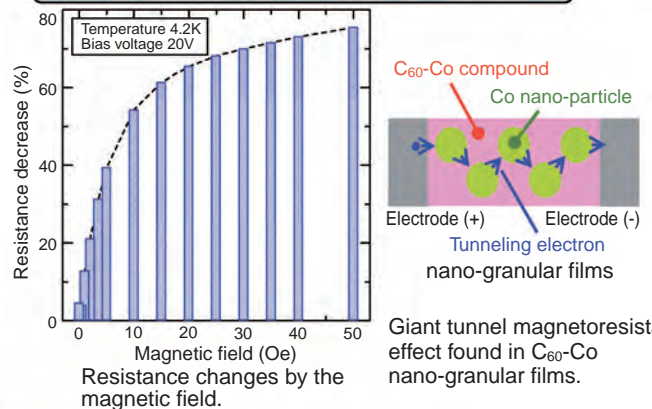
In order to promote this research, we are collaborating with other research sections in JAEA, and several international collaborations are ongoing. In addition, we accept new research subjects based on public suggestions within the framework of the Reimei Research Promotion project of JAEA.

### Superheavy element nuclear science



Automated rapid ion-exchange apparatus AIDA for the study of liquid-chromatographic behavior of superheavy elements.

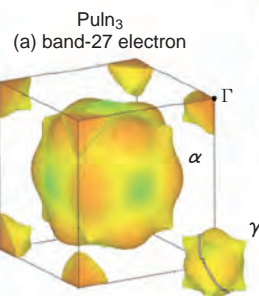
### Extreme environment and substance science



### Actinide material science



Single crystal growth of a plutonium compound  $PuIn_3$  and observation of its Fermi surface.



### Material and life sciences

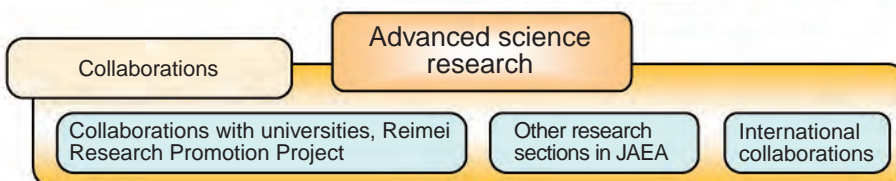
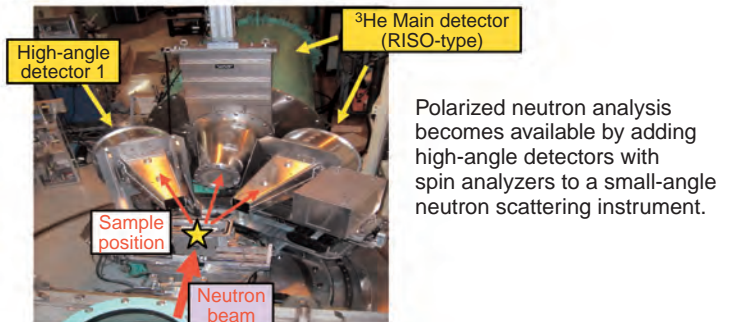


Fig.6-1 Four research fields in Advanced Science Research Center

## 6-1 Unusual Magnetic and Orbital Ordering in Np Compounds — Neutron Scattering Study of Actinides in JRR-3 —



Fig.6-2 Triple-Axis Spectrometer LTAS in JRR-3

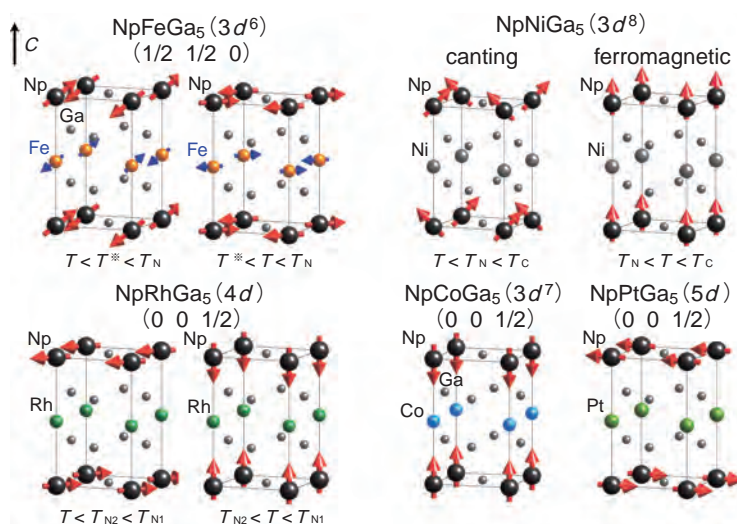


Fig.6-3 Variety of magnetic structures in NpTGa<sub>5</sub>

Actinide compounds with 5f electrons exhibit highly interesting electronic properties. Strong magnetism in rare earth compounds is a consequence of the localized nature of 4f electrons at atomic sites. On the other hand, 5f electrons in light actinides such as uranium, neptunium, and plutonium have an itinerant character.

Neutron scattering studies of neptunium compounds have been carried out using the low energy cold neutron triple axis spectrometer LTAS (Fig.6-2) installed in the guide hall of the research reactor JRR-3 in JAEA. Only a few actinide compounds have been studied by neutron scattering, and actually these were the first experiments of actinide neutron scattering done in Japan. Neutrons with spin 1/2 are the most powerful probe for studying magnetic structure. The size and the direction of the magnetic moment carried by actinide elements are important information for determining the electronic state of 5f electrons.

Our systematic experiments revealed a variety of the magnetic structure in Np compounds NpTGa<sub>5</sub> (T = Fe, Co, Ni, Rh, or Pt), depending on the transition metal element T as shown in Fig.6-3. For T = Fe, Ni, and Rh, a double transition has been observed. Neutron polarization analysis clarified that the magnetic moments of Np and Fe in NpFeGa<sub>5</sub> are

perpendicular to the crystallographical *c*-axis, namely in the tetragonal basal plane. However, the magnetic moments are tilted in the ground state structure. In NpNiGa<sub>5</sub> the magnetic moment of Np exhibits a ferromagnetic ordering with the magnetization parallel to the *c*-axis below the Curie temperature  $T_c = 18$  K, while there is a stable non-collinear (canting) structure in the ground state. We found a very unusual reduction of the magnetic moment from the canting to the ferromagnetic phase with application of the magnetic field. These results indicate that the 5f electronic state changes with the magnetic transitions.

The itinerant character of 5f electrons in NpTGa<sub>5</sub> is shown by a good agreement of the observed Fermi surface topology with band structure calculation. The theoretical study based on the magnetic and quadrupole interactions explains the variety of the magnetic structures and the double transition, where the orbital degree-of-freedom plays an important role. Our study indicates a possible orbital (quadrupole) ordering in the itinerant many body 5f electron system with strong correlation. Further experimental and theoretical study should be carried out in order to determine the order parameter in this highly interesting system.

### Reference

Metoki, N., Neutron Scattering Study on UTGa<sub>5</sub> and NpTGa<sub>5</sub>, Journal of the Physical Society of Japan, vol.75, supplement, 2006, p.24-29.

## 6-2 Large Magnetoresistance Effect Found in Fullerene-Cobalt Thin Films — Organic Molecule Mediates Electron Spin —

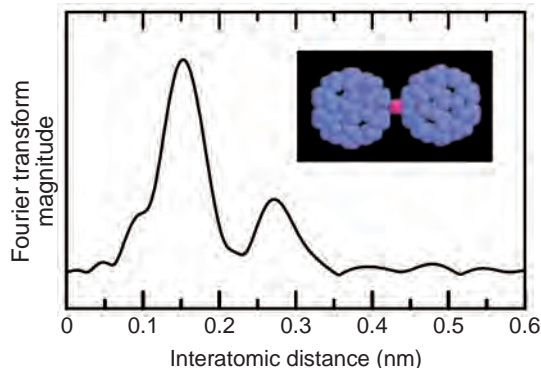
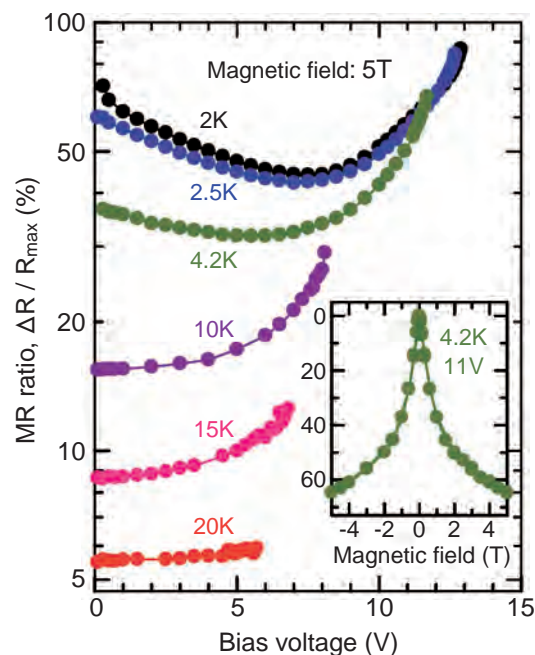


**Fig.6-4 (upper)**

Radial structural function (uncorrected for phase shift) and the resulting simulation model (inset) of the local atomic structure around Co atoms in the  $C_{60}$ -Co compound. The function is obtained through the analysis of the X-ray absorption spectrum at the Co K-edge. It is revealed that a Co atom (red) bridges between  $C_{60}$  molecules (blue).

**Fig.6-5 (right)**

Bias voltage dependences of the magnetoresistance (MR) ratio in a magnetic field of 5 T in the temperature region of 2-20K and a MR reduction/magnetic field curve (inset). The MR ratio reaches above 80% depending on the bias voltage.



In the last few decades, electronics devices have come to be highly integrated, supported by the rapid advances of micro-fabrication technologies. But now, we are coming to a critical stage needing a break-through idea different from the existing ones. “Spintronics” has received intensive attention as a promising evolutionary approach. In the spintronics devices, the degree of freedom of electron spin (up and down spins) is utilized for data processing and recording, in addition to the electron charge used in conventional electronics devices. A key issue required for the progress of spintronics is how to manipulate the electron spin. For highly efficient spin-manipulation, new materials systems capable of higher spin-polarization have been explored intensively. In these systems, the conductivity of spin-polarized electrons can be controlled over a wide range by applying a magnetic field. Here, we call the ratio of the magnetic-field induced resistance change to the maximum resistance ( $\Delta R/R_{\max}$ ) the magnetoresistance (MR) ratio. Only inorganic systems have been a subject of the study of the MR effect up to now. The MR ratio, however, is less than 30% in the typical reported system that comprises hybrid films composed of an insulating matrix and embedded metal nanoparticles (so-called granular films).

Recently, we have found that a very large MR effect occurs

in granular films of fullerene ( $C_{60}$ ) based compounds, not obtainable with an inorganic insulating matrix.  $C_{60}$  is an organic molecule made of 60 carbon atoms and with a shape similar to a soccer ball. Firstly, we have found a method of formation of the  $C_{60}$ -transition metal (Co) compounds, mixing the relevant substances in an ultra high vacuum (Fig. 6-4). We have also found that the granular films of the  $C_{60}$ -Co compound matrix containing Co nanoparticles are obtained in a certain composition range. The granular-structured  $C_{60}$ -Co films exhibit a MR ratio higher than 80% (Fig.6-5) associated with the tunneling effect of spin-polarized electrons. The observed MR ratio is the highest one found in granular systems, and, surprisingly, the ratio is higher than the theoretically predicted upper-limit (50%) with complete spin-polarization. It is also found that range of MR ratio change becomes several times larger and smaller depending on the bias voltage. This behavior is definitely different from the small change reported for inorganic systems.

Our results show clearly that the organic molecule based systems have a considerable advantage for spintronics. Such systems are expected to lead to “molecular spintronics” by incorporating the optical functions and the electrical field effects of organic molecules.

### Reference

Sakai, S. et al., Tunnel Magnetoresistance in Co Nanoparticle/Co- $C_{60}$  Compound Hybrid System, Applied Physics Letters, vol.89, 2006, p.113118-1-113118-3.

## 6-3 A New Method for Material Synthesis under a Million G — Research into New Materials Utilizing “Mega-Gravitoronics” —



**Fig.6-6 Mega-gravity generator (JAEA)**  
Introduced in the magazine Newton, Nov. 2004

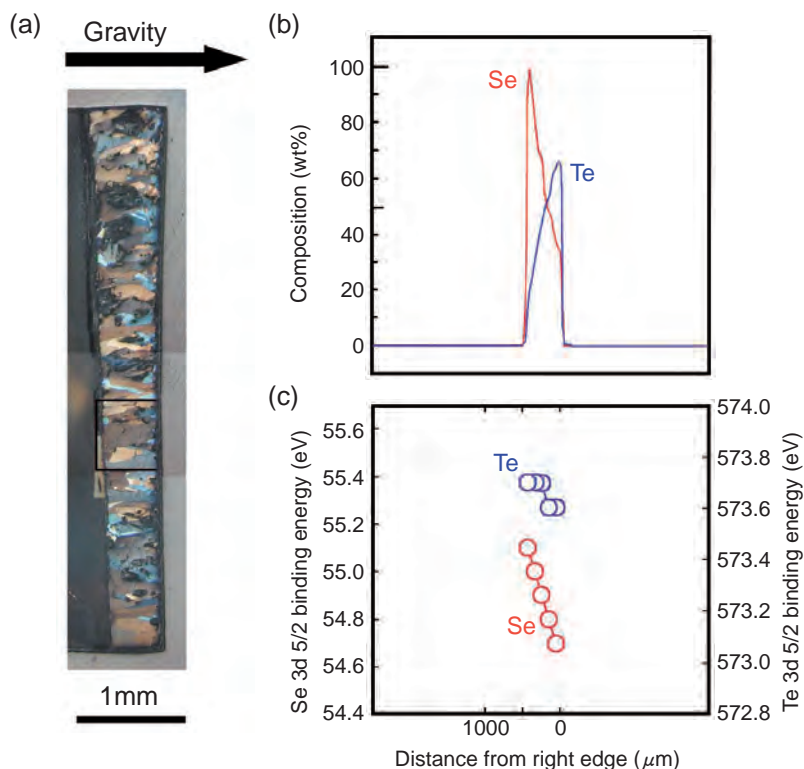


**Fig.6-7**

- (a) Cross-section diagram of a Se-Te sample.  
 (b) Result of chemical composition analysis.  
 (c) Position dependence of 3d-electron binding energy suggesting a continuous modification of band-gap.

Under micro-gravity as in a space shuttle, it is possible to blend micro particles homogeneously together. On the other hand, under an extremely large gravity field of 1 million G, small differences between each atom play an important role for the atomic arrangement and for the interatomic diffusion. Our group focused our research interests on utilizing the extreme environment of mega-gravity as a new platform of the synthesis of novel functional materials (research into “Mega - gravitoronics”), and for clarification of the unexplained mechanism of fast atomic sedimentation and diffusion under mega-gravity. Fig.6-6 shows our mega-gravity (MG) generator developed in collaboration with the Mashimo laboratory in Kumamoto university. Fig.6-7 shows an example of a novel functional material developed with selenium-tellurium (Se-Te) semiconductors. The Se-Te semiconductor is a continuous solid solution, and both constituent atoms blend well with each other in a entire range

of relative concentrations. A homogenous Se-Te sample with a composition rate of 70:30 at% was subjected to the MG process, under 1.02 MG at 260°C for 100 h. It changed to an orientational crystal with a composition gradient structure (Fig.6-7(a)). The obtained sample has an atomic-scale composition gradient structure (Fig.6-7(b)), and its lattice constant continuously changes with the change of the composition ratio. As shown in Fig.6-7(c), the binding energy of 3d electron in a Se or Te atom is also continuously modified depending on the composition ratio (found in collaborative research with Kumamoto University). This suggests that we have made a novel material, which has a continuously changing band-gap width. We expect to establish a method of isotope centrifugal separation directly using atomic sedimentation by mega-gravitoronics in the future.

### Reference

Huang, X., Okayasu, S. et. al., Formation of Atomic-Scale Graded Structure in Se-Te Semiconductor under Strong Gravitational Field, Journal of Applied Physics, vol.101, 2007, p.113502-1-113502-5.

## 6-4 Artificial Enzymatic Synthesis of Cellulose

### — Elucidation of Self-Organization Mechanism of Reaction Products by Using Small-Angle Neutron Scattering Method —

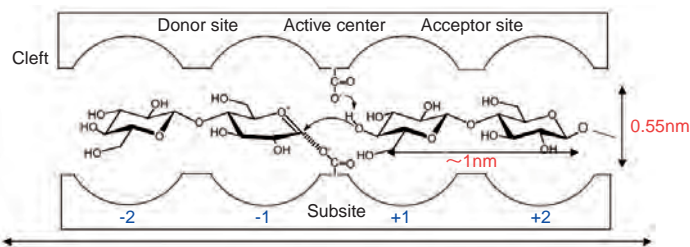


**Fig.6-8 Schematic illustration of a so-called cleft, a specific reaction site in an enzyme**

It contains a donor site, which recognizes the monomer, a pair comprising an active center and a subsite, which activate the monomer and chemically link the activated monomer into the end of the growing polymer chain, and an acceptor site, which anchors the growing polymer, in a very narrow space of about 3 nm in length and 0.55 nm in cross-sectional width.

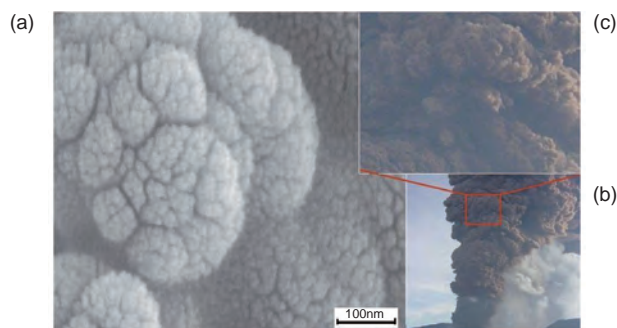


**Fig.6-9**

Field-emission scanning electron micrograph of a part of the self-similarly rough surface formed by cellulose molecules (a), similar to volcano fumes rising from a crater (b, c). Part c is an enlargement of the part of b encompassed by the red square.

Cellulose, one of the important naturally made polymers, is biosynthesized at specific reaction sites in plants and bacteria. Synthesized cellulose molecules self-organize in-situ into crystalline fibrils. The specific reaction site is the so-called cleft found in active enzymes (Fig.6-8). Artificial syntheses of cellulose have been tried since 1941, based on traditional organic chemistry approaches, but none of them has succeeded. Kobayashi et al. first reported a successful synthesis based on enzymatic polymerization using cellulase as the catalytic enzyme and  $\beta$ -cellobiosyl fluoride as a substrate monomer (J. Am. Chem. Soc., vol.113, 1991, p.3079-3084).

In order to gain basic understanding of complex bioactivities concerning the cellulose synthesis and its self-organization into the cellulose fibrils, we attempted to explore the simple system employed by Kobayashi et al. using the time-resolved small angle neutron scattering spectrometer at the JRR-3 research reactor in JAEA. We elucidated for the first time in the world the following facts.

(1) The enzyme molecules form aggregates having sizes greater than 200 nm in the reaction medium. (2) 1 g of active enzymes creates about 14 kg of cellulose during the whole reaction time, which means that one active enzyme creates about 5 cellulose molecules per second. (3) A large number of cellulose molecules, which have sprung out from the cleft assemble themselves into aggregates in the reaction medium and end up completely wrapping the enzyme aggregates. The surface of the cellulose aggregates (Fig.6-9(a)) has a self-similar roughness characterized by surface fractal structure with fractal dimension of 2.3 over an extremely wide length scale ranging from 30 nm to 30  $\mu$ m, quite unique among the manifestations of fractal geometry. This surface structure is quite analogous to that formed by fumes from a volcano crater (Fig.6-9(b), (c)), except for the difference in length of a factor of  $10^9$ . The similarity of the two patterns shown in Fig.6-9 together with the above fact (2) help us to intuitively understand the enormous energy that the enzymatic reaction potentially has.

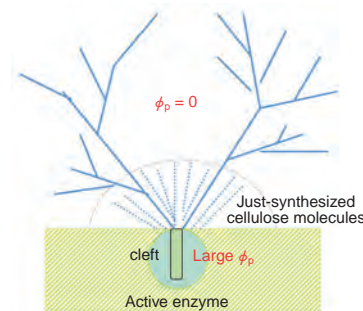


**Fig.6-10 Schematic diagram showing the interface between the enzyme aggregate (the shaded green part) and the reaction medium**

The cleft in the active enzyme (shown by the blue circle) keeps spurting out polymerized cellulose molecules, as a volcano crater springs out fumes. The cellulose polymers formed are soon aggregated into dendritic fibrils (shown by the blue dendrites) in the reaction medium, and they form a surface-based fractal object as shown in Fig.6-9(a). The large difference between the concentration ( $\phi_p$ ) of the cellulose molecules dissolved in the cleft and those in the reaction medium is expected to be a key factor in the spurting out of the cellulose molecules from the cleft and the formation of the fractal structure.

#### References

- Hashimoto, T. et al., Chemical Reaction at Specific Sites and Reaction-Induced Self-Assembly as Observed by In-Situ and Real Time SANS: Enzymatic Polymerization to Synthetic Cellulose, *Biomacromolecules*, vol.7, no.9, 2006, p.2479-2482.
- Tanaka, H., Hashimoto, T. et al., Self-Assembly of Synthetic Cellulose during In-Vitro Enzymatic Polymerization Process as Studied by a Combined Small-Angle Scattering Method, *Macromolecules*, vol.40, no.17, 2007, p.6304-6315.

## 6-5 Dependence of Yield of DNA Damage Refractory to Enzymatic Repair on Ionization & Excitation Density of Radiation

### — Exploring the Induction Mechanism of Clustered DNA Damage —

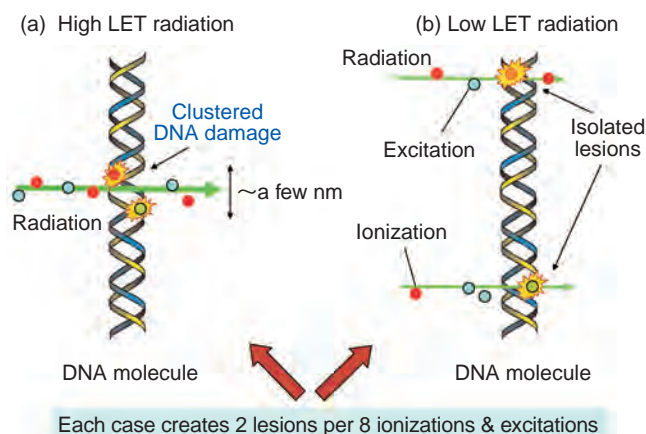


**Fig.6-11 Induction of DNA damage by ionizing radiation**  
Radiation causing ionization & excitation in high density (high LET radiation) induces a clustered DNA damage site (a) which is defined as multiple lesions within a few nm in a DNA molecule. Low LET radiation, on the other hand, creates randomly isolated damage (b). These cases have the same number of lesion.

Many chemical modifications are frequently produced in the genomic DNA (DNA damage) by ionizing radiation from its environment, such as radiation from radioactive materials in soil or cosmic radiation from space. Living systems, on the other hand, have through evolution developed several enzymatic DNA repair systems, which efficiently remove this damage from DNA to maintain the genomic code. If this damage is not repaired in a cell, it may cause serious genetic changes such as mutations, which may lead to cancer. The object of our study is to clarify the nature of damage, which is difficult for the repair enzymes to repair.

It has been proposed that radiation produces multiple lesions within a few nm in DNA molecules, so-called clustered DNA damage (Fig.6-11(a)). This densely localized damage might distort the tertiary structure of DNA and consequently interfere with the binding of repair enzymes to the damage site. Previous measurements of the damage yield (damage per unit dose) using chemical analysis, however, have not distinguished clustered damage from isolated lesions produced by radiation (Fig.6-11).

To investigate the interference of clustered damage with repair enzymes, we observed the damage repair by a repair enzyme. A DNA sample irradiated with He ion beams was mixed with a DNA repair enzyme, glycosylase, and kept at 37 °C for 30 min. This enzyme specifically excises damaged base moieties from DNA and then cuts the DNA strand at the

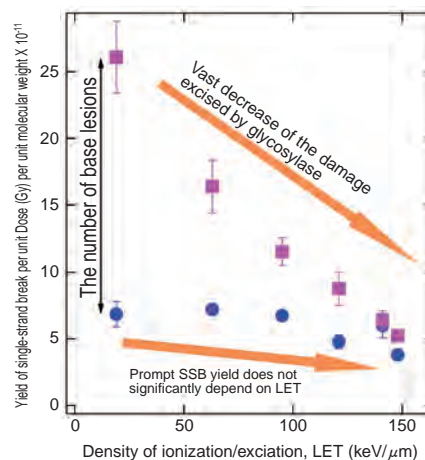


**Fig.6-12 Dependence of frequency of DNA damage induction on ionization & excitation density of radiation track**  
The yield of single-strand break created by the activity of Nth protein (■), which is one of the glycosylases, drastically decreases with increasing level of ionization & excitation density (LET), indicating that the damage induced by higher LET inhibits the activity of the repair enzyme. On the other hand, the yield of single-strand breaks directly induced by radiation (●) does not exhibit significant LET dependence.

damaged site (single-strand break (SSB)). The frequency of the enzymatically induced SSB was analyzed using a gel electrophoresis method. The density of lesion in a cluster is predicted to strongly depend on the number of ionizations and excitations along the He ion track (linear energy transfer (LET)) in the sample. The LET of the He ion beam was systematically changed to determine the LET dependence of the number of the enzymatically induced SSB.

Fig.6-12 shows the obtained yield of the enzymatically induced SSB plotted together with the yield of SSB directly induced by irradiation. The yield of SSB produced by the glycosylase drastically decreases with the increase of LET. This result indicates that higher LET radiation efficiently causes cluster-types of DNA damages, so that the repair activity of the enzyme is strongly inhibited. On the other hand, the yield of the promptly induced SSB by irradiation, which has been used as one of the standards of DNA damage, does not exhibit significant LET dependence (Fig.6-12). The enzymatic “probes” reveal that the yield of this DNA damage strongly depends not only on LET but also the types of particles of radiation, ions or photons (Yokoya, A., Invited Talk at the IXth International Workshop on Radiation Damage to DNA, 2006). These results are important for various fields of applied radiation science, such as risk-assessment of radiation or radiation-surgery on cancer.

#### Reference

Urushibara, A., Yokoya, A. et al., DNA Damage Induced by the Direct Effect of He Ion Particles, Radiation Protection Dosimetry, vol.122, no.1-4, 2006, p.163-165.

## Formation of Basis for R&D of Nuclear Energy, and Creation of Innovative Nuclear Energy Utilization Technology

The R&D activities of nuclear science and engineering research at the Japan Atomic Energy Agency have the four roles shown in Fig.7-1. In order to carry out these roles, nuclear data and reactor engineering, fuels and materials engineering, environment and radiation science, and nuclear applied heat technology are being conducted.

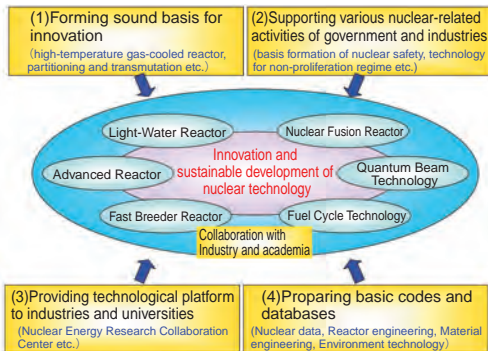


Fig.7-1 Roles of nuclear science and engineering research

### Nuclear data and reactor engineering

Various types of research are being performed to investigate the feasibility of advanced and innovative nuclear systems and to establish the basic technology for these systems, i.e. nuclear data, advanced nuclear and thermal design methods, etc. Detailed two-phase analysis codes processed with supercomputing technology as well as model experiments for code validation are being developed to establish new thermal design methods for advanced water reactors, super critical water reactors, and fast reactors. The feasibility of a tight-lattice core for an advanced water reactor, which aims at effective use of Pu in light water reactors, was confirmed as shown in Topic 7-1. Basic study on transmutation technology for long-lived nuclides is being conducted so as to reduce the burden of radioactive waste management. The effectiveness of partitioning and transmutation technology for waste management was evaluated as shown in Topic 7-2.

### Fuels and materials engineering

Basic studies on advanced nuclear fuel and cycle

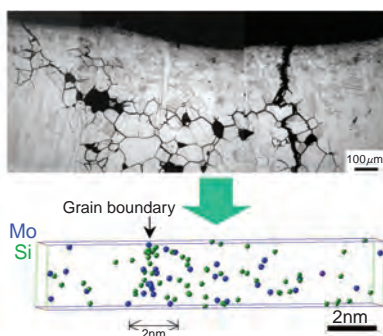


Fig.7-2 Stress corrosion cracking observed in the core shroud of a light water reactor (upper), and concentration of Mo and Si atoms at a grain boundary revealed by 3-dimensional atom probe (lower).

technology and the degradation of nuclear power plant materials are being made. In the advanced nuclear fuel cycles, minor actinides (MA: Np, Am, Cm), which are classified as high level radioactive wastes in the current nuclear fuel cycle, are expected to be recycled to reduce the burden of waste disposals. Topic 7-3 and Topic 7-4 describe important progress in fundamental technology of MA separation by aqueous and pyrochemical processes. Excellent results were also obtained for research into nuclear power plant materials to understand mechanisms of stress corrosion cracking (Fig.7-2), irradiation damage and corrosion degradation.

### Environment and radiation sciences

The R&D on environmental behavior, radiation protection and technology for strengthening the non-proliferation regime are carried out. For radiation protection, a model was established for estimating the cosmic ray spectra at any location in the atmosphere. Based on the model, we developed software named "EXPACS" that enables us to calculate the cosmic radiation doses instantaneously with precision by specifying the altitude, latitude and longitude, and time of interest (Fig.7-3). It is incorporated into JISCARD (Japanese Internet System for Calculation of Aviation Route Doses) of National Institute of Radiological Sciences (NIRS), and is utilized to enforce the administered radiation dose limits recommended for aircrews of Japan.

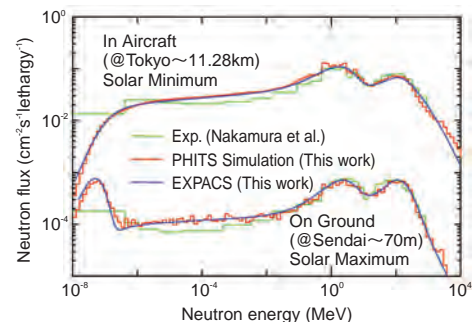
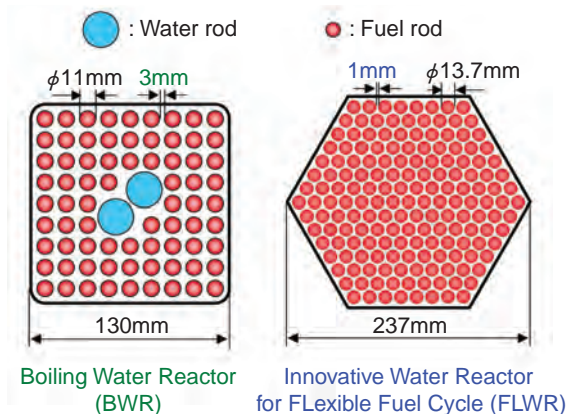


Fig.7-3 Results of quick estimation of cosmic ray spectra at arbitrary points by EXPACS

### Nuclear applied heat technology

To expand nuclear energy application to heat utilizing industries, we continue extensive efforts of research and development for the high-temperature gas-cooled reactor (HTGR) technology and for the HTGR-heated hydrogen production system. Using the High Temperature Engineering Test Reactor (HTTR), safety demonstration tests simulating the events of partial loss of reactor coolant and inadvertent control rod withdrawal have been conducted as shown in Topic 7-7. Even in such abnormal events the reactor responds by self modulating to new stable states without any deviation from safe operating conditions. The planned first commercial HTGR power plant named GTHT300 is conceptually designed based on these results, and promises to have excellent plant economy as shown in Topic 7-8.

## 7-1 Experimental Investigation of Thermal Margin in Tight-Lattice Rod Bundle — Large-Scale Experiments under High Pressure Conditions —



**Fig.7-4 Comparison of the specifications of two rod bundles**

An FLWR core has a triangular tight-lattice configuration to reduce the moderation of neutrons. Since an amount of coolant through the core is considerably smaller than that through a conventional BWR core, the confirmation of thermal-hydraulic feasibility is one of the most important R&D tasks for the FLWR.

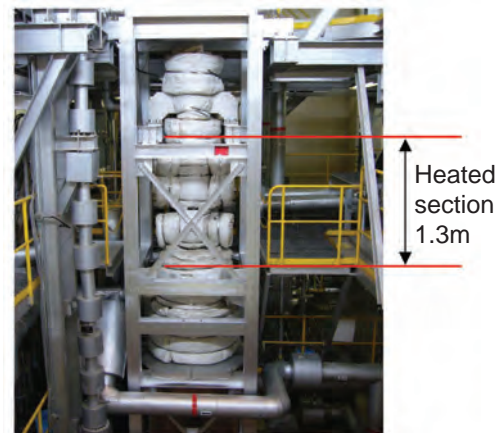


**Fig.7-5 Appearance of a test section for large-scale experiments**

We investigated the thermal-hydraulic characteristics of the FLWR core using a test section with 37-rod bundles under high pressure conditions simulating the FLWR operating conditions.

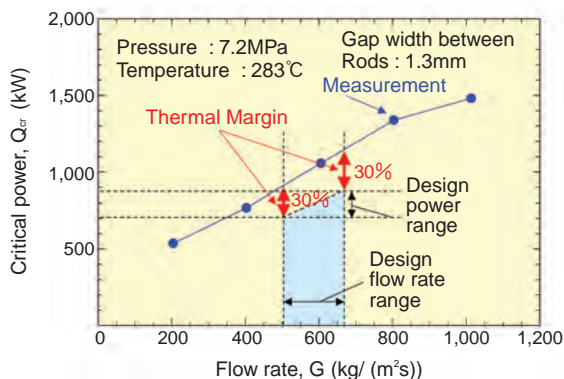


**Fig.7-6 Experimentally derived thermal margin under FLWR operating conditions**

We demonstrated that there are thermal margins, which are large enough to cool the FLWR core.

An Innovative Water Reactor for Flexible Fuel Cycle (FLWR) aims at the achievement of a high conversion ratio of plutonium mixed oxide (MOX) fuel, based on well-tested BWR technology. Since the FLWR makes plutonium multi-recycling possible, the reactor fills the need for effective utilization of uranium resources and long-term energy supply. Fig.7-4 shows a comparison of the specifications of rod bundles of a boiling water reactor (BWR) and the FLWR. The FLWR core has a tight-lattice bundle structure, and it is operated under low mass velocity and high void fraction conditions. These conditions make core cooling difficult, and the FLWR thermal-hydraulic characteristics under such conditions are not known well. The confirmation of thermal-hydraulic characteristics is, therefore, one of the most

important R&D requirements for the FLWR design.

We investigated the thermal-hydraulic performance of the FLWR core using a test section with 37-rod bundles under high pressure conditions simulating the FLWR operating conditions. Fig.7-5 is a photograph of the test section. We measured critical power and pressure drop in the tight-lattice rod bundles under steady state and transient conditions.

Fig.7-6 shows a typical thermal margin observed under the FLWR operating conditions. The result obtains that the FLWR has sufficient thermal margins for cooling of the core.

Present study is the result of “Development of a Fuel Assembly for Very High Burnup Water-cooled Breeder Reactor” entrusted by the Ministry of Education, Culture, Sports, Science and Technology of Japan (MEXT).

### Reference

Tamai, H. et al., Pressure Drop Experiments using Tight-Lattice 37-Rod Bundles, Journal of Nuclear Science and Technology, vol.43, no.6, 2006, p.699-706.

## 7-2 Proposal for Future Waste Management

### — Reduction of the Repository Size for the High Level Wastes (HLW) by Introducing Partitioning and Transmutation (PT) Technology —

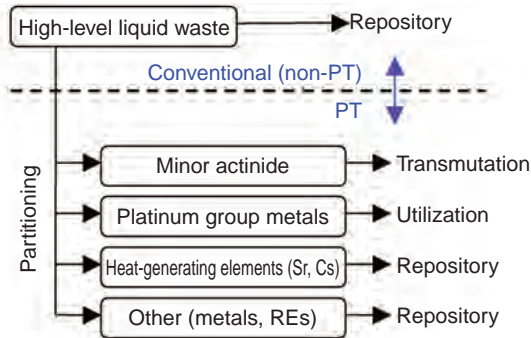


**Fig.7-7 Outline of PT technology**

High-level liquid waste is partitioned and managed according to properties of components.

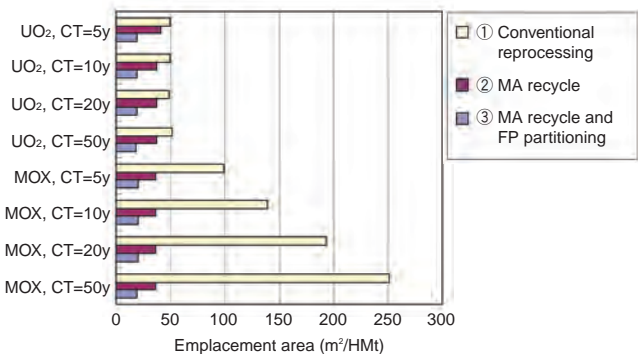


**Fig.7-9 The emplacement area of the repository for various spent fuels from light water reactors**

“UO<sub>2</sub>”, “MOX” and “CT” mean uranium fuel, mixed-oxide fuel and cooling period before reprocessing, respectively. The impact of PT technology is large for the mixed-oxide fuels.

In Japan’s current policy, the high-level radioactive liquid waste from reprocessing plants is vitrified into glass waste forms and is disposed of deep underground. In the PT technology, minor actinides (MAs), platinum group metals (PGMs), and heat-generating elements (Sr-Cs) are separated from the liquid waste as illustrated in Fig. 7-7. Then, MAs are transmuted by a “transmuter” and PGMs are utilized. An accelerator-driven system or a fast reactor will be employed as the transmuter. Sr-Cs and the remaining elements including metals and rare earths are disposed of underground. We sought to determine rational waste management methods, from the processing to storage and disposal, for these two element groups according to the properties of each group.

The heat-generating elements and the other elements are processed into calcined Sr-Cs waste and glass with high concentrations of waste, respectively. The former generates very high heat and the latter generates very low heat.

If the waste is disposed of in the same type of emplacement configuration as the conventional configuration

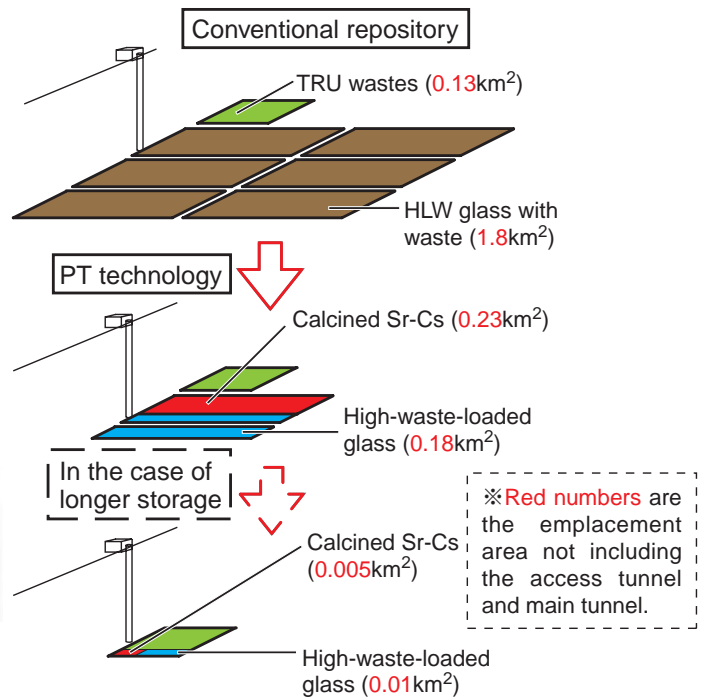


**Fig.7-8 Reduction of the HLW repository size for HLW, using PT technology**

The repository for the TRU wastes is to be attached to a repository for forty thousand pieces of waste glass. The size of the repository is reduced to one-fourth by introducing PT technology. Moreover, all of the HLW can be compactly disposed of similarly to the TRU wastes if the calcined Sr-Cs waste is stored longer before disposal.

using glass, the area of the repository will be reduced to one-fourth (Fig.7-8). This is because the calcined Sr-Cs, which tolerates high temperature and is easy to store, is stored for 130 years, and the number of glass pieces is reduced in number from forty thousand to eight thousand by high-waste-loading. Moreover, both waste forms can be very compactly disposed of in an emplacement configuration similar to that of the TRU wastes if longer storage is adopted; 320 years for the calcined Sr-Cs and 45 years for the high-waste-loaded glass.

We also studied the impact of PT technology on the repository size in various cases of spent fuel (Fig.7-9). Note that a large area is required in the case of plutonium fuel due to the accumulation of <sup>241</sup>Am when the storage period before reprocessing is prolonged. Even in such case, the repository becomes compact by transmuting the MA. The compact repository achieved by PT technology means the area that had been used for one repository can be used for a longer term.

**Reference**

Oigawa, H., Nishihara, K. et al., Parametric Survey for Benefit of Partitioning and Transmutation Technology in Terms of High-Level Radioactive Waste Disposal, Journal of Nuclear Science and Technology, vol.44, no.3, 2007, p.398-404.

## 7-3 Attempts to Improve Radiolytic Stability of Amidic Extractants for the Separation of Actinides

— Development of an Improved Extractant, Based on the Reaction Mechanism of Radiolysis —

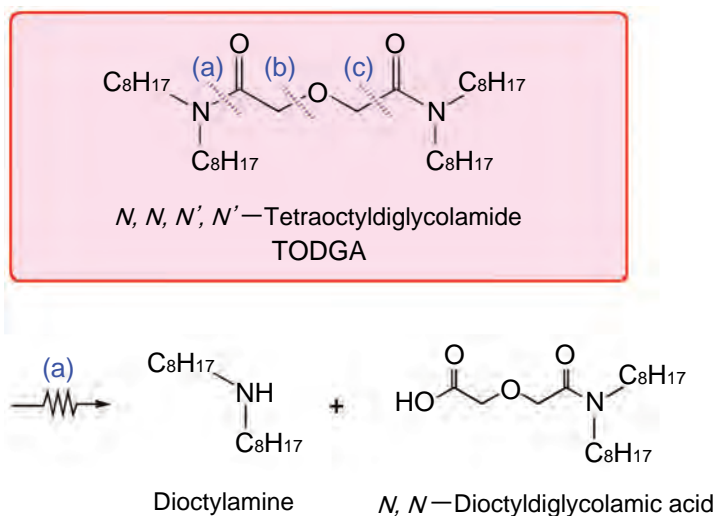


**Fig.7-10 Main reaction of TODGA radiolysis**

The bonds ((a), (b), and (c)) tend to be broken by irradiation of TODGA or its solution in *n*-dodecane with  $\gamma$ -rays. In the presence of nitric acid, the cleavage of the amide-bond (a) mainly occurs.

For the purpose of reduction in the long-term environmental burden of radioactive waste, we have developed an efficient extractant for the recovery of long-lived minor actinides from spent nuclear fuel. A tridentate diamide,  $N, N, N', N'$ -tetraoctyldiglycolamide (TODGA) efficiently extracts tri- and tetra-valent actinides from nitric acid into *n*-dodecane at high acidity.

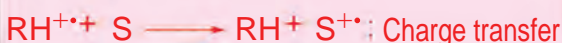
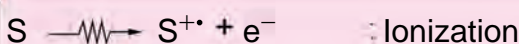
In order to evaluate the applicability of TODGA to the extracting process in high radiation fields, we investigated the radiolysis of TODGA and its effect on the extraction of actinides. We also attempted to develop an improved amidic extractant, based on the reaction mechanism of the radiolysis of TODGA in the solution.

Fig.7-10 shows the main reaction of the radiolytic degradation of TODGA by  $\gamma$ -rays. It was found that amide-bonds and bonds in the vicinity of ether oxygen were relatively weak against radiation. In particular, in the presence of nitric acid, the cleavage of the amide-bond (a) is dominant, and mainly diethylamine and  $N, N$ -diethylglycolamic acid are formed. Furthermore, the radiation effect on the extraction of actinides was investigated using a solution of TODGA pre-irradiated with  $\gamma$ -rays. Good extraction at high acidity was maintained even after irradiation up to a dose corresponding to dozens of cycles in the actual process. This result suggests

RH : *n*-Dodecane ( $n\text{-C}_{12}\text{H}_{26}$ )



S : TODGA



Ionization potential :  $\text{RH} > \text{S}$

**Fig.7-11 Reaction mechanism of TODGA radiolysis in *n*-dodecane**

The radiolysis of TODGA in *n*-dodecane is caused not only by a direct ionization reaction, but also by a charge transfer reaction between the solvent (RH) and the solute (S).

that there are some radiolytic degradation products contributing to the extraction of actinides.

Next, the radiolytic stability of TODGA in *n*-dodecane containing various additives was investigated. Since *n*-dodecane has a sensitization effect on the radiolysis of TODGA in the solution, reduction of the mole fraction of *n*-dodecane by the addition of benzene or  $N, N$ -diethylhexanamide protects TODGA from radiation.

From our pulse radiolysis study, we concluded that the sensitization effect of *n*-dodecane was mainly due to a charge transfer reaction from the radical cation of *n*-dodecane ( $\text{RH}^{+\bullet}$ ) to the TODGA molecule (S) as shown in Fig.7-11. The ionization potential of TODGA is less than that of *n*-dodecane, and the difference in the ionization potentials brings about the charge transfer reaction. Accordingly, by using solvents whose ionization potentials are lower than TODGA, TODGA can be protected from radiation.

In addition, it was confirmed that the radiolytic stability of diamide was effectively improved by the substitution of alkyl groups with aromatic groups, which are much more resistant to radiation damage. A still more improved extractant, which has high radiolytic stability as well as high ability to extract actinides, is being developed.

### Reference

Sugo, Y. et al., Influence of Diluent on Radiolysis of Amides in Organic Solution, Radiation Physics and Chemistry, vol.76, issue 5, 2007, p.794-800.

## 7-4 Toward Clarification of Minor Actinides Behavior in Pyrochemical Processes — Preparation of Minor Actinide Chlorides without the Use of Corrosive Gases —

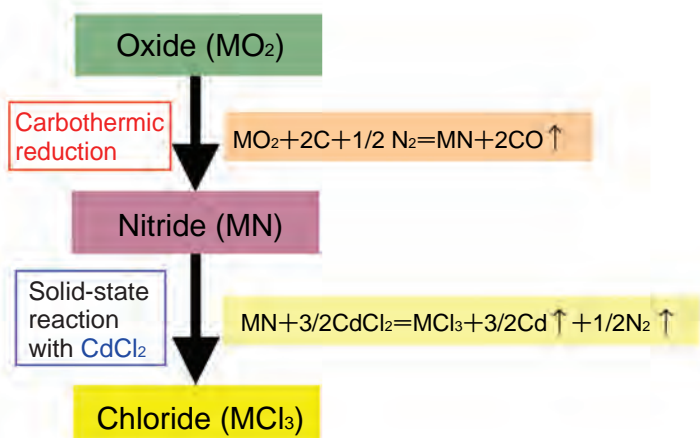


**Fig.7-12 Outline of the method for the synthesis of MA chlorides**

MA chlorides are synthesized from MA oxides without the use of corrosive gases such as chlorine. M stands for MA elements including Am.



**Fig.7-13 Appearance of the synthesized Am chloride ( $\text{AmCl}_3$ )**

$\text{AmCl}_3$  in fine powder form was obtained by heating the pellets of the mixture of AmN, which was synthesized by carbothermic reduction, and  $\text{CdCl}_2$  at 600-723K in vacuum.

In the advanced nuclear fuel cycles, minor actinides (MA: Np, Am, Cm), which are classified as high level wastes in the current nuclear fuel cycle, are to be recycled to reduce the burden of waste disposals. R&D of pyrochemical processes using molten salts as a solvent for treating MA-bearing fuels is underway. The pyrochemical processes are expected to be suitable for the treatment of spent nuclear fuels with high radioactivity and decay heat, and to have some advantages over hydrochemical processes in proliferation resistance, compactness, and economy. To develop the pyrochemical processes, understanding of MA behavior in molten salts is necessary, but few data are available. In order to obtain such data precisely, we installed a hot facility to handle MA chlorides in an inert gas atmosphere, because MA chlorides easily react with moisture and oxygen in air. A new method for the synthesis of MA chlorides on a gram scale without the use of HCl or  $\text{Cl}_2$  gas, which are used conventionally, was needed because these gases can corrode the materials of the hot facility.

We developed a method for the synthesis of MA chlorides from MA oxides, which are relatively easy to obtain, without the use of corrosive gasses. This method consists of two

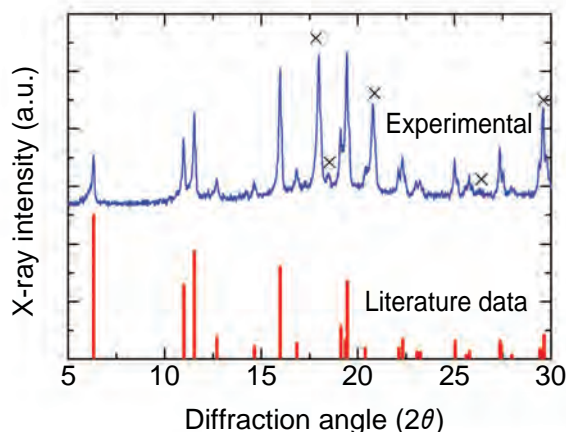


**Fig.7-14 The X-ray diffraction pattern of the synthesized Am chloride ( $\text{AmCl}_3$ )**

All the observed peaks correspond to the reported peaks of  $\text{AmCl}_3$  synthesized by a conventional method. No peaks which can be assigned to impurities were found. The peaks assigned to the Pt sample holder are marked with X.

steps. First, nitrides are synthesized from the oxides by carbothermic reduction. Then, chlorides are synthesized by the solid-state reaction of the nitrides with cadmium chloride ( $\text{CdCl}_2$ ) (Fig.7-12). We succeeded in synthesizing high purity MA chlorides including americium trichloride ( $\text{AmCl}_3$ ) (Fig.7-13, Fig.7-14) in the Module for TRU High Temperature Chemistry (TRU-HITEC) maintained with argon gas. The solid-state reaction of the nitrides with  $\text{CdCl}_2$  is suited for synthesis not only of MA chlorides but also of other chlorides with high purity, because reagents containing oxygen are not used; they can easily react with chlorides to form stable by-products such as oxides.

Our experiments using the prepared MA chlorides are elucidating the behavior of MA in molten chlorides and the behavior of americium during the electrolysis of americium nitride in molten chlorides. We will continue to study on the behavior of MA in pyrochemical processes.

This study was carried out within the collaborative research program of TRU behavior in pyrochemical processes with Tohoku Electric Power Company, Tokyo Electric Power Company and The Japan Atomic Power Company.

### Reference

Hayashi, H. et al., Synthesis of Americium Trichloride by the Reaction of Americium Nitride with Cadmium Chloride, Journal of Alloys and Compounds (2007), DOI:10.1016/j.jallcom.2007.02.011, in press.

## 7-5 Radiation Dose Assessment for a Heavily Exposed Person without any Dosimeters — Dose Assessment by Measuring Activated Sodium in the Body —

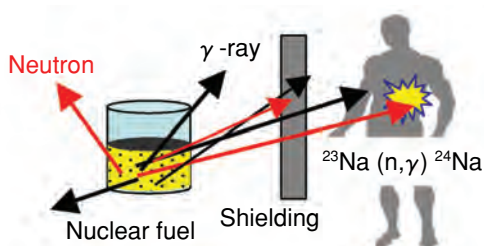


**Fig.7-15 Activation of sodium due to neutron exposure in a criticality accident**

Sodium-23 ( $^{23}\text{Na}$ ) in the human body is activated through neutron exposure in a criticality accident. The radioactivity of sodium-24 ( $^{24}\text{Na}$ ) can be measured with radiation meters.

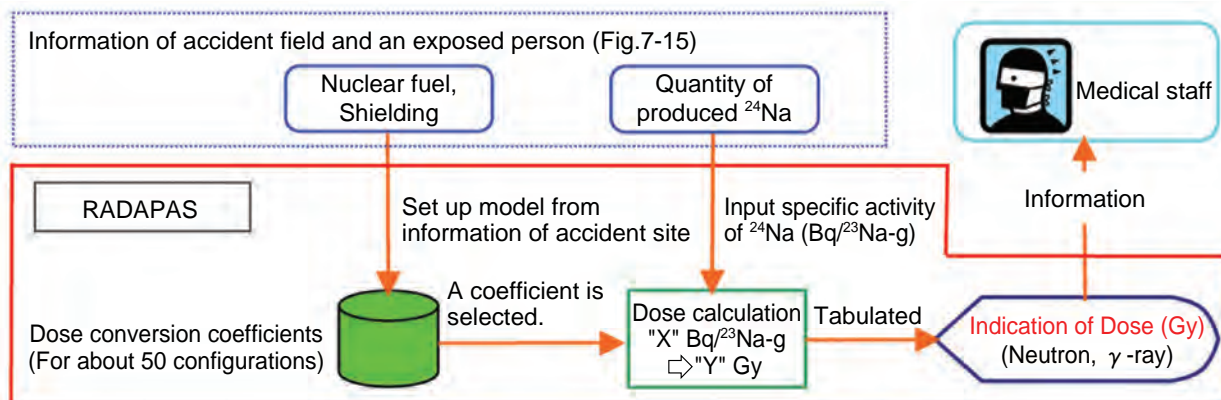


**Fig.7-16 Flowchart of dose assessment by RADAPAS, based upon source configuration data**

A user sets up a source configuration of nuclear fuel and the surrounding shielding, which determines the characteristics of radiation in a field. The database contains dose conversion coefficients for more than 50 configurations. Radiation dose induced in a body can be calculated from the radioactivity of  $^{24}\text{Na}$  using a conversion coefficient, which is automatically selected, based upon the source configuration. Radiation dose is calculated right after the conditions are input, and then the dose information can be given to the medical staff.

If a criticality accident occurs, radiation dose assessments should be performed upon heavily exposed persons, because it is essential to carry out the appropriate medical treatment according to degree of the given dose. In past accidents, however, some persons not carrying any dosimeters have suffered from heavy exposure. In such a case, radiation dose can be assessed from the activated sodium ( $^{24}\text{Na}$ ) in the body due to neutron exposure, as depicted in Fig.7-15. As the type and energy distribution of radiation in a field significantly affect the relation between the radiation dose and production of  $^{24}\text{Na}$ , dose conversion is not so easy. This method had been therefore criticized for lack of quickness and accuracy soon after a criticality accident.

Thus, we developed a program, named RApid Dose Assessment Program from Activated Sodium in human body in Criticality Accidents (RADAPAS). RADAPAS consists of a database containing dose conversion coefficients and a dose calculation program. Fig.7-16 is the dose assessment flowchart of RADAPAS. The nuclear fuel source configuration significantly affects the characteristics of radiation in a field.

A user can interactively set the conditions of the nuclear fuel and the surrounding shielding with a Graphical User Interface (GUI). A coefficient is automatically selected from a database in RADAPAS, corresponding to the source configuration. After that, the user inputs the activity of the produced  $^{24}\text{Na}$ , and then radiation dose from neutrons and  $\gamma$ -rays is calculated. The database has conversion coefficients for more than 50 hypothesized source configurations, which were derived by radiation transport calculations. Thus, radiation dose can be accurately calculated from the radioactivity of  $^{24}\text{Na}$  and the result is displayed in a chart. In addition, RADAPAS can carry out dose assessment more accurately if the radiation characteristics in a field have been analyzed in detail.

The applicability of RADAPAS to a dose assessment after a criticality accident was verified with an experiment at the Transient Experiment Facility (TRACY). Thus, radiation dose can be rapidly and accurately given to medical staff after an unexpected accident, where no useful information can be obtained from any dosimeters.

### Reference

Takahashi, F. et al., Development of Rapid Dose Assessment Program from Activated Sodium in Human Body for Criticality Accident, Hoken Butsuri, vol.41, no.3, 2006, p.180-187.

## 7-6 Estimation of Quality and Quantity of DNA Damage Sites — New Method to Characterize DNA Damage Produced by Radiation —

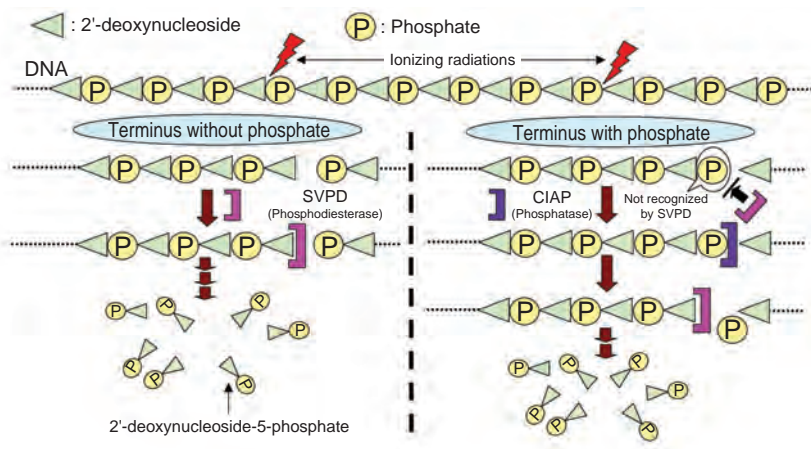


**Fig.7-17 Protocol to analyze DNA strand-break termini using SVPD**

A 2'-deoxynucleoside is constructed from a nucleobase and a 2'-deoxyribose. Ionizing radiation also injures nucleobases, some of which can be removed by piperidine. The lesions are cleaved, leaving a terminus with phosphate. Then, it is possible to estimate the yield of the lesions using the increase in the amount of termini with phosphate in piperidine-treated irradiated DNA.

Environmental factors stimulating a living body, such as ionizing radiation, can injure DNA which is important for heredity. Ionizing radiation has the ability to cause a variety of types of damage in DNA. This radiation may be classified into  $\gamma$ -rays, X-rays, neutrons, and heavy ion particles. Each type of radiation has an individual DNA damage spectrum. Utilizing this fact, we have developed a new-concept analytical method to estimate the DNA damage spectrum. There are three categories of detection methods so far; one is a method using an antibody recognizing a specific type of damage, the second one uses chemicals reactive to a specific functional group on the damaged site, and the third one uses a supercoiled plasmid DNA. Though these methods are useful to detect damage whose type is known, it is difficult to know the overall spectrum of DNA damage containing undetermined damage. The new method introduced here will be a powerful technique to view overall DNA spectrum.

DNA damage is generally classified into two categories. one is "strand break", which occurs by cleavage of a molecular chain of DNA. The other is "nucleobase damage", which occur by destruction of a part of a nucleobase, carrying genetic information of the organism. There are two kinds of termini in the strand break pattern: the termini with or

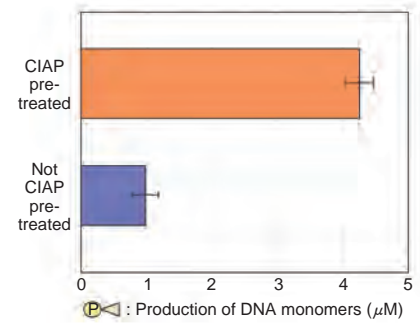


**Fig.7-18 Production of DNA monomers from DNA strand-break termini by SVPD**

**Table 7-1 DNA damage by  $^{60}\text{Co}$   $\gamma$ -rays**

Category of lesions	Yield ( $\mu\text{mol}/\text{J}$ , $\times 10^{-9}\text{Gy}^{-1}\text{Da}^{-1}$ )
Total termini	0.102
Termini without phosphate	0.024
Termini with phosphate	0.078
Nucleobase damage	0.084

without phosphate (Fig.7-17). We have developed the protocols to quantify (1) termini without phosphate, (2) termini with phosphate, and (3) nucleobase damage. An enzyme, snake venom phosphodiesterase (SVPD), recognizes a terminus without phosphate and cuts DNA monomers sequentially from this terminus. Then, the yield of (1) can be quantified since the amount of the DNA monomers produced during incubation for a given period is proportional to that of damage (1). Furthermore, pre-treatment of irradiated DNA by another enzyme, calf intestine alkaline phosphatase (CIAP), enables damage (2) to be recognized by SVPD since CIAP removes phosphate and so converts damage (2) to damage (1) (Fig.7-17, Fig.7-18). On the other hand, pre-treatment of irradiated DNA by a chemical, piperidine, can convert some of the (3) damage to terminals (2), which can become recognizable after CIAP pre-treatment as mentioned previously (see caption in Fig.7-17). The results obtained from the analysis are shown in Table 7-1. Other methods of DNA damage analysis cannot give us these data in principle. This new analytical protocol is a unique idea, and analyses using a variety of combinations of other enzymes made possible by this methodology will elucidate unknown DNA damage.

### Reference

Akamatsu, K., A Novel Methodology for Characterizing Strand-Break Termini and Damaged Bases in Plasmid DNA Exposed to Ionizing Radiation, *Analytical Biochemistry*, vol.362, issue 2, 2007, p.229-235.

## 7-7 Demonstration of Excellent Safety Characteristics of HTGR — Coolant Flow Reduction Test Using HTTR —

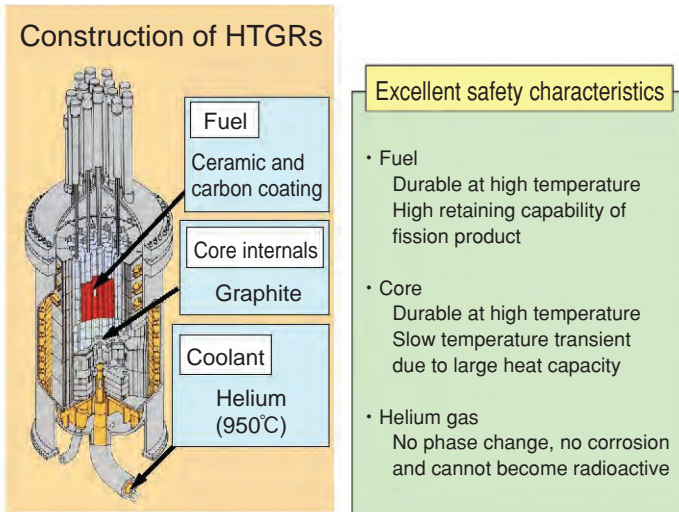


**Fig.7-19 Excellent safety characteristics of HTGR**

HTGR uses TRISO coated fuel particles for fuel, helium which does not undergo chemical change even at high temperature for coolant, and graphite which has large heat capacity for core internal structures. Such characteristics mean that the possibility that significant core damage will occur in the HTGR is extremely small.

Working for a wide variety of energy sources ensuring a stable supply, as well as global environmental protection, we are leading the world in R&D of the high temperature gas-cooled reactor (HTGR). The high temperature durability of coated fuel particles with fourfold ceramic and carbon coatings can effectively retain fission products. The large heat capacity of the core made with graphite can restrain rapid temperature rise. Helium gas, the primary coolant does not change phase and does not react chemically, so that there is no corrosion of reactor components.

HTGR has been evaluated highly for its excellent safety characteristics, judged to be the reactor least likely to incur significant core damage even if an earthquake stronger than that envisioned occurs, as shown in Fig.7-19. There is worldwide demand that such excellent safety characteristics of HTGR which is a next-generation nuclear plant producing heat of 950°C be demonstrated with an actual reactor.

“HTTR” is the only reactor in the world producing heat of 950°C and the nearest reactor of the next-generation HTGR. Therefore, the success of the safety demonstration test performed at HTTR, the coolant flow reduction test of the fuel and core structures performed under very strict conditions, is very important.

In the initial tests, reactor power rose step by step from

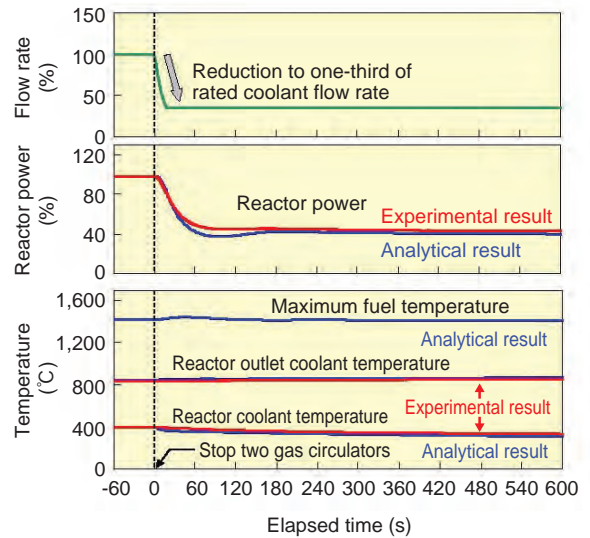


**Fig.7-20 Experimental results at full reactor power (30MW)**

The experimental results demonstrated the excellent safety characteristics of the reactor, the reactor power becoming stable even if the coolant flow drops to one-third.

30% capacity (9MW) and the final test was successfully completed at full reactor power (30MW) for the first time in the world.

In the test, two out of three gas circulators were stopped so that the coolant flow was reduced to one third of the rated value. The fuel and graphite temperature rose because the cooling capability of the core decreased due to the reduction of the coolant flow. As the number of fission reactions decreased due to the inherent self-regulating characteristics, the reactor power decreased and became stable naturally. The reactor inlet and outlet coolant temperatures changed little and remained stable as shown in Fig.7-20.

Improvement of the safety analysis code is in progress; with this, prediction of the reactor power which is accurate within 8% becomes possible. The experimental results confirmed the excellent safety characteristics of the reactor even with rapid reduction of the coolant flow. It is considered that HTGR doesn't need an emergency shutdown system. As a next stage, we are planning a more severe test with loss of the coolant flow in HTTR. The present study is the result of project “Quantitative Demonstration of HTGR Inherent Safety Features” entrusted to the Japan Atomic Energy Agency by the Ministry of Education, Culture, Sports, Science and Technology of Japan (MEXT).

### Reference

Takamatsu, K. Nakagawa, S. et al., Core Dynamics Analysis for Reactivity Insertion and Loss of Coolant Flow Tests Using the HTTR, Proceedings of the 15th International Conference on Nuclear Engineering (ICONE15), Nagoya, Japan, 2007, ICONE15-10158, in CD-ROM.

## 7-8 Outstanding Economic Efficiency of HTGR for Electricity Generation — Design Study on the HTGR with Gas Turbine —

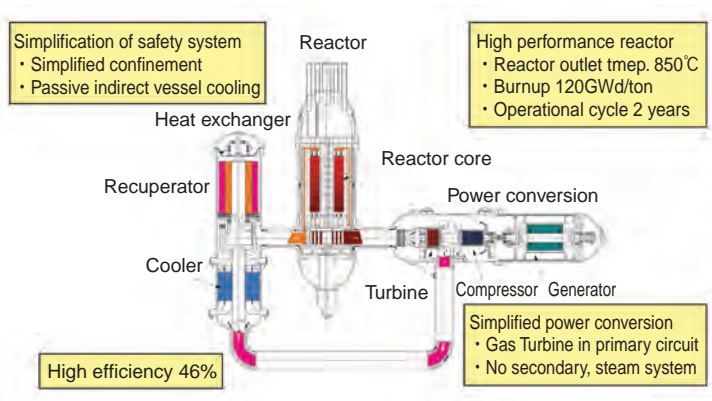


**Fig.7-21 Technical features contributing to excellent economics**

The GTHTR300 reactor has a simple system layout, including a power conversion unit and a heat exchanger unit (Fig.7-21). The capital cost is ¥200k/kWe (Fig.7-22). The passively-safe reactor requires a low-power-density core, resulting in large cost; the power conversion unit and the balance of the plant are less costly due to their overall design simplicities. The cost of electricity including costs of capital, fuel and O&M is ¥4/kWe

We have been developing an advanced electricity generation system using the Gas Turbine High Temperature Reactor 300 (GTHTR300) to contribute to reducing greenhouse gas emissions and preventing climate change. The 850 °C reactor helium gas coolant is directly used to power a gas turbine for generation of electricity (Fig.7-21). The efficiency of electricity generation is as high as 46% which is substantially better than the 33% of the Light Water Reactor with a 300°C steam turbine. The design simplicity is another important feature of the GTHTR300, which does not include a secondary system and a steam supply system, as does the LWR. The HTGR, designed to be inherently and passively safe, is limited to a low power density of 6MW/m<sup>3</sup> which makes its core larger in size than the LWR. On the other hand, the unique strong safety features result in design simplicity of the GTHTR300 engineered safety system.

The fuel, consisting of ceramic coated particles, is highly resistant to irradiation and is capable of maintaining integrity in fuel burnup of 120 GWd/t or higher. However, the fuel fabrication is a complex and thus costly technical process.

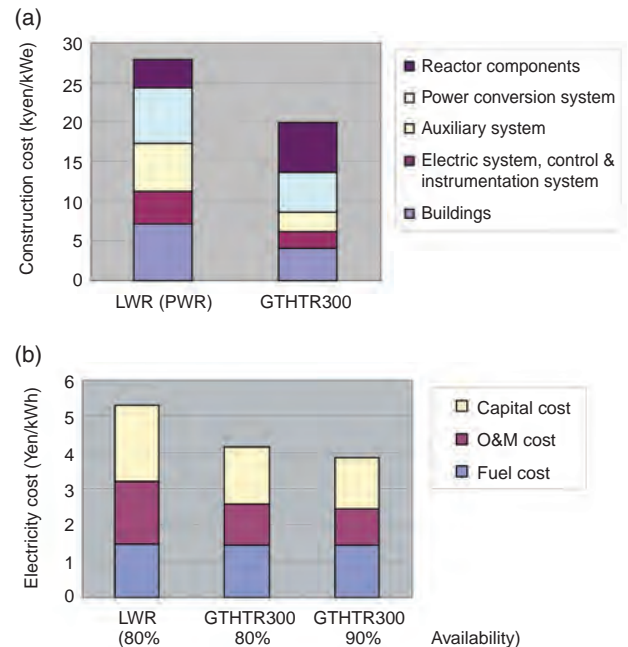


**Fig.7-22 Cost comparison between LWR and GTHTR300**

Considering the merits and drawbacks of the system, we have evaluated the economics of the GTHTR300 and compared it with that of the current large scale LWR. The economic evaluation reflects the system basic design. The estimated capital cost per unit of electricity is approximately 25% less than that of the LWR (Fig.7-22 (a)). The fuel cycle cost is comparable with that of the LWR, since the high fabrication cost is offset by the low backend cost because the amount of spent fuel is only about 1/3 of the LWR, which reduces the reprocessing cost. The cost of operation and maintenance is about 35% less than that of the LWR because the use of chemically inert helium gas as reactor coolant simplifies maintenance of reactor components.

In sum, the GTHTR300's net cost of electricity generation with a plant usage rate of 80% is estimated to be ¥4.2/kWh, as opposed to the ¥5.3/kWh of the LWR (Fig.7-22 (b)). The GTHTR300 thus offers an economically competitive option for nuclear power generation.

This design study was entrusted by MEXT.

### Reference

Takei, M., Kunitomi, K. et al., Economical Evaluation on Gas Turbine High Temperature Reactor 300 (GTHTR300), Nippon Genshiryoku Gakkai Wabun Ronbunshi, vol.5, no.2, 2006, p.109-117 (in Japanese).

## To Establish the Nuclear Fuel Cycle

We execute various types of research and development of spent nuclear fuel reprocessing and mixed oxide (MOX) fuel fabrication, etc., including joint research projects, to promote development of nuclear fuel cycle technology in Japan.

Moreover, we actively carry out technical co-operation based on the results of our research and development with Japan Nuclear Fuel Ltd. (JNFL), which is engaged in the nuclear fuel cycle business as private entrepreneur in Rokkasho village, Aomori Prefecture.

### 1. Technological Development of Spent Fuel Reprocessing

JAEA's Tokai Reprocessing Plant (TRP) terminated reprocessing operations based on the service contract with electric power companies at the end of FY2005, and changed over to research and development operations in FY2006.

In the "07-1 campaign" starting in February 2007, TRP began a reprocessing examination that used "FUGEN type B" MOX spent fuel whose content of plutonium and burn-up were higher than the fuel which had been reprocessed before ("FUGEN type A" MOX spent fuel). We are planning examination of dissolution characteristics and solvent degradation etc. that will examine the features of the MOX spent fuel over several years. We also will continue research concerning behavior and separation etc. of minor actinide nuclides such as Neptunium and technological development to upgrade light-water reactor spent fuel reprocessing technologies such as safeguard technology.

As for the vitrification technology of high-level radioactive waste, we will continue operation of an improved type of glass melter which has been operating since FY2004, and accumulate data on the operation stability of this melter. Moreover, we will carry out technological development into a long-lived melter and glass melter dismantlement.

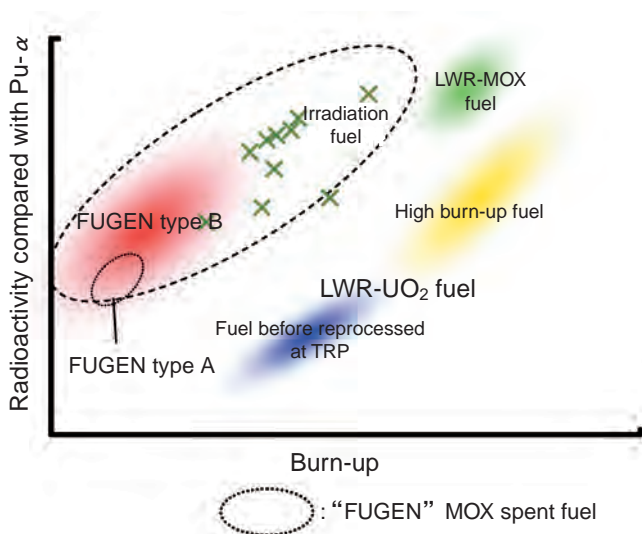


**Fig.8-1 Features of "FUGEN" MOX spent fuel (ex.)**

"FUGEN" MOX fuel has characteristics close to those of LWR-MOX fuel, such as high specific  $\alpha$ -radioactivity of Pu, in spite of its relatively low burn-up.

### 2. Technical Co-operation

#### (1) Technical Co-operation to Enrichment Businesses

We continue to execute technical co-operation to JNFL, dispatching engineers and transferring enrichment technology of JAEA etc. for the super-efficient new material centrifuge (new model) cascade examination that JNFL began in April, 2006.

Moreover, as entrusted by JNFL, we executed quality control of the centrifuge for cascade examination, operation management of the Rokkasho Enrichment Plant, and consulting for the uranium adhesion amount measurement system for the centrifuge etc.

#### (2) Technical Co-operation to Reprocessing Business

We provided technical co-operation allowing the smooth execution of an active examination of the Rokkasho Reprocessing Plant (RRP) that JNFL had been carrying out since March 2006, such as dispatch of an engineer who had operation experience in TRP and dispatch of an analysis technical leader as urgent support when there was pollution trouble, etc.

Moreover, entrusted by JNFL, JAEA executed technological training of JNFL engineers in TRP, electromagnetic field analysis of a micro wave denitrate heater, and measurement of physical properties of powder uranium oxide that had been obtained from the RRP uranium-plutonium mixture denitrate facility, etc.

In addition, JAEA and JNFL concluded an agreement to extend expiration date of their "Agreement concerning providing technical assistance during trial operation of reprocessing plant" in May, 2007.

#### (3) Technical Co-operation to MOX Fuel Fabrication Business

The MOX fuel fabrication business of JNFL is now in the stage of safety assessment by the government prior to permission for operation. We have started negotiations for a co-operation plan, including dispatch of engineers, for construction and operation of the MOX fuel fabrication plant with JNFL.

Moreover, entrusted by JNFL, we executed technological training of JNFL engineers in the Tokai MOX Fuel Fabrication Facility, did a confirmatory examination of MOX fuel powder adjustment equipment, etc.

#### (4) Other Technical Co-operation

We dispatched engineers according to a request from the Nuclear Material Control Center (NMCC), and executed technical co-operation concerning nuclear material management in the Rokkasho district.

Moreover, we accepted a request from JNFL and concluded an agreement for technical co-operation to enable use of the technical knowledge that we gained in its cooperation with JNFL, to promote the Global Nuclear Energy Partnership (GNEP) that the United States Department of Energy (USDOE) advocates in cooperation with French company AREVA, in June, 2007.

## 8-1 Accurate Measurement of Plutonium Nitrate Solution — Accuracy & Reliability by Digital-Quartz Transducers Confirmed by Comparison of Two Densities and by Applying Them to Solution Mass Monitoring —

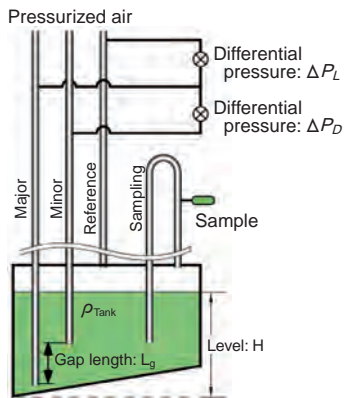


**Fig.8-2 Measurement of solution density and volume in a tank**

Spent nuclear fuel used in the light water reactor is dissolved and reusable uranium and plutonium are extracted in the form of nitrate solution at the Tokai reprocessing plant. These solutions have to be converted to mixed oxide (MOX) powder to reuse them as nuclear fuel. We have developed and adopted a method to convert directly the mixed nitrate solution to MOX, which has high resistivity to nuclear proliferation because it is absolutely impossible to make pure plutonium oxide. Considering the danger of pure plutonium nitrate solution, we have carried out very carefully and strictly the measurement and management of plutonium.

Plutonium solution before mixing with uranium solution is stored in a tank shown in Fig.8-2. The difference of back pressures between three tubes filled with air is measured accurately using two digital-quartz pressure transducers. The differential pressure between the Major and the Minor tubes ( $\Delta P_D$ ), the differential pressure between the Major and the Reference tubes ( $\Delta P_L$ ) and the solution volume ( $V$ ) are expressed in terms of the solution density ( $\rho_{\text{Tank}}$ ), gravity acceleration ( $g$ ), solution level ( $H$ ), vertical differential length between the Major and the Minor ( $L_g$ ) and the tank-specific (fixed) calibration function ( $F$ ) to determine  $V$  from  $H$ :

$$\begin{aligned} \cdot \Delta P_D &= \rho_{\text{Tank}} \cdot g \cdot L_g \\ \cdot \Delta P_L &= \rho_{\text{Tank}} \cdot g \cdot H \\ \cdot V &= F(H) \end{aligned}$$

$L_g$  and  $g$  are constants, so  $\rho_{\text{Tank}}$ ,  $H$ , and  $V$  can be calculated from  $\Delta P_D$  and  $\Delta P_L$ . These equations are derived from measurement principles, and actual equations include some corrections for such factors as pressure distribution inside the tubes. It is very important that accurate measurement is done while the solution is motionless. Plutonium mass is determined from  $\rho_{\text{Tank}}$  and  $V$  measured by this method,

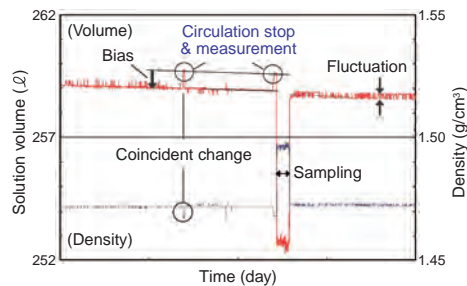


**Fig.8-3 Example of continuous volume monitoring data**

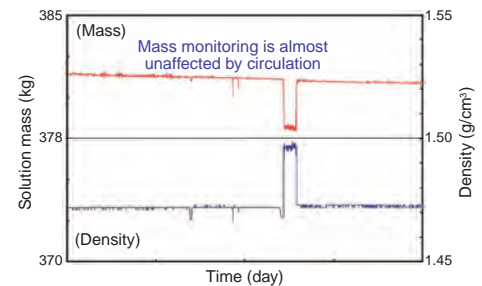


**Fig.8-4 Example of continuous mass monitoring data**

$\rho_{\text{Labo}}$ , the solution density and the plutonium concentration of the test sample at the temperature of the laboratory measured by another method. These two density results are corrected for the temperature difference between tank and sample. These results should match after considering the temperature dependency. If the results do not match, it is assumed that there is/are unexpected error/s. In such a case, re-measurement is carried out fully or partly in order to complete accurate determination of plutonium mass.

However, the solution has to be circulated by air to remove hydrogen gas generated by alpha radiation except at the time of accurate precise measurement. During the circulation, a small change in volume caused by motion of solution or change in temperature is observed. Here, we introduced solution mass defined as  $\rho_{\text{Tank}} \times V$ , and it became clear that we can distinguish clearly the change in volume by appearance and the correct change such as evaporation.

An example of continuous volume monitoring is shown in Fig.8-3. The time when circulation is stopped is very short, and this volume is correct. The air affects  $\Delta P_D$  measurement, and  $\rho_{\text{Tank}}$ , causes both the changed appearance of  $H$  and the minus bias of around 0.2% and fluctuation of  $V$ .

Another example of continuous mass monitoring is shown in Fig.8-4, where the effect of  $\rho_{\text{Tank}}$  observed in Fig.8-3 is amazingly reduced. In addition, gradual decrease of mass due to evaporation is observed correctly and it was confirmed that there was little change in volume due to temperature before/after sampling.

As a result, it is possible to measure correctly and stably the amount of solution using this continuous mass monitoring method even though there is circulation.

### Reference

Hosoma, T., Mukai, Y. et al., Reduction of Fluctuation and Small Bias Observed in Continuous Volume Monitoring taken in an Annular Tank for Plutonium Nitrate, Symposium on International Safeguards: Addressing Verification Challenges, (IAEA-CN-148), Vienna, Austria, 2006, p.192-194.

## 8-2 Contributions to Safeguards and Further Efficiency

### — Safeguards Improvement for the Tokai Reprocessing Plant —

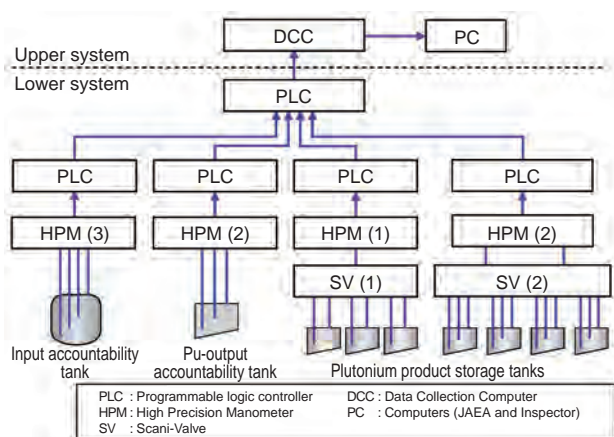


**Fig.8-5 Outline diagram of solution measurement and monitoring system**

This system consists of the upper system (recording with computer, etc.) and the lower system (measuring instruments and their control devices). The level and the density of each tank are calculated from differential pressure measured with high precision manometers connected to a couple of dip-tubes installed in the tanks, the measured data being recorded in the computer. The high precision manometer has a structure such that an inspector can authenticate it.

Tokai Reprocessing Plant (TRP) has actively cooperated with the implementation of safeguards (SG) by Japan and IAEA, and has also actively engaged in the development of technology for the strengthening and the efficiency of these safeguards.

In past activities, the inspector of the plant requested that an “SG Improvement Plan” be drawn up for the strengthening and efficiency of the IAEA’s SG. The improvement plan consisted of four areas and ten tasks. TRP engaged in implementation of each item after repeated discussions with the inspector. This resulted in improvements of the weak points of SG for TRP and efficiency in inspection. The current SG system instituted following the “SG improvement plan” is a platform for introducing integrated safeguards including short notice random inspections of TRP in the future.

(1) Improvement of system for verification of facility design information

All the facilities covered by the IAEA’s SG provide answers to the Design Information Questionnaire (DIQ) to IAEA. The DIQ elicits very important information, and the inspector develops the SG approach for a facility on the basis of the DIQ. TRP contributes to the smooth implementation of IAEA’s SG by providing the process diagram and detailed drawings of the primary tank, and information such as Pu amount and its distribution in the process, the operational method of each process, and measurement methods.

Additionally, the procedure for verifying the design information continuously was established based on the discussions with the inspector. The guarantee of the validity of the facility’s declarations is strengthened because the procedure enables the IAEA to verify the absence of undeclared design change by which nuclear material (NM)

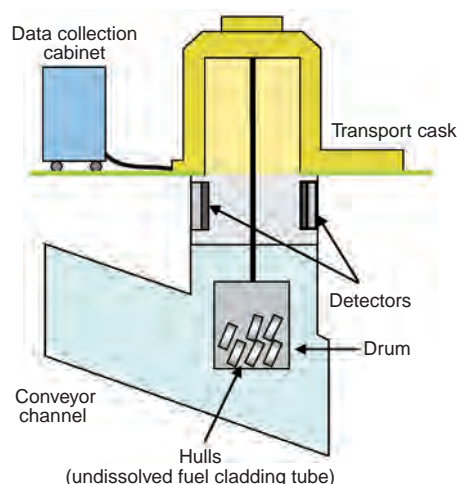


**Fig.8-6 Outline diagram of Hull measurement and monitoring system**

This system consists of control part (computer, etc.) and measurement part (neutron detector, etc.). The neutrons emitted from spontaneous fission of  $^{244}\text{Cm}$  in the drum are measured, and the amounts of Pu and U in the drum are calculated using the ratios of  $^{244}\text{Cm}/\text{Pu}$  and  $^{244}\text{Cm}/\text{U}$  calculated by a burnup calculation code.

could be diverted.

(2) Improvement of reliability of verification for primary tank on SG

TRP developed the Solution Measurement and Monitoring System by addition of a tamper detection function and function for authentication thereof by the inspector, and addition of an important tank, input accountability tank, on SG to the existing system that measures the solution level of the tanks in which an important Pu product is measured or stored (Fig.8-5). The system enables inspectors to measure the level of Pu solution independently and to detect the absence of fraudulent solution changes. Also, the transparency of the handling of the Pu solution was further improved.

(3) Establishment of waste verification method

TRP developed an unattended non-destructive assay system in cooperation with Los Alamos National Laboratory in order to measure a slight amount of NM associated with fuel cladding tube (Hulls) remaining after spent fuel is dissolved (Fig.8-6). The system enables quantity inspection for waste and verification that the hulls are one of the causes of Shipper Receiver Difference (SRD: difference in the amounts of NM in the reactor and at TRP). The efficiency of inspection is also improved using a system that is unattended.

(4) Improvement of NM accountability

TRP has engaged in methods to investigate the cause of SRD, and SRD has been decreased by reevaluation of nuclear loss (Decrease of Pu by radioactive decay) of the spent fuel, establishment of the analytical method to detect a slight amount of NM contained in the undissolved residuals in the high active liquid waste, etc. Accurate accountability control was developed through this improvement.

#### Reference

Onizawa, T. et al., Safeguards Improvement for the Tokai Reprocessing Plant (TRP), Symposium on International Safeguards: Addressing Verification Challenges, (IAEA-CN-148), Vienna, Austria, 2006, p.203-205.

## R&D for Decommissioning and Rad-Waste Management

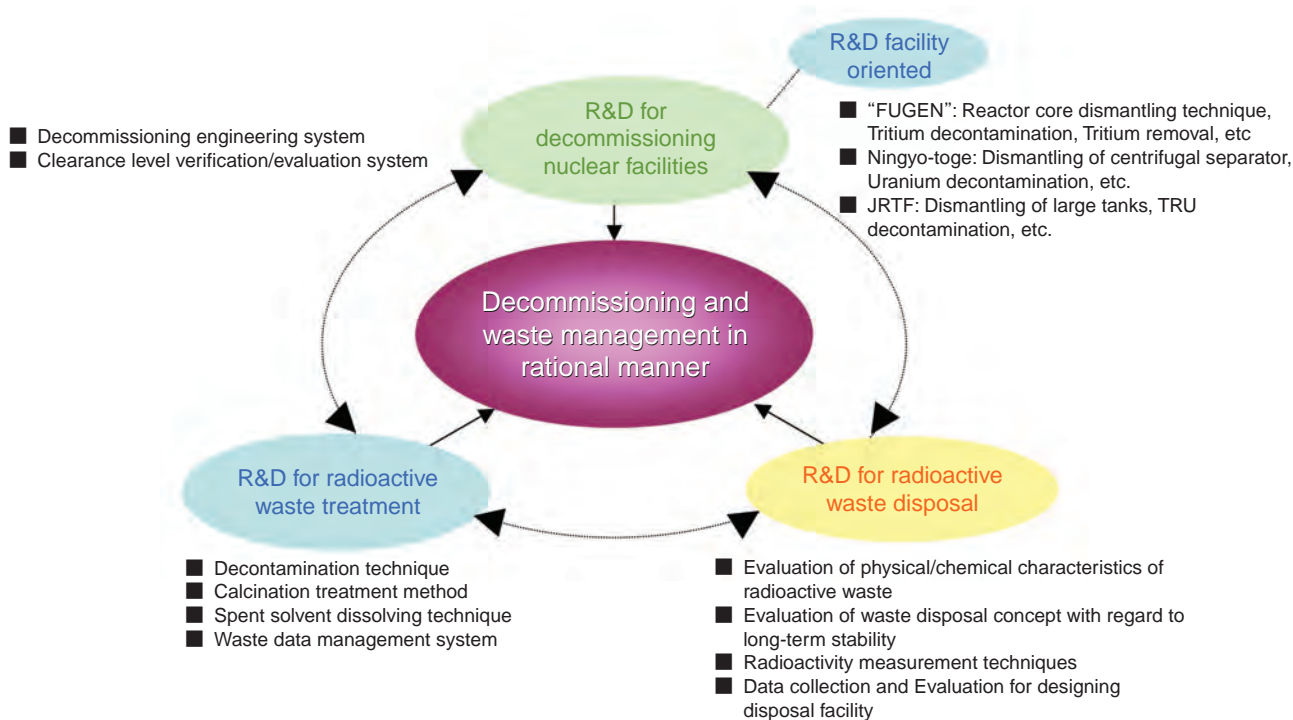


Fig.9-1 Research & Development for decommissioning and rad-waste management

It is the facility owner's and/or waste generator's responsibility to decommission unneeded facilities and to treat/dispose of generated radioactive waste, respectively. Research & Development (R&D) might be necessary for decommissioning and rad-waste management measures allowing these processes to be carried out in a cost effective manner while securing safety. We therefore determined the technology necessary for decommissioning and rad-waste management measures supporting the R&D shown in Fig.9-1, and then dedicated our midterm plan (2005-2009) to development of this base technology. The major progress achieved in this R&D is as follows.

### R&D for Decommissioning

A lot of know-how and data on removal remote handling, waste management, etc. have been gained through past decommissioning experiences. Utilizing this knowledge effectively, we are developing a decommissioning engineering system and a clearance level verification/evaluation system to support the planning of decommissioning and clearance implementation, respectively. A prototype version of clearance level verification/evaluation system was built and the relevant data on clearance were collected for the system.

In addition, R&D is under way at facility sites, considering specific conditions. At the Fugen site, performance of abrasive water jet cutting was tested for reactor components (Topic 9-1). Decontamination capability of a uranium contaminated centrifuge machine at the Ningyo-toge site was tested. The waste storage tanks contaminated with transuranic nuclides were dismantled to evaluate the

efficiency of techniques applied at the reprocessing test facility in the Tokai site.

### R&D for Waste Treatment

For accumulation of data on calcination treatment, studies are in progress to evaluate the behavior of aluminum metal materials during melting and oxidation, obstruction of smoke exhaust routes by metal materials with low-melting-temperature, and transfer of radio nuclides in the calcination process. Further, decomposition treatment of organic waste liquids was tested using actually used solvents. In addition, basic designs for the waste data management system with input/output functions for waste identification, etc. were studied, and radioactivity data is continuously being collected for the database.

### R&D for Waste Disposal

For disposal of radio-isotope and laboratory waste, studies were conducted on selection of essential nuclides for safety evaluation and physical, chemical and radiological characteristics of wastes. Evaluation of influence of cement and nitrate content on nuclide migration in disposal systems, and long-term stability of transuranic waste disposition is being carried out, and nuclide migration behavior studies are planned.

A multi- $\gamma$ -ray measurement device was built for simplified and rapid measurement of radioactivity for evaluation of waste disposal. A simplified tritium measurement method was also developed for giving clearance to concrete debris (Topic 9-2).

## 9-1 Cutting Method for a Narrow Space with Little Heat Generation — Dismantling of the Core by the Abrasive Water Jet Cutting —

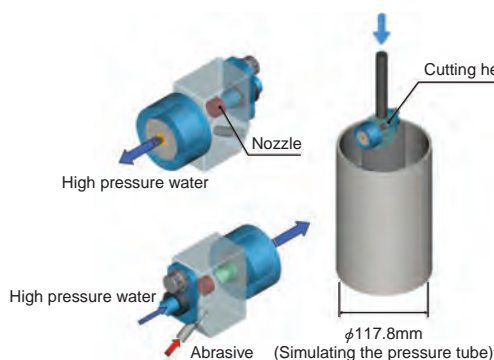


Fig.9-2 Downsized AWJ cutting head



Fig.9-3 Specimen used in the experiment (The tubes were arranged coaxially and cut from inside simultaneously)

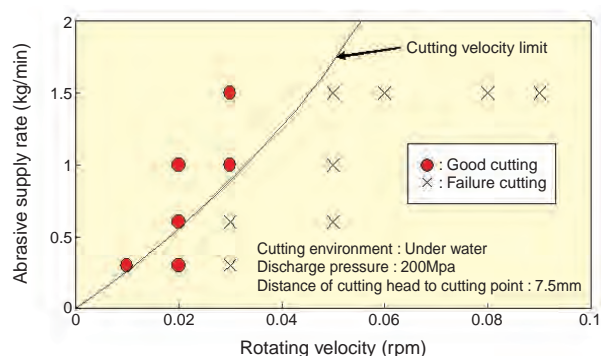


Fig.9-4 Relationship between rotating velocity of cutting head and abrasive supply rate (Specimen: thick double-tube)

Care must be taken to prevent the diffusion of radioactive materials during dismantling of nuclear facilities. In the case of cutting structural materials of the facilities, fume and/or dross may be generated due to the melting or the evaporation of the materials with heat. Especially, for the dismantling of structure containing the radioactive materials, it is desirable to choose a cutting method that produces few fumes, to suppress the diffusion of the radioactive materials. Moreover, it is required that the cutting device can be used in facilities with complicated and narrow geometries as in reactor cores.

Considering the above, the abrasive water jet (AWJ) cutting method, the head of which is relatively small, was selected as one of the favored technologies for dismantling of the core of "FUGEN". In this method, the heat generated by cutting is low, because structural materials are cut by high-pressure (200-400 MPa) water with abrasive discharged from the cutting head.

The core of "FUGEN" contains many vertical pressure tubes arranged at small intervals. It is, therefore, necessary to cut the pressure tube from its inside since this is the wider space, in the dismantling work. A downsized AWJ cutting

head (Fig.9-2) which can be inserted inside the pressure tube, has been developed. Appropriate cutting conditions for dismantling the core were also determined in the experiments using a double-tube specimen simulating the pressure and calandria tubes, arranged coaxially. The experiments were carried out under the water to simulate the actual conditions of the dismantling work.

As the results of the experiments, it was confirmed that the AWJ cutting method generates few fumes, and is able to cut the two tubes at the same time (Fig.9-3). It was also clarified that the relationship between the abrasive supply rate and the nozzle rotating velocity can be expressed by considering the momentum conservation between the abrasive and the water, and the kinetic energy of the abrasive transferred to the structural materials (Fig.9-4). The optimum abrasive supply rate and cutting velocity can be also estimated using the above relation.

It is concluded that the AWJ cutting method is practical for dismantling nuclear facilities that have completed their missions. Useful data for optimizing the method were obtained in this study.

### Reference

Nakamura, Y. et al., Applicability Examination and Evaluation of Reactor Dismantlement Technology in the Fugen -Examination of Double Tubes Cutting by Abrasive Water Jet-, Proceedings of 14th International Conference on Nuclear Engineering (ICONE14), Miami, USA, 2006, ICONE14-89380, in CD-ROM.

## 9-2 Measurement of Low Concentrations of Tritium in Concrete — Confirmation of Tritium Contaminant Clearance —

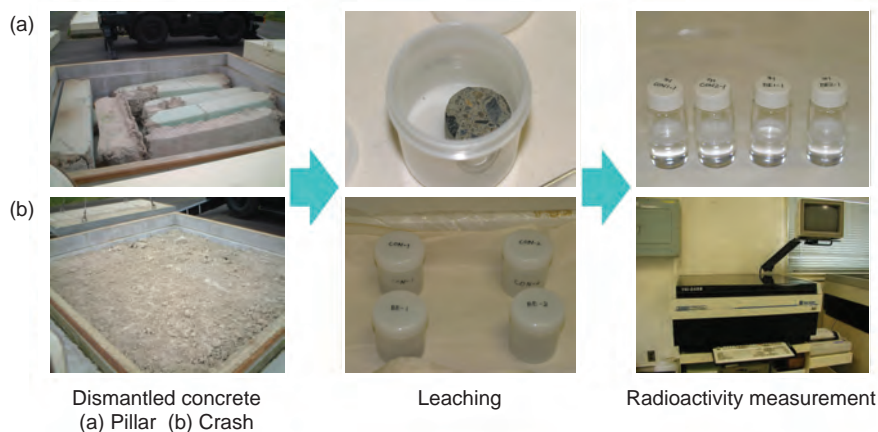


Fig.9-5 Schematic diagram of tritium measurement by a leaching method

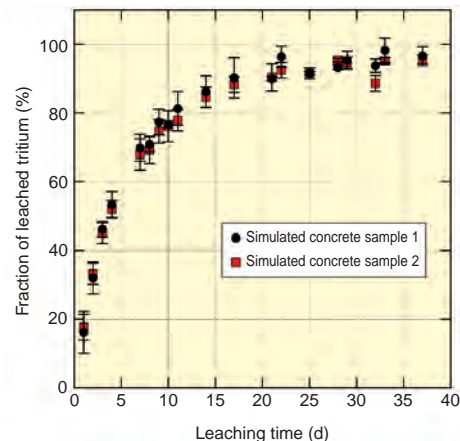


Fig.9-6 Leaching behavior of tritium in simulated concrete samples

Decommissioning of nuclear facilities generates a lot of waste such as concrete and metal. The radioactivity of some of the waste is lower than the clearance level, the radioactivity level below which radiation sources can be released from regulatory control. From the viewpoint of reduction of the amount of radioactive waste and efficient use of resources, effective use of the concept of clearance is important.

When the Japan Research Reactor No.3 (JRR-3) was modified, a lot of concrete waste was generated. This concrete waste had a possibility of contamination with tritium generated by the neutron capture reaction of deuterium. However, about four thousand tons of this concrete was estimated to be under the clearance level for radioactivity. Therefore, it was necessary to establish a reliable method to determine whether tritium concentration was lower than the clearance level in this concrete.

Because tritium is a low energy  $\beta$ -ray emitter, its concentration in concrete cannot be determined by an external radiation measurement method. In order to confirm the tritium concentration in a massive amount of concrete, it is necessary to analyze a lot of representative samples. A leaching method, where the sample is immersed in water and the tritium in a sample is leached into the water, was applied to measure the concentration of tritium in the concrete

because this method is able to analyze a lot of samples at once (Fig.9-5).

Tritium measurement with the leaching method was generally carried out using crushed concrete or a few g of a massive sample. However, it is known that some tritium is lost during sample powdering or milling. Therefore, *ca.* 50g of a massive sample was used for analysis of tritium to avoid a loss of tritium during sample preparation. Two kinds of simulated concrete samples doped with tritium were immersed in 100g of water, and the relation between the fraction of leached tritium and leaching time were investigated (Fig.9-6, reference). The result shows that 95% of the tritium in the concrete is leached into the dipped water in 30days. Based on this result, tritium concentration in dismantled concrete samples from “JRR-3” was determined. The tritium concentration determined by the leaching method was in good agreement with that determined by the heating method (sample was heated 2h at 1173K and evaporated tritium was recovered with a cold trap and measured). This indicates that the leaching method is a useful and reliable method to analyze tritium in concrete. Also, the detection limit of the leaching method is over 100times lower than the tritium clearance concentration. Therefore, it is clear that the present leaching method is sufficient to confirm the tritium concentration in dismantled “JRR-3” concrete for clearance.

### Reference

Fujiwara, A. et al., Analysis of Tritium of Clearance Level in Concrete, Nippon Genshiryoku Gakkai Wabun Ronbunshi, vol.6, no.1, 2007, p.58-64 (in Japanese).

## Atomic Energy R&D by Computer Simulation

— Toward Establishment of Advanced Technology for Atomic Energy R&D —

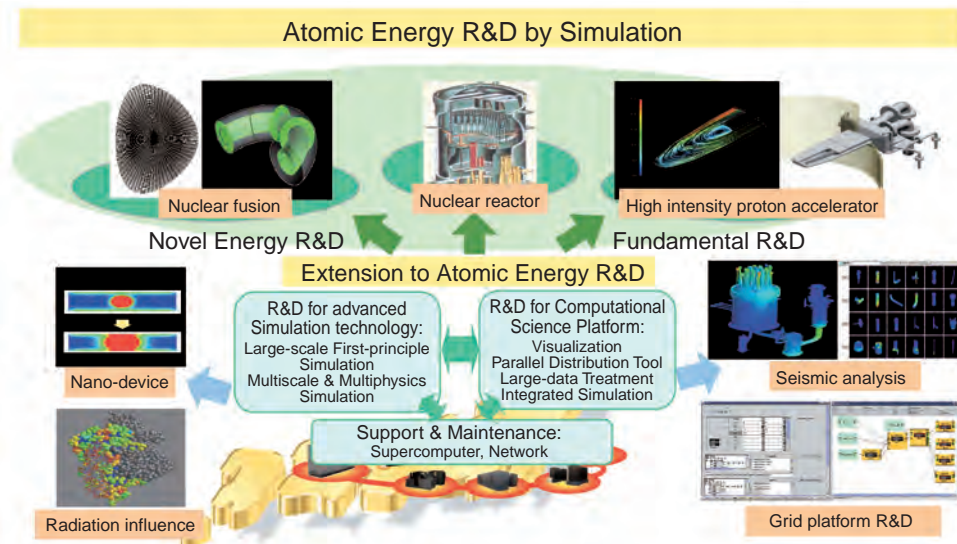


**Fig.10-1 Center for Computational Science and e-Systems**

Three of CCSE's missions and directions of its R&D are schematically depicted. Combining the three missions i.e., operation & maintenance of facilities, R&D for computational science platforms, and R&D for advanced simulation technology, CCSE aids users in atomic energy R&D and proposes new advanced simulation technologies.

Supercomputers which emerged in 1980's were quickly utilized for atomic energy research and development (R&D). The reason is that the computer simulation was considered to be able to replace previous techniques in atomic energy R&D, which encountered various difficulties due to economical and environmental limitations. The first of these simulations was done on computers with performance poorer than the present PC, but the supercomputer advancement has been so remarkable that they now can perform quite large-scale simulations with a parallel architecture composed of thousands of CPU's.

At the present, CCSE maintains a supercomputer and its support facilities including a network, and supports several users by allowing effective access to its rich computer resources. Moreover, CCSE developed a computational science platform to efficiently operate the parallel processing on computer resources distributed over sections and studies advanced techniques exploring a new field of atomic energy research by using massively parallel calculations.

Based on the previous experience, we believe that combining three computation technologies, for maintenance & support of facilities, a computational science platform, and advanced simulation, is crucial for promoting atomic energy research. Fig.10-1 schematically displays the R&D directions of CCSE. Following this strategy, CCSE has so far produced some achievements which have had a great impact on atomic energy R&D. The following are the latest typical results.

Firstly, CCSE has created a virtual research laboratory whose computer capacity is beyond 50 TFLOPS (1 TFLOPS=1000 billions operations per second) by participating in the ITBL project, which was carried out as a part of Japan's IT policy. Now, CCSE is utilizing this resource to study seismic activity, nanodevices, irradiation influence on the human body, etc. Especially, the seismic analysis study has successfully created 3-dimensional virtual shaking platform prototype which can evaluate 2000 parts of a nuclear plant. If such a study evolves further and we can freely construct a nuclear plant in virtual space, then dramatic reductions of the period for design and the cost for construction are expected.

Next, CCSE has succeeded in realizing a virtual strength test in atomic level simulations for reactor materials. Although the number of simulated atoms is still limited to within a few hundred atoms, a first principle simulation applying a stress into the grain boundary, in which impurities can be segregated and damage can be caused, is now executable. In such a simulation, one can examine several times how the boundary becomes fragile with the impurity segregation etc. If simulation technology progresses further, materials design based on simulations will be really possible.

CCSE continually accelerates R&D for computer science and simulation technology, which in turn dramatically advances atomic energy R&D.

## 10-1 A Simulation Study of Intricate Crack Shapes

### — Large-Scale Simulation of Stress Corrosion Cracking Shape —

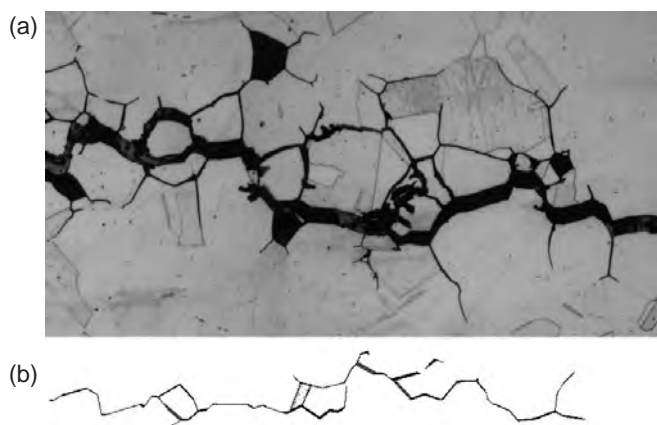


**Fig.10-2 Intricate crack shape typical of stress corrosion cracking**

In stress corrosion cracking, cracks follow interfaces between crystal grains, resulting in intricate crack shapes. The upper photo(a) shows a crack observed in a real material, and the lower picture(b) is a result of computer simulation.

Inside a nuclear reactor, metal components are subjected to neutron irradiation and high-temperature coolant water, and after several decades of operation, cracks can appear in components which are otherwise resistant to cracks and corrosion. This kind of phenomena is called “Stress Corrosion Cracking” (SCC), because it occurs only when the material is subjected to both tensile stress and a corrosive environment. However, the exact mechanism of interaction between stress and corrosive environment remains unclear. Since prediction of SCC progression is crucial for safety assessment of nuclear reactors, intensive experimental studies have been carried out to measure SCC progress speed in operational environments, and SCC progression in a real reactor over several decades into the future is estimated. If the exact mechanism of SCC is identified, we can provide a theoretical foundation for these estimations. Therefore this topic has been intensively studied.

One of the typical features of SCC is an intricate crack shape as shown in Fig.10-2. Metal material is usually composed of many crystal grains whose size is about 0.05 mm, and cracks follow the interface between these grains in SCC in a zigzag shape. Many branches of cracks are also a typical feature of SCC. In experiments, one can only observe a two-dimensional intersection of cracks, so the actual three-dimensional shape is not known, making it difficult to

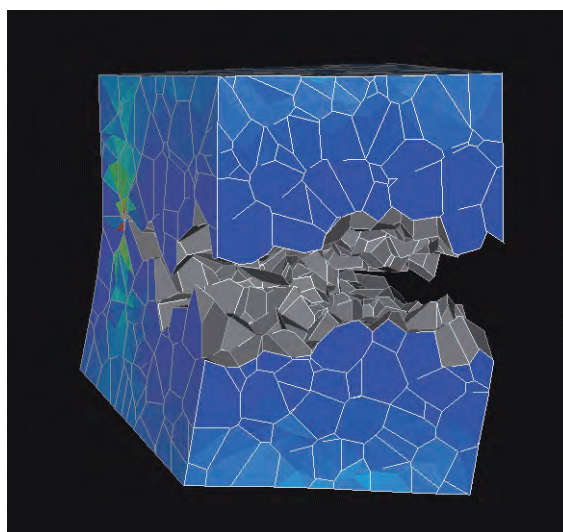


**Fig.10-3 A three-dimensional model reproducing crack shapes**

This is a three-dimensional visualization of the simulation model. The colors indicate the strength of local tensile stress. The crack opening is exaggerated 100 times.

estimate the exact tensile stress acting at the crack tip which drives the SCC progression. If this intricate crack shape could be reproduced by a computer simulation, one could identify the mechanism which generates the intricate shape, and also see the three-dimensional shape of the cracks, which might be a clue to identify the mechanism of SCC.

In this study, a metal material composed of ten thousand grains is modeled and crack propagation in it is simulated by a large-scale computation of tensile stress distribution (Fig.10-3). In the simulation, a very simplified model is used: the crack proceeds at the interface of grains which is under the strongest tensile stress. In spite of the simplicity of the model, the resultant crack shape reproduces the essential features of experimentally observed crack shape very well, especially the frequent branching of the cracks. Since this branching behavior is difficult to explain by an intuitive model of stress distribution, it has been attributed to corrosion. The present simulation takes the heretofore unseen three-dimensional crack shape into account and reproduces the intricate crack propagation behavior in all directions, which results in the intricate crack shape including the branches. This simulation shows the potential of computer simulation to reproduce intricate three-dimensional shapes, which is difficult to reproduce by intuitive reasoning.

#### Reference

Itakura, M. et al., Branching Mechanism of Intergranular Crack Propagation in Three Dimensions, Physical Review E, vol.71, 2005, p.055102-1-055102-4.

## 10-2 Detection of Nuclear Plant Structure Vibration

— Vibration Analysis Technology for Simultaneous Evaluation of Different Wavelengths —

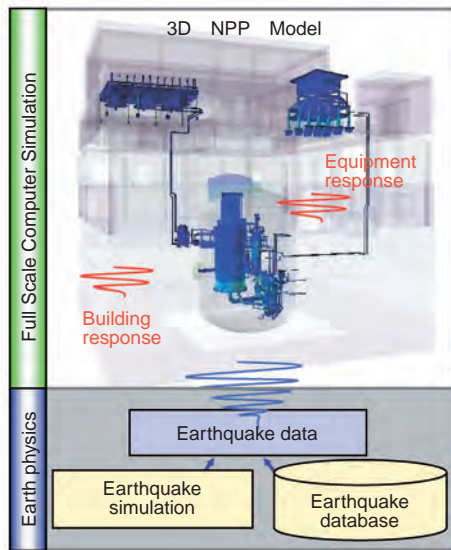


**Fig.10-4 Vibration simulator for full-scale nuclear plant**

We are developing a technology to enable the reproduction of various phenomena in nuclear plants by using a three-dimensional numerical model of an entire plant in a computer system.

Since research and development for a more reliable inspection of safety of nuclear plants is an extremely important problem, we are cooperating with industry to examine this problem, establishing a special committee of the Atomic Energy Society of Japan. To solve this problem, a maintenance management experiment or an aging inspection experiment using an actual nuclear reactor or a nuclear plant under real conditions in a real environment is necessary. However, this kind of experiment has the disadvantages of large costs and long time being required, and hence, it is not easy to perform such experiments. Therefore, at the Center for Computational Science and E-systems, we began a trial of a safe and effective safety evaluation of a nuclear plant employing computational science technology. As the first step, we are tackling the issue of research and development of simulation of three-dimensional vibration of an entire nuclear plant, which cannot be done using an experimental vibration table.

This technology, referred to as vibration simulator for full-scale nuclear plant, digitizes a three-dimensional model of an entire nuclear plant in a computer and makes it possible to simulate various phenomena that occur in a nuclear plant by combining the conventional technology on earthquake and ground motions (Fig.10-4). The calculation of the resonances of a complicated structure with high precision through vibration analysis is one of the indispensable technologies required to realize this vibration simulator for full-scale nuclear plant.

In the resonance phenomenon, the vibration energy of

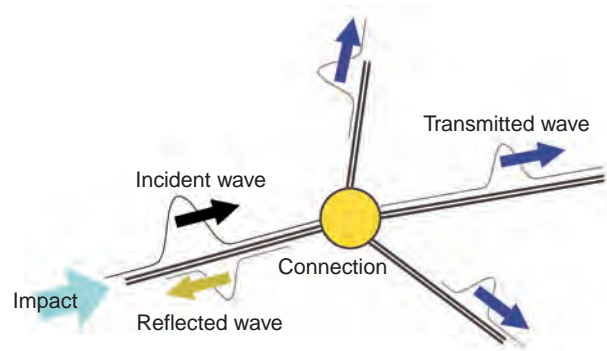


**Fig.10-5 Wave reflections and transmissions at a connection**

The repetition of reflections and transmissions of the wave, which are generated at points of discontinuity such as connections, contribute to the vibration phenomenon of the structure. The simulation of these waves enables the development of a vibration reduction plan and preventive measures against vibration.

earthquakes transmits as a wave in a structure, leading to the reflection and transmission of the wave at connections, which are points of discontinuity (Fig.10-5). This phenomenon repeats itself at a lot of connections, and the structure is strongly shaken where the energy is concentrated and the vibration is amplified. Resonance is generated over a wide frequency range that varies from the vibrations of the entire structure to some local vibrations of a structural component. Further, in the worst case scenario, the resonance may lead to the collapse of the structure in a few seconds. The aim of this study is to improve the safety of a nuclear plant by analyzing the resonance state through computational science technology, and to provide solutions for the reduction of resonance in a complicated structure.

It was possible to evaluate the problem of resonance of vibrations in the entire structure by conventional computational science technology; however, local structure vibration could not be evaluated with sufficient precision because the reflected wave could not be sufficiently modeled by conventional technology. Therefore, we attempted to develop a wave propagation simulation technique that can evaluate the vibrations of local structures as well as those of entire structures. Our proposed technique was applied to a piping structure and was successful in simultaneously treating entire and local structure vibrations; this technique could be applied to an actual nuclear plant. As a result, it can be used to calculate the resonances of a complex structure with high precision and provide solutions for reducing them.

### Reference

Nishida, A., Wave Propagation Properties of Frame Structures -Formulation for Three-Dimensional Frame Structures-, JSME International Journal Series B, vol.49, no.2, 2006, p.360-367.

## 10-3 Measuring Twisting Modulus of DNA

### — Predicted Effects of Local Conformational Coupling and External Restraints on the Torsional Properties of Single DNA Molecules —

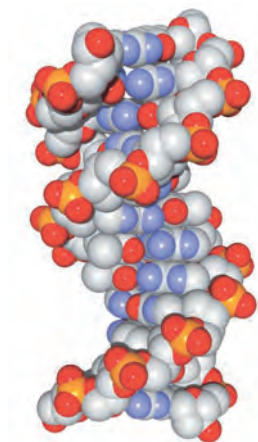


**Fig. 10-6 Three dimensional structure of DNA**

Three DNA conformations, A-DNA, B-DNA and Z-DNA, have been observed in naturally occurring biological systems. Most common conformation in cells is the B-DNA shown in the figure. The DNA in the figure has 12 base pairs and is 4 nm in length. Each somatic cell in human has about 6 billion base pairs, making the DNA 2m long.

DNA is a string-like material with diameter of about 2 nm and carries genetic information for almost all organisms on earth. DNA is the longest material in a cell. For example, if all DNA molecules in a cell were connected to make a single string, the string would be 2m in length (see legend to Fig.10-6). It is quite surprising that such a long DNA is folded and stored in a nucleus with diameter of 10  $\mu$ m.

People tend to focus on the genetic information which DNA carries. When it comes to the DNA folding problem, however, it is important to study the spatial structure of DNA and its bending properties. The structural property of DNA is important for biological reasons as well. For various biological activities, the genetic information on DNA needs to be read. In such occasions, physical force, which causes bending and twisting of DNA, is often applied on DNA. The reaction of DNA against such a force has been revealed to be involved in the control of the reading of the genetic information.

The bending and twisting moduli of DNA are the most fundamental structural properties of DNA. Many researchers have measured these mechanical constants with various experimental techniques. However, there still is controversy about them.

Recently, single molecule manipulation technique using

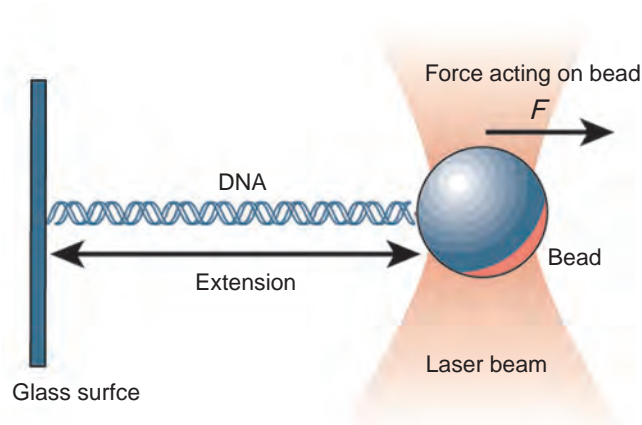


**Fig.10-7 Single DNA manipulation experiment using optical tweezers**

One end of the DNA is attached to a glass surface, and another end to a bead, which is trapped in a laser beam. A rightward force is applied to the bead and the DNA is extended.

optical tweezers is often applied to biomolecules (Fig.10-7). In this technique, a bead is attached to a molecule of interest, and a laser beam is applied on the bead, thereby generating a force on the bead. Researchers can apply forces on the molecule by moving the bead, and/or ascertain the position of the molecule by observing the position of the bead. The experiment is performed under optical microscopy.

A single molecule manipulation experiment involving DNA was expected to yield accurate mechanical constants of DNA, and indeed, the bending moduli derived from the experiments were consistent with those derived from other experimental techniques. The twisting moduli, however, were appreciably larger than the previous values.

We tried to find the reason for the inconsistency of the twisting moduli of DNA by computer simulation. We simulated a DNA in the single molecule manipulation experiment by applying a force on both ends of the DNA. We also simulated a DNA without any force applied. We found that the twisting modulus becomes larger when the force is applied on both ends than when no force is applied, and that the local conformational couplings of DNA, which has been discovered recently, induce the increase of the twisting moduli.

#### Reference

Matsumoto, A. et al., Predicted Effects of Local Conformational Coupling and External Restraints on the Torsional Properties of Single DNA Molecules, Multiscale Modeling and Simulation, vol.5, issue 4, 2006, p.1227-1247.

## 10-4 Nanosecond Neutron Detection with Superconductor $\text{MgB}_2$ — Ultra-Fast Response Revealed by Simulations and Experiments —

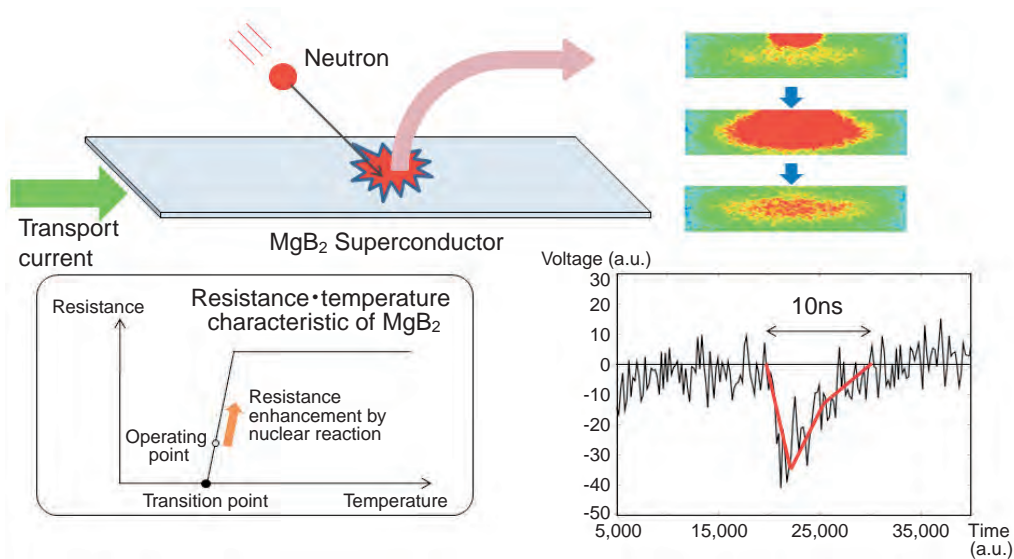


**Fig.10-8** Transport current is applied to  $\text{MgB}_2$  superconducting thin film and the operating temperature is set close to the transition point (see the upper left-hand panel). Then, if a neutron hits and a nuclear reaction occurs, the reaction heat energy depresses the superconductivity and brings about the resistance enhancement. (see the lower left-hand panel). In this situation, we predict by numerical simulation that the strength of the voltage signal over time to be as shown in the lower right-hand side figure.

One can make a highly accurate irradiation detector by taking advantage of the properties of a superconductor, whose electrical resistance abruptly goes to zero at the superconducting transition temperature. Thus, even the tiny heat created by one radiation particle brings about a large electrical signal in superconductors (Fig.10-8). It is expected that superconducting radiation detector will develop high accuracy and be utilized as an essential detector for X- and  $\gamma$ -rays in astrophysics to study the origin and the development of the universe. Moreover, its ability to count only a single photon and identify a very small amount of actinide compound is considered to be quite useful in future quantum communication and the microanalysis of nuclear materials, respectively. However, very little is known on the mechanism of the radiation detection except for simple principle as described above. That is why studies for making ultra high accuracy detectors mainly follow empirically observed rules.

In order to aid the researchers engaging in measurement and experiment and contribute to its detector development in general, the research group in CCSE has tried to develop a method of predicting the detection processes by simulation.

In the developed simulation, an equation expressing the superconducting transition dynamics close to the transition point, the heat diffusion, and the Maxwell equations describing the heat transfer and the subsequent creation of the electrical signal are solved together. Thus, this code can reproduce the detection process via the superconductivity depression by the heat diffusion (Fig.10-8).

By utilizing this simulation code, we performed a simulation for the neutron detection of superconductor  $\text{MgB}_2$  and predicted the detector performance prior to experiments. Researchers have desired greatly information about the response speed of the electrical signal. The reason for this is that they have to change their measurement setups according to the speed of response. The simulation revealed that the response time is on the order of a nanosecond, and the experiments in JRR-3 really confirmed that the prediction is valid. Thus, it is found that the simulation code works well and the response speed is much faster than the previous detectors. This indicates that  $\text{MgB}_2$  has good potential as an ultra-high-speed neutron detector. Presently, further experiments and simulations are underway.

### Reference

Machida, M. et al., Direct Numerical Simulation on Non-Equilibrium Superconducting Dynamics after Neutron Capture in  $\text{MgB}_2$  Superconductor, Nuclear Instruments and Methods in Physics Research A, vol.559, issue 2, 2006, p.594-596.

## Scientific & Technical Development for Nuclear Nonproliferation Supporting Peaceful Use of Nuclear Energy

We have two primary missions regarding nuclear nonproliferation. One mission is to support the government in developing nonproliferation-related policies through research and study.

The other mission is to support government and international organizations by performing nuclear nonproliferation technology development. Other important missions of JAEA are to support denuclearization, nuclear material control JAEA completed installation and tests of particle collection/nuclide measurement equipment at the Okinawa Monitoring Station; its operation began after certification Feb. 2007 as a CTBTO certified facility. at its own facilities, and human resource development.

### Policy Research and Study

We are performing two major policy studies, i.e., “the Evaluation of the Safeguards Achievements in Japan”, and “the Study of Peaceful Use of Nuclear Energy in Asia and Improvement of Its Transparency and Confidence Building”, based on in-house technical knowledge.

In 2006, we released the results of these projects investigating which measures are necessary for nuclear nonproliferation in peaceful use of nuclear energy, using Japan as a model, at an international forum and the working group meeting held by JAEA. Also, we performed investigation and research concerning assuring fuel supply and strengthening of nonproliferation by meetings of knowledgeable people and investigation of various countries’ intentions.

### Technical Development relating to nuclear nonproliferation

Development of the advanced safeguards system which will be applied to effective and efficient safeguards for the future Fast Breeder Reactor fuel cycle is underway. In collaboration with US as part of GNEP, cooperative research plans for next generation safeguards/physical protection have been discussed.

Regarding environmental sampling for safeguards, we are performing development of the fission track method with which a uranium particle less than  $1 \mu\text{m}$  can be detected, and technical development for upgrading of analytical accuracy is underway.

We have upgraded the “JOYO” Remote Monitoring System to get improved security of communication, and have started its field trials, as a technical development for

improvement of the reliability of, and confidence in, peaceful use of nuclear energy.

We also contribute to the Generation IV International Forum and INPRO (International Project on Innovative Nuclear Reactors and Fuel Cycles), and we are performing research on evaluation methodology for the proliferation resistant features of future nuclear cycle systems.

### Support of Denuclearization

As technical development to contribute disarmament and denuclearization of the world, we have performed cooperative research with Russia to use surplus nuclear weapons plutonium as MOX vipac fuels in fast breeder reactors. The effectiveness of this method was recognized by both the US and the Russian Federation, and its application in Fast Breeders has been indicated.

Concerning CTBT (Comprehensive Nuclear-Test-Ban Treaty), at Tokai laboratory, we continue to perform precise analysis of environmental specimens collected at nuclide stations in the world.

In Takasaki Monitoring station we installed Noble Gas Analytical Equipment which can detect nuclear explosions under the ground, adding to the existing Particle Collection/Nuclide Analytical System.

Following Takasaki monitoring station, the technical level of the Tokai laboratory and Okinawa Monitoring Station was certified by the CTBT Organization Preparatory Committee in fiscal 2006, so that all of the monitoring stations/laboratories established by JAEA commenced their operations as certified CTBT organization facilities (Fig.11-1, Fig.11-2).

### Nuclear Material Management

Concerning safeguards, we contribute to IAEA safeguards implementation in technical aspects by conducting several technical development projects based on the agreement for technical cooperation with US Department of Energy.

Concerning physical protection, we continue technical development for strengthening of physical protection measures. For example, we conducted performance tests of a system for detection an intruder into the grounds of a facility, consisting of surveillance cameras and image processor, etc.

Concerning nuclear material transportation, we are performing technical development of safe and effective transportation of MOX powder, etc.

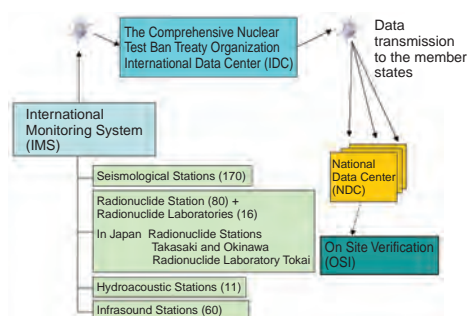


**Fig.11-1 Comprehensive Nuclear-Test-Ban Treaty (CTBT) international verification**  
CTBT Organization Preparatory Committee is organizing to establish the International Monitoring System (IMS) with installation of monitoring stations/ radionuclide laboratories in which four different technologies to monitor the globe for nuclear explosions - seismic, infrasound, hydroacoustic and radionuclides, are used. Also, the committee is preparing a verification system by which relevant information could be provided to all of the member states of CTBT.



**Fig.11-2 CTBT Okinawa Radionuclide Monitoring Station**

JAEA completed installation and tests of particle collection/nuclide measurement equipment at the Okinawa Monitoring Station; its operation began after certification Feb. 2007 as a CTBTO certified facility.

# 11-1 Design of Safeguards System for an Advanced Nuclear Fuel-Cycle System – Development of Safeguards System Simulator –

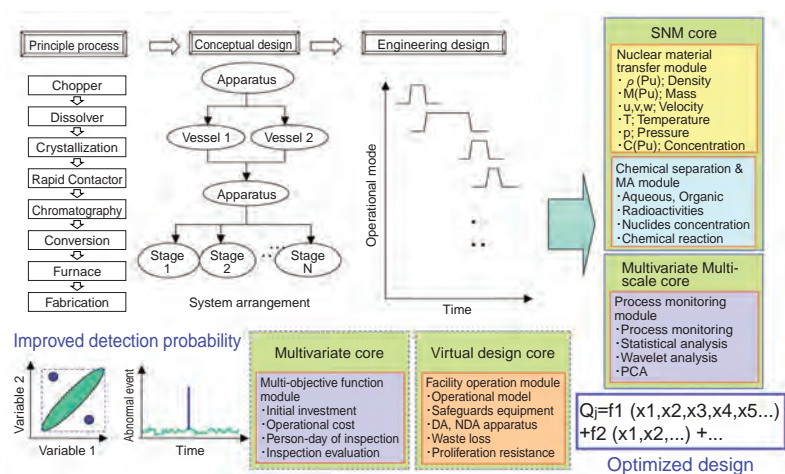


**Fig.11-3 Overview of safeguards system simulator**

In order to design an advanced nuclear fuel-cycle system, the fundamental process, apparatus arrangement, and material flow have to be clarified. At this time, the measurement accuracy of Pu is achieved with a Nuclear Material Accounting core in a simulator, abnormal event detection with a Multivariate and Multi-scale core, and optimal selection of safeguards apparatus with a Multiple Objective Optimization core. A Virtual Design core will enable us to investigate the safeguards system even in the facility design phase.

Japan is unique as the only country that has established a safeguards system for a series of nuclear fuel cycle facilities, including uranium enrichment, fuel fabrication, reactor and reprocessing. This is a result of implementing under full compliance of IAEA safeguards with various nuclear material accounting (NMA) methods and safeguards technologies and promoting peaceful use of nuclear technologies and nuclear nonproliferation.

In an inspection of nuclear fuel reprocessing facilities to verify no diversion of Pu, which might result in production of nuclear weapon, NMA has to be implemented correctly and timely. However, in safeguards technologies adopted in NMA for nuclear facilities, quantitative measures taken in the design stage using numerical simulation have been fairly limited so far. During construction of the facilities, any changes or addition of measuring or monitoring equipment often results in large expenditures. Historically, after the completion of facility design or just before the construction of facility, the investigation of the safeguards system has been started. However, in order to strengthen international safeguards, the start of safeguards system considerations after the completion of the design has led to an increase of development cost due to of the need for the additional safeguards apparatus to comply with standards.

Under these circumstances, a study of an advanced safeguards system which is applicable to future nuclear fuel-cycle facilities has been started. In the initial design stage, the safeguards system should be considered more quantitatively, and cost-effective performance meeting the IAEA criteria should be estimated before a facility construction. Therefore,

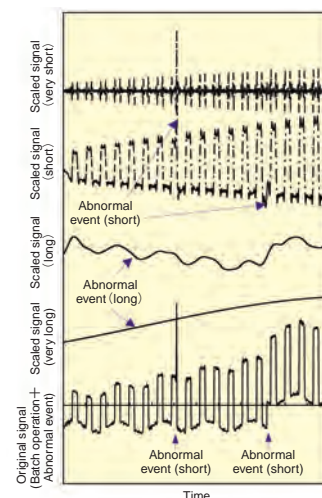


**Fig.11-4 Abnormal event detection**

For the purpose of detecting an abnormal event effectively and efficiently by observing the signals output by the process, a wavelet decomposition method in which a signal is decomposed into frequency and time domains has been developed. Multi-scale nature in the wavelet decomposition can be effectively used for the abnormal event detection.

the development of a safeguards system simulator, which is capable of predicting the NMA performance under the planned facility operation conditions, has been initiated to plan the safeguards system along with the rest of the facility design. The whole diagram of the safeguards system simulator is shown in Fig.11-3.

After deciding the design of the facility process and the arrangement of various apparatuses, we can investigate nuclear material flow and accounting characteristics of the facilities. At this time, using the Nuclear Material Accountancy core in this simulator, the accounting characteristics and a material unaccounted for are investigated to evaluate the effectiveness of safeguards system before it is constructed. This simulator core was originally developed by JAERI, which is the former organization of JAEA, more than 10 years ago, and has been remodeled by improving the pre- and post-processor functions.

Moreover, application of a wavelet decomposition method has been investigated using simulation results of numerical operations applied to an abnormal event signal. The wavelet decomposition method is the orthogonal function decomposition in time and frequency domains. As shown in Fig.11-4, the abnormal event is effectively detected. In this way, process monitoring is investigated before the facility operation. A Multivariate and Multi-scale core has been developed for this purpose.

We have been developing a Multiple Optimization core and a Virtual Visualization core, and the safeguards system simulator will enable us achieve reliable safeguards design in the near future.

## References

- Suzuki, M. et al., Development of Safeguards System Simulator, Proceedings of 15th International Conference on Nuclear Engineering (ICONE15), Nagoya, Japan, 2007, ICONE15-10297, in CD-ROM.
- Suzuki, M. et al., Numerical Consideration for Multiscale Statistical Process Control Method Applied to Nuclear Material Accountancy, Journal of Nuclear Science and Technology, vol.43, no.10, 2006, p.1270-1279.

We have been promoting a wide range of R&D activities systematically by coordinating between R&D sectors, including the R&D Directorates whose activities have been described in previous chapters and 12 R&D Centers located in various places in Japan.

The R&D Directorates of JAEA have been promoting R&D for their respective purposes with the experimental equipment/facilities at each R&D Center. The R&D Centers have not only been operating and managing various types of equipment/facilities but have also been working on innovations and improvements for them, and in addition have themselves been developing experimental techniques, management techniques and equipment/facilities necessary for various R&D projects of JAEA.

In this chapter, those developments which have been made over recent years at each R&D center are introduced.

### Tsuruga Head Office

For the prototype FBR “MONJU”, modification works including the exchange of thermometers of the secondary cooling system and the modification on sodium leakage countermeasures have been conducted. Following these modification works, functional tests of the improved components and systems will be carried out.

We made a draft of a booklet of possible accidents and troubles during the functional tests and operation of “MONJU”. 118 items are listed and their outlines, countermeasures, and preventative design considerations are described.

“FUGEN” began the legal procedures for the decommissioning implementation last November. After that, its name and structure will be changed and the R&D activity on decommissioning technology will start.



Booklet on possible accidents and troubles during the functional tests and operation of “MONJU” (<http://www.jaea.go.jp/04/turuga/cases/>)

### Tokai Research and Development Center, Nuclear Science Research Institute (NSRI)

NSRI, as a Center of Excellence (COE) in nuclear research and development, has safely and successfully operated research reactors, tandem accelerators, criticality testing facilities and nuclear fuel facilities while conducting related technology development in order to fulfill various needs of these facilities.

One technology developed at NSRI is advancement of a cure for virulent tumor by boron neutron capture therapy (BNCT) using research reactors. In 2006, NSRI has established a technique to irradiate patients in a seated position, to cure lung cancer. As a result, 34 irradiation treatments were conducted in 2006, many more than the 12 treatments of 2005. Meantime, NSRI also has been developing radiation calibration fields matching the national standard in order to establish the reliability of radiation measurements. These radiation calibration fields at the Facility of Radiation Standards have been available for common use since last November.



Japan Research Reactor No.3 beam hall at the 15th anniversary of its upgrade

### Tokai Research and Development Center, Nuclear Fuel Cycle Engineering Laboratories

In Tokai Reprocessing Technology Development Center, reprocessing experiments were carried out using fuel (11.7 tons, of which about 2.5 tons were mixed oxide) used up by “FUGEN”. Moreover, experiments were carried out at the Plutonium Fuel Development Center to determine the manufacturing conditions etc. of the pellets with low density for “MONJU”.

Besides this, at the Tokai Reprocessing Technology Development Center, construction of the Low-level Radioactive Waste Treatment Facilities (LWTF) that started on March 20, 2002 was completed on September 15, 2006, and the test operation (cold test) have begun.

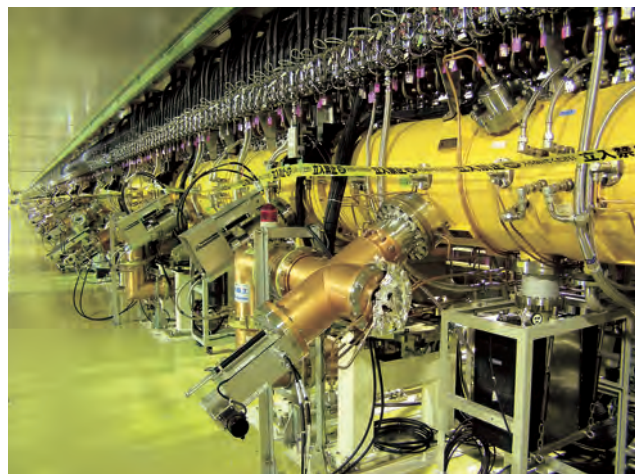


LWTF

### J-PARC Center

At J-PARC, the construction of three buildings for the Linac, the 3 GeV Proton Synchrotron and the 50 GeV Proton Synchrotron, has been completed, and those accelerator components are being installed and tested. Linac, the first of these accelerators, has achieved a proton beam with an acceleration energy of 181 MeV, the initial goal, on January 24 this year.

After adjustments are made to Linac during this year, the 3 GeV Proton Synchrotron and the 50 GeV Proton Synchrotron are scheduled to start the beam operation, aiming for the full operation of the J-PARC facilities in April, 2009.



“Linac” First stage accelerator of J-PARC

### Oarai Research and Development Center

In the development of Fast Breeder Reactor (FBR) cycle system technology, the development of the high burn-up fuel and the minor actinide containing fuel for FBR has been conducted using the experimental fast reactor “JOYO” and post irradiation examination facilities. Experimental research for the economic operation, safety and reliability of FBR, especially sodium safety handling technique has been carried out using the sodium and its related test facilities. In the development of high temperature gas reactor, safety demonstration tests have been conducted using the High Temperature engineering Test Reactor (HTTR). The development of hydrogen production technology with the iodine-sulfur process and the thermochemical-electrolysis hybrid cycle have been conducted.

Concerning nuclear reactors, the Japan Materials Testing Reactor (JMTR) obtained consent from the government for refurbishment, with restart planned in FY2011, and “JOYO” won the Nuclear Historic Landmark Award from the American Nuclear Society (ANS), since its contributions to the development of FBR cycle system technology for 30 years were highly evaluated. In activities as a member of the local society, the number of visitors of Oarai Science Museum exceeded 1,000,000, and Oarai Science Museum is contributing to the local community through education in science including nuclear technology.

### Naka Fusion Institute

Naka Fusion Institute, in close cooperation with the Fusion R&D Directorate, aims at utilizing fusion energy for the future. Following the conclusion of the Agreement for ITER (to be built in France) in November 2006, the Agreement for Broader Approach Activities (to complement the ITER Project) with Europe was concluded in February 2007, and a project to upgrade JT-60 has been initiated as a part of this cooperation. In order to introduce the forefront of fusion R&D to the public, the Institute frequently organizes site tours for neighboring junior high school students, and for high school students from all over Japan (Super Science High Schools). Also, we open our site and some facilities to the local residents in October every year.



“Nuclear Historic Landmark Award” plaque

Takashi Nagata (left)

Director of Oarai Research and Development Center (JAEA)

Harold F. McFarlane (center)

President of the American Nuclear Society

Soju Suzuki (right)

Director of Experimental Fast Reactor Division

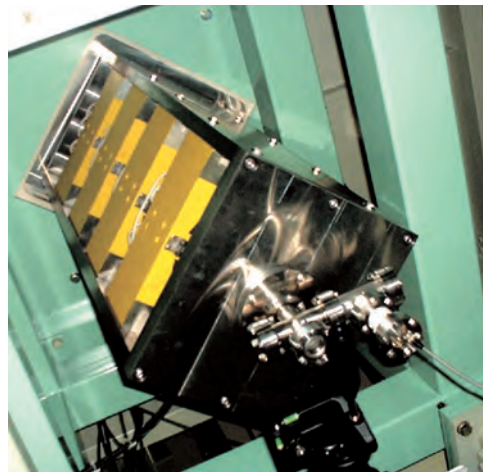
Oarai Research and Development Center (JAEA)



Local residents visited Naka on the Open-Site-Day

### Takasaki Advanced Radiation Research Institute

The Takasaki Advanced Radiation Research Institute, opens its four ion accelerators at “TIARA”, an electron accelerator, and  $\gamma$ -ray irradiation facilities to researchers both inside and outside JAEA for R & D on new functional or earth-friendly materials, biological technology, quantum beam analysis and radiation resistance tests of materials/apparatuses. In this fiscal year, the formation of a microbeam of 260-MeV Ne having a diameter less than  $1\ \mu\text{m}$  was achieved in vacuum for the first time in the world, and the fabrication of a fine 3D polymer structure with a depth/width ratio higher than 10 also was realized using proton beam writing technology.



The quadrupole magnet system for formation of heavy ion microbeams of hundreds of MeV.

### Kansai Photon Science Institute

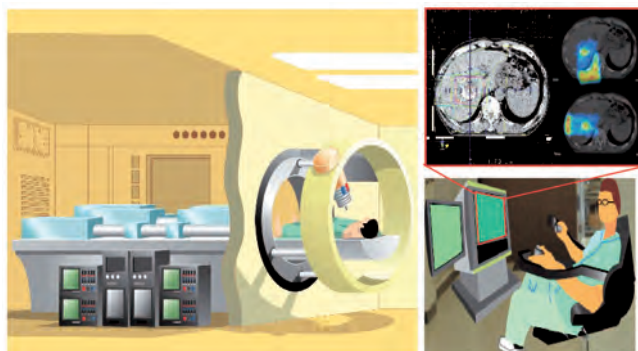
The new project, creation of a “Photo Medical Industrial Valley”, has been proposed in the “Formation of creative base for innovations integrating frontier fields” program funded by Special Coordination Funds for Promoting Science and Technology commissioned by the Ministry of Education, Culture, Sports, Science and Technology (MEXT), and a feasibility study has been commissioned in fiscal year 2006.

Preparations for “Photo Medical Industrial Valley” construction were made in collaboration with industries and universities in the Keihanna region (extending over Kyoto, Osaka, and Nara prefectures, a new base of culture, science, and research for the 21st century.).

Facility sharing began in fiscal year 2006, and facilities have been used by universities and the corporations in 57 cases.

For public relations, there were openings of facilities to the public, cooperation in local events, science camps, science seminars, etc..

In the science museum, commemorative ceremony upon the 200,000th visitor and the fifth anniversary was held, and a Yamashiro Science festival and a teacher seminar were held in cooperation with the local board of education.



Compact laser-driven proton beam device for cancer treatment (concept)

### Horonobe Underground Research Center

As part of the research into geological isolation technology to dispose of high-level radioactive waste collected from spent fuels of nuclear power plants safely, geological research, research and development on geological disposal technology, and joint research with other research laboratories and universities were carried out in the 2006 fiscal year.

Moreover, the construction of an underground research laboratory and a public information house has progressed.

The public information house opened June 30, in which corners for surveillance studies and publicizing the results thereof are set up.



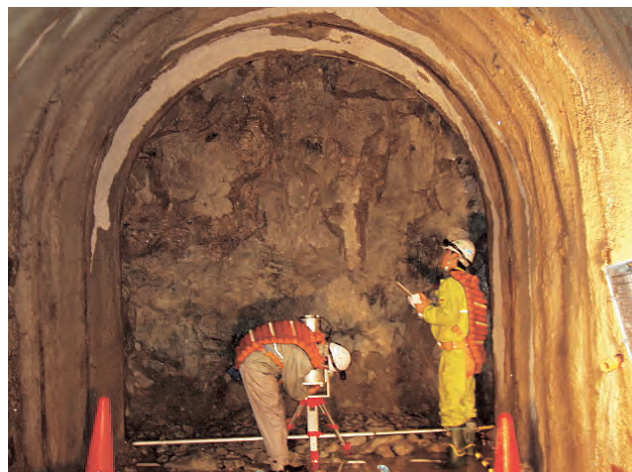
Inside the PR facility (corner introducing research and development of the Center)

### Tono Geoscience Center

We conduct general Research & Development (R&D) on techniques for characterization of deep geological environments in granite, and on the long-term stability of a geological disposal of High-Level radioactive Waste (HLW).

In 2006, we excavated two research shafts to the depth of 200.2m for the Main Shaft and 193.6m for the Ventilation Shaft. We also started the excavation of a sub stage horizontal tunnel at the depth of 200m by drilling pilot boreholes at the bottom of the shafts, and we investigated more in detail the geological conditions of the rock down to a depth of 500m.

In July 2007, The Mizunami Underground Research laboratory celebrated its 5th anniversary of the start of its construction.



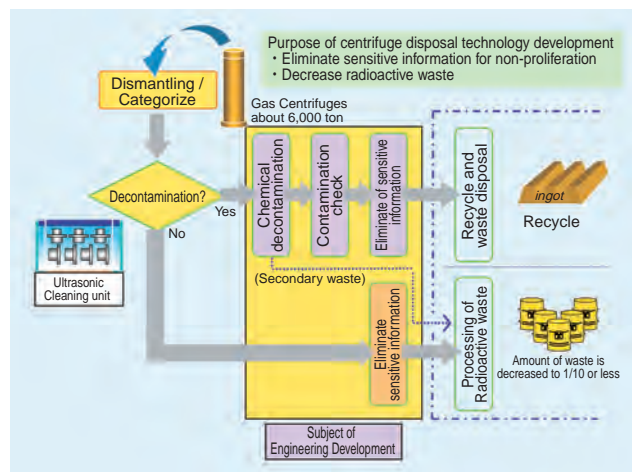
Geological inspection of a sub stage horizontal tunnel at the depth of 200m

### Ningyo-toge Environmental Engineering Center

The Ningyo-toge Environmental Engineering Center has been developing the dry decontamination technology using iodine heptafluoride (IF7) gas as a part of decommissioning technology R&D for uranium enrichment facilities. The decontamination testing is being performed through JFY 2008 at the Uranium Enrichment Demonstration Plant. Development of wet decontamination technologies using diluted sulfuric acid is ongoing for decontamination technology of decommissioned gas centrifuges.

Data acquisition has been carried out, including water level and chemical composition of ground water, to advance the reclamation of the Ningyo-toge Mine in the future.

Preparation for the construction of a brick factory which will use waste rock from the Katamo Waste Rock Yards as raw materials, was started.



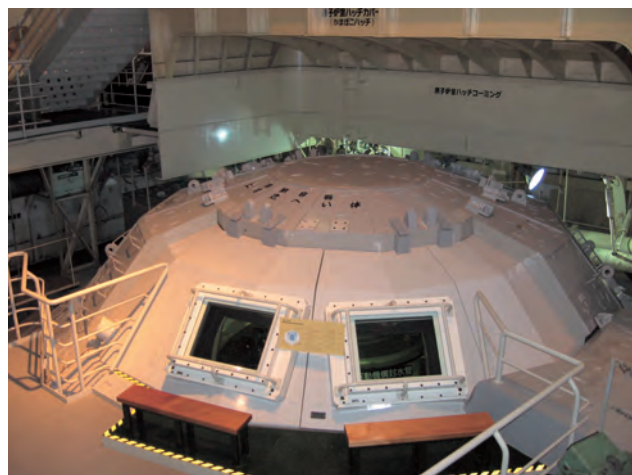
General flowchart of the centrifuge disposal technology development

### Aomori Research and Development Center

Tandetron AMS has had an open door policy for general users since Spring 2006. Tandetron AMS measured 1,094 graphite samples and 502 iodine samples in the fiscal year of 2006, the highest numbers in our history. At the same time, we have been developing a pre-treatment system for  $^{14}\text{C}$  in dissolved organic carbon which uses ultraviolet rays and  $^{14}\text{C}$  in the atmosphere. Also under development are pre-treatment methods for  $^{129}\text{I}$  in seawater and seaweeds.

In decommissioning the nuclear ship "MUTSU", radioactive wastes were surveyed and spent fuels were re-assembled for re-processing at the Hot Material Examination Facility in the Nuclear Science Research Institute. The decommissioning plan of "MUTSU" got approval from the Japanese regulating authority in October 2006.

A symposium was held at Mutsu, Aomori in November for Environmental Sciences under the auspices of JAMSTEC (Japan Agency for Marine-Earth Science and Technology), JMSF (Japan Marine Science Foundation) and JAEA to give information about our activities to the local public.



Reactor room of Nuclear ship "Mutsu"

## 12-1 Shortening the Modification Period in “MONJU”

### — Discussion of One-Loop Operation of Primary Heat Transport System in Fast Breeder Reactor “MONJU” and the Execution —

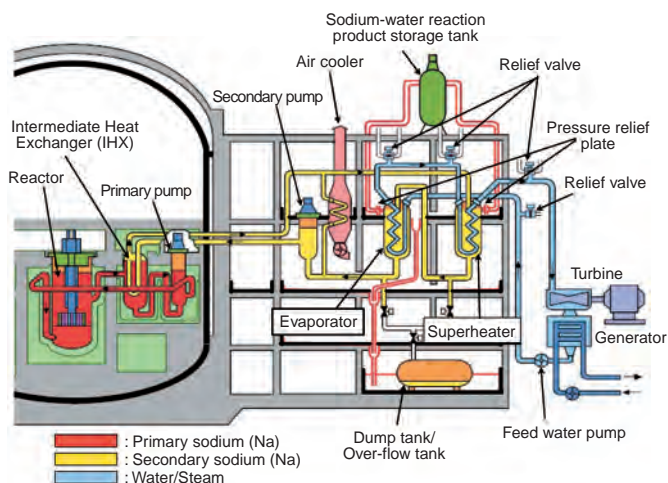


Fig.12-1 Overview of “MONJU”

The main heat transport system of “MONJU” is divided into three systems: the primary heat transport system (PHTS) to extract heat from the reactor core, SHTS to transmit heat of PHTS to the steam-water system and the steam-water system to turn a turbine-generator. They are composed of three loops. Fig.12-1 is an overview of “MONJU”.

The modification work for restartup started in March 2005. The main content of the modification work is as follows.

1. Change or removal of thermocouple wells in SHTS
2. Improvement of sodium leak countermeasures
3. Improvement of steam generator (SG) safety

Before the above-mentioned modification work was started, shortening the modification period was discussed. In the discussion, PHTS one-loop operation (All of sodium in the SHTS was drained and one-loop of the PHTS was circulated) was discussed.

Two conditions to change to PHTS one-loop operation are as follows. First, the heat loss must exceed the reactor core decay heat. Secondly, it is possible to make the difference between the heat loss and the decay heat smaller than the capacity of preheater, which is to keep the temperature of the in-vessel sodium at 200°C.

Concerning the first condition, the estimated heat loss in

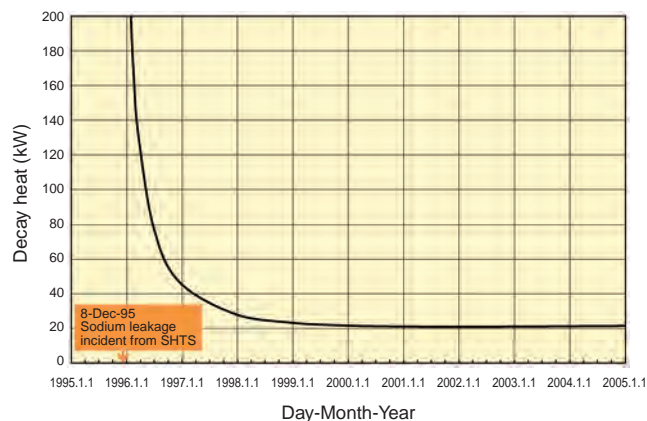


Fig.12-2 The change of decay heat after sodium leakage

the primary system was in the range of 110-160 kW in one-loop operation, and the calculated decay heat was 21.2 kW (Fig.12-2). Although the heat input of the primary pump was considered, it was clear that circuit heat loss greatly exceeded the decay heat. The FPGS90 analytic code was used for the evaluation of the decay heat, because there is no means to measure it directly when the system is cold on standby. The heat loss was calculated by the HVAC method. The HVAC method calculates the heat loss from each piece of equipment and pipe by calculating the total heat loss of all equipment and the pipes in the targeted room from the temperature fluctuation of heat exchanger inlet-outlet in RV nitrogen atmosphere air-conditioning system and distributing the heat loss according to ratios derived from the design.

Concerning the second condition, because the normal set value of the preheater can not keep the in-vessel sodium at about 200°C, the set value of the primary preheater was changed and the heat loss of one-loop operation of PHTS was reduced.

One-loop operation of PHTS was able to be executed by means of these measures. It brings about not only shortening of the construction period but also reduction of the electrical consumption within the power plant.

#### Reference

Goto, T. et al., One-Loop Operation of Primary Heat Transport System in MONJU during Heat Transport System Modifications, Proceedings of 14th International Conference on Nuclear Engineering (ICONE14), Miami, USA, 2006, ICONE14-89242, in CD-ROM.

## 12-2 Heavy Ion Beams Lead the Way to Super Heavy Element Science — Development of Heavy Ion Injector in Terminal of Tandem Accelerator —

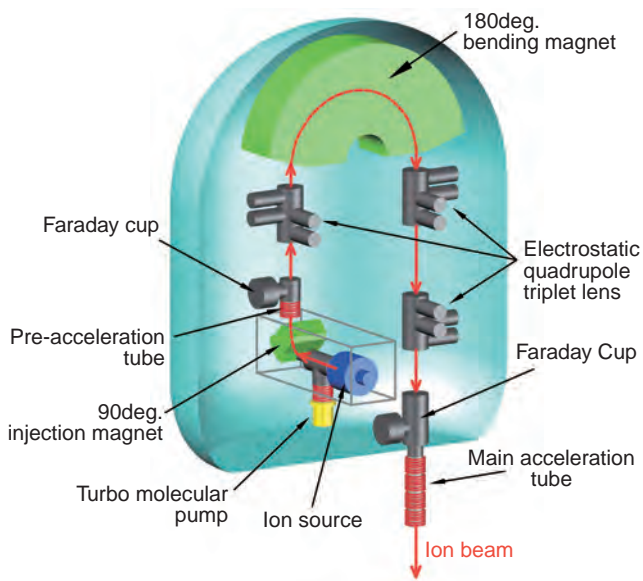


**Fig.12-3 Layout of in-terminal heavy ion injector**

A multi charged heavy ion injector has been developed for the high voltage terminal of a tandem accelerator. The ion beam generated by the ion source is bent with a 90° injection magnet and 180° bending magnet, and then accelerated through the main 20MV acceleration tube toward the earth potential.

Nuclear reactions, nuclear structures, and chemical properties of super heavy elements are researched using high energy heavy ions from the JAEA tandem accelerator. The ion beams are used also for research involving irradiation of nuclear reactor fuel because the beam energy can be tuned to the energy of fission fragments. A high intense heavy ion beam is necessary for the production of the super heavy elements with short lifetimes and small production rates. This irradiation is also necessary for research where particle flux as in a nuclear reactor is needed.

The tandem accelerator efficiently works because the carbon foil in the terminal changes negative ions to positive multi-charged ions. Carbon foils are, however, consumed quickly, and are not suitable for intense heavy ion beam acceleration. Therefore, we started developing a heavy ion injector (Fig.12-3) in the terminal of the accelerator to accelerate the positive ions from a permanent magnet type electron cyclotron resonance (ECR) ion source. The energy is also increased because higher charge state ions are generated by the ECR ion source than carbon foil.

The high voltage terminal is in a severe environment, i.e. it is filled with the pressurized insulation gas to 5.5 atm and itself is held at a voltage of 20MV at maximum. The capability to withstand high pressure and electrical discharge

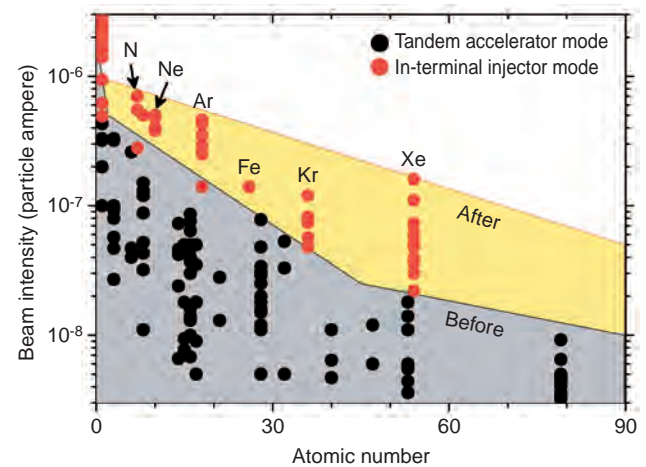


**Fig.12-4 Ion species and intensity of beam accelerated by in-terminal heavy ion injector**

Solid circles show accelerated ion beam intensity. The vertical scale indicates the beam current divided by ion charge, which is proportional to the number of ions. With this injector rare gas ions can be accelerated, and intensity is 2~10 times that of conventional devices.

is indispensable to the in-terminal ion injector. The components of the injector, namely the ion source, beam line devices, power supplies and vacuum components, have been confirmed to be pressure-resistant. A control system with optical fibers and circuits was designed to prevent damage from electrical discharges, and these electrical devices were heavily shielded. Since ion pumps do not work for inert rare gases, a turbo molecular pump and a rotary pump were newly developed for high pressure gas. The exhaust gas from the pumps was designed to accumulate in a closed vessel. Even when the pumping system fails, the high vacuum is held.

The accelerated ions from new injector are shown in Fig.12-4. Rare gas ion beams can be generated, and the intensities were 2~10 times those of conventional devices. Xe ion energy reached 300MeV, making this the only accelerator that provides beams in a wide energy range of 50~300MeV. In addition, the beam quality was greatly improved compared with the tandem acceleration mode because there was neither the energy spread nor the beam divergence which is caused by the carbon foil.

Intense beams of Kr and Xe in this way have become available not only for production of super heavy elements but also irradiation research on high burn-up nuclear fuel.

### Reference

Matsuda, M. et. al., Rearrangement of In-Terminal ECR Ion Source Injector, JAEA-Review 2006-029, 2006, p.14-15.

## 12-3 Toward a Better Understanding of High Burnup Fuel Behavior during Scenario Accidents in Nuclear Power Reactors

### — Design of Experimental Capsule for Irradiated Fuel Experiments —

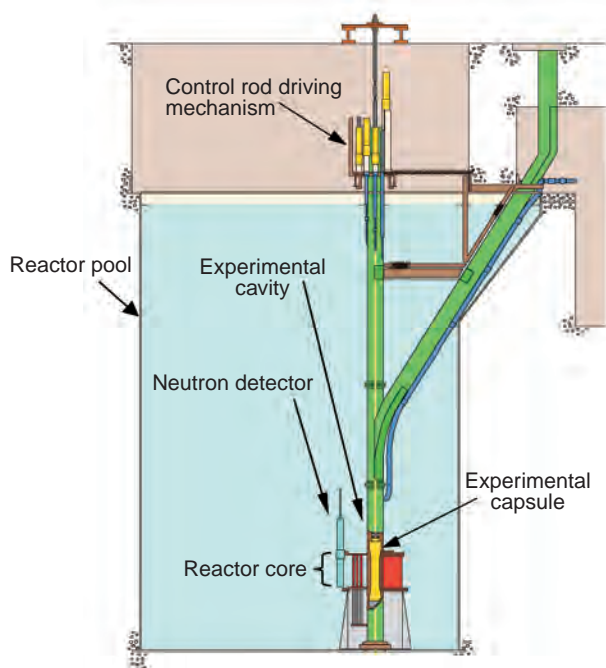


**Fig.12-5 Vertical cross section of NSRR**

The experimental capsule must be designed to prevent a leak of fission products that are released from failed fuels.

The Nuclear Safety Research Reactor (NSRR) (Fig.12-5) was built to investigate fuel behavior under Reactivity Initiated Accident (RIA) conditions. The first criticality was achieved in June 1975. NSRR started experiments with fresh fuels of power reactors to investigate fuel behavior, and the results were referred to in setting the regulatory guidelines. Recently, there is a growing concern about the data of irradiated fuels, and tests with high burnup fuels are among the main experiments in the NSRR program.

At NSRR, 18 types of experimental capsules have been developed to simulate various operational conditions. One of them, the type X-IV atmospheric pressure capsule (type X-IV capsule, Fig.12-6) produced in 2006, is used for experiments concerning  $\text{UO}_2$  fuels irradiated in power reactors.

The type X-IV capsule is used with irradiated fuels, so it has to be completely free of leaks of fission products that are released from damaged fuels. Accordingly, it requires imperviousness equivalent to the pressure vessel of a power reactor. On the other hand, the thickness of the capsule wall must be as thin as possible to get enough neutron flux to the

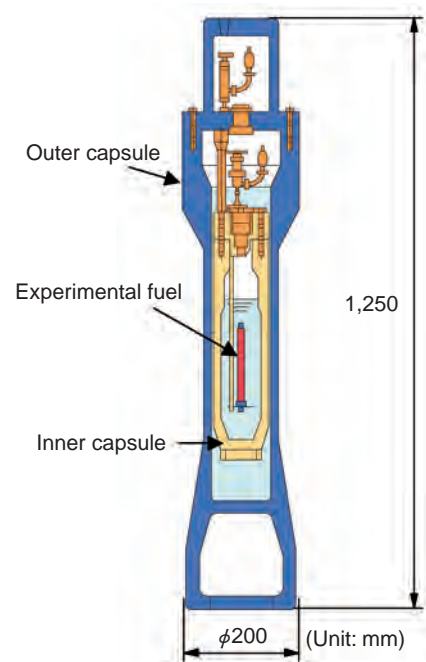


**Fig.12-6 Vertical cross section of Type X-IV atmospheric pressure capsule**

The experimental capsule is doubly-sealed with the Outer and Inner Capsules. Fuel is installed to the Inner Capsule along with water.

experimental fuels. Therefore, the capsule was designed to be a double container system which is composed of inner and outer capsules. In the inner capsule, the thickness of the capsule wall was reduced as much as possible in the vicinity of experimental fuel and thickened in the upper area where high stress would be applied.

Although the strength of experimental capsules had been evaluated based on the relevant national regulation (Notification No.501), we applied the alternative design standard JSME S NC1-2005 to the type X-IV capsule. The standard was defined by Japan Society of Mechanical Engineers (JSME) and reflects the latest technical knowledge.

Dozens of these type X-IV capsules have been already manufactured and used for many experiments. Results from the experiments have been applied to the fuel design of power reactors and regulatory information. We will keep carrying out these experiments to support research programs for a better understanding of high burnup fuel behavior under RIA conditions.

#### Reference

Murao, H. et al., Design of Type X-IV Atmospheric Pressure Capsule for Irradiation Test Based on JSME S NC-1 2005, JAEA-Technology 2006-062, 2006, 32p. (in Japanese).

## 12-4 Precise Estimation of the State of Oceans in the Past, Present and Future — Simulation of the Marine Diffusion of Radioactive Materials Using LAMER —

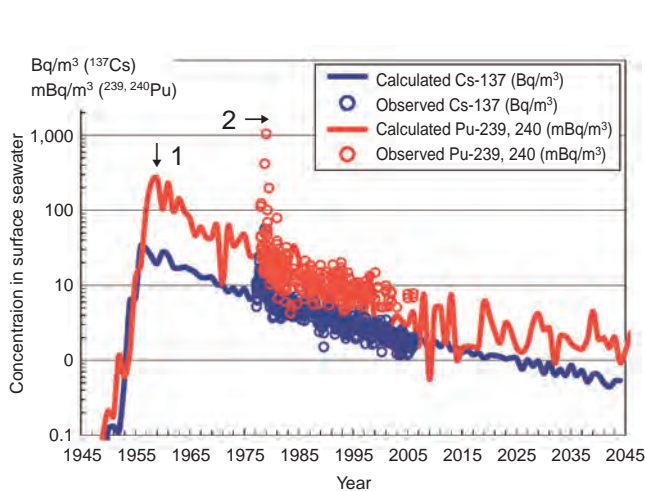


**Fig.12-7 Changes in the cesium - 137 ( $^{137}\text{Cs}$ ) and plutonium-239, 240 ( $^{239,240}\text{Pu}$ ) concentrations in the surface seawater collected off the shore of Tokai**

This figure shows the chronological variations of  $^{137}\text{Cs}$  (blue) and  $^{239,240}\text{Pu}$  (red) concentrations in the surface seawater off the shore of Tokai from 1945 to 2045. The lines indicate the values calculated by LAMER, and the circles indicate our monitoring data around the Tokai Reprocessing Plant. These data seem to agree well. It is possible to forecast the concentrations in the past and future. "1" indicates the effect of the atmospheric nuclear tests at Bikini and Enewetak atolls around 1954, and "2" indicates the local effect of China's atmospheric nuclear tests in 1978 and 1980. The fluctuation in the calculated value (especially for Pu) is traceable to statistical reasons, and doesn't indicate a real phenomenon.

For risk assessment of nuclear cycle facilities and worldwide environmental conservation, it is important to grasp how radioactive materials (e.g.  $^{137}\text{Cs}$ ,  $^{239,240}\text{Pu}$ , etc.) will disperse in the marine environment in an accidental marine release of liquid radioactive effluent from a nuclear cycle facility. We have developed the LAMER (Long-term Assessment Model of Radionuclides in the Oceans) program, and validated LAMER's worldwide diffusion model using the fallout of  $^{137}\text{Cs}$  and  $^{239,240}\text{Pu}$  from past atmospheric nuclear tests.

LAMER consists of a Part A, which calculates the decadal behavior of radionuclides in marine environment, and a Part B, which calculates the risk from the intake of marine products considering the concentration, intake amounts of marine products and dose coefficients. The worldwide diffusion model in Part A for worldwide marine assessment of liquid radioactive effluent was developed and validated for use over a long period.

This worldwide diffusion model is required to be able to assess the long-term and worldwide effects, not only for a

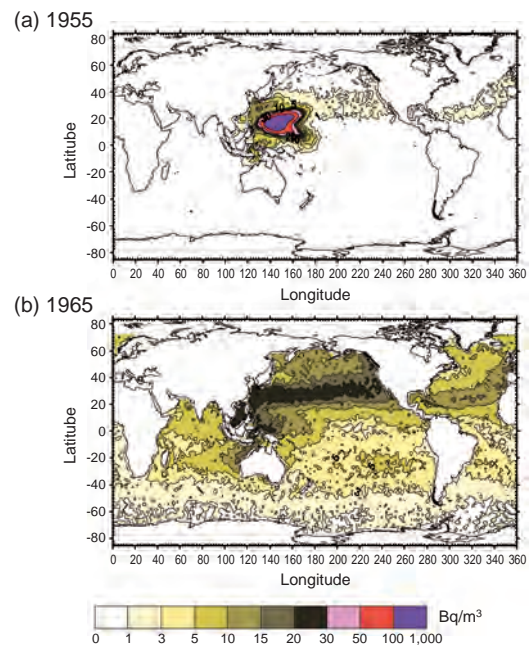


**Fig.12-8 Contour maps of the  $^{137}\text{Cs}$  concentrations in the surface seawater calculated by LAMER in (a) 1955, and (b) 1965**

In (a)1955, when the atmospheric nuclear tests began around Bikini atoll,  $^{137}\text{Cs}$  concentrations around Bikini were higher than those in the other places. Then, the transportation of  $^{137}\text{Cs}$  by Kuroshio current and the atmospheric nuclear tests by the former Soviet Union dispersed the  $^{137}\text{Cs}$  all over the north Pacific in (b)1965.

soluble element (Cs) but also an insoluble element (Pu). In order to satisfy this requirement, the computer programs to calculate three-dimensional velocity fields by an oceanic general circulation model, horizontal and vertical transport of soluble elements by an advection-diffusion model, and vertical transportation of insoluble elements by a scavenging model were developed.

The precision of this worldwide simulation model was validated by the observed data of atmospheric nuclear fallout. Over 80 percent of 152 calculated  $^{137}\text{Cs}$  profiles agreed with the observed  $^{137}\text{Cs}$  profiles reported by other organizations. The calculated data around the Tokai Reprocessing Plant also agreed with our environmental monitoring data. This means that the  $^{137}\text{Cs}$  in seawater near the Tokai Reprocessing Plant originated not from the plant but from the fallout (Fig.12-7). This model will be useful in monitoring for a new radioactive source in the ocean, since this simulation can forecast the future background level from fallout. Additionally, with this model it is possible to visualize how a radionuclide is dispersed by the ocean current, as in Fig.12-8.

### Reference

Nakano, M., Simulation of the Advection-Diffusion-Scavenging Processes for  $^{137}\text{Cs}$  and  $^{239,240}\text{Pu}$  in the Japan Sea, Radioactivity in the Environment, vol.8, Elsevier, 2006, p.433-448.

## 12-5 Study on Physical Properties of Fast Reactor Fuel for Future Commercialization — Study on Thermal Conductivities of Uranium-Plutonium Mixed Oxide Fuels —

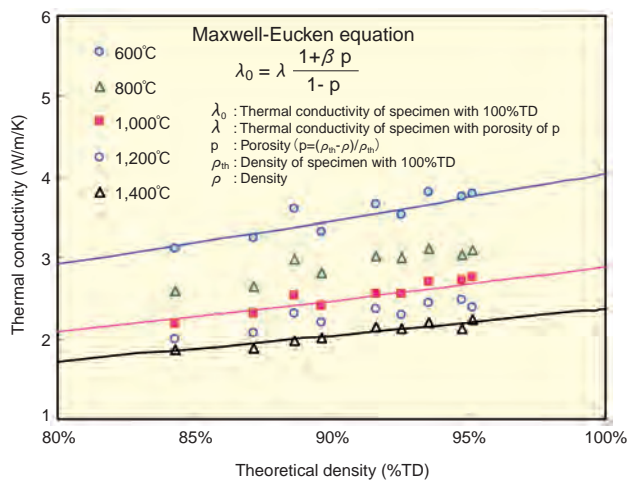


**Fig.12-9 Dependency of thermal conductivity on density**  
The symbols are the thermal conductivities evaluated experimentally. Conductivity tends to decrease with decrease in density. Solid lines were calculated with the Maxwell-Eucken equation. The calculated values show a good agreement with experimental ones. This result shows that Maxwell-Eucken equation makes possible correction of density in the range from 85 to 95%TD.

A sodium-cooled fast reactor using oxide fuel is considered the most practical reactor for the next-generation nuclear fuel cycle system. Research and development for practical use of this reactor is being carried out. In fuel design, evaluation of reactor and fuel characteristics is needed for operating this reactor at high linear heat rate, so that we can obtain large amounts of energy from the reactor, without melting the fuel. We can carry out rational fuel design by using data with high reliability. Thermal conductivity is one of the most important thermal physical properties in fuel design.

The thermal conductivity of uranium-plutonium mixed oxide (MOX) used as fast reactor fuel is changed by density, oxygen to metal ratio (O/M ratio), etc. The specifications of densities of this fuel are different according to the characteristics of reactors. The prototype fast-breeder reactor “MONJU” uses the low-density type fuel with theoretical density (%TD) of 85%. The density of this type of fuel is adjusted by controlling porosity. If the storage time between reprocessing of the irradiated fuel and MOX fuel loading into the reactor becomes long, a considerable amount of  $^{241}\text{Am}$  accumulates in the MOX fuel, which may affect its thermal and mechanical properties.

In this study, three kinds of MOX fuels with different Am-content were prepared, and their thermal conductivities were measured at temperatures from 600 to 1,500 °C. From these results, the effects of Am-content (from 0.7 to 3%) and density (from 85 to 95 %TD) on thermal conductivity were

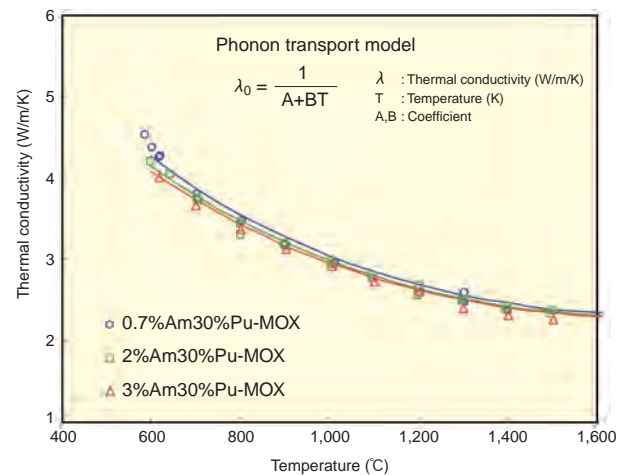


**Fig.12-10 Dependency of thermal conductivity on Am-content**

The symbols are the thermal conductivities evaluated experimentally. The thermal conductivities of MOX fuels containing Am decreased slightly with increase in Am-content. The thermal conductivities up to about 1500 K satisfied the classical phonon transport model,  $\lambda_0 = (A+BT)^{-1}$ . The coefficient A increased linearly with an increase of the Am-content.

clarified. Fig.12-9 and Fig.12-10 show the dependency of thermal conductivity on density and Am - content, respectively. From the analysis of these dependencies, the influences of density and Am - content on thermal conductivity could be described theoretically.

Some reports on thermal conductivity of MOX fuel have been published, but the ranges of Pu-content, density and O/M ratio of specimens were less than 20%, more than 90%TD and from 1.96 to 2.00 respectively. These measurement ranges are not sufficient for the thermal conductivity evaluation of fast reactor fuel in fuel design. In addition, there is no report that describes the influence of Am-content on thermal conductivity. In this study, the thermal conductivities of (U, Pu, Am) $\text{O}_2$  solid solutions were measured as a function of density (85 to 95 TD%). The evaluation formula on the density dependency of thermal conductivity obtained in this measurement was confirmed to apply to low-density type fuel like that of “MONJU”. The thermal conductivities of (U, Pu, Am) $\text{O}_2$  solid solutions were measured as functions of Am-content (0.7 to 3.1%) for the first time in this study. It was found that the thermal conductivities of MOX fuels decreased slightly with increasing Am-content in the range of a few percent. We are now investigating thermal conductivities of MOX fuels over wide ranges of temperature (to 2,000 °C) and O/M ratio (from 1.91 to 2.00), and will proceed to carry out comprehensive tests for evaluation of fast reactor fuel characteristics in the future.

### Reference

Morimoto, K. et al., Thermal Conductivity of (U, Pu, Am) $\text{O}_2$  Solid Solutions, Journal of Alloys and Compounds (2007), DOI:10.1016/j.jallcom.2006.12.159, in press.

## 12-6 Measurement and Analysis of Deflection of Fuel Pins Irradiated in a Fast Reactor — Evaluation of Irradiation Effects Using the X-ray CT Technique —

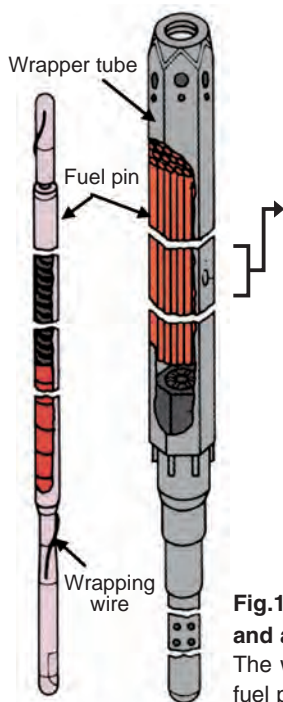


**Fig.12-11 Schematic diagram of fuel pin and assembly for "JOYO"**

The wrapper tube completely surrounds the fuel pin bundle.

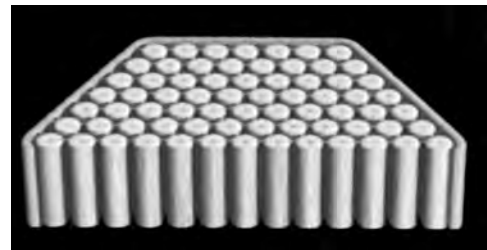


**Fig.12-12 Three-dimensional X-ray CT image of the irradiated fuel assembly**

It is possible to observe displacement of a fuel pin in the irradiated fuel assembly.

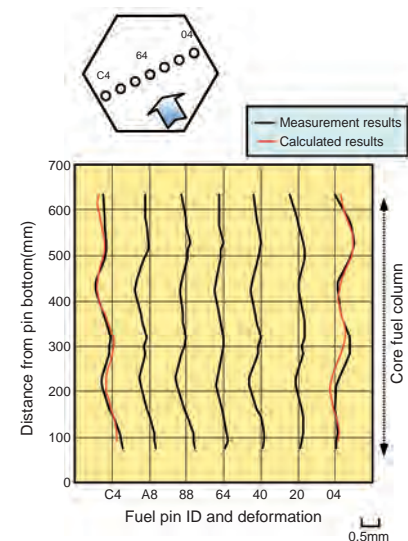


**Fig.12-13 Comparison between the observed and calculated fuel pin deflection**

Large displacement toward the outside of the fuel assembly occurs in the region of the core fuel column; this result agrees with the prediction.

Under irradiation, the fuel pins of a fast breeder reactor (FBR) are deflected by different amounts along the axial direction. Three factors can be envisaged that cause pin deflection: (1) bundle-duct interaction, (2) wrapping wire tension against pin, (3) thermal bowing of fuel pin. It is, however, difficult to observe fuel pin deformations in the actual assemblies because the wrapper tube prevents direct inspection (Fig.12-11). In order to observe the structural change in the interior of irradiated fuel assembly such as fuel pin deflection, a non-destructive post irradiation examination technique using X-ray computer tomography (X-ray CT) was developed (Fig.12-12).

In this study, X-ray CT images were taken on 20 cross sections along the full length of a fuel assembly which had been irradiated in "JOYO" to 78 GWd/t maximum burnup, and the deflection behavior of a fuel pin along the axial direction in the assembly was analyzed from the obtained CT images. Fig.12-13 shows the horizontal deflections of the center of 7 fuel pins in a fuel assembly along the axial direction. As shown in this figure, the displacement of all of fuel pins coincided with the wrapping wire winding pitch over the full length of fuel pins. Furthermore, the displacements of the fuel pins loaded in the outermost portions of the assembly are large, compared with the fuel pins of the central region.

The fuel pins are deflected in the axial direction by the three factors described previously. Of these factors, the contribution of bundle-duct interaction to the fuel pin deflection is negligibly small, because the neutron fluence of

this assembly was low level. Thus, the fuel pin deflection induced by wrapping wire tension and thermal bowing was evaluated.

In the case of the fuel pins loaded in the outermost array, the cladding temperature rises more on the side facing inward than on the opposite outer side. This temperature difference results in a tendency for the pin to deflect outward (thermal bowing). In our calculation, it is estimated that the maximum displacement of the fuel pin loaded in the outermost array is about 0.2 mm.

Additionally, the fuel pins will undulate with the pressure imparted by wrapping wire tension, with the undulations coinciding with the pitch of the wrapping wire. In the calculation, the fuel pin displacement induced by the wrapping wire tension is about 0.16 mm.

Overall deformation was obtained as the sum of these two deformations. The calculated deformation along the axial direction of two fuel pins loaded in the outermost array in the assembly are shown in Fig.12-13. The red lines on the graph correspond to calculated results. The results agree with each other.

The composition of X-ray CT images of the successive cross sections taken at a short interval made it possible to determine the deformation of fuel pins along the axial direction. The results obtained for the fuel assembly irradiated in "JOYO" showed good agreement with predictions. This knowledge makes it possible to predict the deflection of fuel pins loaded in the assembly under irradiation.

### Reference

Katsuyama, K. et al., High Energy X-ray CT Study on the Central Void Formations and the Fuel Pin Deformations of FBR Fuel Assemblies, Nuclear Instruments and Methods in Physics Research B, vol.255, issue 2, 2007, p.365-372.

## 12-7 Measuring Irradiation Time until Metal Specimen Rupture in Sodium Cooled Reactor — In-Pile Creep Rupture Experiment of Cladding Materials for Fast Reactor —

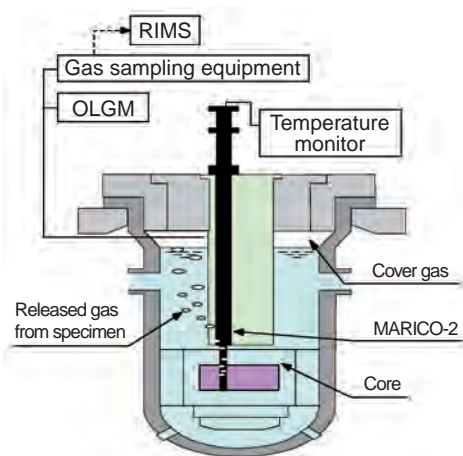


**Fig.12-14 Creep rupture detection and Identification system**

Both the temperature change in each capsule and OLG (the  $\gamma$ -ray spectrometry of the cover gas) indicate creep rupture events. The sampled cover gas is measured by means of the RIMS to obtain isotopic ratios of xenon tag gas in order to identify the ruptured specimen.

An on-line creep rupture experiment was conducted in the experimental fast reactor Joyo to evaluate the creep rupture strength of Oxide Dispersion Strengthened ferritic steel (ODS) under neutron irradiation. ODS has been developed as a candidate fuel cladding material for the next generation fast reactor because of its high temperature resistance and low swelling properties. Out-of-pile experiments in both argon and sodium environments have shown that ODS has higher creep rupture strength than the currently used austenitic stainless steel and the ferritic steel developed for the wrapper tube. The effect of neutron irradiation is the remaining item which needed to be confirmed in order to make mechanical designs with this material.

The Material Irradiation Rig with Temperature Control (MARICO) was developed to conduct this experiment in the Joyo reactor. ODS specimens (with no fuel) pressurized by helium gas up to 22 MPa were used to accelerate the creep rupture testing. The specimens were irradiated in the Joyo's core region, with the temperature maintained constant  $\pm 4$  °C.

In order to determine when a specimen ruptured, two Chromium/Aluminum thermo couples were installed inside each capsule containing the ODS irradiation specimens. One

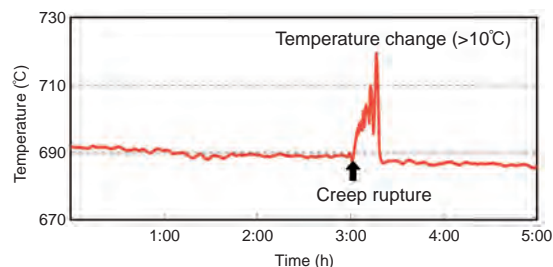
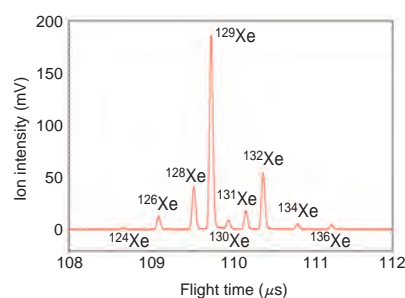


**Fig.12-15 Creep rupture detection by temperature change**

The temperature change of more than 10°C indicates a capsule which contains a ruptured specimen.



Tag gas no.	Xenon nuclides ratio to $^{129}\text{Xe}$		
	$^{126}\text{Xe}$	$^{131}\text{Xe}$	$^{132}\text{Xe}$
1	0.632	0.896	0.891
2	0.069	0.101	0.298
3	0.209	0.890	0.101
4	0.630	0.301	0.101
5	0.629	0.102	0.892
6	0.071	0.888	0.889
Measurement result	0.065	0.099	0.295

**Fig.12-16 Tag gas isotopic ratio measured by RIMS**

No. 2 tag gas was identified by RIMS successfully.

was located at the center of the capsule for temperature control and the other was installed at the upper end of the capsule to measure the temperature increase due to the change of the thermal conductivity when the coolant space was filled with the released gas (Fig.12-14, Fig.12-15).

A few cm<sup>3</sup> of a unique blend of stable xenon and krypton tag gas was contained in each specimen along with the helium fill gas. In the event of a specimen rupture, the gases were released into the coolant sodium and transferred into the argon cover gas region. The tag gas was measured by means of  $\gamma$ -ray spectrometry which monitors the activated tag gas nuclides produced by (n,  $\gamma$ ) reactions (OLGM, Fig.12-14), and Resonance Ionization Mass Spectrometry. Both methods have high sensitivity to the xenon and krypton tag gases diluted in the cover gas to a level as low as a few ppb (Fig.12-14, Fig.12-16).

The experiment was carried out from April 2006 until May 2007. Fourteen ODS specimens out of 24 total were ruptured, and all were successfully identified by means of the temperature change and tag gas measurements. These results are expected to be useful for the design of future fast reactor fuel.

### Reference

Ito, C. et al., In-Pile Creep Rupture Experiment of ODS Cladding Materials in the Experimental Fast Reactor Joyo, Proceedings of the 15th International Conference on Nuclear Engineering (ICONE15), Nagoya, Japan, 2007, ICONE15-10226, in CD-ROM.

## 12-8 Upgrading of HTTR Burnup Characteristics Evaluation Method — Improvement of BP Burnup Characteristics —

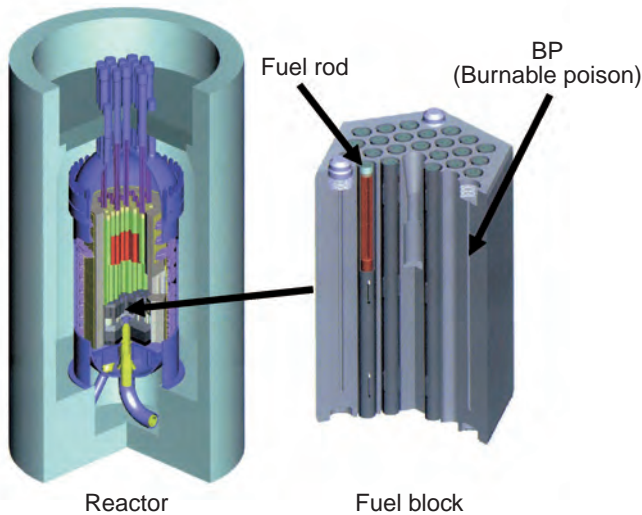


**Fig.12-17 HTTR fuel block**

The HTTR core is a fuel block with pile structure. The fuel block is a graphite block containing fuel rods and BP rods with absorb neutron.

The High Temperature Gas-cooled Reactor (HTGR) is a proposed reactor type with high inherent safety features, with capability as a heat source, for hydrogen production, and for high efficiency power generation. The High Temperature Engineering Test reactor (HTTR) made by JAEA is the first HTGR in Japan. HTTR achieved the outlet coolant temperature of 950°C in 2004, which is the highest attained in the world.

The fuel block of HTTR is a hexagonal graphite block containing 33 fuel rods. The fuel block also contains two burnable poison (BP) rods at corners of the block. The HTTR core consists of 150 fuel blocks (Fig.12-17).

In HTTR, control rod position should be kept constant during one burnup period (660 days) keeping the profile of power distribution in the core which will achieve outlet coolant temperature of 950°C while keeping fuel temperature below its allowable limit. The change in reactivity during burnup should be compensated for by the BPs. Therefore, it is important to evaluate the burnup characteristics of BP for “HTTR” operation.

From the results of criticality tests, it was clear that the excess reactivity was less than the predicted value. To improve the prediction accuracy, improvement of calculation model was carried out. In the improvement, a detailed BP cell model (hereafter “the detailed model”) was developed. In the

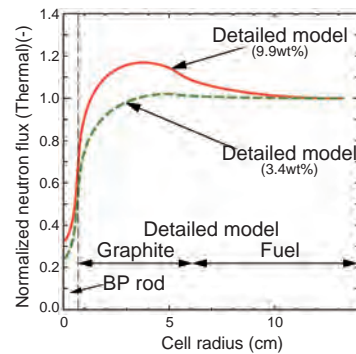


**Fig.12-18 Neutron flux distribution around BP rod**

Detailed model shows the change of neutron flux distribution with change in fuel enrichment

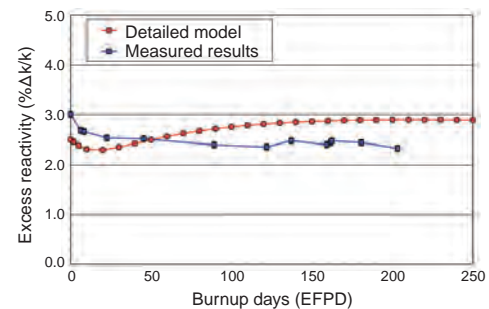


**Fig.12-19 Comparison of measured and calculated excess reactivity**

Results calculated by the detailed model yield almost constant values. The discrepancy with the measured results was less than 1%  $\Delta k/k$ .

model, a BP rod is located in a graphite region which is surrounded by fuel. The configuration of the detailed model corresponds to the actual configuration of the BPs in a fuel block. The model could reproduce the change in neutron flux distribution around a BP rod with different uranium-235 ( $^{235}\text{U}$ ) enrichments. The graphite enhances the BP reactivity effect of the  $^{235}\text{U}$  enrichment (Fig.12-18). The detailed model could evaluate BP reactivity which varies with change in fuel enrichment. Excess reactivity of the HTTR also was evaluated more precisely.

The detailed model was modified to include burnup calculations, because the neutron flux distribution around the BP rod changed with burnup. The model calculated a constant excess reactivity during the burnup period. The discrepancy between the calculated and measured results was small (Fig.12-19). It was clear that the detailed model could reproduce BP reactivity change with burnup precisely. Moreover, axial power distribution in the core was evaluated more precisely by the detailed model.

It was concluded that the detailed model could evaluate core characteristics under high burnup conditions. The detailed model can contribute to improve fuel economy of HTGRs. The model can be improved by experimental data under high burnup conditions.

### Reference

Fujimoto, N. et al., Burnup Characteristics of Burnable Poison and Core Characteristics of HTTR, JAEA-Technology 2005-008, 2006, 45p. (in Japanese).

## 12-9 Fabrication of a Micro-Scale Arc de Triomphe by MeV Focused Proton Beams

— Development of a 3-D's Fine Fabrication Technique Using High Energy Submicron Ion Beams —

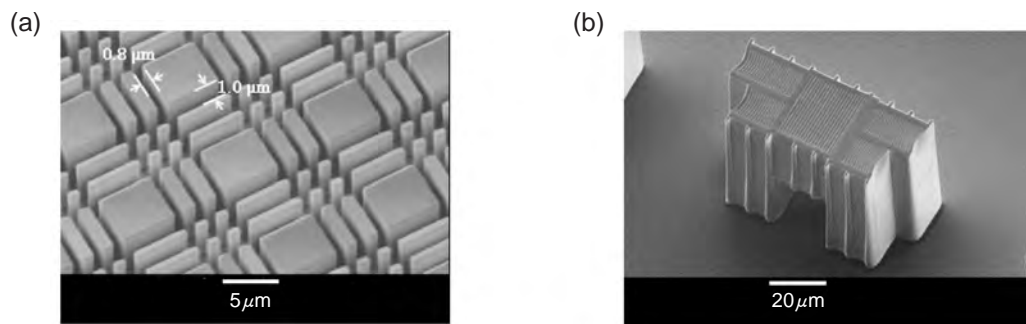


**Fig.12-20** Fine polymer structures fabricated of a polymer using PBW  
(a) grid structure, (b) Arc de Triomphe structure

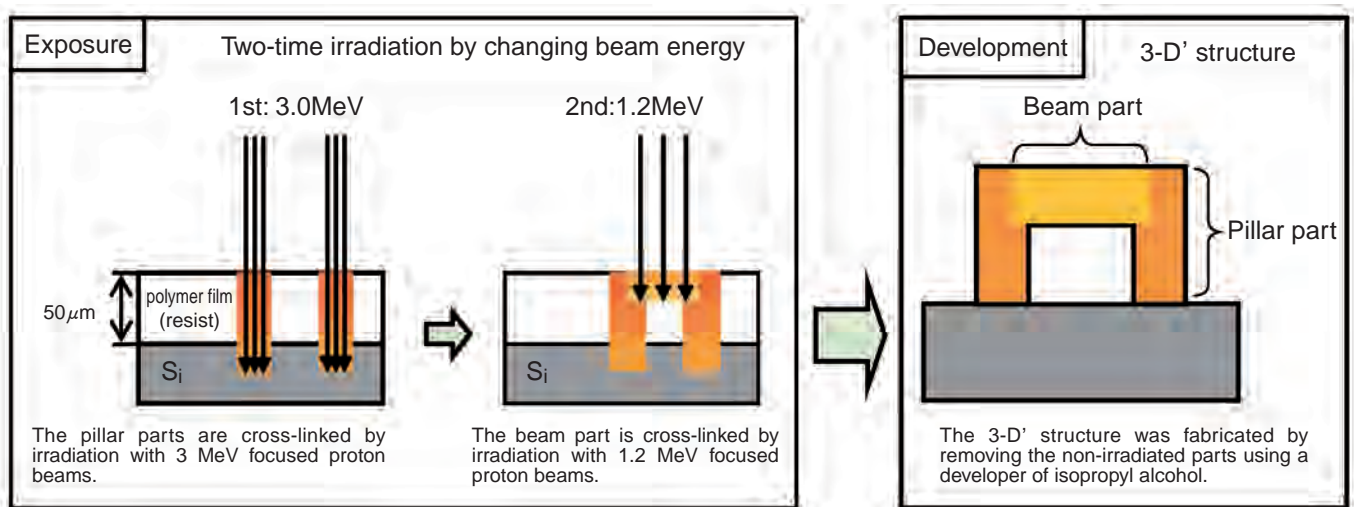


**Fig.12-21** Fabrication process for 3-D polymer structure (negative resist; non-irradiated parts are removed)

Fine polymer fabrication at a scale of micrometer or less has been performed using electron beams. The fabrication with long penetrable ranges is, however, difficult due to large straggling effects of the beams in the polymers. The MeV focused proton beams with a diameter of micrometer or less have longer range of penetration into materials of over 100  $\mu$  m, and highly straight trajectories. These advantages allow us to fabricate not only high aspect-ratio structures, but also 3-D structures with cavities by changing the penetration range which depends on the proton beam energy. The technique of focusing proton beams of 3 MeV at a maximum into an area of hundreds of nanometers in diameter has been developed at “TIARA” (the Takasaki Ion Accelerators for Advanced Radiation Application) in the Takasaki Advanced Radiation Research Institute. We, a group of a joint research between JAEA and the Shibaura Institute of Technology, used these advantages for fabrication first in Japan, and through research starting in 2005 have developed a proton beam writing (PBW) technique to fabricate 3-D structures with polymers. The PBW is a detailed fabrication technique using the MeV

focused proton beam scanned following the predetermined patterns over a polymer resist. Fine structures are produced by carrying out the PBW and then removing the irradiated or non-irradiated parts using a developer.

We fabricated the 3-D structures with horizontal resolution on the scale of hundreds of nanometers or maximum processing depth of 50  $\mu$  m. The fine 3-D structures fabricated by PBW are shown in Fig.12-20; (a) a thin PMMA film (a positive resist; irradiated parts were removed) coated on a silicon substrate and (b) a 3-D structure with a cavity (Arc de Triomphe shape) using the irradiation of SU-8 (a negative resist; non-irradiated parts were removed). The former shows that the spatial resolution of PBW reaches the scale of hundreds of nanometers. The fabrication process of Fig.12-20(b) is development after exposure to 3 MeV and 1.2 MeV focused proton beams 1  $\mu$  m in diameter and then performing the development, as illustrated in Fig.12-21. This 3D structure fabrication method demonstrates that the PBW technique at JAEA has reached the top-level in the world.

### Reference

Uchiya, N., Ishii, Y. et al., Micro-machining of Resists on Silicon by Proton Beam Writing, Nuclear Instruments and Methods in Physics Research B, vol.260, issue 1, 2007, p.405-408.

# 12-10 Battle Against Water Inflow: Five-year History of Mizunami Underground Research Laboratory

## — Development of Post-Grouting Technology for Deep Shaft —

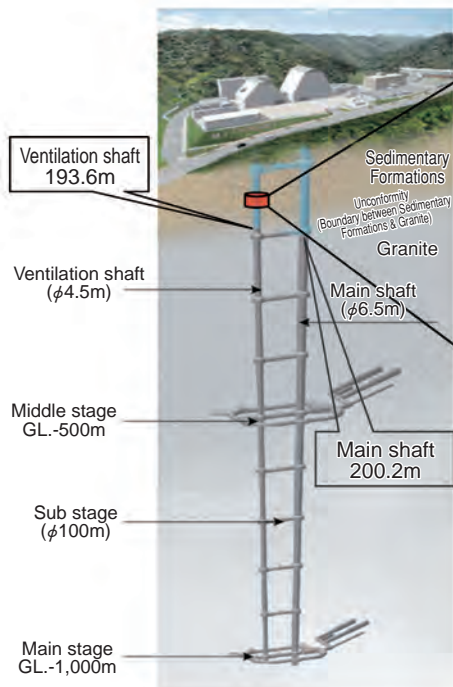


**Fig.12-22 Conceptual design of MIU, location of the post-excitation grouting experiment in red (GL-140~ - 148 m). Depth of shafts as of March 2007.**

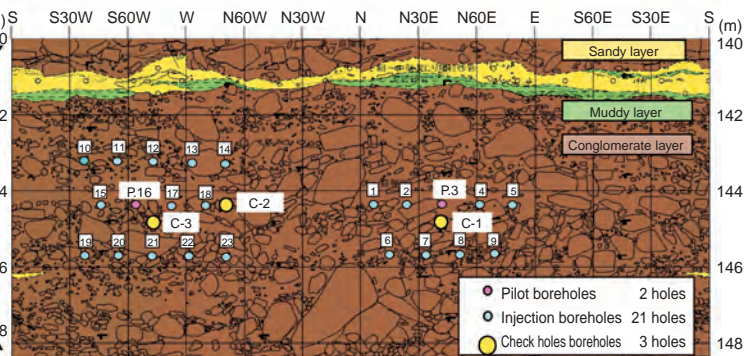


**Fig.12-23 Geological description and borehole layout for the post-grouting (Red area in Fig.12-22)**

**Table 12-1 Test results**

Borehole No.	Test interval (m)	Lugeon value (Lu)	Inflow pressure (MPa)	Hydraulic conductivity (m/sec)	Inflow rate (L/min)	Grouting stage / Test area
P.16	4.6~7.7	20.1	0.169	2.78E-06	6.5	Before grouting
C-3	5.6~7.0	4.2	0.219	7.79E-07	0.0	After grouting / Inside grouting zone
	6.7~9.5	3.1	0.228	4.25E-07	1.1	After grouting / Inside grouting zone
	12.0~14.5	11.4	0.258	1.76E-06	18.0	After grouting / Outside grouting zone

The Mizunami Underground Research Laboratory (MIU) is currently being constructed to establish techniques for investigation, analysis and assessment of deep geological environments, and to develop a range of engineering expertise for application in deep underground excavations in crystalline rocks such as granite. Construction of shafts and galleries is being executed to confirm the results of the predictions made in the surface-based investigation phase. The construction phase started on July 8th, 2002, five years ago. Recently, shaft excavation has progressed to about GL-(below ground level) 200m where a substage tunnel is under construction (Fig.12-22).

Consideration of environmental impact due to the excavation, optimization of costs for treatment of groundwater as well as reduction of inflow water is indispensable for continuing the excavation of MIU. Post-excitation grouting (hereafter “post-grouting”) on the shaft walls at GL-142~--146m has been conducted as part of development of techniques for reducing water inflow (Fig.12-23). Post-grouting is a technique of injection of cement materials in the rock mass after excavation. The post-grouting on the shaft walls has seldom been performed previously, and is one of the engineering techniques which must be developed for the continuation of the construction of

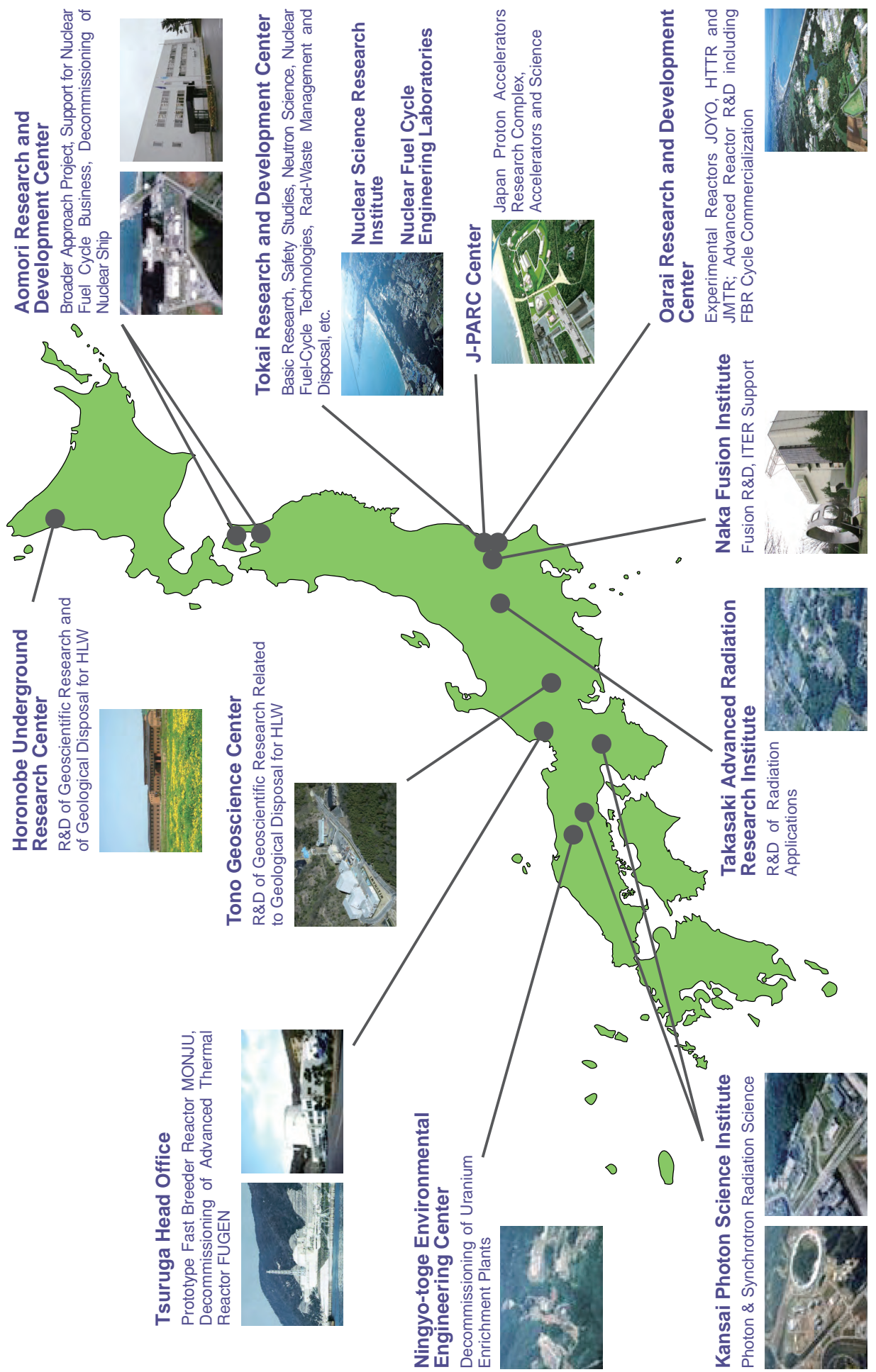
the shaft. In the post-grouting, hydraulic testing such as injection and recovery method have been carried out in the drilled boreholes from the shaft wall. From the testing, Lugeon value defined as water injection rate with constant injection pressure of 0.98MPa and hydraulic conductivity (flux of water in the rock mass per unit of water head) were obtained. These values were compared, not only before and after the grouting, but inside and outside of the injection area. The results of the test showed that both Lugeon value and hydraulic conductivity after post-grouting were decreased to one fifth of the values before grouting. The water inflow was hardly observed in the injected volume after grouting (Table 12-1). On the other hand, the inflow rate after post-grouting was higher than the one before outside the injected volume. From the tests of the post-grouting, the strategy and methods applied were confirmed to be effective in reducing permeability of the rock.

Although pre-excitation grouting technique will be the basic method for reducing inflow water, the post-grouting technique will be also applied in case of an unacceptable inflow volume. In this way, the construction of MIU proceeds while protecting the environment and optimizing the costs of water treatment by reducing the water inflow.

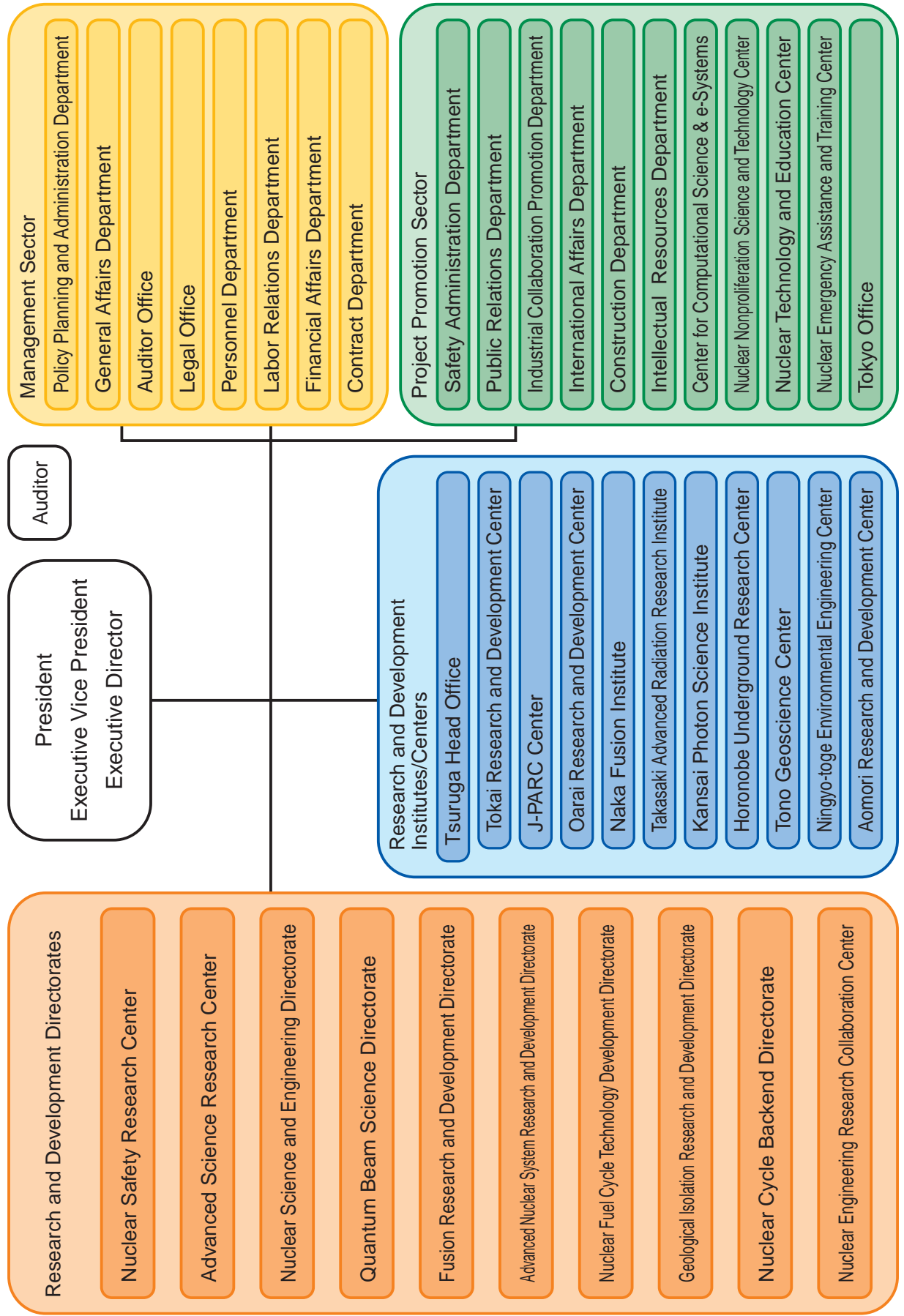
**Reference**

Kuji, M. et al., Countermeasures Plan for Reducing Water Inflow into Deep Shafts at the Mizunami Underground Research Laboratory, Proceedings of 15th International Conference on Nuclear Engineering, (ICONE15), Nagoya, Japan, 2007, ICONE15-10413, in CD-ROM.

# R&D Centers of JAEA



# Japan Atomic Energy Agency – Outline of Organization –



About the Design of the Cover :

The cover is designed to envisage a hopeful future shining in the sky with a blue color derived from the color of the JAEA logo. This is accompanied with white colored hexagons similar to the pattern in a tortoise shell symbolizing the wish of people for longer lives since ancient times in Japan. Coincidentally, this shape is the same as that of the core fuel assemblies both of the prototype Fast Breeder Reactor, "MONJU", and the High Temperature Test Reactor, "HTTR".

The picture in the upper left shows a geological structure at the Mizunami Underground Research Laboratory in the Tono Geoscience Center, where R&D in the safety geological disposal technologies of high-level radioactive wastes is expected to make great progress.

The figure in the lower right is the advanced superconducting tokamak "JT-60SA", with the superconducting coils which can be used in the Broader Approach Activities in the field of fusion energy research. It will be exploited as a "satellite" facility of ITER.



## **JAEA R&D Review 2007**

### **Editorial Board**

**Chief editor:** Hisao Ojima

**Vice editor:** Shunichi Miyakawa

**Editors:** Toru Nakatsuka, Hideo Kaburaki, Yu Hashimoto,  
Ken Muramatsu, Yuichiro Nagame, Takemasa Shibata,  
Takamasa Mori, Yasuhiko Kobayashi, Atsushi Yokoyama,  
Yoshitaka Ikeda, Makoto Ishikawa, Munetaka Myochin,  
Kiyoshi Tamayama, Yoshihiko Nagasato, Yoshifumi Yamaguchi,  
Hiromichi Ogawa, Michio Yoshizawa, Kenji Kikuchi,  
Koji Kawata, Kazunori Hirao, Takuji Kojima

**Published by** Japan Atomic Energy Agency (JAEA)

**Editorial Office:** Intellectual Resources Section, Intellectual Resources Department  
2-4 Shirakatashirane, Tokai-mura, Naka-gun, Ibaraki-ken 319-1195, Japan  
Phone: +81-29-282-6387      Facsimile: +81-29-282-5920  
e-mail: ird-seika\_shi@jaea.go.jp



Japan Atomic Energy Agency